STRUCTURAL AND FUNCTIONAL STUDIES ON BOVINE INOSITOL MONOPHOSPHATASE

By

Rajji Rani Badyal B.Sc. (Hons)

A thesis submitted to the department of Biochemistry and Molecular Biology,
University of Southampton

For the degree of
Doctor of Philosophy

December, 2000

UNIVERSITY OF SOUTHAMPTON

ABSTRACT

FACULTY OF SCIENCE
DIVISION OF BIOCHEMISTRY AND MOLECULAR BIOLOGY

Doctor of Philosophy

STRUCTURAL AND FUNCTIONAL STUDIES ON BOVINE INOSITOL MONOPHOSPHATASE

By Rajji Rani Badyal B.Sc. (Hons)

Inositol monophosphatase is a homodimeric enzyme that catalyses the dephosphorylation of inositol monophosphates to inositol and inorganic phosphate. It has a dual role in that it recycles the inositol, which is critical in brain tissue since it lacks an adequate import system for this moiety and secondly it carries out the final step in the *de novo* conversion of glucose to inositol. The enzyme has an absolute requirement for Mg^{2+} ions for catalytic activity although uncompetitive inhibition takes place at high concentrations. In addition, the enzyme is inhibited uncompetitively by Li^{+} ions. Kinetic studies have reported the existence of two metal binding sites, a high affinity site with a K_d of 300μM and a lower affinity site with a K_m value of 3mM. The X-ray structure of the human enzyme has provided much insight into the structural features required for Mg^{2+} and substrate binding. Based on these findings, corresponding residues in the structurally homologous bovine enzyme located within loop regions, near the active site and at the dimer interface were mutated. Several spectroscopic techniques were employed to determine if these residues were structurally or functionally significant. A G76S mutant displayed unchanged metal binding affinities for both sites 1 and 2. The mutant G69S displayed reduced metal binding affinity at both sites and also for substrate. The stability of this mutant with respect to the denatured state was significantly lower than that of the WT enzyme. The mutation H188Q at the dimer interface displayed a similar site 1 K_d to the WT enzyme, however, its specific activity was markedly increased; it displayed decreased affinity for both Mg^{2+} binding to site 2 and for substrate. The E30P mutant displayed an increased affinity for Mg^{2+} binding at site1 and for substrate, but the affinity for Mg^{2+} binding at site 2 was unchanged. Mutant C218D displayed a 3-fold and 2-fold decrease in affinity at sites 1 and 2 respectively. Crystals of WT BIMP were grown for the first time, in the presence of the natural Mg^{2+} ligand. The X-ray structure has been successfully determined at 1.6Å in the laboratory of Professor Steve Wood in Southampton. Three Mg^{2+} binding sites are present in each subunit of the BIMP dimer. The Mg^{2+} binding sites in subunit B are identical to those seen in the Mn^{2+} and Ca^{2+} bound human enzyme structures. However, the third site for Mg^{2+} in subunit A is differently located and only partially occupied. The significance of the third Mg^{2+} binding site of BIMP in the proposed mechanism of the enzyme is discussed.

ACKNOWLEDGEMENTS

I would like to thank Dr. Mike Gore for offering me the opportunity to study for a PhD in his group and for his help and encouragement at all times.

I would especially like to thank Nicki Muir for her help in the early stages of this work and Dr Raj Gill, Fiyaz Mohammed and Professor Steve Wood for their help on the structural aspects of this work. I would also like to thank all past and present Gore group members, especially Vicky, Mark, Doug, Nick, Hazel, Annie, Nina and Steve for their help and friendship when things were not going to plan and everyone else in 4061 who livened up the lab on many a day.

I am grateful to my sister Seema and my brothers Raj and Pawan who at times probably thought that they were doing this PhD with me, and to Martin, Marco, Matt, Colin, Paul, Amir, Gopi, Anu, Val and Wendy for making sure I had fun outside the lab.

Most of all I am especially grateful to my parents for being a constant source of support and encouragement throughout my education and it is to them that I dedicate this thesis.

To my family

LIST OF ABBREVIATIONS

A	- Adenine
2'-AMP	- 2'-Adenosine monophosphate
Analar	- Analytical grade
APS	- Ammonium persulphate
BCA	- Bichinconinic acid
BIMP	- Bovine inositol monophosphatase
cAMP	- Cyclic adenosine monophosphate
CAPS	- 3-[Cyclohexylamino]-1-propane sulphonic acid
CD	- Circular dichroism
cDNA	- Complementary DNA
CIAP	- Calf intestine alkaline phosphatase
C218A	- Cysteine (residue 218) to alanine replacement
C218D	- Cysteine (residue 218) to aspartate replacement
Da	- Dalton
DAG	- Diacylglycerol
DEP	- Diethylpyrocarbonate
ΔG	- Change in free energy
dH_2O	- Distilled water
ddH_2O	- Distilled deionised water
DMSO	- Dimethylsulphoxide
DNA	- Deoxyribonucleic acid
Dnase I	- Deoxyribonuclease I
dNTP	- Deoxynucleotide triphosphate
dsDNA	- Double stranded DNA
E.coli	- Escherichia coli
EDTA	- Ethylenediaminetetraacetic acid
EG	- Ethylene glycol

EGTA	- Ethylenebis(oxyethylenenitrilo) tetraacetic acid
$E\text{-}P_i$	- Phosphoenzyme intermediate
E30P	- Glutamate (residue 30) to proline replacement
F1,6-BP	- Fructose 1,6-bisphosphatase
2'-GMP	- 2'-Guanidine monophosphate
G	- Guanine
G69D	- Glycine (residue 69) to aspartate replacement
G69S	- Glycine (residue 69) to serine replacement
G76S	- Glycine (residue 76) to serine replacement
h	- Planck's constant
HIMP	- Human inositol monophosphatase
H100Q	- Histidine (residue 100) to glutamine replacement
H188Q	- Histidine (residue 188) to glutamine replacement
H217G	- Histidine (residue 217) to glycine replacement
H217Q	- Histidine (residue 217) to glutamine replacement
IAA	- Iodoacetic acid
IC_{50}	- Concentration of inhibitor required to give 50% inhibition
I269SC	- Isoleucine (residue 269) to stop codon replacement
IMPase	- Inositol monophosphatase
Ins(1)P	- Inositol 1-phosphate
Ins(2)P	- Inositol 2-phosphate
Ins(3)P	- Inositol 3-phosphate
Ins(4)P	- Inositol 4-phosphate

$Ins(1,4,5)P_3$	- Inositol 1,4,5-triphosphate
$Ins(1,3,4,5)P_4$	- Inositol 1,3,4,5-tetrakisphosphate
IPP	- Inositol polyphosphate 1-phosphatase
IPTG	- Isopropyl-β-D-thiogalactosidase
k_{app}	- Apparent rate of reaction
k_1	- Rate of association
k_{cat}	- Turnover number
k_{cat}/K_m	- Specificity constant
K_d	- Dissociation constant
k_{-1}	- Rate of dissociation
kDa	- Kilodalton
k_{eq}	- Equilibrium constant
K_i	- Inhibition constant
$K_m$app	- Apparent Michaelis-Menten constant
K_m	- Michaelis-menten constant
LB-broth	- Luria Bertani broth
L-690,330	- 1-(4-hydroxyphenyloxy)ethane-1, 1-bisphosphonic acid
MPD	- 2-methyl-2, 4-pentanediol
M_r	- Relative molecular mass
4-MUFP	- 4-methylumbelliferyl phosphate
4-MUFone	- 4-methylumbelliferone
n	- Hill coefficient
NADH	- Reduced nicotinamide adenine dinucleotide
NEM	- N-ethylmaleimide
4NP	- 4-nitrophenyl phosphate
OD	- Optical density
PCR	- Polymerase chain reaction
PEG	- Polyethylene glycol
P_i	- Inorganic phosphate
PM	- Pyrene maleimide
PtIns	- Phosphatidylinositol

$PtIns(4,5)P_2$	- Phosphatidylinositol 4,5-bisphosphate
Q	- Quantum yield
R	- Gas constant
RET	- Resonance energy transfer
RNA	- Ribonucleic acid
Rnase A	- Ribonuclease A
R191A	- Arginine (residue 191) to alanine replacement
SDM	- Site-directed mutagenesis
SDS-PAGE	- Sodium dodecyl sulphate polyacrylamide gel electrophoresis
ssDNA	- Single stranded DNA
SC	- Stop codon
T	- Thymine
TEMED	- N,N,N',N'tetramethylethylenediamine
T_m	- Melting temperature
Tris	- Tris(hydroxymethyl)aminomethane
U	- Uracil
U-DNA	- Uracil-rich DNA
UV	- Ultraviolet
V_{max}	- Maximum rate of reaction
WT	- Wild-type

CONTENTS

LIST OF FIGURES AND TABLES

Chapter 1 Introduction

Figures

Chapter 3 Site-directed mutagenesis of inositol monophosphatase.

3.11 The characteristic CD spectra of the three major secondary structural elements found in proteins.

3.12 (a) The Far UV CD spectra for WT inositol monophosphatase.

3.13 (a) The fraction of WT unfolded (in the absence of Mg^{2+} ions) monitored as a ratio at 320nm and 360nm in the presence of urea.
(b) The percentage of WT enzyme in the unfolded state in urea.
(c) The conformational stability of unfolding for WT enzyme in the presence of Mg^{2+}.

Chapter 4 The use of fluorescence spectroscopy to study equilibrium and pre-equilibrium binding.

4.1 (a) The fluorescent pyrene maleimide label covalently attached to an enzyme thiol group.
(b) The fluorescence emission spectra of the modified and native WT enzyme.

4.2 The fluorescence emission spectra for WT, G76S, G69S, H188Q, E30P and C218D enzymes at pH 8.0 (λ^{ex} = 280nm, λ^{em} = 340nm).

4.3 The rates of pyrene maleimide labelling of (a) WT, (b) G76S, (c) G69S, (d) H188Q and (e) E30P enzymes.

4.4 The fluorescence emission spectra of pyrene-maleimide labelled (a) WT, (b) G76S, (c) G69S, (d) H188Q, (e) E30P and (f) C218D enzymes and the signal change on addition of 20mM Mg^{2+} ions.

4.5 The titration of Mg^{2+} ions into (a) WT, (b) G76S, (c) G69S, (d) H188Q, (e) E30P and (f) C218D enzymes in 50mM Tris.HCl containing 250mM KCl pH 8.0 at 25°C.

4.6 (a) The far UV CD spectra in the absence and presence of 30mM Mg^{2+}.

4.7 (a) The near UV CD spectra of WT enzyme in the absence and presence of 10mM Mg^{2+} ions.
(b) The titration of Mg^{2+} ions into WT enzyme monitored using near UV CD spectroscopy.

4.8 (a) The spectral changes in the near UV region for G76S upon addition of 10mM Mg^{2+} ions.

(b) The titration of Mg^{2+} ions into the G76S mutant in the near UV region.

4.9 (a) The near UV CD spectra of the G69S mutant in the absence and presence of 10mM Mg^{2+} ions.

4.10 (a) The near UV CD spectra of the H188Q mutant in the absence and presence of 10mM Mg^{2+} ions.

(b) Titration of Mg^{2+} ions into the H188Q mutant monitored in the near UV region of the CD spectrum.

4.11 (a) The spectral changes observed in the near UV CD region upon addition of 10mM Mg^{2+} ions to the E30P mutant.

(b) The titration curve of Mg^{2+} addition into the E30P mutant.

4.12 (a) The near UV CD spectra of the C218D mutant in the absence and presence of 10mM Mg^{2+} ions.

(b) Titration of Mg^{2+} ions into the C218D mutant monitored in the near UV region.

4.13 A typical reaction progress curve observed when 3μM enzyme is reacted with 400μM Mg^{2+} ions at pH 8.0, 25°C. The lower plot describes the residuals to the fitted curve which in this case was by a double exponential algorithm.

4.14 The relationship between k_{app} and the final concentration of Mg^{2+} ions.

4.15 The dependence of the second phase of the reaction on the final concentration of Mg^{2+} ions.

4.16 The dependence of the rate of decrease of fluorescence intensity when a solution of 6μM enzyme in the presence of 400μM Mg^{2+} ions is mixed with an equal volume of a solution of EDTA.

4.17 The rapid decrease in fluorescence intensity noted when a solution of pyrene-labelled enzyme (6μM) in the presence of 400μM EDTA in 10mM Tris-HCl buffer, pH 8.0 is reacted with an equal volume of 10mM EDTA in 10mM Hepes buffer adjusted to the pH required to generate the final pH indicated. The inset shows a plot of the value of k_{app} against the pH of the resultant solution.

Chapter 5 The observation of the effect of mutagenesis on metal ion and substrate binding by steady state kinetics.

Chapter 6 Crystallisation and structural determination of recombinant bovine inositol monophosphatase.

6.5 A crystal of WT BIMP obtained using the hanging drop method. The crystal grew over a one-month period in 0.1M Na Hepes pH 8.5, 0.1M Na acetate, 15% v/v PEG 4K and 10mM Mg^{2+} ions at 25°C.

6.6 A 1° oscillation diffraction image of WT BIMP crystal obtained at ESRF Grenoble.

6.7 An illustration of the placement of a molecule HIMP within the unit cell of the bovine enzyme.

6.8 A Ramachandran plot of the ϕ and ψ angles of bovine inositol monophosphatase refined to1.6Å.

6.9 The structure of the BIMP dimer, showing three Mg^{2+} ions in the active site of subunit B and three Mg^{2+} ions in the active site of subunit A.

6.10 (a) The active site structure for subunit A of BIMP complexed to Mg^{2+} ions. Mg^{2+} ions are labelled 1, 2 and 3 and are shown together with active site water molecules and the electron density around the active site.

6.10 (b) The active site structure for subunit B of BIMP complexed to 3 Mg^{2+} ions shown together with active site water molecules and the electron density.

6.11 The active site structure of HIMP, complexed to Mn^{2+} and Cl^- ions (1IMC.pdb).

6.12 The active site of bovine inositol monophosphatase showing the positions of the three Mg^{2+} ions and their corresponding ligands.

6.13 (a) The active site of subunit A of bovine inositol monophosphatase.

6.13 (b) The active site of subunit B of bovine inositol monophosphatase.

6.14 The human inositol monophosphatase structure complexed with 3 Ca^{2+} and D-Ins(1)P (Ganzhorn *et al.*, 1997, 1AWB.pdb)

6.15 (a) Superposition of the substrate binding region of BIMP (monomer B) on that of the HIMP structure complexed either with Gd^{3+} and D-Inositol(1)P or with the Ca^{2+} and D-Inositol(1)P.

6.15 (b) Superposition of the substrate binding region of BIMP (monomer B) on that of the HIMP structure complexed with Gd^{3+} and L-Inositol(1)P.

6.16 A crystal of G76S BIMP obtained using the hanging drop method. The crystal grew in 0.1M Tris.HCl pH 8.5, 0.3M Na acetate, 22.5% v/v PEG 4K and 10mM Mg^{2+} ions at 25°C and diffracted to 1.3Å at ESRF Grenoble.

6.17 Shows low resolution images of crystals formed in the presence of (a) Mg^{2+} and inhibitor I, (b) Mg^{2+} and inhibitor II, (c) Li^{+} and inhibitor I, (d) Mg^{2+} and Li^{+}, (e) Zn^{2+}, (f) Zn^{2+} and inhibitor I, (g) Zn^{2+} and inhibitor II, (h) Zn^{2+}, Li^{+} and inhibitor I (i) Li^{+}, Mg^{2+} and inhibitor I, (j) Li^{+}, Mg^{2+} and inhibitor II and (k) Li^{+}, and inhibitor I.

List of tables.

CHAPTER 1

INTRODUCTION

CHAPTER 1

Introduction

1.1 The phosphatidylinositol cell signalling pathway: Function and role of inositol monophosphatase

Inositol monophosphatase is an important enzyme in the phosphatidylinositol secondary messenger signalling pathway of the brain (Figure1.1). It plays a central role in the recycling of the inositol moiety liberated by the hydrolysis of its monophosphate ester substrates for the resynthesis of phosphatidyl-inositol phospholipids (Figure 1.4(a)). It is also responsible in the brain for catalysing the final step in the *de novo* synthesis of inositol from glucose-6-phosphate (Eisenberg, 1967).

The binding of an agonist to a cell surface receptor activates phospholipase C, (via a guanidine nucleotide exchange protein) which utilises the membrane bound phosphatidylinositol 4,5-bisphosphate (PtdIns(4,5)P_2) as a substrate. PtdIns(4,5)P_2 is hydrolysed to two second messengers, diacylglycerol (DAG) and inositol 1,4,5-trisphosphate (Ins(1,4,5)P_3). The lipid-soluble diacylglycerol is retained in the plane of the cell membrane where it binds to and activates protein kinase C, promoting the phosphorylation of target proteins in the cell (Nishizuka, 1984). Inositol 1,4,5-trisphosphate is released into the cytoplasm where it acts upon specific receptors inside the target cell and stimulates the release of calcium from intracellular stores (Berridge and Irvine, 1989). The Ins(1,4,5)P_3 calcium mobilising signal is terminated by the metabolism of Ins(1,4,5)P_3 by one of two routes.

The first route involves phosphorylation of Ins(1,4,5)P_3 at the 3-position, giving rise to inositol 1,3,4,5-tetrakisphosphate (Ins(1,3,4,5)P_4, which together with Ins(1,4,5)P_3 may have a role in calcium mobilisation (Downes *et al.*, 1989; Vallejo, 1987). In the second route Ins(1,4,5)P_3 is metabolised by an

Figure 1.1 A summary of the phosphatidylinositol cell signalling pathway.

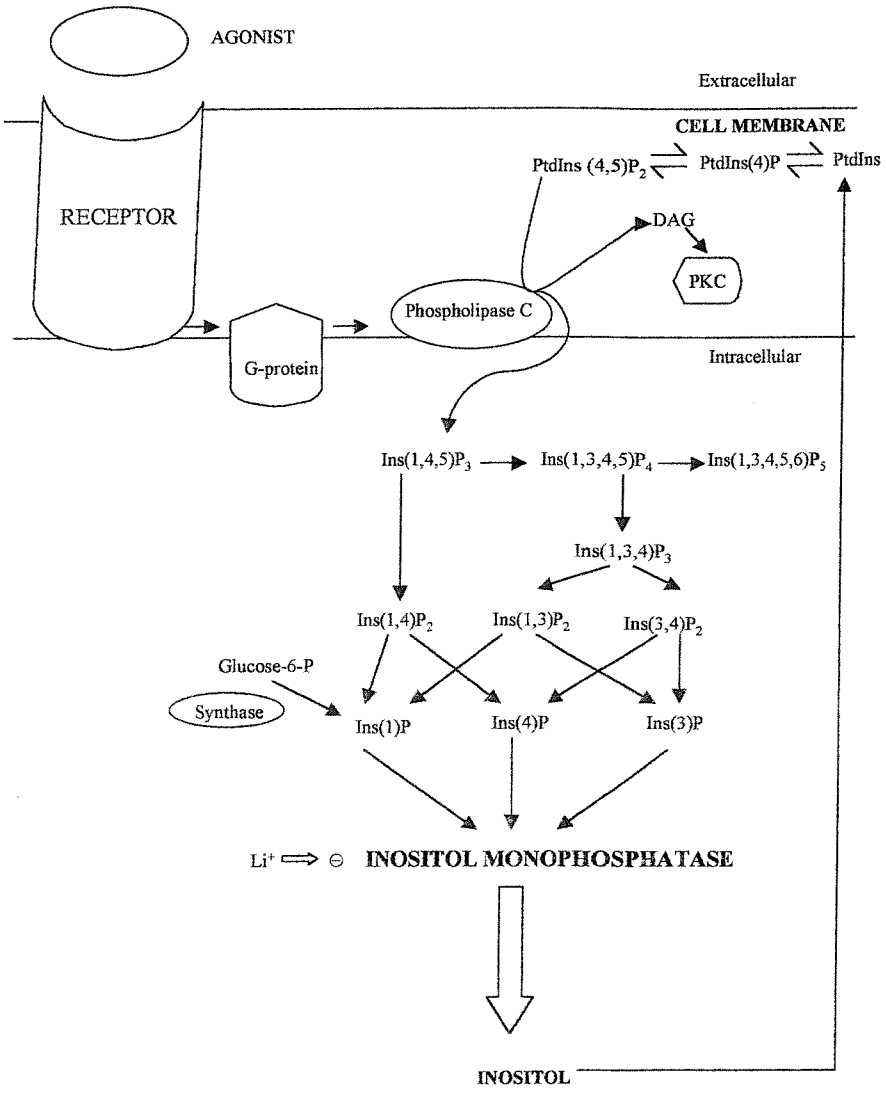
AGONIST
Extracellular
CELL MEMBRANE
PtdIns (4,5)P2
PtdIns(4)P
PtdIns
RECEPTOR
DAG
PKC
Phospholipase C
G-protein
Intracellular
Ins(1,4,5)P3
Ins(1,3,4,5)P4
Ins(1,3,4,5,6)P5
Ins(1,3,4)P3
Ins(1,4)P2
Ins(1,3)P2
Ins(3,4)P2
Glucose-6-P
Synthase
Ins(1)P
Ins(4)P
Ins(3)P
Li+
INOSITOL MONOPHOSPHATASE
INOSITOL

array of phosphatases and hydrolases into monophosphate esters, all of which act as substrates for inositol monophosphatase. Inositol monophosphatase is then responsible for the hydrolysis of these inositol monophosphates to inorganic phosphate (P_i) and inositol, which is then used for the resynthesis of the membrane bound PtdIns(4,5)P_2.

1.2 Pleckstrin homology domains (PH domains)

Although signalling roles for inositol phospholipids that involve their hydrolysis to second messengers have been well documented, recent work (Bottomley *et al.*, 1998) has shown additional roles that do not require their hydrolysis. In these roles, phosphoinositides function as signals on membranes that recruit and or activate protein complexes at the cytosolic interface. These signals are used in processes such as signal transduction, cytoskeletal assembly, membrane budding and fusion processes. Such processes would normally be restricted to certain membrane domains. Phosphoinositides achieve this by binding to small protein modules known as PH domains.

PH domains, termed plextrin homology domains, initially discovered in platelet protein kinase C substrate plextrin, consist of approximately 120 amino acid residue modules. These PH domains have been identified in various signalling proteins including protein-tyrosine kinases, ser-threonine kinases and all phospholipase C isoforms (Musacchio *et al.*, 1993; Gibson *et al.*, 1994). Although their sequence homology is low (10-20%), NMR and X-ray studies have shown remarkable similarities in the structures of PH domains from different proteins. All comprise of two orthogonal β-sheets of three and four antiparallel β-strands capped with a C-terminal α-helix which contains a conserved tryptophan residue (Figure 1.2). The loop regions are thought to be the main regions of variability which in turn explain the varied phosphoinositide-binding specificities and affinities.

It is believed that specific recognition of PtdIns(4,5)P_2 and Ins(1,4,5)P_3 by

Figure 1.2 A ribbon diagram of the pleckstrin-homology (PH) domain of Phospholipase C attached to Ins(1,4,5)P_3 (adapted from Ferguson *et al.*, 1995).

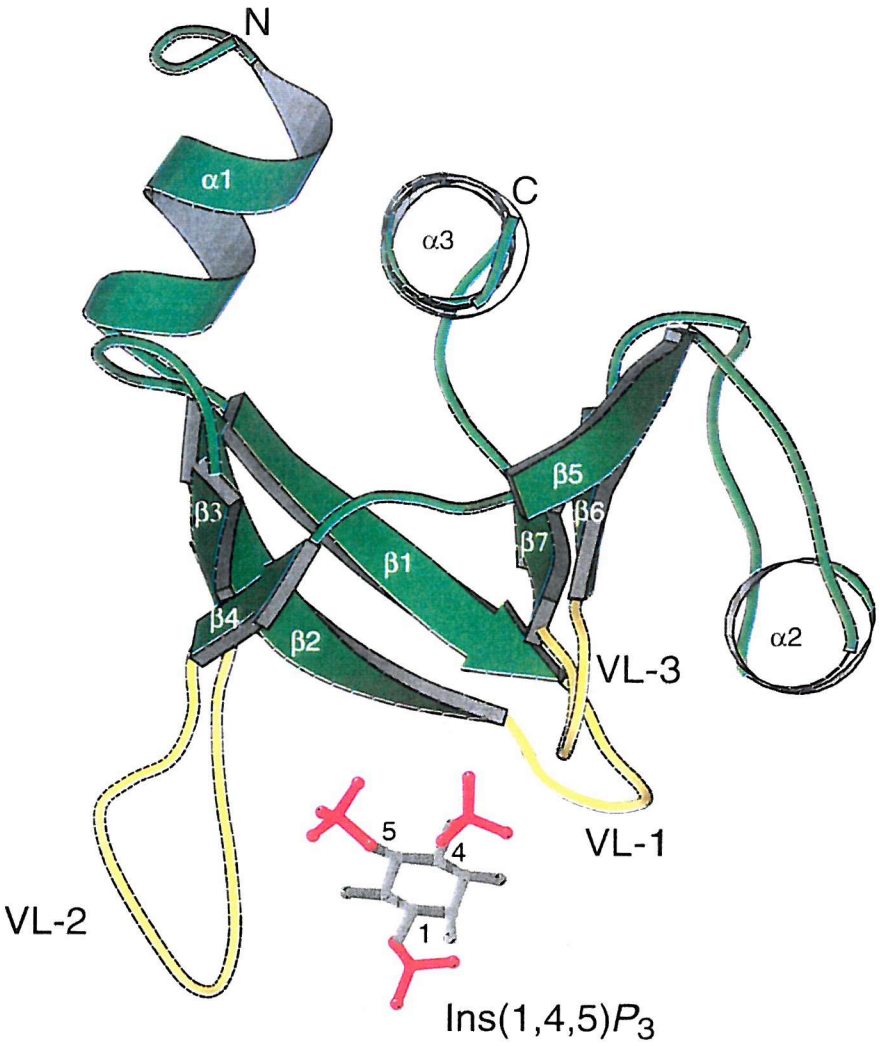
N
C
α1
α3
β5
β3
β6
β7
β1
β4
β2
α2
VL-3
VL-1
VL-2
5
4
1
Ins(1,4,5)P_3

the PH domain of phospholipase C may play a role in regulation of the enzyme. Furthermore, it has been proposed that the PH domain of phospholipase C attaches the enzyme to the membrane surface containing its substrate (PtdIns(4,5)P_2) and allows a 'processive' form of PtdIns(4,5)P_2 hydrolysis. Based on *in vitro* studies using this PH domain, high levels of Ins(1,4,5)P_3 would be expected to prevent enzyme attachment to the membrane surface (via competition with PtdIns(4,5)P_2) and therefore prevent this 'processive' form of PtdIns(4,5)P_2 hydrolysis, thereby reducing the catalytic efficiency of phospholipase C. This may represent a possible mechanism of product inhibition of the enzyme *in vivo*.

1.3 Inositol monophosphatase and Li^+

Li^+ ions, in the form of citrate and carbonate salts, have been used successfully for over 50 years in the treatment of manic depression. In order to determine the mechanism of action of Li^+, the phosphatidylinositol cell signalling pathway has attracted much interest. To achieve the desired therapeutic effect a concentration of 0.5 to 1.0mM Li^+ ions is required *in vivo*, but serious side effects occur at plasma concentrations exceeding 2mM (Nahorski *et al.*, 1991). Both inositol monophosphatase and inositol polyphosphate phosphatase (which hydrolyses Ins(1,4)P_2 and Ins(1,3,4)P_3) are inhibited by Li^+ ions in an uncompetitive manner (K_i = 0.8mM; Hallcher and Sherman, 1980; Gee *et al.*, 1988). This inhibition has been more closely investigated for inositol monophosphatase due to its central role in inositol recycling. Following the studies of Hallcher and Sherman, (1980); Berridge *et al.*, (1989) suggested that Li^+ inhibition of inositol monophosphatase could reduce the supply of inositol available for PtdIns synthesis. This reduction in the supply of PtdIns would lead to a reduction in the resynthesis of PtdIns(4,5)P_2 and subsequently second messenger (Ins(1,4,5)P_3 and DAG) production in stimulated cells. Furthermore, plasma inositol cannot easily cross the blood-brain barrier (Spector and Lorenzo, 1975), which means that inositol monophosphatase is the primary route of inositol synthesis in the brain. This would explain why the observed antimanic effects of Li^+ are CNS

related. One alternative route for inositol production, is the *de novo* synthesis of Ins(1)P from glucose in the brain catalysed by the enzyme inositol-1 phosphate synthase (Eisenberg, 1967). However, once again, ins(1)P can only be converted to inositol by the action of inositol monophosphatase.

Uncompetitive inhibition is very rare in metabolic pathways, and is defined as inhibition which results in parallel Lineweaver-Burk plots (Cornish-Bowden, 1986). In terms of mechanism, Li^+ ions inhibit by binding to the enzyme.substrate (E.S) or enzyme.intermediate (E.I) complexes. This implies that cells that are signalling very rapidly will have their signalling systems progressively inhibited by Li^+ ions with the degree of inhibition increasing as the stimulation increases. In contrast, cells that are signalling normally will be little affected by Li^+, as levels of inositol monophosphatase in the form of E.S or E.I complexes are low. Thus uncompetitive inhibition is particularly useful for inhibitory drugs.

1.4 The primary structure of inositol monophosphatase and homologous proteins

Inositol monophosphatase has been successfully isolated, purified and sequenced from a number of sources including bovine (Gee *et al.*, 1988; Diehl *et al.*, 1990), rat (Takimoto *et al.*, 1985) and human brain (McAllister *et al.*, 1992). The sequences of the enzyme from the three species were found to be 79% identical with the human enzyme and that from bovine brain being most similar (85% identical, Figure1.3). The bovine enzyme exists as a homodimer with a subunit molecular weight of 30kDa (Gee *et al.*, 1988) encoded by a 277 amino acid open reading frame. The predicted protein sequence revealed no unusual regions of hydrophobic character. In addition, no consensus sequences for calcium binding, ATP binding or phosphorylation were identified (Diehl *et al.*, 1990). Further studies showed that the brain derived enzyme is not post-translationally modified or myristylated and nor is it a substrate for protein kinase C or cAMP protein kinase.

Figure 1.3 The aligned amino acid sequences of human and bovine inositol monophosphatase (blue) showing motifs A, B and C (shown in red). Regions possessing homology to F1, 6-BP, IPP and the products of genes *qa*-x, *qut*G, *suh*B and HAL2 are also shown (adapted from Atack *et al.*, 1993).

1 M-A-D-P-W-Q-E-C-M-D-Y-A-V-T-L-A-R-Q-A-G-E-V-V-C-E-A- 26

M-A-D-P-W-Q-E-C-M-D-Y-A-V-T-L-A-G-Q-A-G-E-V-V-R-E-A- 26

27 I-K-N-E-M-N-V-M-L-K-S-S-P-V-D-L-V-T-A-T-D-Q-K-V-E-K-M- 53

36 IPP, *qa*-x, *qut*G, *suh*B, *cys*Q, HAL2

L-K-N-E-M-N-I-M-V-K-S-S-P-A-D-L-V-T-A-T-D-Q-K-V-E-K-M- 53

54 L-I-S-S-I-K-E-K-Y-P-S-H-S-F-I-G-E-E-S-V-A-A-G-E-K-S-I-L-T-D- N-84

63 69 — MOTIF C 72

L-I-T-S-I-K-E-K-Y-P-S-H-S-F-I-G-E-E-S-V-A-A-G-E-K-S-I-L-T-D-N-84

85 P-T-W-I-I-D-P-I-D-G-T-T-N-F-V-H-R-F-P-F-V-A-V-S-I-G-F-A-V 113

87 MOTIF A 100

P-T-W-I-I-D-P-I-D-G-T-T-N-F-V-H-G-F-P-F-V-A-V-S-I-G-F-V-V- 113

114 N-K-K-I-E-F-G-V-V-Y-S-C-V-E-G-K-M-Y-T-A-R-K-G-K-G-A-F-C- 141

N-K-K-M-E-F-G-I-V-Y-S-C-L-E-D-K-M-Y-T-G-R-K-G-K-G-A-F- C- 141

142 N-G-Q-K-L-Q-V-S-Q-Q-E-D-I-T-K-S-L-L-V-T-E-L-G-S-S-R-T-P-E-T-171

N-G-Q-K-L-Q-V-S-H-Q-E-D-I-T-K-S-L-L-V-T-E-L-G-S-S-R-T-P-E-T-171

172 V-R-M-V-L-S-N-M-E-K-L-F-C-I-P-V-H-G-I-R-S-V-G-T-A-A-V-N-M- 200

189 — F1,6-BP 194

V-R-I-I-L-S-N-I-E-R-L-L-C-L-P-I-H-G-I-R-G-V-G-T-A-A-L-N-M- 200

201 C-L-V-A-T-G-G-A-D-A-Y-Y-E-M-G-I-H-C-W-D-V-A-G-A-G-I-I-V-T- 229

qa-x, *gut*G, *suh*B 219 MOTIF B

C-L-V-A-A-G-A-A-D-A-Y-Y-E-M-G-I-H-C-W-D-V-A-G-A-G-I-I-V-T- 229

(E213)

230 E-A-G-G-V-L-M-D-V-T-G-G-P-F-D-L-M-S-R-R-V-I-A-A-N-N-R-I- 257

233

E-A-G-G-V-L-L-D-V-T-G-G-P-F-D-L-M-S-R-R-V-I-A-S-S-N-K-T- 257

258 L-A-E-R-I-A-K-E-I-Q-V-I-P-L-Q-R-D-D-E-D 277

L-A-E-R-I-A-K-E-I-Q-I-I-P-L-Q-R-D-D-E-D 277

Although inositol monophosphatases show little overall sequence identity with other proteins, three regions of local similarity have been identified (Figure 1.3). These being, motif A consisting of residues 87-100, motif B, (219-233) and motif C (69-72) (Atack *et al.*, 1995). These motifs contain most of the key residues involved in metal and substrate binding and also those involved in nucleophilic water activation. Sequence comparison data have also revealed that the corresponding regions also occur in two other phosphatases. Inositol polyphosphate 1-phosphatase (IPP), a monomeric enzyme of 400 amino acids that catalyses the hydrolysis of the 1-phosphate from Ins(1,3,4)P_3 and Ins(1,4)P_2 (Ke *et al.*, 1989) and fructose 1,6-bisphosphatase, a tetrameric enzyme in the gluconeogenesis pathway catalyses the hydrolysis of fructose-1,6-bisphosphate to fructose-6-phosphate (Zhang *et al.*, 1993(a) and 1993(b)). Both of these enzymes, like inositol monophosphatase, are uncompetitively inhibited by Li^+ ions and have a requirement for two Mg^{2+} ions for catalytic activity (Ke *et al.*,1989; Zhang *et al.*, 1993(a) and (b)). Diehl *et al.*, (1990) reported local sequence similarity (35-40%) between inositol monophosphatase and the *qa*-x gene product of *Neurospora crassa*, the *qut*G protein from *Aspergillus nidulans* and the *suh*B and *cys*Q proteins of *E. coli*. By aligning the sequences of these genes with the sequence of inositol monophosphatase, regions of hydrophobicity were seen to be conserved in the structural core of the enzyme (Figure 1.3). Furthermore the *qa*-x, *qut*G and *suh*B proteins have conserved metal-binding glutamate residues corresponding to E213 in inositol monophosphatase, a residue known to be involved in substrate binding (Bone *et al.*, 1992).

Chen and Roberts, (1998) have recently identified, cloned and purified the inositol monophosphatase (*MJ109*) gene from the hyperthermophilic organism *Methanococcus jannaschii*. The sequence homology between the *MJ109* gene product and human inositol monophosphatase prompted Chen and Roberts to express the protein in *E.coli*. The purified protein was found to be active and displayed kinetic characteristics such as Mg^{2+} requirement, Li^+ inhibition, substrate specificity, dimer formation and heat stability comparable to those determined for mammalian inositol monophosphatase. However, the inhibition at low Li^+ and high Mg^{2+} concentrations characteristic of IMPase is absent,

and the rates of hydrolysis with substrates glucose-1-phosphate and p-nitrophenyl phosphate are high. These differing aspects between the two sources could be attributed to sequence disparity observed in the active site regions of *Methanococcus jannaschii* and human inositol monophosphatase.

The Sop B protein recently discovered in the enteric bacteria, *Salmonella dublin*, perturbs the inositol phosphate signal transduction pathway as a route of mediating its virulence. This protein shows remarkable sequence homology to mammalian inositol polyphosphate 4-phosphatases and the recombinant form exhibits inositol monophosphatase activity in *in vitro* studies (Norris *et al.*, 1998).

Galactosemia is a disorder that results from a deficiency in the enzymes that convert galactose to glucose, and this gives rise to the accumulation of galactose-1-phosphate. It has recently been discovered that expression of human inositol monophosphatase in *Saccharomyces cerevisiae* (Bakers' yeast) defective in galactose-1-phosphate metabolism suppresses galactose toxicity in a Li^+ sensitive manner. It was proposed that the accumulated galactose-1-phosphate in this condition could act as a substrate for inositol monophosphatase and in doing so interfere with its normal functioning in the signal transduction pathway. In this way disruption in the signal transduction pathway (via IMPase) could result in a decrease in free inositol in galactosaemic patients and this could be a possible cause of neurological abnormalities such as mental retardation, which are symptomatic of this disorder Mehta *et al.*, (1999).

3'-Phosphoadenosine 5'-phosphate phosphatases (PAP) are enzymes present in bacteria, yeast, plant and animal cells which function by catalysing the hydrolysis of the 3'-phosphate from PAP to adenosine 5'-phosphate (AMP) and inorganic phosphate. PAPs are Mg^{2+}-dependent, Li^+-sensitive enzymes and belong to the same family as F1,6-BP, IPP and IMPase. It was thought that since the human enzyme is lithium sensitive, it could represent a potential target of lithium therapy and in doing so it may help explain some of the side effects of this therapy. Yenush *et al.*, (2000) have successfully characterised

the human enzyme which hydrolyses both PAP (<1μM) and inositol-1, 4-bisphosphate (K_m = 0.4μM) and found it to be extremely sensitive to therapeutic levels of Li^+ (IC_{50} = 0.3mM). Spiegelberg *et al.*, (1999) have shown that methionine supplementation to yeast cultures (*S. cerevisiase*) growing in the presence of Li^+ ions alleviates Li^+ toxicity. When similar studies were carried out using a human model no such reduction in Li^+ toxicity was observed. This observation was attributed to the differences in the metabolism of methionine between yeast and humans.

1.5 Substrate specificity

Inositol monophosphatases isolated from a number of sources demonstrate broad substrate specificities. Inositol monophosphatase can dephosphorylate all monophosphates with the exception of Ins(2)P (Gee *et al.*, 1988; Ragan, 1990; Nahorski *et al.*, 1991). This is as a result of the ester linkage being in the axial position relative to the ring (Figure 1.4(b)). *In vivo* the two main substrates for the enzyme are Ins(1)P and Ins(4)P and Gee *et al.*, (1988) have shown that bovine inositol monophosphatase hydrolyses both enantiomers of Ins(1)P and Ins(4)P. Although the D and L enantiomers of Ins(4)P were found to be much better substrates for the enzyme, giving rise to V_{max} values of 39.8μmol/min/mg and 51.0μmol/min/mg of protein compared to 13.3μmol/ min/mg and 15.6 μmol/min/mg protein for (D/L)-Ins(1) P (Gee *et al.*, 1988). The K_m for Ins(1)P and Ins(4)P have values of 0.16mM and 0.23mM respectively. None of the inositol polyphosphates in the phosphatidylinositol cell signalling pathway act as substrates for the bovine enzyme, however, the enzyme is able to hydrolyse several structurally diverse phosphates. In particular 2'-AMP, 2'-GMP, β-glycerophosphate and α-glycerophosphate show 50, 44, 33 and 13% of the specific activity seen with Ins(1)P (Attwood *et al.*, 1988). This notable lack of substrate specificity has initiated numerous studies in this field in order to determine the groups necessary for substrate binding. The requirement for at least one hydroxyl group α to the phosphate group was highlighted by Attwood *et al.*, (1988). Further studies by Baker *et*

Figure 1.4 (a)The structure of phosphatidylinositol.
(b) The structure of myo-inositol showing the OH at the 2-carbon atom in the axial position (Parthasarathy and Eisenberg., 1986).
(c) The structure of the L-690,330 bisphosphonate inhibitor (Atack *et al.*, 1993).

(a)

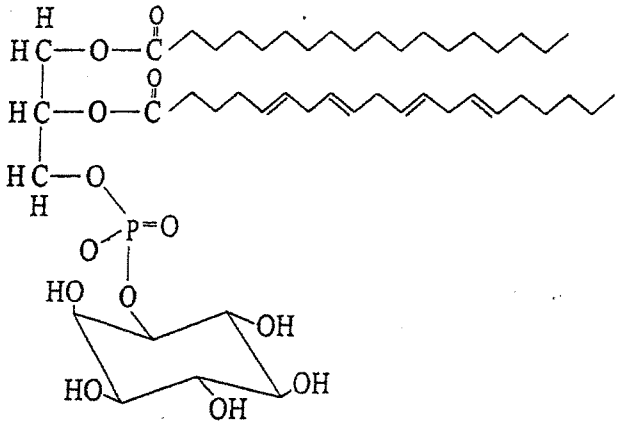

(b)

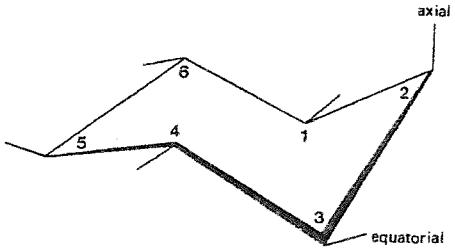

(c)

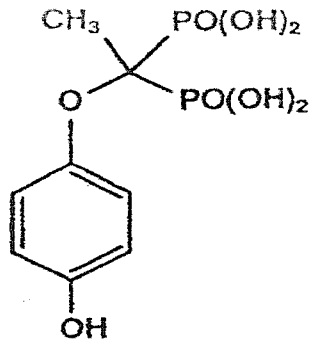

al., (1989) involved the synthesis of 2-dehydroxylated and 6-dehydroxylated forms of Ins(1)P and these have demonstrated that both of these groups have important roles in binding to the enzyme and the mechanism of hydrolysis. This observation has been further supported by the X-ray crystallographic studies of Bone *et al.*, (1990). 4-nitrophenyl phosphate (Attwood *et al.*, 1988) and 4-methylumbelliferyl phosphate (Gore *et al.*, 1992) act as alternative substrates, and it is thought that the role of the 6-hydroxyl group in hydrolysis is achieved by the nitrophenyl ring in the case of 4-nitrophenyl phosphate and possibly by the aromatic nature of the 4-methylumbelliferyl phosphate, since these compounds only contain the phosphate group. The effect of substituting the 6-OH group at the α-position gave rise to the production of powerful substrate-based inhibitors of inositol monophosphatase (Baker *et al.*, 1991). Phosphate (P_i), but not inositol, was shown to be a competitive inhibitor with respect to substrate, Ins(1)P, with a K_i value of 0.52mM (Gee *et al.*, 1988).

Atack *et al.*, (1993) synthesised and investigated the *in vivo* and *in vitro* properties of a bisphosphonate-containing inhibitor (L-690,330) of inositol monophosphatase (Figure 1.4(c)). Studies have shown that this competitive inhibitor inhibits IMPase more potently *in vitro* (~1000-fold) than Li^+. However, *in vivo* testing of L-690,330 resulted in the accumulation of inositol monophosphates at only 40% of the level observed for Li^+, which could be explained by the polar nature of this inhibitor which restricts its access into the CNS. In addition, the competitive mode of inhibition of L-690,330 (c.f. uncompetitive inhibition using Li^+) which can be overcome with increases in substrate concentration (as would be seen *in vivo* for overactive neurones), suggests that this inhibitor would become less effective at increasing substrate concentrations. Consequently the ability of L-690,330 to exert the same *in vivo* effects as Li^+ is as yet undemonstrated and presently limits its use therapeutically.

1.6 Chemical modification

Chemical modification studies (Greasley *et al.*, 1993) have shown that inositol monophosphatase can be modified at two sites by pyrene maleimide (Cys141 and Cys218). Stoichiometric addition of pyrene maleimide allowed the predominant modification of residue 218 and the fluorescent properties of this thiol specific reagent has allowed metal ligand interactions with the enzyme to be monitored (Greasley *et al.*, 1994). It was found that modification by this reagent leads to no concomitant loss in enzyme activity. Interestingly it was found that modification of C218 by IAA reagent leads to a 20% increase in enzyme activity (Knowles *et al.*, 1992). This is in contrast to the inhibition noted when the enzyme reacts at the same site with N-ethylmaleimide (McAllister *et al.*, 1992). These studies further support the existence of two Mg^{2+} binding sites. Site 1 of high affinity has been elucidated by Mg^{2+} binding to pyrene labelled enzyme, (K_d was 300μM) and the presence of a lower affinity site 2 has been demonstrated by kinetic studies (K_m = 3mM).

It has been suggested that an arginine residue located at the active site (Gee *et al.*, 1990) plays a role in the functioning of inositol monophosphatase (Jackson *et al.*, 1990). Modification of the enzyme by the arginine-specific reagent phenylglyoxal resulted in total loss of enzyme activity. The presence of substrate protected the enzyme from phenylglyoxal inactivation. The inclusion of Li^+ ions in addition to the substrate potentiated the protective effect. Phosphate also protected against inactivation while inositol failed to show any form of protection. It was therefore concluded that one or more arginine residues are located within the active site of the enzyme and may be involved in ionic bond formation with an oxygen atom of the phosphate moiety. The modified arginine residue has never been identified, but one possible candidate is R191 from the neighbouring subunit. However, further studies carried out by Rees-Milton, (1994) showed that this arginine residue was not susceptible to modification by the bulkier reagents 1-pyreneglyoxal and dansyl camphor-10-sulphonic, contradicting the findings of Jackson *et al.*, (1990). Detailed X-ray crystallographic analysis of the enzyme (Bone *et al.*, 1994(a)

and (b)) has shown that the reaction mechanism does not involve an arginine side chain, but most probably involves two Mg^{2+} ions and acidic residues (E70, D90, D93 and D220) in the enzyme.

1.7 Proteolysis of inositol monophosphatase

Studies by Greasley *et al.*, (1993) demonstrated that trypsin cleaves the peptide bond between K36 and S37 which are situated on a loop close to the amino terminus which is highly susceptible to proteolysis. Further ligand protection studies demonstrated that the cleavage could be prevented by the inclusion of Ins(1)P (0.6mM) and LiCl (10mM), suggesting that a movement of this N terminal α-helical region takes place upon Mg^{2+} and substrate binding (preceding catalysis), thereby making residues Lys36-Ser37 inaccessible to the protease. An analogous site has been found in F1,6-BP (T66-G67; Marcus *et al.*, 1987), and this enzyme has been shown to undergo a conformational change upon binding of its substrate (2'-AMP) and Mg^{2+} ions during catalysis (Ke *et al.*, 1990).

1.8 The role of metal ions

Inositol monophosphatase has an absolute requirement for Mg^{2+} ions for catalytic activity (Hallcher and Sherman, 1980), however, high concentrations of this ion (>5mM) result in uncompetitive inhibition (with respect to substrate) of the enzyme. The amount of inhibition by Mg^{2+} varies appreciably with substrate structure and pH. Ganzhorn *et al.*, (1990) showed that using Ins(1)P as the substrate, the K_i for Mg^{2+} at pH 8.0 and 37°C is 4mM, whereas when 4-methylumbelliferyl phosphate is the substrate, concentrations as high as 100mM fail to inhibit the enzyme (Gore *et al.*, 1992). Studies by Gee *et al.*, (1988), further confirmed the Mg^{2+} ion dependence of the bovine enzyme (K_m = 2-3mM). Other divalent cations such as $Ca^{2+}$and Mn^{2+} ions were shown to be powerful competitive inhibitors of the enzyme with respect to the

cofactor Mg^{2+}, with characteristic K_i values of 18μM and 2μM respectively (Hallcher and Sherman, 1980). Monovalent ions such as K^+ and Na^+ have been shown to have no effect on enzyme activity.

The uncompetitive nature of inhibition (with respect to Ins(1)P) by Li^+ has been extensively studied. At higher concentrations Li^+ has been seen to show non-competitive inhibition with respect to Mg^{2+} ions (Ganzhorn *et al.*, 1990). It has been proposed that the uncompetitive inhibition of inositol monophosphatase (with respect to substrate) mediated by Mg^{2+} at high concentrations and that due to Li^+ arises at the same site and not at two different sites (Pollack *et al.*, 1994).

1.9 Structure of inositol monophosphatase

The X-ray crystallographic structure of human inositol monophosphatase has been determined to 2.1Å in the presence of gadolinium ions (Bone *et al.*, 1992). Crystals of the human enzyme were prepared in the presence of the heavy metal gadolinium (Gd^{3+}), and sulphate (which corresponds to phosphate binding) and high Li^+ ion concentrations (Bone *et al.*, 1992). The structure identified only one metal (Gd^{3+}) binding site per monomer of inositol monophosphatase (Figure 1.5). However, there is a complication in that Li^+ is virtually invisible in an X-ray crystallographic image at this relatively low resolution since it has only two electrons. This together with the uncompetitive nature of inhibition denies the possibility of characterising an E-Li^+ intermediate.

Figure 1.5 shows the X-ray crystallographic structure of a dimer of inositol monophosphatase. Each subunit of the enzyme is composed of a five-layered sandwich of alternating α-helices and antiparallel β-sheets. This αβαβα structure has also been reported for the homotetramer F1,6-BP (Zhang *et al.*, 1993(a) and 1993(b)) and a similar αβαβ structure is present in the IPP monomer. Figure 1.6 (a), (b) and (c) shows the homologous regions of

Figure 1.5 The structure of a dimer of human inositol monophosphatase depicting the single Gd^{3+} site (shown in dark blue) per monomer (Bone *et al.*, 1992).

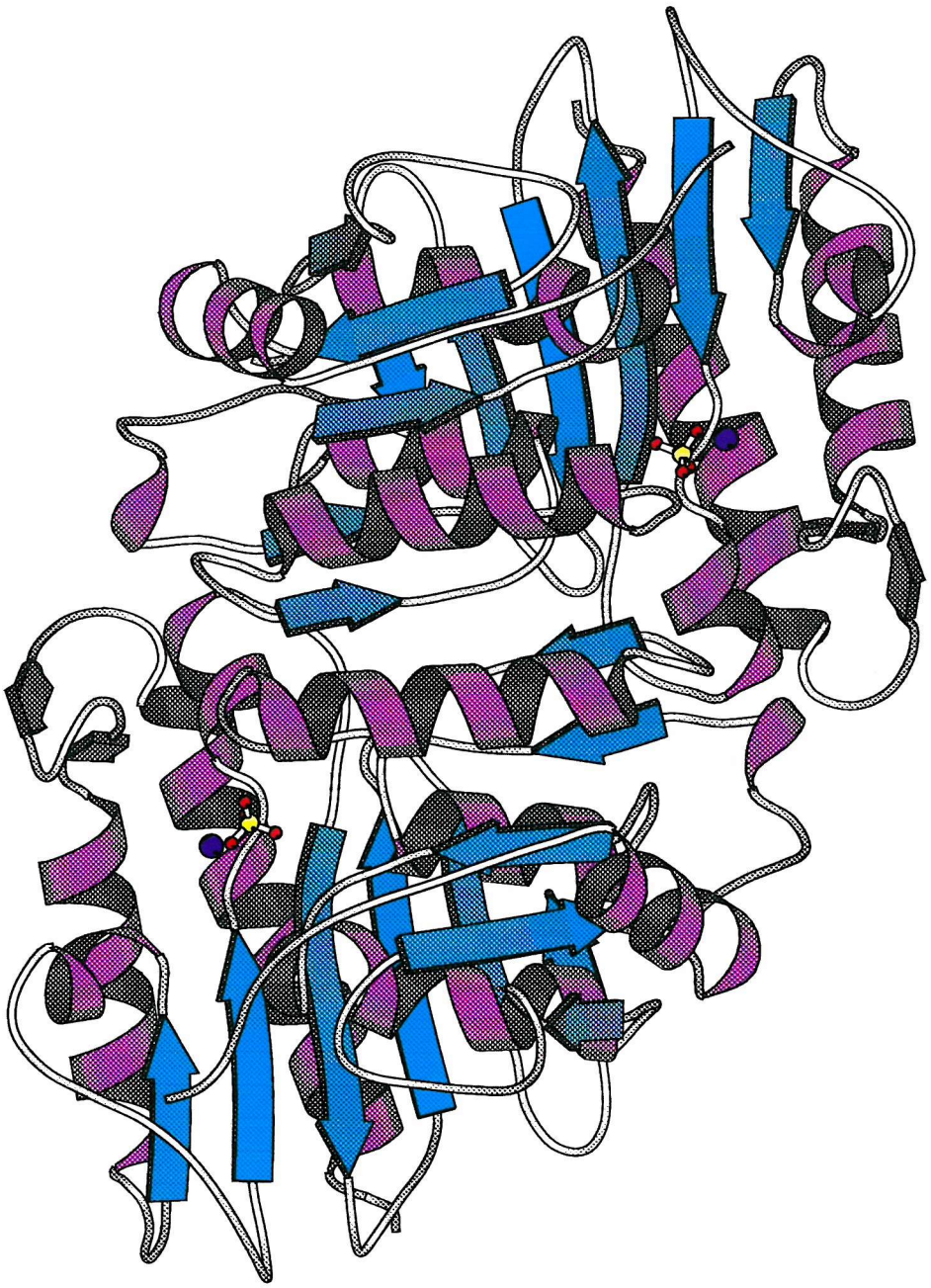

Figure 1.6 The structures of (a) IMPase, (b) F1,6-BP and (c) IPP depicting the shared regions of secondary structure (shown in blue).


(a)

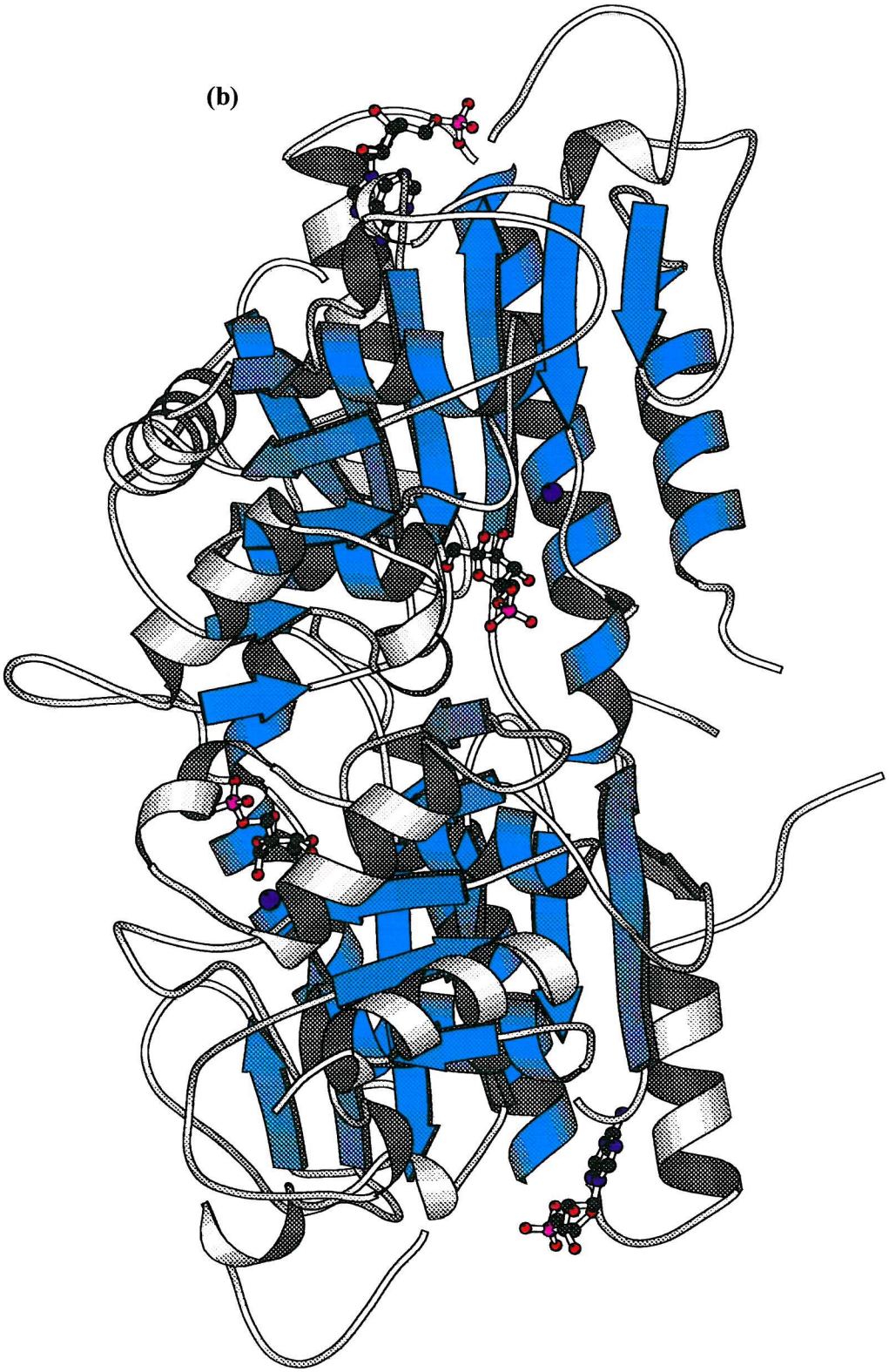
(b)

(c)

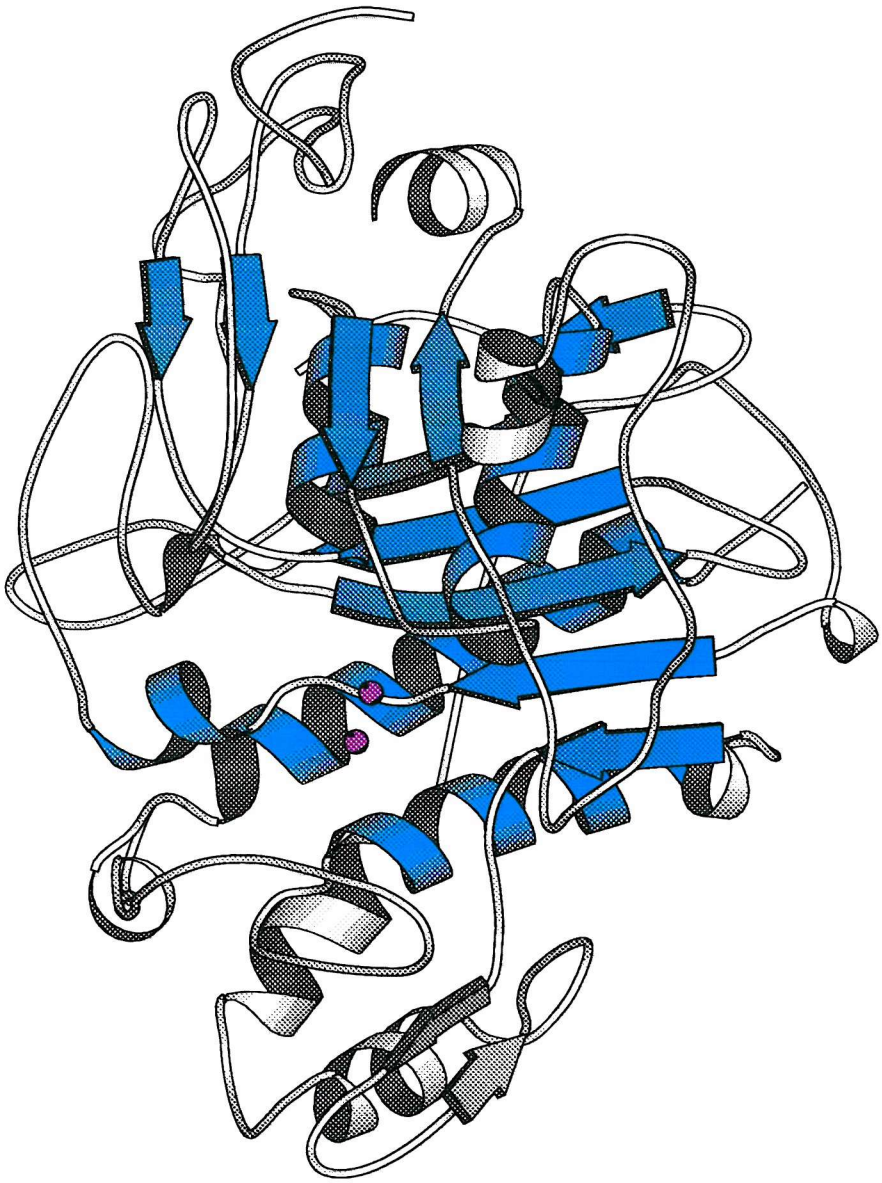

secondary structure observed for the three enzymes. Consequently the tertiary ($\alpha\beta\alpha\beta\alpha$) structure is a characteristic signature of the phosphatase activity of these proteins, more so indeed than the sequence homology.

The active site centre of each monomer forms a large hydrophilic cavern capable of accomodating the Ins(1)P substrate and an additional 30 solvent molecules as depicted in Figure1.7. The active site does not appear to be shared between the subunits although protrusion of residues from one subunit into the active site of the other is observed (Bone *et al.*, 1992). For instance the side chain of Arg-191 protrudes into the adjacent active site where it interacts with solvent molecules at a distance of 11Å from the metal binding site (Figure 1.8). This residue corresponds to R243 in F1,6-BP and is found to be conserved (Zhang *et al.*, 1993(a) and 1993 (b)).

The subunit interface is extensive and involves a number of interactions throughout the chain length. In particular, 10% of the surface area on each subunit is concealed upon dimer formation (Bone *et al.*, 1992) and 17% of the residues on each subunit are close enough to partake in the exclusion of solvent from the interface (Connolly, 1983). The dimer structure is stabilised by the formation of 18 hydrogen bonds between the subunits (Bone *et al.*, 1992).

Although Gd^{3+}-containing structures are misleading from the point of view of metal binding, they are useful with regards to providing information about substrate binding. The total inhibition of the enzyme by Gd^{3+} meant that it was possible to grow crystals of human inositol monophosphatase in the presence of substrates Ins(1)P, Ins(3) or the substrate-based phosphate-containing inhibitor (2,4-dihydroxy inositol-1-phosphate) in order to identify residues in the active site involved in substrate binding. The structures of complexes of human inositol monophosphatase with these substrates and inhibitory Gd^{3+} ions have been determined to 2.2-2.3Å resolution by Bone *et al.*, (1994(a)). Figure1.9 depicts the inositol monophosphatase structure in the presence of $Gd^{3+}$and L-Ins(1)P and Figure 1.10 depicts the structure of HIMP

Figure 1.7 The structure of a monomer of inositol monophosphatase depicting the active site showing the two Mn^{2+} binding sites (dark blue) and P_i.

Figure 1.8 The structure of a monomer of inositol monophosphatase, highlighting the protrusion of R191 from one subunit into the active site of the adjoining subunit.

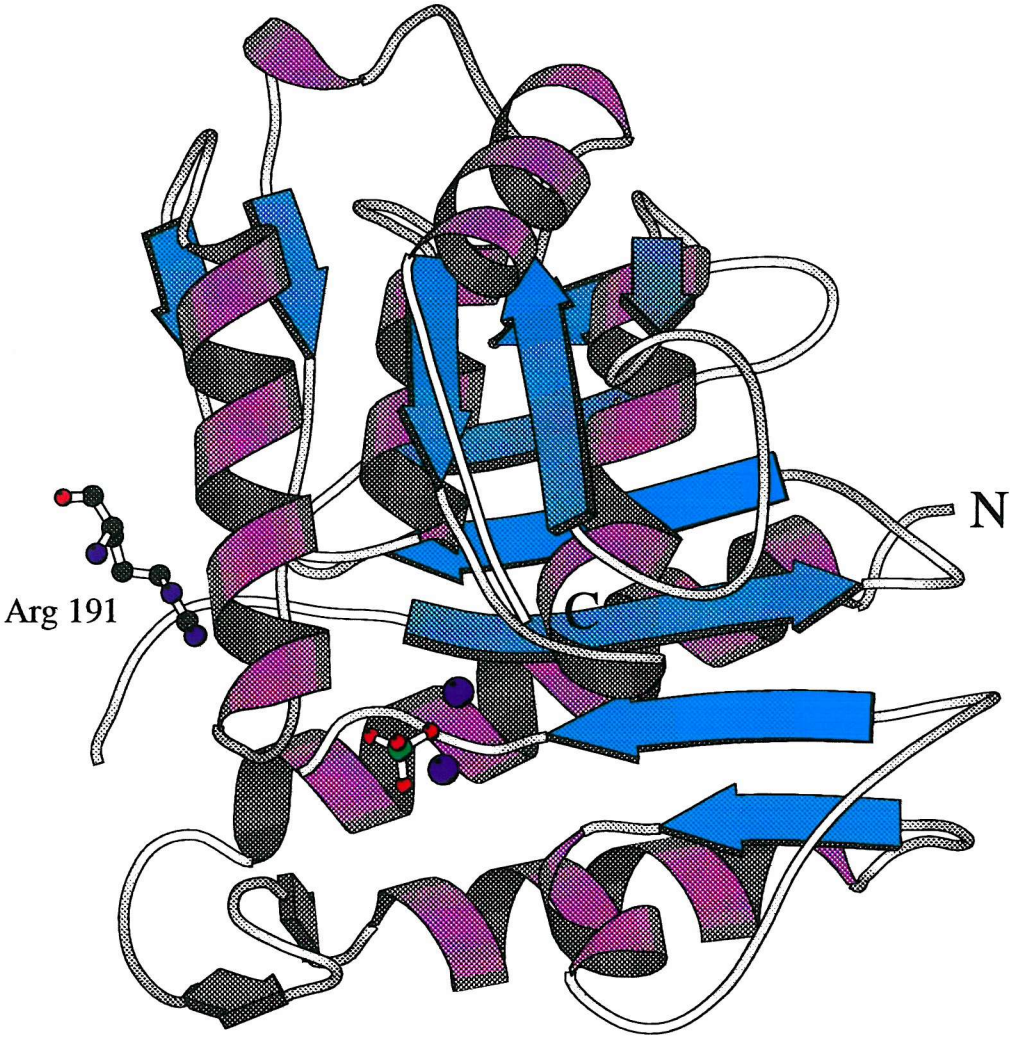
Arg 191
N
C

Figure 1.9 The structure of the active site of inositol monophosphatase, containing L-Ins(1)P and Gd^{3+} ion (shown in purple).

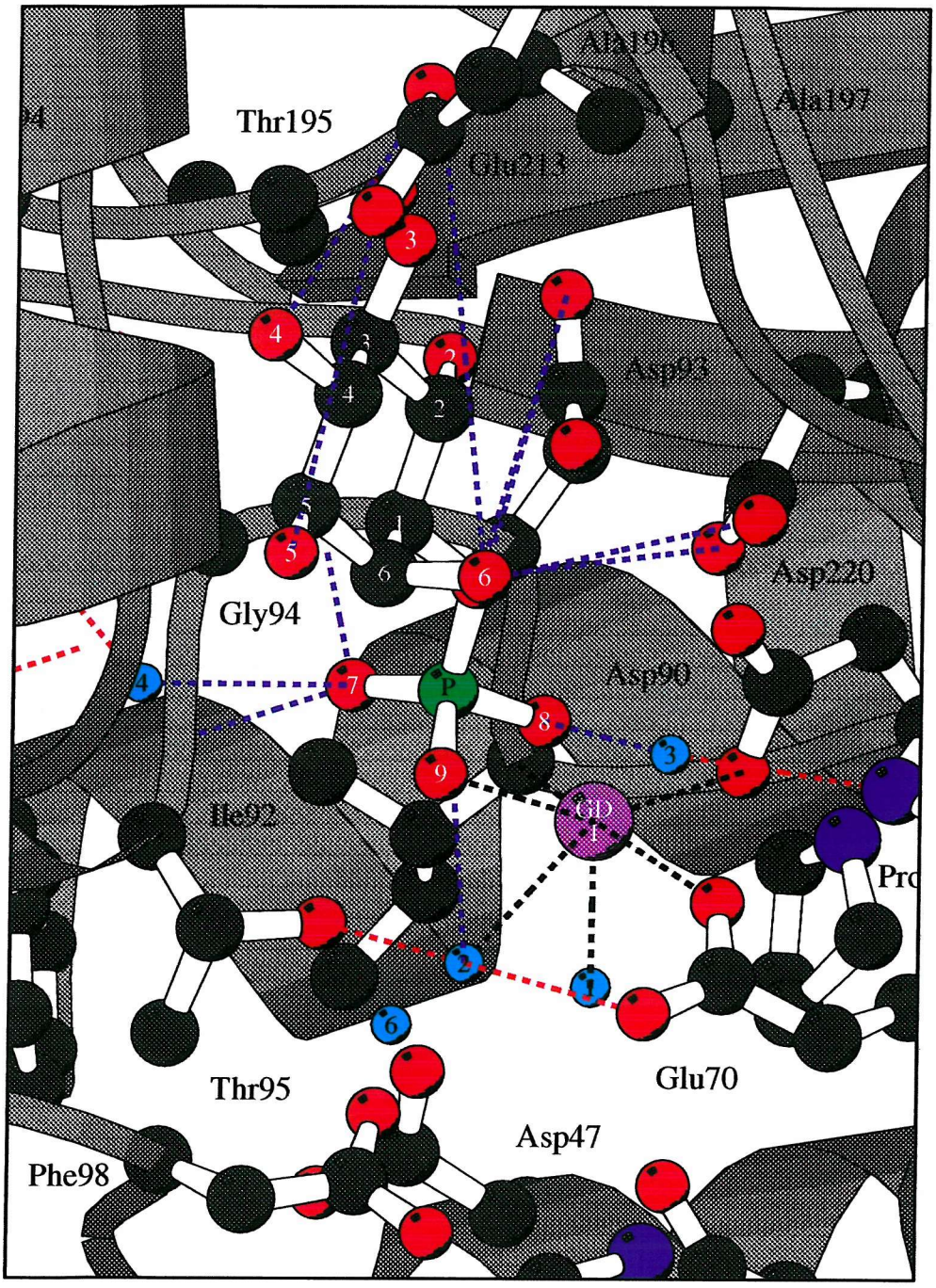
Ala196
Ala197
Thr195
Glu213
Asp93
Asp220
Gly94
Asp90
He92
Thr95
Glu70
Asp47
Phe98

Figure 1.10 The structure of the active site of inositol monophosphatase containing D-Ins(1)P and Gd^{3+} ion (shown in purple).

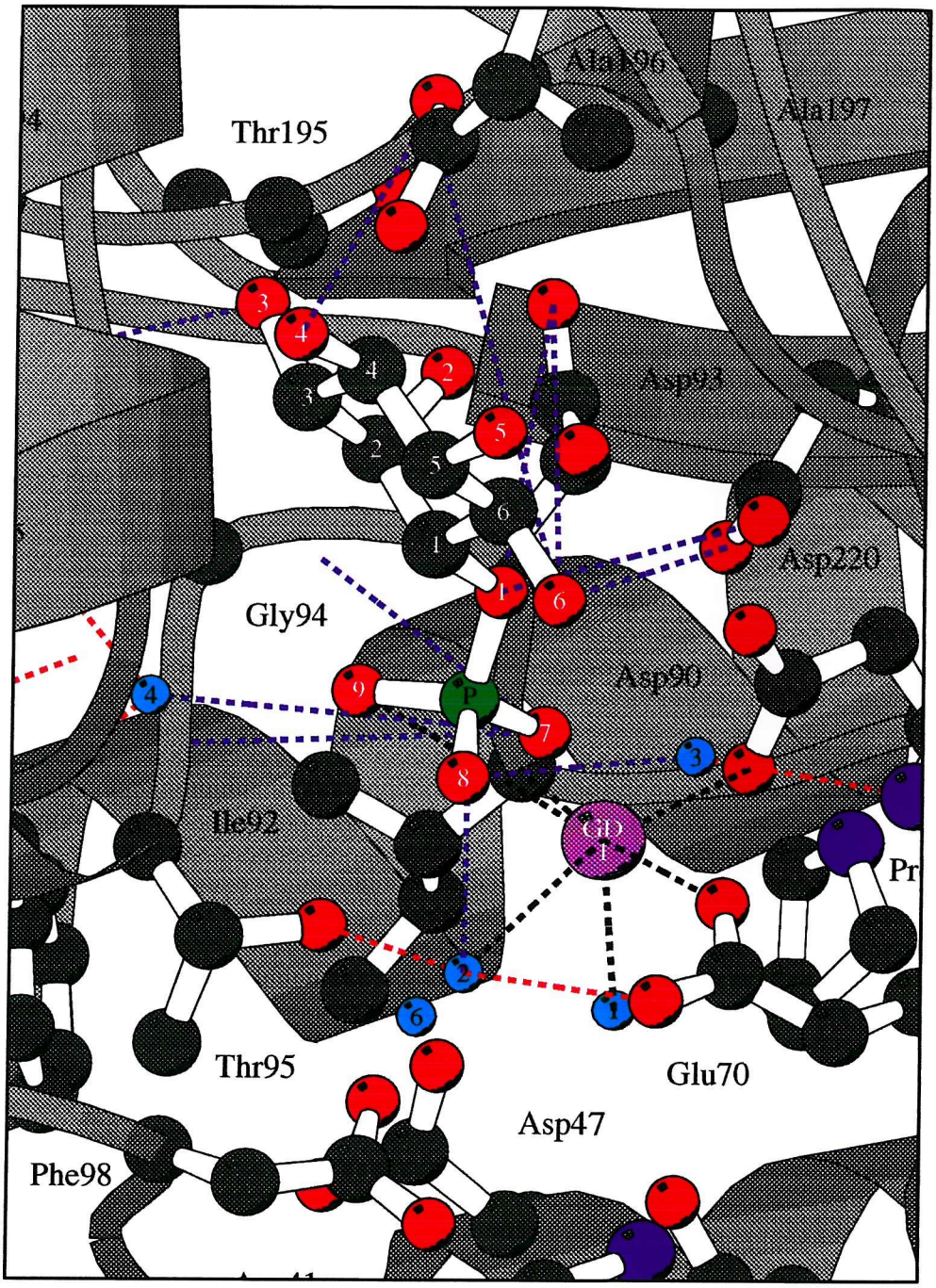
Ala196
Ala197
Thr195
Asp94
Asp220
Gly94
Asp90
Ile92
Thr95
Glu70
Asp47
Phe98

in the presence of Gd^{3+} and D-Ins(1)P). Essentially each substrate utilises the same residues to form the same number of hydrogen bonds with inositol monophosphatase. Only three out of the five hydroxyl groups on the substrate make hydrogen bonds, these being the 2-hydroxyl, which forms 2 hydrogen bonds with D93 and A196, the 4-hydroxyl which forms a bond with the side chain of E213 and the 6-hydroxyl group which forms a minor interaction with D220. Like inositol, the phosphate moiety of the substrate makes very weak interactions with the enzyme. The phosphate group forms hydrogen bonds with the main chain amide groups of residues G94 and T95. The higher valency of Gd^{3+}, which manifests in it possessing an additional 2-3 metal binding ligands relative to $Mn^{2+}$and Mg^{2+} and the presence of Li^{+} ions failed to provide any useful information regarding metal-binding to the enzyme.

Consequently, the structure of the enzyme was subsequently resolved to 2.6Å in the presence of Mn^{2+} (Figure1.11) and Mn^{2+} and phosphate (Figure1.12). In the Mn^{2+} only complex, three Mn^{2+}-binding sites were identified, one of which (ligated by E70) was expelled from the active site of each subunit in the presence of phosphate and was therefore considered not to be involved in the enzyme mechanism. The results of these studies suggest that the enzyme accomplishes phosphate ester hydrolysis using two metal ions (Bone *et al.*, 1994b). Metal binding site 1 has octahedral coordination geometry, the metal ion being ligated via the carboxylate oxygens of residues D90 and E70 and the backbone carbonyl group of I92 (Figure 1.13). Metal binding site 2, which has tetrahedral geometry, is formed by interactions with the carboxylate oxygens of residues residues D90, D93 and D220. The phosphate group of the substrate also appears to form hydrogen bond interactions with the two metal ions. Bone *et al.*, (1994b) have also determined the structure of apo-inositol monophosphatase at 2.5Å resolution. Residues 70-75, a two-turn α helix that is involved in metal coordination, moves away from the metal binding site by 2-3Å when metal ions are absent. Furthermore, residues 30-40, which interact with the protein and solvent molecules of the metal binding site, become highly disordered in the absence of cations (Figure 1.14). Ganzhorn *et al.*, (1997) have recently solved the structure of human inositol monophosphatase

Figure 1.11 The structure of the active site of inositol monophosphatase containing 3 Mn^{2+}ions (shown in light blue).

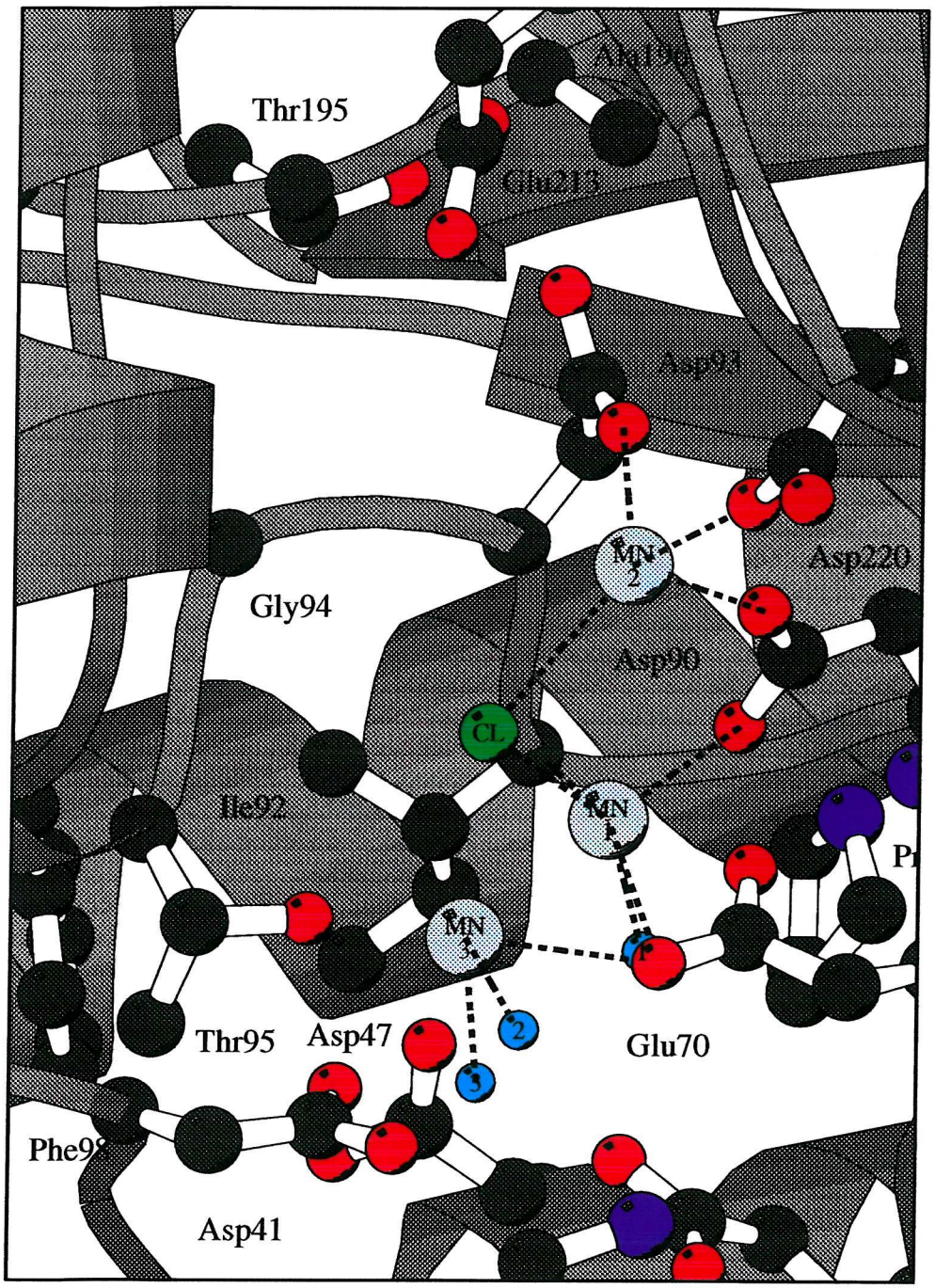
Thr195
Glu213
Asp91
Asp220
MN 2
Gly94
Asp90
CL
Ile92
MN 1
MN 3
Thr95
Asp47
Glu70
Asp41

Figure 1.12 The structure of the active site of inositol monophosphatase containing 2 Mn^{2+} ions (purple) and P_i.

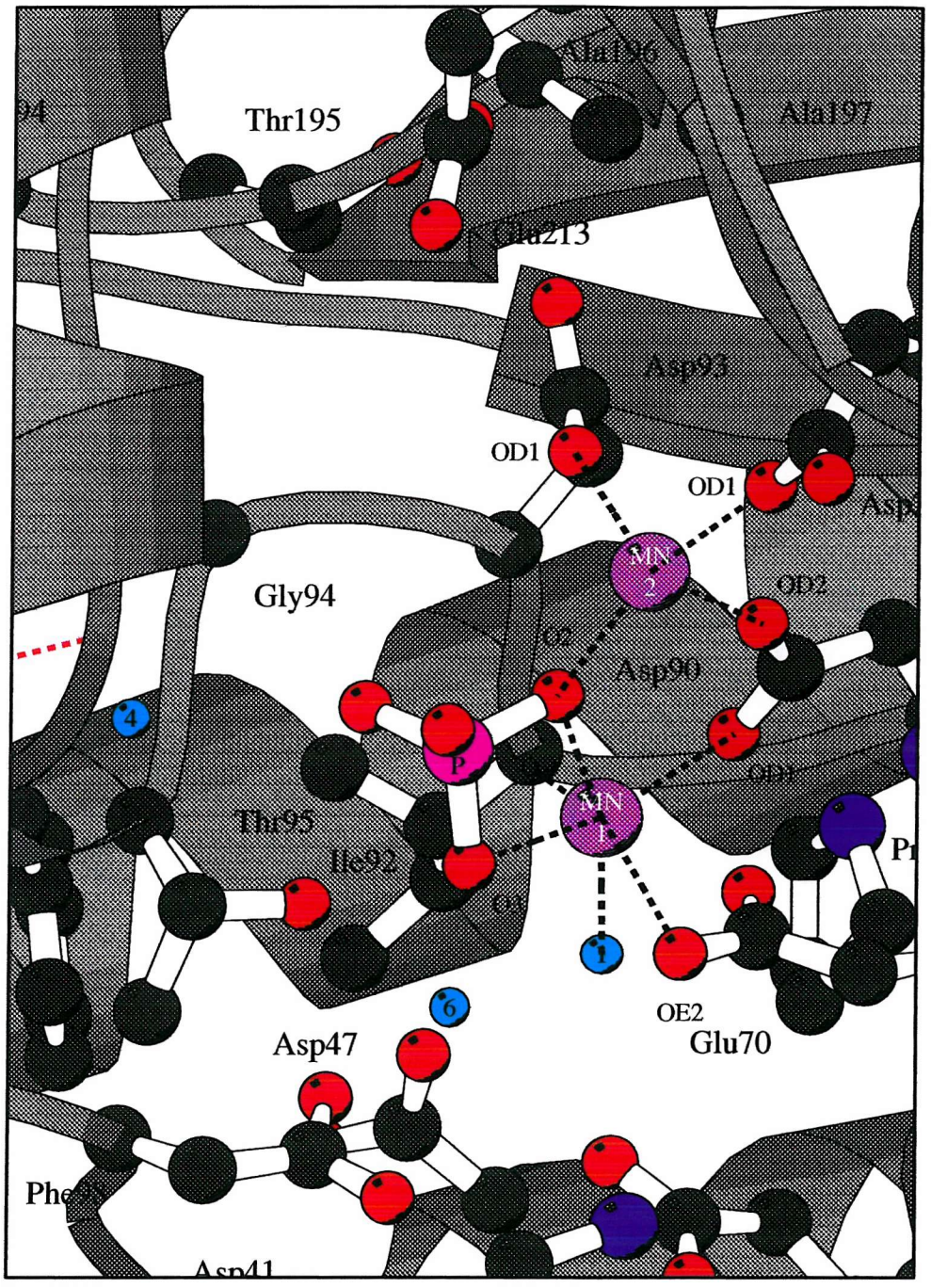
Thr195
Ala196
Ala197
Asp93
OD1
OD1
MN
2
OD2
Gly94
Asp90
P
MN
1
Thr95
Ile92
OE2
Glu70
Asp47
Asp41

Figure 1.13 The active site of inositol monophosphatase. The key interactions formed by the side chains of E70, D90, D93 and D220 with the Mn^{2+} ions (purple) are shown together with the interactions between the phosphate oxygen and the Mn^{2+} ions. The putative water nucleophile is shown in cyan (adapted from Pollack *et al.*, 1994).

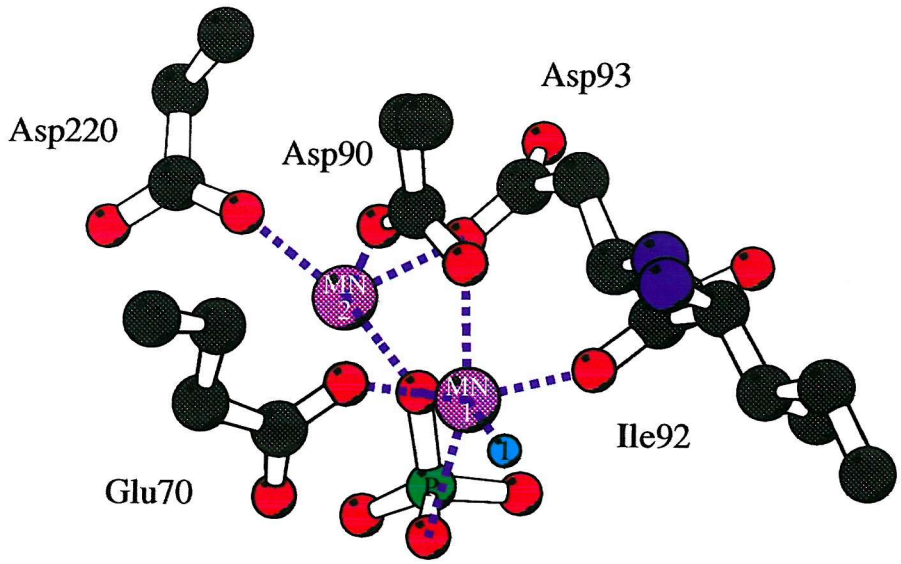
Asp220
Asp90
Asp93
MN
2
MN
1
Ile92
Glu70

Figure 1.14 The active site structure of apoinositol monophosphatase.

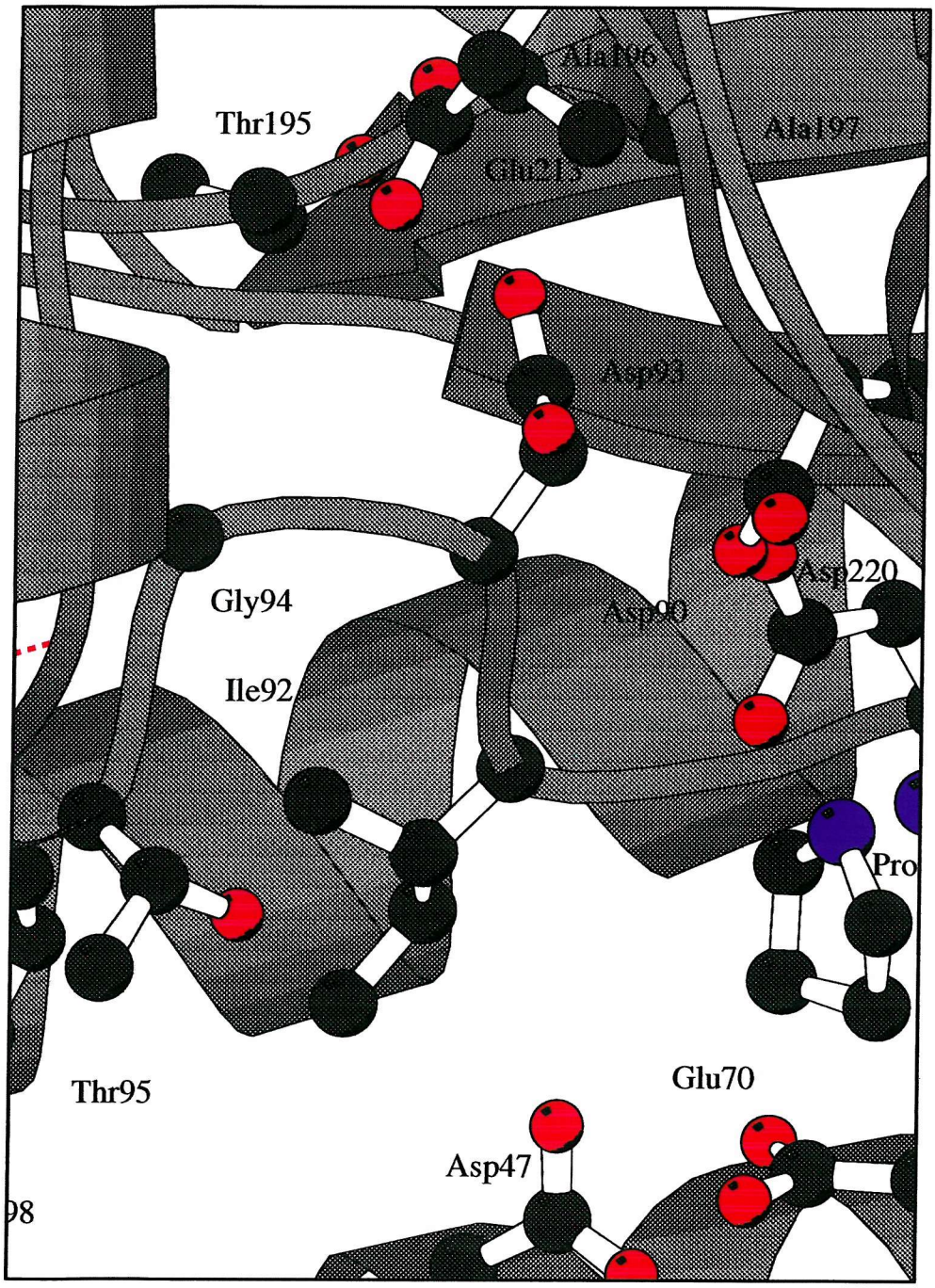
Ala196
Thr195
Ala197
Glu213
Asp93
Gly94
Asp90
Asp220
Ile92
Pro
Thr95
Glu70
Asp47
98

complexed with Ca^{2+} and D-Ins(1)P. This structure shows that the metal ions essentially interact with the same residues at sites 1 and 2, however, in addition, a third site was identified with a unique protein ligand (E70). Additionally, the phosphate moiety of the substrate molecule interacts with each of the three Ca^{2+} binding sites. The existence of the third site has been corroborated by kinetic data also presented in this study.

1.10 Mechanism of inositol monophosphatase

Shute *et al.*, (1988) initially proposed a ping-pong mechanism from the burst phase release of [^{14}C]Inositol from [^{14}C]Ins(1)P in the presence of high concentrations of Li^{+}. Such a mechanism was based on similar findings for alkaline phosphatase where the substrate phosphate is transferred to the enzyme via nucleophilic attack by an enzyme serine residue. The resultant phosphoenzyme is then hydrolysed by an extrinsic nucleophile such as water releasing the phosphate and enzyme for the next catalytic cycle. However, all attempts to trap an E-P_i complex of inositol monophosphatase failed and it was concluded that a ping-pong mechanism was unlikely. Rapid equilibrium dialysis experiments performed by Greasley and Gore, (1993), disproved the mechanism proposed by Leech *et al.*, (1993) and revealed that P_i binding can only take place in the presence of Mg^{2+}. Therefore the mechanism proposed by Leech *et al.*, (1993) was amended to include a second Mg^{2+} ion. Studies by Greasley *et al.*, (1994) using pyrene fluorescence to monitor Mg^{2+} binding to pyrene labelled enzyme provided a K_d value of 300μM, a value 10-fold lower than the K_m reported by Gee *et al.*, (1988). X-ray crystallographic work (Bone *et al.*, (1994(b)) and metal titration curves (Greasley *et al.*, (1994)) and molecular modelling data (Pollack *et* al., 1994) have further confirmed the existence of two metal ions in the catalytic mechanism. In addition, indirect evidence for a 2-metal mechanism of inositol monophosphatase comes from the observation that F1,6-BP and IPP also hydrolyse phosphate groups via a 2-metal mechanism through nucleophilic attack by water. Figure 1.15 shows a schematic representation of the current accepted two metal ion mechanism

Figure 1.15 The mechanism of inositol monophosphatase based on two metal ions (Thorne *et al.*, 1996).

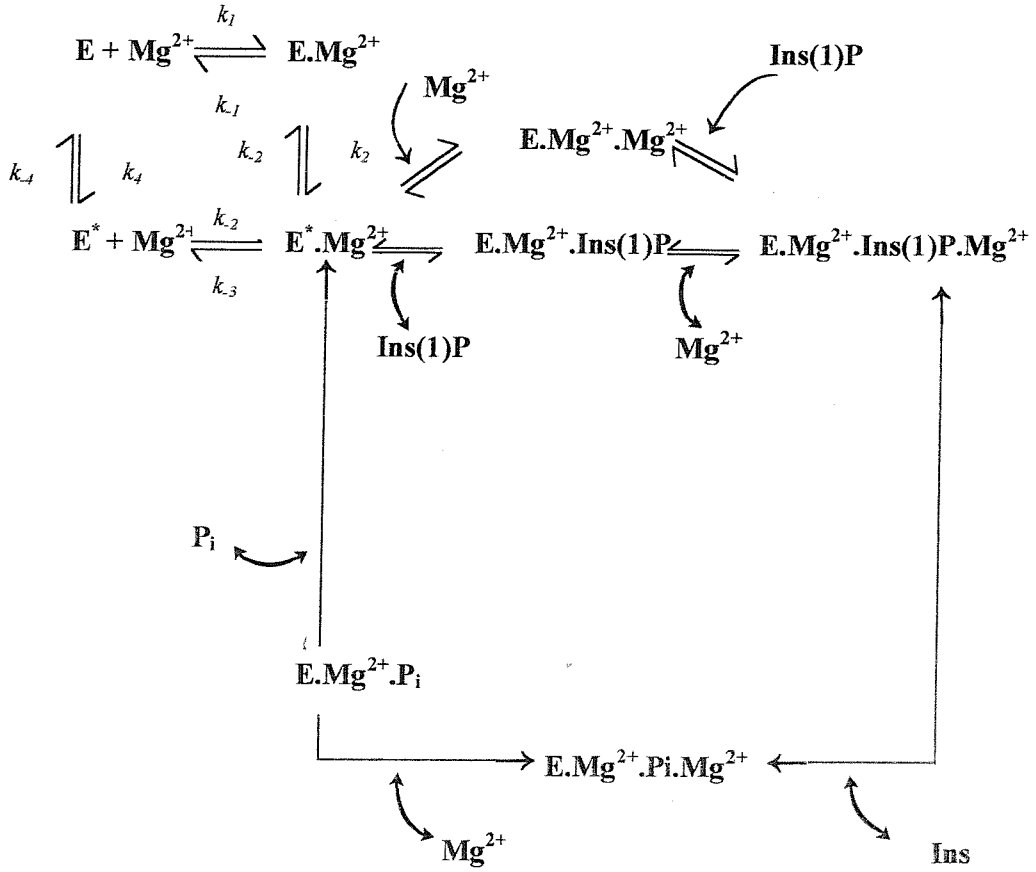
k1
E + Mg2+
E.Mg2+
k-1
Mg2+
Ins(1)P
k-4
k4
k-2
k2
E.Mg2+.Mg2+
k-2
E* + Mg2+
E*.Mg2+
E.Mg2+.Ins(1)P
E.Mg2+.Ins(1)P.Mg2+
k-3
Ins(1)P
Mg2+
Pi
E.Mg2+.Pi
E.Mg2+.Pi.Mg2+
Mg2+
Ins

(adapted from Thorne *et al.*, 1996) while Figure 1.16 depicts the same schematic mechanism proposed by Pollack *et al.*, 1994 (adapted from Atack *et al.*, 1995). When a Mg^{2+} ion is present at site 1, substrate binds with the stabilisation energy being contributed by the interaction between the phosphate and this $Mg^{2+}1$. The binding of a second Mg^{2+} ion then activates a water molecule ligated to residues E70 and T95, and this nucleophilic water molecule attacks the phosphate phosphorus and cleaves the phosphate bond. This is followed by debinding of the inositol moiety leaving the phosphate bound at both metal binding sites in a Michaelis complex rather than a phosphoenzyme intermediate. The site 2 metal then debinds leaving the P_i in a $E.Mg^{2+}.P_i$ complex. At this stage rapid dissociation of the P_i results in the regeneration of inositol monophosphatase with the site 1 Mg^{2+} ready for the subsequent catalytic cycle. However, in the presence of Li^+ions, site 2 becomes occupied by Li^+ thus preventing the P_i group leaving and resulting in a highly stable quaternary complex ($E.Mg^{2+}.P_i.Li^+$) which effectively inhibits the enzyme. Ganzhorn *et al.*, (1996) have recently proposed a role for a third metal ion in the catalytic mechanism (Figure 1.17). The existence of up to three Mn^{2+} ion binding sites was originally identified by work carried out by Bone *et al.*, (1994(b)). Initial velocity data of the K36Q mutant were best described by a rapid equilibrium ordered mechanism, with two Mg^{2+}ions binding before and the third binding after the substrate (Ganzhorn *et al.*, 1996). This third metal ion (ligated to E70) has been suggested to aid Mg^{2+} at site 1 in the activation of a water molecule. However, at present its role remains unclear.

Recent NMR experiments using [^{16}O, ^{17}O, ^{18}O]-thio phosphate labelled inositol have demonstrated that hydrolysis of Ins(1)P is accompanied by the inversion of configuration of the P_i group (Fauroux *et al.*, 1999) in support of the model for hydrolysis proposed by Bone *et al.*, (1992). This observation is also consistent with the proposed mechanism for F1, 6-BPase, (Zhang *et al.*, 1993(a) and (b)).

Figure 1.16 A schematic representation of the mechanism of inositol monophosphatase based on two metal ions proposed by Pollack *et al.*, 1994 (adapted from Atack *et al.*, 1995).

(A) In the absence of substrate, a Mg^{2+} ion is present at site1.

(B) Ins(1)P binds with most of the energy of binding being contributed by the interaction between the phosphate and site 1 Mg^{2+}.

(C) The second Mg^{2+} ion binds at site 2, activates the water molecule hydrogen-bonded to residues E70 and T95, which results in nucleophilic attack on the phosphate group.

(D) After cleavage of the phosphate bond, the inositol departs leaving the Pi ligated by both Mg^{2+} ions.

(E) The Mg^{2+} at site 2 rapidly debinds and a ternary $E.Mg^{2+}.Pi$ complex is resultant in which the phosphate is ligated primarily by the site 1 Mg^{2+}.

(F) Rapid debinding of Pi results in regeneration of IMPase with Mg^{2+} at site 1, for the subsequent catalytic cycle. However, in the presence of Li^{+}, site 2 may become occupied by Li^{+} prior to the debinding of Pi, thus giving rise to a very stable quaternary ($E.Mg^{2+}.Pi.Li^{+}$) complex which inhibits the enzyme.

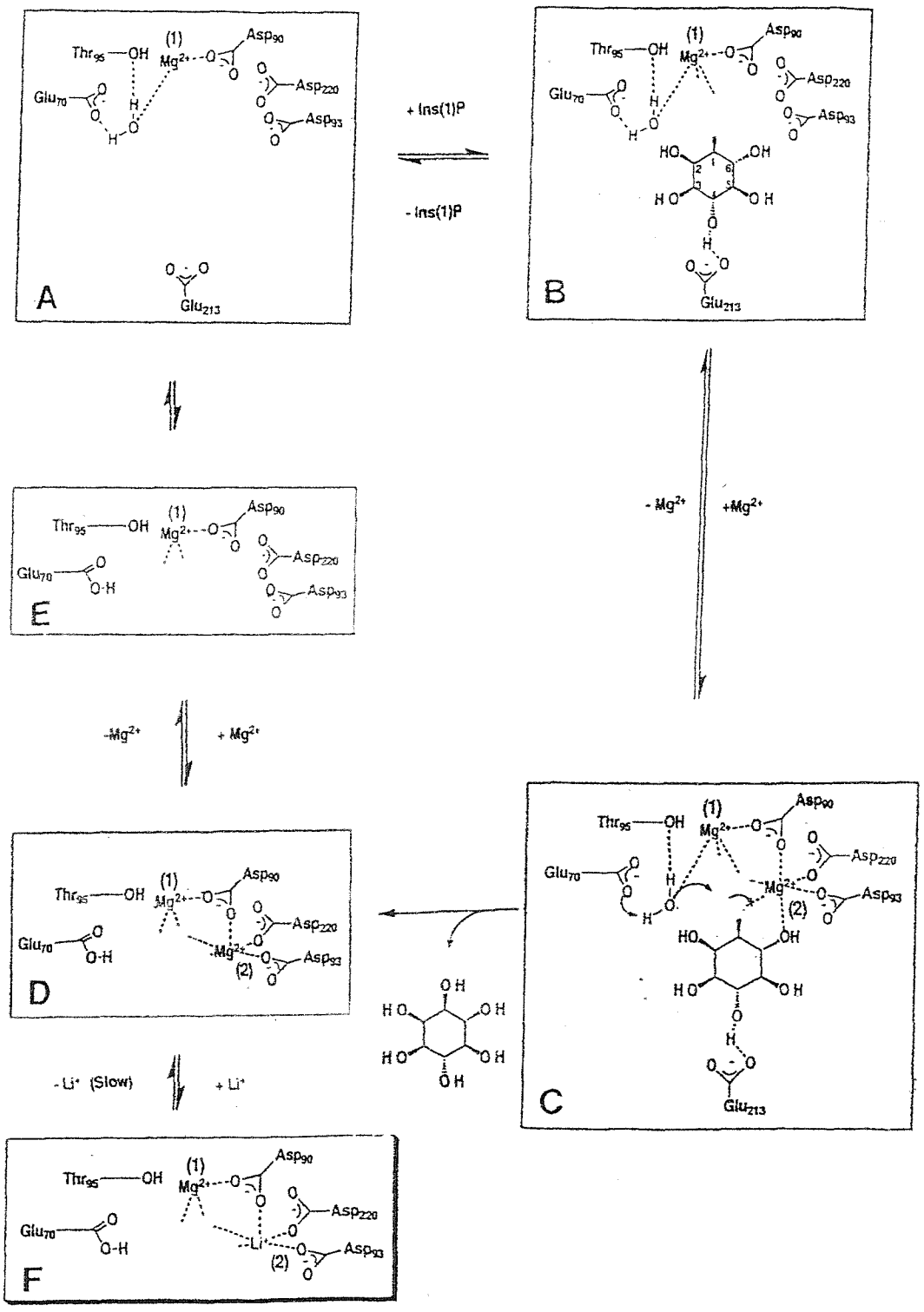
A
B
C
D
E
F
+ Ins(1)P
- Ins(1)P
- Mg2+
+Mg2+
-Mg2+
+ Mg2+
- Li+ (Slow)
+ Li+
Thr95
Glu70
Asp90
Asp220
Asp93
Glu213
(1)
(2)

Figure 1.17 The three metal ion mechanism proposed by Ganzhorn *et al.*, (1996), S represents Ins(1)P.

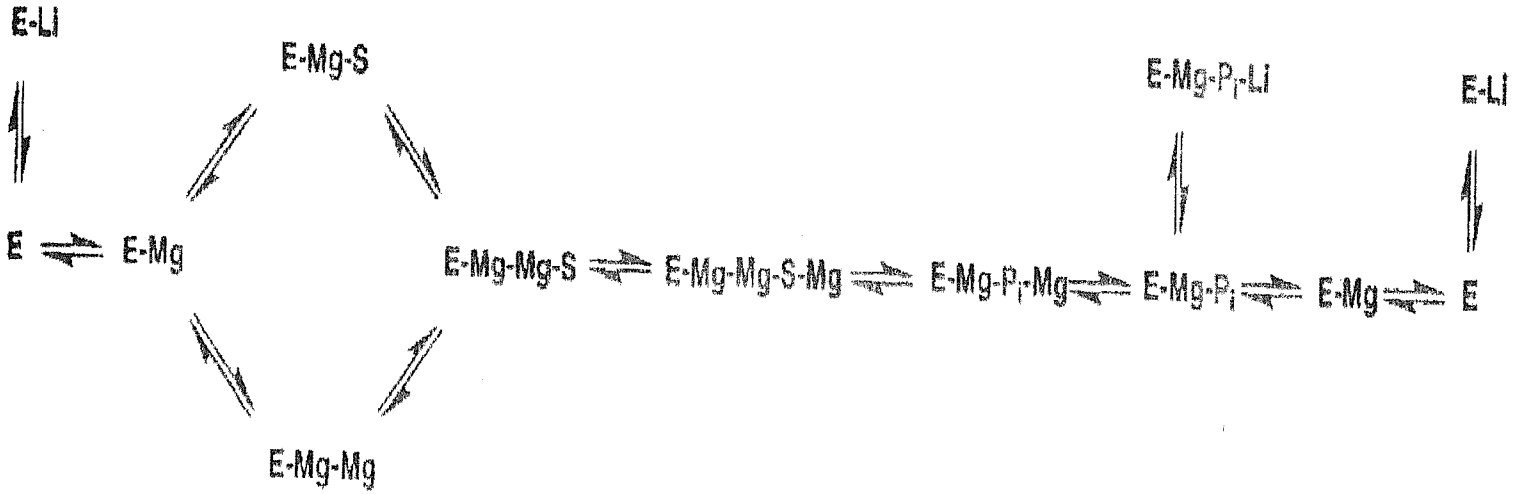
E-Li
E-Mg-S
E-Mg-Pi-Li
E-Li
E
E-Mg
E-Mg-Mg-S
E-Mg-Mg-S-Mg
E-Mg-Pi-Mg
E-Mg-Pi
E-Mg
E
E-Mg-Mg

1.11 Spectroscopic studies used to monitor ligand binding to two metal binding sites: the importance of two metal ions in the structure/function of BIMP

Stopped flow spectroscopy has been used to investigate metal ion binding to pyrene labelled enzyme at site 1. In these studies the on-rate (k_1) and the off-rate (k_{-1}) were determined over a range of Mg^{2+} ion concentrations. These constants were then used to calculate the dissociation constant (K_d) for WT enzyme, which was found to agree closely with the value determined from metal ion titrations at site 1 determined for pyrene labelled enzyme (equilibrium metal ion binding studies of Greasley *et al.*, 1994). From these studies two phases are used to describe the binding of Mg^{2+} to the pyrene labelled enzyme; an initial fast increase in fluorescence caused by Mg^{2+} binding and a slow increase in fluorescence that is independent of Mg^{2+} ion concentration (Thorne *et al.*, 1996). The slow increase in fluorescence is suggestive of a rate limiting conformational change that occurs upon Mg^{2+} binding to site 1 (the high affinity site) (Thorne *et al.*, 1996).

Mg^{2+} binding to WT, H217Q and W219F substituted enzymes was monitored using CD spectroscopy; it was possible to monitor metal ion interactions both at site 2 (using far UV CD signal changes) and at site 1 (using near UV CD signal changes). Titration of Mg^{2+} ions into WT, H217Q and W219F produced saturation curves with K_d values of 3.9mM, 6.8mM and 29.1mM respectively when the CD was monitored at 225nm. In addition, Li^+ ions perturbed the signal at this wavelength, corroborating results from previous studies that Li^+ ions bind at site 2 (Rees-Milton *et al.*, 1997). Mg^{2+} ion binding was also followed in the near UV CD region by monitoring changes at 275nm. Titration of Mg^{2+} ions yielded K_d values of 275μM, 292μM and 302μM for WT, H217Q and W219F respectively, which agreed closely with values for WT suggesting no change in the affinity at site 1 in the mutant enzymes.

1.12 Aims of the project

Although the structure of the human enzyme has been determined to 2.6Å resolution in complexes with Mn^{2+} and Mn^{2+} plus phosphate. This resolution is not high enough to be able to visualise Li^{+} ions in the complex. Furthermore, the structure of the bovine enzyme has not yet been solved and this does have sequence differences from the human enzyme. In addition, no such structure exists for an enzyme-Mg^{2+} complex. The aim of this project was to successfully crystallise the bovine enzyme in a form that would permit higher resolution structural determination in order to identify residues important for Li^{+} binding and stability. Based upon findings from the studies of Bone *et al.*, 1992; Bone *et al.*, 1994(a) and (b), residues predicted from the structure of Bone to be important for stability and those contained within conserved loop regions will be mutated and ligand binding examined using a variety of spectroscopic techniques.

CHAPTER 2

MATERIALS AND METHODS

CHAPTER 2

Materials and methods

2.1 MATERIALS

Most of the analytical grade chemicals were obtained from Sigma-Aldrich Co.Ltd., Poole or BDH Ltd., Poole, Dorset. Other chemicals were obtained from the following companies:

Amersham Pharmacia Biotech, Chalfont, Buckinghamshire:
Thermo Sequenase fluorescent primer cycle sequencing kit.

Bio-Rad Laboratories Ltd., Hemel Hempstead, Hertfordshire, UK:
SDS-PAGE low molecular weight protein standards.

Boehringer Mannheim UK Ltd., Lewes, Sussex:
Restriction and modification enzymes and buffers:
Dithiothreitol, DNase I, T4 DNA ligase, T4 DNA polymerase and
T4 DNA polynucleotide kinase.

Dynatech Laboratories Ltd., Billingshurst, Sussex:
Microtitre plates.

E. Merck, Darmstadt, Germany:
Tryptone

Hampton Research, Laguna Niguel, U.S.A:
22 mm circle cover slides
Linbro plates

Lab. M, Bury, Lancashire:
Yeast extract
Agar No.1.

Melford Laboratories, Chelsworth, Suffolk:
Ampicillin
IPTG

Molecular Dimensions Limited, Luton, Bedfordshire:
Structure screen reagents, kits 1 and 2.

National Diagnostics, Hessle, Hull:
Protogel (30% acrylamide and 0.8% bis-acrylamide)

Oswel DNA Services, Southampton, Hants:
Oligonucleotides for sequencing primers or for mismatch mutagenesis.

Pharmacia AB, Uppsala, Sweden:
Agarose (NA grade)

QIAGEN Ltd., Crawley, West Sussex:
QIA prep spin miniprep plasmid kit
Qiaex II Gel Extraction kit

The 2,4-dihydroxycyclohexane1-phosphate (inhibitor) was kindly provided by Professor R. Baker, Merck Sharpe and Dohme Research Laboratories, Essex.

2.2 MICROBIOLOGICAL METHODS

2.2.1 Bacterial strains

E. coli strain	Genotype	Reference	Use
E. coli CJ236	dut1, ung1, thi-1, relA1/pCJ105 (Cam^r F′)	Kunkel *et al.*, (1987)	Site-directed mutagenesis
E. coli JM103	(Δ(lac-proAB), supE, thi, rpsL, endA, sbcB15[F′, traD36, proAB, $lacI^q$, lacZΔ15])	Messing *et al.*, (1981)	Site-directed mutagenesis
E. coli DH5α	supE44, ΔlacU169 (ϕ 80 lacZΔM15), hsdR17, recA1, endA1, gyrA96, thi-1, relA1	Hanahan, (1983)	DNA preparations
E. coli BL21(DE3)	hsd 5 gal (λcIts857 ind 15am 7nun5 lacUV5-T7 gene1	Moffatt & Studier, (1986)	Protein preparations

2.2.2 Cloning vectors

M13 mp18/19 phage was used for the production of single-stranded template DNA for sequencing and mutagenesis. PRSET5a T7 polymerase expression vector was transformed into competent BL21(DE3) cells and used for the production of protein.

2.2.3 Strain storage

Bacterial strains were stored at 4°C for short-term storage on LB agar plates, which were viable for 2-3 weeks.

For long-term storage, bacterial strains were grown in 10ml cultures of LB until they reached mid-log phase (OD_{600nm} = 0.6). The cells were pelleted, resuspended in 850µl LB, and aliquoted into 150µl sterile glycerol in sterile cryotubes. These stocks were stored at -80°C, and replaced every twelve months.

2.2.4 Bacterial growth media

LB medium was used for the growth of bacteria for the production of plasmid DNA and recombinant proteins. Where necessary, the media was supplemented by the addition of ampicillin (50µg/ml), after autoclaving and cooling of the media. The ampicillin was added in order to successfully select for cell transformed with the plasmid DNA carrying the gene of interest. Similarly CJ236 *E. coli* cell growth was selected for by the addition of 30µg/ml chloramphenicol, since the CJ236 strain contains the chloramphenicol resistance gene.

Luria Bertani broth (LB)	g/litre
Tryptone	10
Yeast extract	5
NaCl	5

1.5% w/v of agar no.1 was added prior to autoclaving to solidify the LB for the production of plates.

H-plates	g/litre
Tryptone	10
NaCl	8
Agar no.1	12

H-top agar	g/litre
Tryptone	10
NaCl	8
Agar no.1	8

2xTY broth	g/litre
Tryptone	16
Yeast extract	10
NaCl	5

2xTY was used for the growth of CJ236 for the production of single stranded plasmid DNA for mutagenesis.

LB freeze culture media	g/litre
Tryptone	10
Yeast extract	5
NaCl	5
K_2HPO_4	6.3
KH_2PO_4	1.8
Na citrate	0.45
$MgSO_4.7H_2O$	0.09
$(NH_4)_2SO_4$	0.9
Glycerol	44mls

2.2.5 Sterilisation

All media, stock solutions, Eppendorf tubes and pipette tips were sterilised by autoclaving at 120°C and 15 psi for 20 minutes. Heat labile chemicals such as ampicillin (50μg/ml), and IPTG (400mM) were filter sterilised through 0.45μm disposable Millipore filters.

2.3 MOLECULAR BIOLOGY METHODS

2.3.1 Preparation of competent cells

Bacterial cells were rendered competent by the calcium chloride method (Cohen *et al.*, 1972). An overnight LB culture (10ml), was diluted 1:100 into LB, and incubated with shaking at 37°C until mid-log growth phase was obtained (OD_{600} = 0.6). Following this, the cells were pelleted in a bench centrifuge at maximum speed for 5 minutes, and resuspended in 5mls of ice cold, sterile 50mM $CaCl_2$. The cells were then incubated on ice for 30 minutes, repelleted and finally resuspended in 1ml of cold sterile $CaCl_2$. The competent cells were then stored on ice and used within 12 hours.

2.3.2 Transformation of competent cells with plasmid DNA

1-3μl (typically 2ng-10ng) of plasmid DNA was added to 200μl of competent cells and incubated on ice for 30 minutes. The cells were then heat shocked at 42°C for 90 seconds and returned to ice for four minutes to permit recovery from heat shock. Subsequently the cells were plated out onto LB agar plates containing ampicillin (50μg/ml), and incubated overnight at 37°C.

2.3.3 Transfection of M13 DNA

M13 DNA was transfected into competent cells as for plasmid DNA, using the transformation method but, with one modification. Following heat shock, 4mls of sterile H-top agar containing 200μl cells at 42°C was added and the mixture

was poured onto H-plates and allowed to set. The plates were then incubated at 37°C overnight to produce phage plaques on an *E. coli* lawn.

2.3.4 Preparation of plasmid DNA

Plasmid DNA was prepared using the QIAprep spin miniprep kit. The kit was used according to the manufacturer's instructions and typically yielded up to 20μg of high-copy plasmid DNA from 4ml of bacterial culture. The yield and quality of the plasmid DNA prepared was determined by agarose gel electrophoresis. Plasmid DNA from this was used for cloning, restriction endonuclease digestion, ligations etc.

2.3.5 Phenol extraction

Phenol/chloroform solution was used to remove protein contaminants from DNA samples. One volume of phenol was added to the DNA solution followed by vortexing to form an emulsion. The sample was then centrifuged for 5 minutes, resulting in an upper aqueous layer, and a lower phenol layer separated by a precipitate at the interface. The aqueous layer containing the DNA was carefully removed and transferred to a new tube before the procedure was repeated twice. The aqueous phases were pooled and extracted with an equal volume of chloroform to eliminate residual phenol.

2.3.6 Ethanol precipitation of DNA

DNA was concentrated by precipitation of its sodium salt with ethanol. DNA was precipitated by the addition of 0.1volume of 3M sodium acetate pH 5.0 and 2.5 volumes of ice-cold absolute ethanol. The solution was mixed and incubated at -70°C for 30 minutes. The sample was then centrifuged at 4°C for 15 minutes, and the layer of ethanol (supernatant) was carefully removed taking care not to disturb the DNA pellet. 1ml of 70% ice-cold ethanol was added to the DNA pellet, followed by centrifugation for 5 minutes and the

resultant desalted pellet was air dried for 30 minutes and finally resuspended in 20µl sterile water.

2.3.7 Measurement of DNA concentration

DNA concentration was estimated by measuring the optical density at 260nm. 2µl of DNA was diluted into 1ml of sterile distilled water.
For double-stranded DNA an OD_{260} of 1 in a 1cm path length cuvette corresponds to 50µg/ml DNA. For single-stranded DNA an OD_{260} of 1 corresponds to 40µg/ml DNA.

2.3.8 Agarose gel electrophoresis

Agarose mini gels were used for the analysis of the quality and yield of single and double-stranded plasmid DNA (Maniatis, 1982). Agarose was used at 0.8 to 1% w/v in 1 x TBE and boiled to dissolve into solution. After cooling to 50°C, ethidium bromide was added to a final concentration of 0.1µg/ml. The solution was then poured onto a gel casting plate with a comb positioned at one end and allowed to set. The gel was then submerged in a gel tank containing 1 x TBE. Samples were prepared by the addition of 1µl of 6x gel loading buffer and 5µl of DNA and DNA standard size markers were run in adjacent wells (λ DNA/ EcoR I and Hind III). Samples were loaded into the wells and electrophoresed at 100V for 20-30 minutes. DNA bands were visualised on a UV transilluminator.

10x TBE	g/litre
Tris.HCl	108
Boric acid	55
EDTA	9.3

Ethidium bromide (10mg/ml stock)

6x gel loading buffer

0.25% w/v bromophenol blue

30% v/v glycerol

2.3.9 Purification of DNA from agarose gels

DNA fragments were purified from agarose gels using the QIAquick gel extraction kit (Qiagen). The purification is based on solubilisation of the agarose gel followed by adsorption of the DNA to Qiaex II silica beads in the presence of high salt. The kit was used according to the manufacturer's instructions.

2.3.10 Site-directed mutagenesis

Site directed mutagenesis was carried out using a protocol based on the method described by Kunkel *et al.*, 1987.

2.3.11 Preparation of M13mp18 containing the WT BIMP gene

One of the prerequisites of the Kunkel procedure of site directed mutagenesis is that the gene of interest (bovine inositol monophosphatase gene) be inserted into the M13mp18 bacteriophage vector. The inositol monophosphatase gene in the PET11a vector, was excised using the restriction enzymes *Bgl II* and *Hind III* and gel extracted using the QIAquick gel extraction kit (see section 2.3.9). M13mp18 was also cut using the same two restriction enzymes (*Bgl II* and *Hind III*). Subsequently typical "sticky end" ligations were set up in a total volume of 10µl, containing the BIMP gene, linearised M13mp18 vector, together with DNA ligase, 10x ligation buffer, and water (see section 2.3.22). The ligation mixtures were incubated in a water bath at 25°C and then allowed to cool overnight at 4°C.

2.3.12 Transfection of JM103 with M13mp18 containing the BIMP gene

JM103 cells were made competent and 200µl were incubated with 1µl of the ligation reaction mixture, followed by heat shock at 42°C for 90 seconds. Transfection was carried out as described in section 2.3.3. A number of plaques were picked from the plates and grown for 6 hours, before DNA was prepared and digested to confirm correct ligation. Subsequently, the double stranded M13 DNA containing the BIMP gene was retransfected into competent cells and used in section 2.3.13.

2.3.13 Preparation of single stranded U-DNA

5µl of an overnight culture of *E. coli* CJ236 was used to inoculate 10ml of LB broth containing chloramphenicol (35µg/ml) and grown with shaking at 37°C for 6 hours. In addition, a single plaque arising from a successful ligation was excised from a transfection plate (section 2.3.12) and added to 1ml LB broth and heated to 60°C for 5 minutes (solubilises the agar) in the preparation of a phage solution. The solution was vortexed and centrifuged for 5 minutes. 100µl of this supernatant (phage solution) was then added to the 10ml of mid-log phase CJ236 culture and then the 10ml solution was grown overnight with shaking at 37°C. The cells were pelleted in a bench centrifuge and the supernatant containing the single stranded DNA poured into a sterile microfuge tube containing 150µl of 4M NaCl and 150µl of 40% PEG (precipitates bacteriophage DNA). The tube was incubated on ice for 1 hour to allow phage precipitation. The phage was then pelleted by centrifuged for 10 minutes and resuspended in 100µl of high salt buffer (300mM NaCl, 100mM Tris.HCl, 1mM EDTA, pH 8.0). This was followed by centrifugation and the resultant solution was subjected to phenol extraction and ethanol precipitation. Finally the resultant single stranded DNA was resuspended in 20µl of sterile water and the yield and quality determined by agarose gel electrophoresis.

2.3.14 Oligonucleotide synthesis

All oligonucleotides were synthesized and HPLC purified by OSWEL DNA services.

2.3.15 Phosphorylation of oligonucleotides

Oligonucleotides were phosphorylated on a 200pmol scale. 100ng of purified oligonucleotide was incubated with 3µl of 1M Tris.HCl, pH 8.0, 1.5µl of 0.2M $MgCl_2$, 1.5µl of 0.1M DTT (Dithiothreitol), 1.3µl of 10mM ATP and 21.5µl of sterile water. Phosphorylation was catalysed by the addition of 1µl of T4 polynucleotide kinase followed by incubation at 37°C for 45 minutes. The enzyme was then inactivated, by heating at 65°C for 10 minutes.

2.3.16 Annealing of mutagenic DNA to single stranded template DNA

2µl of the phosphorylated oligonucleotide (2pmoles) was added to 1µl of single stranded U-DNA (~ 200ng template DNA) in 1µl annealing buffer (10x annealing buffer: 200mM Tris.HCl, pH 7.4, 500mM NaCl, 20mM $MgCl_2$), and sterile water (6µl) added to a final volume of 10µl. The sample was then heated in a 70°C water bath for 3 minutes and cooled slowly to room temperature (~ 25°C).

2.3.17 Synthesis of complementary DNA to single stranded U-DNA

To the annealing reaction was added 2.5µl of T4 DNA ligase, 1µl of T4 DNA polymerase and 1µl of synthesis buffer (10x synthesis buffer: 5mM each dNTP (A, C, G and T), 10mM ATP, 100mM Tris.HCl pH 7.4, 50mM $MgCl_2$, 20mM DTT). The reaction mixture was then incubated on ice for 5 minutes, at room temperature for 5 minutes and finally at 37°C for 90 minutes. The reaction was stopped by freezing at –20°C.

2.3.18 Selection of mutants

The products of the synthesis reaction were transfected into *E. coli* JM103, and the resultant plaques were grown for 5 hours in 10ml of LB broth containing 100µl JM103 and subsequently used for the production of double stranded DNA using the QIAprep spin miniprep kit. DNA was digested using the appropriate restriction enzymes to confirm the presence of the inositol monophosphatase gene fragment. The DNA was then sequenced in order to confirm the presence of the mutation.

2.3.19 DNA sequencing reactions

To 5µl of dsDNA, 1µl of primer, 0.7µl of DMSO and 14.3µl sdH_2O were added. 4.5µl of this solution was aliquoted into each of 4 sterile 0.5ml microfuge tubes. To each of the tubes, 1.5µl of the relevant dideoxynucleotide (A, C, G or T reagents) was added and the mixture overlaid with 30µl of sterile mineral oil. The sequencing reactions were performed on a PTC-100 programmable thermocycler (PCR machine) using the following program:

94°C	30secs	] 1 cycle
94°C	10secs	┐
54°C	30secs	├ 20 cycles
65°C	30secs	┘
94°C	10secs	┐ 5 cycles
70°C	30secs	┘
5°C	Hold	

At the end of the PCR reaction cycles, 4µl of formamide loading dye (formamide, EDTA and fuchsin) was added and the reaction mixtures analysed by automated sequencing.

2.3.20 Automated sequencing

Automated sequencing was carried out on the LI-COR model 4000 automated DNA sequencer followed by analysis of the sequencing gels to confirm the identity of the mutants.

2.3.21 Restriction digestion of DNA

Restriction enzymes (*Hind III* and *Nde I*) were used according to the manufacturer's instructions. The restriction enzymes were inactivated by either phenol extraction or heat. The digested mutant dsDNA was analysed on a 0.8% agarose gel and the appropriate DNA fragment (mutant gene) purified from the agarose gel using the Qiaex II Gel Extraction kit (Qiagen).

2.3.22 Ligation of DNA

In most cases, "sticky-end" ligations were carried out in 10µl volumes with 1µl of DNA ligase and 1µl of DNA ligation buffer used for every 50ng of DNA. Ligation mixes were set up by varying the ratio of insert to vector (pre-digested using restriction enzymes *Nde I* and *Hind III*) with the ligation mix control (LMC) containing vector only. The ligation reactions were placed in a 2l water bath at 25°C and allowed to cool overnight to 4°C.

Reagents: 10 x Ligation buffer (300mM Tris.HCl pH 7.8, 100mM $MgCl_2$, 100mM DTT, 5mM ATP)
T4 DNA Ligase (1unit/ µl)

2.3.23 Dephosphorylation of DNA

CIAP was used to remove the terminal 5′ phosphate group from DNA to prevent religation of the digested vector in ligation experiments. DNA was digested and ethanol precipitated and the resultant pellet was resuspended in 25µl sterile water to which 5µl phosphatase buffer and 5µl CIAP were added.

After incubation at 37°C for 20 minutes a second aliquot of CIAP was added and the incubation continued for a further 20 minutes. The enzyme was then inactivated by heating at 65°C for 20 minutes and protein removed by phenol/chloroform extraction and ethanol precipitation.

2.4 PROTEIN TECHNIQUES

2.4.1 Growth of bacterial cultures for the expression of recombinant bovine inositol monophosphatase

The gene for bovine inositol monophosphatase, was kindly provided by Dr. Ragan (Merck Sharpe and Dohme Research Laboratories) in the pRSET5a vector. The vector was transformed into phage resistant *E.coli* strain BL21 (DE3) and a single colony from an LB amp plate was used to inoculate 10mls of LB medium containing ampicillin (50μg/ml). After an overnight incubation at 37°C, 1ml of this culture was used to inoculate 500ml medium of LB containing 50μg/ml of ampicillin. The cells were incubated with shaking (120 rpm) at 37°C until an OD_{600nm} of approximately 0.9-1.0 was attained and then IPTG was added to a final concentration of 0.4mM. The cells were vigorously shaken at 200 rpm for a further 12 hours before being harvested.

2.4.2 Extraction and purification of recombinant bovine inositol monophosphatase from *E. coli* BL21(DE3)

Cells grown in 4 litres of LB were pelleted in a Sorvall RC-3B centrifuge at 4,500 rpm for 30 minutes at 4°C using a 4 x 11 rotor. The pellet was resuspended in 30mls of 30mM Tris.HCl, 0.1mM EGTA buffer pH 8, and transferred to a 50ml Oakridge tube. Lysozyme and DNase I were added to a final concentration of 0.1mg/ml and the cells were left on ice for 30 minutes. The cells were then sonicated using an MSE Soniprep 150, for 12 cycles of 15 seconds with 45 second intermissions at 22 microns. Triton X-100 was added (0.5% v/v) and the lysed cells were incubated on ice for a further 30 minutes. Insoluble cell debris was removed by centrifuging the sonicate for 30 minutes

at 4°C and 18,000 rpm using a Beckman J2-21 centrifuge and an 8 x 50 ml rotor. The supernatant was separated from the insoluble pellet and then placed in a water bath at 65°C for 1 hour, before being returned to ice. Denatured protein was removed by centrifugation at 10,000 rpm and 4°C for 30 minutes using a Beckman J2-21 and an 8 x 50 ml rotor.

2.4.3 Anion exchange chromatography

The supernatant obtained in part 2.4.2 was then loaded onto a Q-Sepharose anion exchange column pre-equilibrated in 30mM Tris.HCl and 30mM NaCl, pH 8.0 (buffer A). A linear gradient of buffer A and buffer B (30mM Tris.HCl and 300mM NaCl, pH 8.0) was run using a Biorad Econo system, and 8 ml fractions were collected using a flow rate of 2 ml/min. All buffers contained 0.1mM sodium azide to prevent bacterial growth. The column was washed with 30mM Tris.HCl, 2M NaCl, pH 8.0 before reuse. The elution of protein from the column was followed by monitoring the absorbance at 280nm and each peak was assayed for inositol monophosphatase activity using the continuous fluorescence assay of Gore *et al.*, (1992). 5µl of the fractions spanning the peak of enzyme activity were also run on a 12.5% SDS PAGE gel to examine the purity and the degree to which a contaminating 30kDa protease had been removed. The fractions were pooled according to purity and ammonium sulphate was added to a final concentration of 80%. The solution was centrifuged at 15,000 rpm at 4°C for 20 minutes. The 80% precipitate was resuspended using 30mM Tris.HCl (pH 8.0) containing 80% $(NH_4)_2SO_4$ and stored at -20°C. Inositol monophosphatase preparations were typically found to be greater than 95% pure.

2.4.4 Determination of protein concentration

The concentration of the enzyme was determined by the Bichinconinic acid protein assay of Smith *et al.*, (1985) using bovine serum albumin as the standard. The concentration of inositol monophosphatase, was also more

accurately determined by measuring the absorbance at 280nm, and applying the Beer-Lambert law ($A = \varepsilon cl$ where $\varepsilon_{280nm} = 26{,}200\ M^{-1}\ cm^{-1}$).

2.4.5 Determination of enzyme activity

Enzyme activity was determined using the continuous fluorescence assay described by Gore *et al.*, (1992) in 50mM Tris.HCl, pH 8.0 at 37°C. The rate of hydrolysis of the substrate 4-methylumbelliferyl phosphate to product, 4-methylumbelliferone, which fluoresces intensely at 450nm was monitored (λ^{ex} = 388nm; λ^{em} = 450nm) using 7mM Mg^{2+} and 3mM substrate. The fluorimeter was also calibrated by measuring the fluorescence change of increasing concentrations of 4-methylumbelliferone (product) in 50mM Tris.HCl, pH 8.0 at 37°C under the same conditions. Using the product calibration curve and the fluorescence change seen in the assay, the specific activity of the enzyme (nmolproduct/min/mg) was calculated.

2.4.6 Polyacrylamide gel electrophoresis

The discontinuous Tris.glycine method of Laemmli, (1970) was used for the separation of proteins.

Main separating gel:

% Acrylamide	9%	12.5%	15%	18%
ddH_2O (ml)	2.94	2.24	1.74	1.14
Protogel (ml)	1.8	2.5	3.0	3.6
1.875M Tris.HCl, pH 8.8 (ml)	1.2	1.2	1.2	1.2
10% SDS (µl)	60	60	60	60
TEMED (µl)	5	5	5	5
APS (µl)	30	30	30	30

Stacking gel:

ddH_2O (ml)	2.48
Protogel (ml)	0.6
0.625M Tris.HCl pH 6.8 (ml)	0.8
10% SDS (µl)	40
TEMED (µl)	4
APS (µl)	20

APS solutions were freshly made prior to use.

5 x SDS running buffer	g/litre
Tris.HCl	15.15
Glycine	72
SDS	5

2 x Sample buffer (per 10 ml)

0.625M Tris.HCl	2ml
dH_2O	1ml
2-mercaptoethanol	1ml
10% SDS	4ml
Glycerol	2ml
Bromophenol blue dye	Trace

Stain solution (per litre):

Methanol	454ml
Acetic acid	92ml
Coomassie blue	2.5g
dH_2O	454ml

Destain solution (per 5 litres):

Methanol	250ml
Acetic acid	375ml
dH_2O	4375ml

2.4.7 Preparation of buffers, dialysis and production of apo-inositol monophosphatase

All solutions were prepared in Analar grade water and filter sterilised before use. Glassware was washed in 50% Conc.HCl and rinsed using Analar water. For all fluorescence and circular dichroism studies, the enzyme was prepared in 50mM Tris.HCl pH 8.0. The enzyme was then dialysed against 3 x 4l of 50mM Tris.HCl, 20mM EDTA, 1mM EGTA and 0.7mM 1,10-phenanthroline, pH 8.0 to remove all metal ions before a final dialysis against 4l of 50mM Tris.HCl, pH 8.0 for at least 6-8 hours each. Since the pH of Tris.HCl buffer increases inversely with temperature (ΔpH = -0.3 for every 10°C increase in pH with a 1M Tris.HCl solution), all buffers were made using precooled Analar water. All solutions were filter sterilised prior to being used in experiments. Metal ion solutions were prepared as the chlorides in 50mM Tris.HCl, pH 8.0 as 2M stocks. These stocks were diluted to working concentrations as required.

2.5 Kinetic studies

Bovine inositol monophosphatase was prepared as described in section 2.4.7 and all solutions were prepared with Analar grade water/chemicals. All fluorescence experiments were carried out on a thermostated Perkin-Elmer 650S LS-3B fluorescence spectrophotometer. The fluorescence assay of Gore *et al.*, (1992) was used to obtain all K_m, and V_{max} data for $Mg^{2+}$and substrate (4MUFP) or K_i values for Li^+ ions.

All data were analysed using the ENZFIT or Prism graph pad data analysis packages to derive K_m and K_d values (Michaelis-Menten equation).

2.6 Fluorescence studies using pyrene-maleimide-labelled enzyme

2.6.1 Modification of inositol monophosphatase by pyrene maleimide

A 25mM stock solution of pyrene maleimide was prepared in DMSO, and further diluted to working concentrations (1mM) using technical grade ethanol. In all modification protocols using pyrene maleimide, the concentration of ethanol in solution was maintained at less than 5% to prevent protein precipitation. For all the Mg^{2+} ion titrations, 1.5ml of 33μM bovine inositol monophosphatase (~1mg/ml), in 50mM Tris.HCl, pH 8.0, was incubated with 33μM pyrene maleimide (49.5μl of 1mM) at 25°C for 90 minutes. This stoichiometric addition of pyrene maleimide ensures the sole modification of the C218 residue (Greasley *et al.*, 1994). The modification was monitored directly by following the increase in fluorescence of the pyrene moiety (λ^{ex} = 340nm; λ^{em} = 380) which arises upon reaction of the maleimide group with a sulphydryl side chain. A 5.6M excess of pyrene maleimide was used in order to measure the rates of modification of WT and mutant enzymes. The data was then fitted to a double exponential equation (Prism graph pad software). The stoichiometry of modification was determined by measuring the OD at 340nm (ε_{340nm} = 36000 M^{-1} cm^{-1}) and determining the enzyme

concentration using the Bichinconinic acid protein assay of Smith *et al.*, (1985) using bovine serum albumin as the standard.

2.6.2 Fluorescence spectroscopic studies

All experiments using unlabelled and pyrene labelled protein were carried out on a thermostated Hitachi F-2000 fluorescence spectrophotometer. All procedures were carried out using excitation and emission slit widths of 10nm. Experiments were performed in volumes of 1.5ml using 50mM Tris.HCl containing 250mM KCl, pH 8.0, and all data were corrected for dilution upon addition of ligands. Titration of metal ions into pyrene labelled enzyme was performed using λ^{ex} = 340nm and λ^{em} = 375nm at 25°C. All data were collected at 25°C unless otherwise stated.

2.6.3 Fluorescence: correction for quenching by the inner filter effect

Where necessary the protein fluorescence was corrected for the inner filter effect using the equation:

$$F_{corrected} = F_{observed} \times 10^{0.5OD}$$

where the OD was determined at the excitation wavelength.

2.6.4 Stopped-flow fluorescence measurements

Pre-equilibrium studies were carried out using an Applied Photophysics SX17 stopped-flow spectrophotometer equipped with fluorescence detection. When monitoring pyrene fluorescence, an excitation wavelength of 280nm was selected and the emission at wavelengths greater than 360nm collected using a cut-off filter. A narrow band-pass filter was used to select wavelengths between 325nm and 335nm. The instrument was used with 1:1 v/v ratio syringes for metal binding studies, but 5:1 v/v syringes were used for protein folding studies. The temperature of the cell was thermostatically regulated using a Techne TE-8A water bath. All experiments were carried out at 25°C in

50mM Tris-HCl buffer containing 250mM KCl, pH 8.0 unless otherwise stated.

2.6.5 Analysis of pre-equilibrium reaction progress curves

All concentrations quoted are final concentrations after mixing. The reactions were carried out in triplicate and analysed by the manufacturer's software using double and single exponential curve fitting algorithms. In experiments to determine the rate constant for the association of the complex, the pyrene labelled enzyme concentration was kept constant at 3μM and the concentration of Mg^{2+} ions was varied. The use of an excess of metal ions allowed the reactions to be analysed as pseudo-first order processes using the relationship;

$$F_t = F_0 \exp^{-kt} + C$$

where F_o and F_t are the fluorescence intensities at time 0 and time t respectively, k is the apparent first order rate constant for the reaction and C is a constant. However, the reaction progress curves were also routinely analysed by a double exponential equation:-

$$F(t) = A_1\exp(-k_1t) + A_2\exp(-k_2t) + C$$

In which F(t) is the fluorescence at time t, A_1 and A_2 are the amplitudes of the different phases of the change in fluorescence, k_1 and k_2 are the rate constants for the first and second phase respectively and C is a constant.

In addition, the rates of dissociation of Mg^{2+} ions from a complex with the enzyme were determined at different pH values by mixing 1:1 v/v of pre-formed complex with 20mM EDTA. This was repeated for different concentrations of EDTA (2mM-100mM). The buffers used here were 50mM

Tris.HCl, pH 8.0 at 25°C for inositol monophosphatase and 10mM Hepes buffer, pH 8.0 at 25°C for the EDTA.

2.7 Circular dichroism studies

All CD measurements were performed on a Jasco J720 spectropolarimeter. Enzyme was prepared in 50mM Tris.HCl, pH 8.0, dialysed as in section 2.4.7 and filter-sterilised and degassed for experiments. Far UV studies were performed in the wavelength range 195-250nm using protein concentrations of 0.1-0.2mg/ml and a 0.1cm path length cell. Near UV studies were performed in the wavelength range 250-320nm using protein concentrations of 0.5-1.0mg/ml and a 1cm path length cell. For maximal signal to noise ratio, each spectrum measured was an accumulation of three runs at 20nm/min. For metal ion titrations in the far UV region, a slower scan speed of 5nm/min over the range 215-225nm was used. Values of K_d for Mg^{2+} ions were determined at 220nm. For metal ion titrations in the near UV region, the spectra were scanned at 5nm/min over the 280nm range and K_d values were determined at a wavelength of 275nm. As before these spectra were an accumulation of three consecutive scans. When carrying out the metal ion titrations, buffer controls were also performed and corrections for dilution made. Measurement parameters used were; response (8 sec), band width (1.0nm), resolution (0.2nm) and slit width (500μm). All CD spectra were converted to mean residue ellipticity values (θ_m) in units of deg. cm^2 $dmol^{-1}$. The equation used for determining the Molar ellipticity is as follows:

$$\theta_m = \frac{\theta.MRW}{10cl}$$

Where θ denotes the ellipticity measured in mdeg, MRW represents the mean residue weight (115), l is the path length in cm and c is the concentration in mg/ml determined from the absorbance at 280nm.

2.8 Protein unfolding studies

The enzyme was prepared as in section 2.4.7 and dialysed against 50mM Tris.HCl, pH 8.0. 10M urea was prepared in filter sterilised 50mM Tris.HCl, pH 8.0. Enzyme (0.1mg/ml) was incubated in increasing concentrations of denaturant at 32°C for 2 hours. The unfolding was followed by monitoring the changes in protein fluorescence at 320nm and 360nm using an excitation wavelength of 280nm.

2.9 X-RAY CRYSTALLOGRAPHIC STUDIES

2.9.1 Purification and crystallisation

Recombinant bovine inositol monophosphatase was purified as described in section 2.4.7. Then enzyme obtained from the final dialysis was concentrated to 20mg/ml using centricon-10 concentrators. BIMP was crystallized using the hanging drop method. An initial crystal screen was set up using reagents from Molecular Dimensions Limited. This kit contains 100 different sterile filtered reagents. This provided a wide range of trial conditions, the variables being buffer, pH, salt and precipitant.

Inositol monophosphatase (WT/G76S mutant) and Mg^{2+}cocrystals were grown by mixing 2µl of protein (20mg/ml) containing 20mM Mg^{2+} ions (or without 20mM Mg^{2+} ions) with 2µl of the MDL reagent on 22mm coverslides before inverting over a reservoir containing 1ml of the same MDL reagent. This was repeated for the remaining MDL reagents before the wells of the Linbro plates were sealed and allowed to equilibrate for several weeks at 25°C. Twelve of the 100 initial conditions resulted in clusters of needle-like crystals, microcrystals, and quasi crystals after 3 weeks (see chapter 6, Figure 6.3). Conditions yielding crystals were systematically optimised by altering the buffer type (0.1M Tris.HCl/ 0.1M Na Hepes), the pH, the precipitant concentration and the salt concentration. All experiments were carried out at room temperature with the protein being concentrated and stored at 4°C until

the crystallisation conditions were set up. Subsequently the crystallisation trays were placed at 25°C.

2.9.2 Data collection

The native protein crystal (0.6mm x 0.4mm x 0.1mm; Figure 6.5) was prepared for low temperature data collection by soaking it in solution of mother liquor (0.1M Na Hepes (pH 8.5), 15% v/v PEG 4K, 0.1M Na acetate, 10mM Mg^{2+} ions and 20% glycerol). The crystal was then mounted in a mohair loop and flash cooled by plunging it into liquid ethane and then quickly into liquid nitrogen after which it was sealed in a cryovial for transportation. Once at the synchrotron the crystal was rapidly placed in the nitrogen stream of a cryostream (Oxford Cryosystems) which maintained its temperature at 100 K. X-ray data were collected at the ESRF synchrotron (Grenoble, France), at station ID14-EH3 with a 30cm Mar CCD detector by Dr Jon Cooper. 180 images of 1° oscillation were collected.

2.9.3 Structure solution and refinement

Since human inositol monophosphatase shares a high sequence homology with the bovine form, the structure of the recombinant enzyme was solved by molecular replacement using the HIMP structure previously resolved to 2.6Å resolution (Bone *et al.*, 1994(b) (2HHM.pdb)) and refined to 1.6Å. This is covered in more detail in chapter 6.

CHAPTER 3

SITE-DIRECTED MUTAGENESIS OF INOSITOL MONOPHOSPHATASE

CHAPTER 3

Site-directed mutagenesis of the inositol monophosphatase gene

3.1 Introduction

To aid studies aimed at relating structure to function in a protein, certain regions of the protein thought to be important for a specific role can be modified. The mutated protein can then be characterised to detect changes in its structure and relate these to changes in kinetic characteristics. In order to carry out these modifications, a significant amount of information is required with regards to the selection of amino acids for modification. This information can be obtained from a number of sources: protein sequence homology searches may provide data on the conserved nature of particular amino acids within a class of proteins which may serve an important role. Chemical modification studies may provide useful information regarding the importance of specific amino acid residues involved in catalysis, substrate binding, or ligand binding. Ideally, for a particular protein, a structural model of the protein (obtained either by X-ray crystallography or NMR) is the most useful. However, an X-ray structure although providing the location of particular residues, gives little information regarding the role of that particular residue within the protein.

Historically, several techniques have been used to introduce mutations. Before the advent of recombinant DNA technology, techniques employed have generally resulted in the generation of random mutations, where the site of the mutation and the nature of the amino acid replacement are uncontrolled. Random mutagenesis often relies on the use of chemical mutagens. These chemicals primarily modify the side groups of bases in the DNA *in situ.*
Examples of mutagens include: nitrous acid which oxidatively deaminates cytosine to uracil, adenine to hypoxanthine, and guanine to xanthine; sodium bisulfite deaminates cytosine residues to form thymine, but only in single-stranded DNA; hydrazine breaks the rings of the pyrimidines cytosine and

thymine; the base analog 5-bromouracil (5BU) sterically resembles thymine and is therefore incorporated into DNA in place of thymine and effectively induces an A.T → G.C transition; formic acid functions by breaking the glycosyl bonds of adenine and guanine; and hydroxylamine (NH_2OH) also induces G.C → A.T transitions by specifically reacting with cytosine to convert it to a compound that base pairs with adenine.

3.2 Site-directed mutagenesis

Site-directed mutagenesis is an invaluable technique for altering specific amino acids in a protein by changing their codons in the gene sequence. By changing selected amino acids in this way, one can determine which parts of the protein chain are crucial to such fundamental processes as protein folding, protein-ligand interactions and enzymatic catalysis. Several variations of *in vitro* mutagenesis techniques for introducing site-specific mutations have been developed, the simplest and most efficient being that described by Kunkel, (1985) and Kunkel *et al.*, (1987).

In this method, the gene of interest must initially be cloned into a vector whose DNA can exist in both single and double stranded forms (for example bacteriophage M13). This M13 vector containing the gene of interest is then transformed into a bacterial strain that generates the single stranded replicative form, which contains a number of uracil residues in place of thymine (for example *E. coli* CJ326). This allows a strong selection against the non-mutagenised DNA strand. The CJ236 strain, which is a *dut*$^-$ *ung*$^-$ bacterium, is deficient in the enzymes dUTPase and uracil N-glycosylase. The lack of dUTPase (*dut*$^-$) implies inactivation of the enzyme dUTPase, which results in high intracellular levels of dUTP which competes with dTTP (deoxythymine triphosphate) for incorporation into the replicating DNA (Konrad *et al.*, 1975). In addition, uracil N-glycosylase (*ung*$^-$) can no longer replace misincorporated uracil residues should they become incorporated into the DNA. In this way single stranded uracil-rich DNA can be purified and used as a template for the *in vitro* synthesis of an oligonucleotide-primed non-uracil containing mutant

strand. The oligonucleotide (typically18-30 nucleotides long) containing the desired base change is annealed to the template strand and extended by *in vitro* synthesis catalysed by DNA polymerase and subsequent ligation brought about by T4 DNA ligase. The resultant double stranded product (dsM13 DNA) containing the desired mutation is then transformed into an ung^+ strain (JM103). In this strain, there is proficient uracil N-glysoylase, so that the uracil containing parental strand is degraded leaving the non-uracil containing mutant strand to serve as a template for subsequent DNA synthesis, thereby producing a second strand carrying the mutation. The Kunkel, (1985) and Kunkel *et al.*, (1987) method results in a 50-70% mutation efficiency. Figure 3.1 depicts a schematic representation of the procedure.

In other strategies of site-directed mutagenesis, modified nucleotides such as thio-dCTP (Taylor *et al.*, 1985(a)) or methyl-dCTP (Taylor *et al.*, 1985(b)), are incorporated into the newly synthesised strand. The resultant hybrid is incubated with restriction enzymes which destroy the unmodified strand, leaving the mutated strand as the template for subsequent DNA synthesis. After transformation into competent cells, a DNA duplex is synthesised containing the desired mutation. The efficiency of this particular method is greater than 70%, however, the reagents are expensive.

In the mutagenesis protocols discussed above one disadvantage is the requirement for a single-stranded DNA template. This necessitates that the gene of interest must first be cloned into a vector capable of synthesising single-stranded DNA and subsequent subcloning into an expression vector following successful mutagenesis.

The Kunkel, (1985) and Kunkel *et al.*, (1987) method of mutagenesis was used in this project as it is well established within the laboratory and yields a relatively high frequency of mutation (50-70%). The bovine inositol monophosphatase gene (Figure3.2) was cloned and mutated in the M13mp18 vector (Figure 3.3), followed by automated sequencing on a LI-COR 4000 sequencer and then subcloned into the pRSET5a expression vector (Figure 3.4).

Figure 3.1 Schematic representation of the Kunkel (1985, 1987) method of site-directed mutagenesis. This method of oligonucleotide-directed mutagenesis relies on the annealing of a complementary oligonucleotide containing a one or two base mismatch to a single-stranded M13 DNA template. The phosphorylated mismatch mutagenic oligonucleotide then acts as a primer for a DNA polymerase to synthesise the complementary strand *in vitro* in the presence of dNTP's and subsequent ligation with T4 DNA ligase results in a heteroduplex product. When this heteroduplex is transformed into an *E. coli* strain (JM103) that carries out normal replication (i.e. dut^+ ung^+), the mutagenic strand is selectively replicated. Mutant clones are subsequently isolated and confirmed by DNA sequencing.

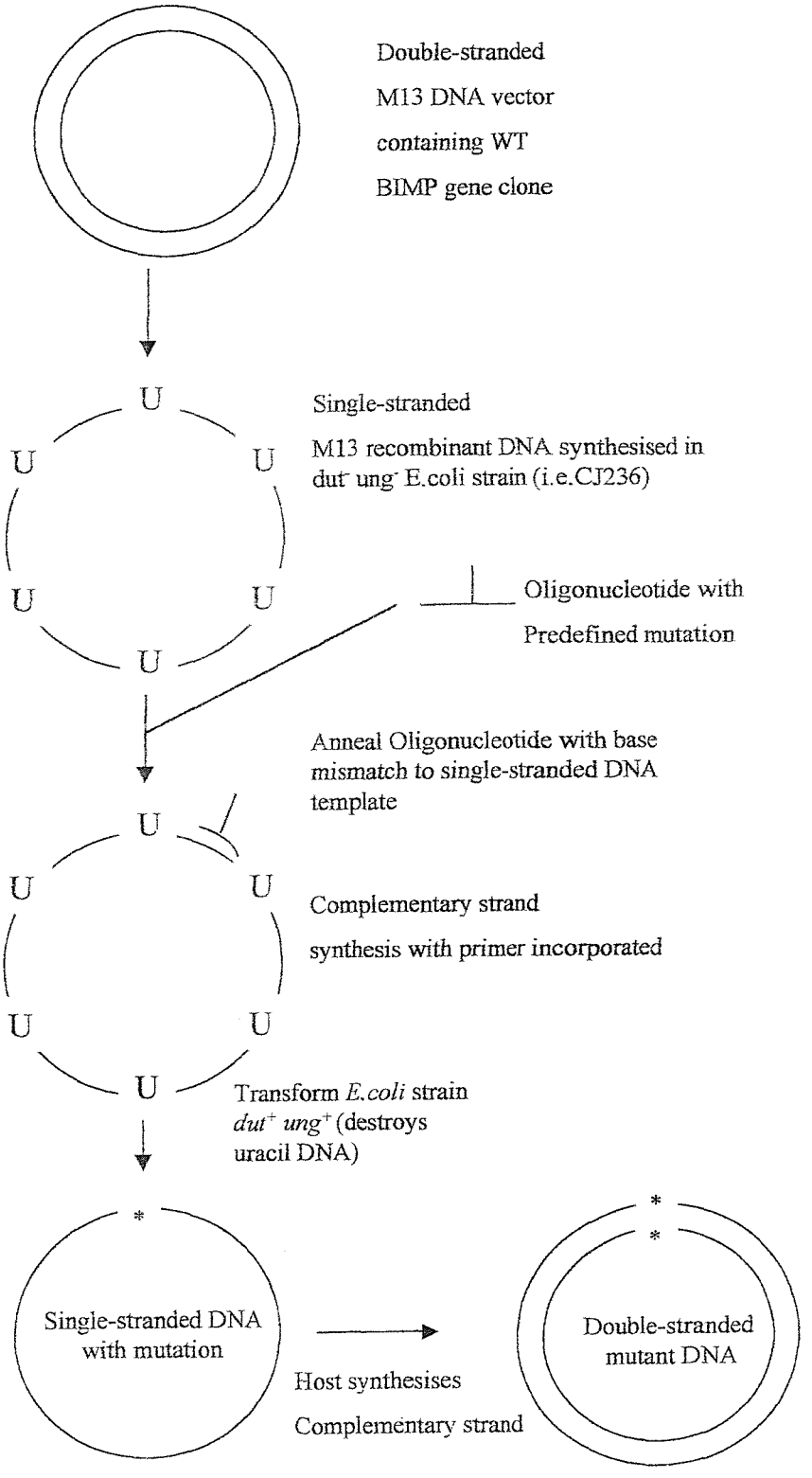
Double-stranded
M13 DNA vector
containing WT
BIMP gene clone
U
U
U
U
U
U
Single-stranded
M13 recombinant DNA synthesised in
dut⁻ ung⁻ E.coli strain (i.e.CJ236)
Oligonucleotide with
Predefined mutation
Anneal Oligonucleotide with base
mismatch to single-stranded DNA
template
U
U
U
U
U
U
Complementary strand
synthesis with primer incorporated
Transform E.coli strain
dut+ ung+ (destroys
uracil DNA)
*
Single-stranded DNA
with mutation
Host synthesises
Complementary strand
*
*
Double-stranded
mutant DNA

Figure 3.2 The nucleotide sequence of bovine brain inositol monophosphatase open reading frame and the derived amino acid sequence (blue) (adapted from Diehl *et al.*, 1990).

```
1    ATGGCTGATCCTTGGCAGGAATGCATGGATTATGCAGTAACCCTGGCAGGACAAGCTGGA  20
     M  A  D  P  W  Q  E  C  M  D  Y  A  V  T  L  A  G  Q  A  G

61   GAGGTGGTTCGTGAAGCGCTCAAGAATGAAATGAATATTATGGTTAAAAGTTCTCCGGCT  40
     E  V  V  R  E  A  L  K  N  E  M  N  I  M  V  K  S  S  P  A

121  GATTTGGTAACTGCTACTGACCAAAAAGTTGAAAAAATGCTTATCACATCCATAAAGGAA  60
     D  L  V  T  A  T  D  Q  K  V  E  K  M  L  I  T  S  I  K  E

181  AAGTATCCATCTCACAGTTTCATTGGTGAGGAATCTGTGGCAGCTGGGGAAAAAAGTATC  80
     K  Y  P  S  H  S  F  I  G  E  E  S  V  A  A  G  E  K  S  I

241  TTAACCGACAACCCTACATGGATCATTGACCCTATTGATGGAACAACTAACTTTGTACAT  100
     L  T  D  N  P  T  W  I  I  D  P  I  D  G  T  T  N  F  V  H

301  GGATTTCCTTTTGTAGCTGTTTCAATTGGCTTTGTGGTAAATAAAAAGATGGAGTTTGGA  120
     G  F  P  F  V  A  V  S  I  G  F  V  V  N  K  K  M  E  F  G

361  ATTGTGTACAGTTGCCTGGAGGATAAGATGTACACTGGCCGGAAAGGAAAAGGTGCCTTT  140
     I  V  Y  S  C  L  E  D  K  M  Y  T  G  R  K  G  K  G  A  F

421  TGTAATGGTCAAAAACTACAGGTTTCACACCAAGAAGATATTACCAAATCTCTCTTGGTG  160
     C  N  G  Q  K  L  Q  V  S  H  Q  E  D  I  T  K  S  L  L  V

481  ACAGAGTTGGGCTCTTCCAGAACACCAGAGACTGTGAGAATTATTCTTTCTAATATAGAA  180
     T  E  L  G  S  S  R  T  P  E  T  V  R  I  I  L  S  N  I  E

541  AGGCTTCTTTGCCTTCCCATCCATGGGATCCGGGGTGTTGGAACAGCAGCTCTGAACATG  200
     R  L  L  C  L  P  I  H  G  I  R  G  V  G  T  A  A  L  N  M

601  TGCCTGGTGGCCGCTGGGGCTGCGGACGCGTATTATGAAATGGGGATCCACTGCTGGGAT  220
     C  L  V  A  A  G  A  A  D  A  Y  Y  E  M  G  I  H  C  W  D

661  GTTGCACGCGCCGGCATCATTGTGACTGAAGCTGGCGGAGTGCTCCTGGATGTCACAGGT  240
     V  A  G  A  G  I  I  V  T  E  A  G  G  V  L  L  D  V  T  G

721  GGACCATTTGATTTGATGTCACGAAGAGTAATTGCTTCAAGCAATAAAACATTAGCAGAA  260
     G  P  F  D  L  M  S  R  R  V  I  A  S  S  N  K  T  L  A  E

781  AGGATAGCCAAAGAAATTCAGATAATACCTCTTCAAAGAGATGATGAAGAT           277
     R  I  A  K  E  I  Q  I  I  P  L  Q  R  D  D  E  D
```

Figure 3.3 A map of the bacteriophage M13mp18 (from Maniatis *et al.*, 1982).

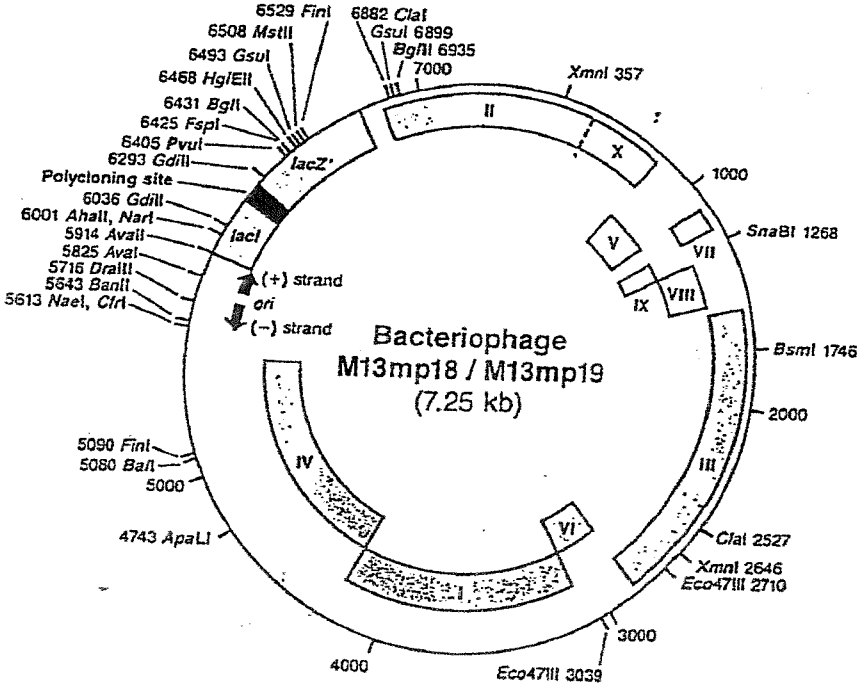

Polycloning Sites
M13mp18

			1	2	3	4	5	6	1	2	3	4	5	8	7	8	9	10	11	12	13	14	15	16	17	18	7	8
			Thr	Met	Ile	Thr	Asn	Ser	Ser	Ser	Val	Pro	Gly	Asp	Pro	Leu	Glu	Ser	Thr	Cys	Arg	His	Ala	Ser	Leu	Ala	Leu	Ala
ATG	ACC	ATG	ATT	ACG	AAT	TCG	AGC	TCG	GTA	CCC	GGG	GAT	CCT	CTA	GAG	TCG	ACC	TGC	AGG	CAT	GCA	AGC	TTG	GCA	CTG	GCC

EcoRI *SacI* *KpnI* *SmaI* *XmaI* *BamHI* *XbaI* *SalI* *AccI* *HincII* *PstI* *SphI* *HindIII*

Figure 3.4 The pRSET5a vector (adapted from Schoepfer, 1993).

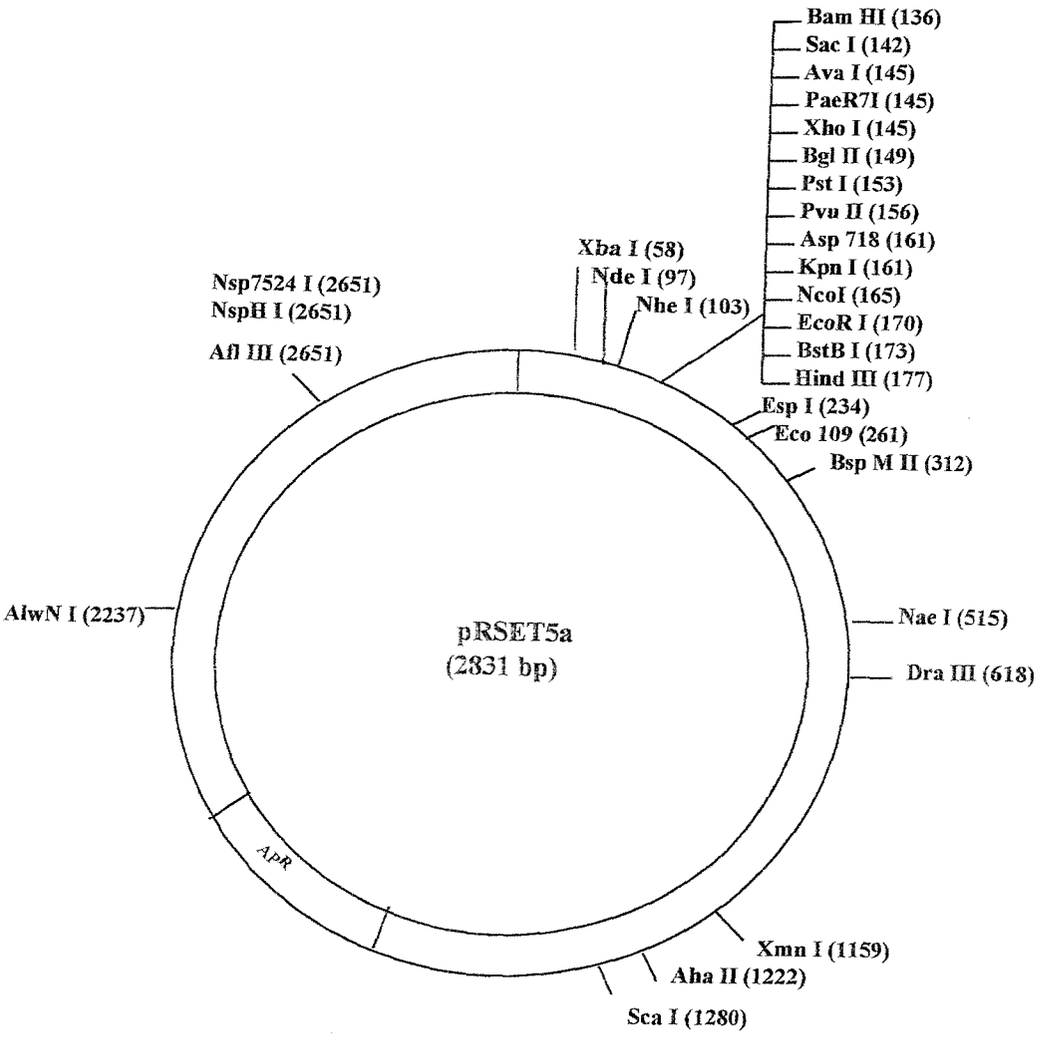
Bam HI (136)
Sac I (142)
Ava I (145)
PaeR7I (145)
Xho I (145)
Bgl II (149)
Pst I (153)
Pvu II (156)
Asp 718 (161)
Kpn I (161)
NcoI (165)
EcoR I (170)
BstB I (173)
Hind III (177)
Esp I (234)
Eco 109 (261)
Bsp M II (312)
Nae I (515)
Dra III (618)
Xmn I (1159)
Aha II (1222)
Sca I (1280)
AlwN I (2237)
Afl III (2651)
Nsp7524 I (2651)
NspH I (2651)
Xba I (58)
Nde I (97)
Nhe I (103)
pRSET5a
(2831 bp)
ApR

3.3 Selection of amino acids for mutation

The selective substitution of one residue for another allows removal of a single reactive group. In the process of mutating a specific amino acid it is imperative to make the change as conservative as possible with respect to size, charge and hydrophobicity. In some cases substitution by a residue that results in a deformation of secondary and therefore tertiary structure may potentially lead to changes in the characteristics of the protein that are not attributable to the side chain substitution alone. In all cases, various kinetic analyses can then be used to probe the role of that particular residue in the mutant protein. Figure 3.5 shows a monomer of inositol monophosphatase highlighting the sites of the mutations made in these studies. Residues 70-75 are located in a loop region of the enzyme which moves away from the metal binding site by approximately ~3Å in the absence of metal ions, breaking 3 intramolecular hydrogen bonds. Therefore substitution of residues G69 and G76 by serine was used to test whether this may impair the movement of this loop. A serine residue was chosen in order to slightly increase the bulk of the residue at positions 69 and 76 and make the environment more hydrophilic. It was expected that G69S might also be useful in studying the role of the adjacent residue E70 which is crucially involved in the catalytic mechanism as it is contained within a conserved region (motif C) of the enzyme. Similarly, residue E30 is located in another loop region of the enzyme and proline was selected as a replacement in order to restrict the movement of this loop region. Examination of the crystal structure (Bone *et al.*, 1992, 1994a and 1994b) shows that residues H100 and H188 form mutual subunit: subunit hydrogen bond interactions and thus by mutating these residues to glutamine, the importance of these residues in the stabilisation of the enzyme may be studied. Further mutations were made including C218 to aspartate and G69 to aspartate. The first mutation is at a site known to influence Mg^{2+} ion binding (Gore *et al.*, 1993) and the latter is adjacent to E70, also involved in metal ion ligation. Here an attempt was being made to influence the pKa of E70 to test its affect on Mg^{2+} ion binding. Other mutations that were made are as follows: R191A and I269 to a stop codon (truncated protein). Upon sequence alignment

Figure 3.5 A monomer of inositol monophosphatase showing the residues mutated and the substitutions made in these studies.

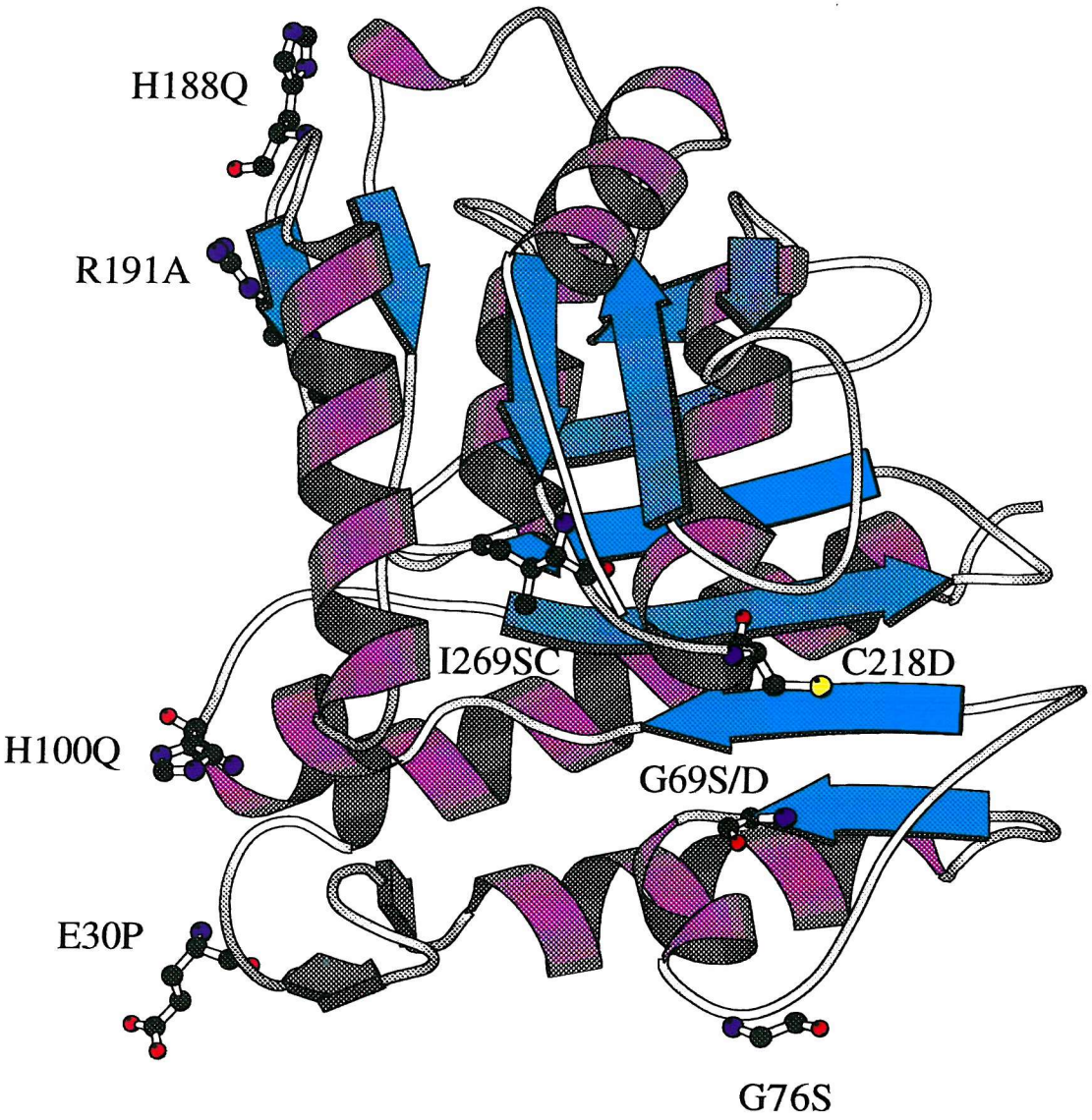
H188Q
R191A
I269SC
C218D
H100Q
G69S/D
E30P
G76S

of the HIMP with F1,6-BP, residue 191 is found to be conserved and corresponded to R243 in the latter enzyme. In the F1,6-BP dimer, residue R243 of one subunit participates in the binding of substrate to the other subunit in the enzyme. It has also been suggested that R243 has an additional structural role in formation of the dimer interface (Zhang *et al.,* 1993(a) and 1993(b)). Therefore, R191 was mutated in order to determine if it fulfilled a similar role in BIMP. Furthermore, the solution of the X-ray crystallographic structure of HIMP demonstrates that the side chain of R191 protrudes from one subunit in the dimer into the active site of the other adjoining subunit, where it interacts with solvent molecules 10Å from the metal binding site (Bone *et al.*, 1992).

The main reasons for mutating residue I269 to a stop codon (SC), was to establish whether the truncated protein expressed and in addition if expression was present, whether it affected dimer formation and stabilisation.

3.4 Production of mutants of inositol monophosphatase

Oligonucleotides (Figure 3.6) were synthesised, purified and quantified by Oswel Ltd, Southampton, and 200pmoles of each were phosphorylated and used with uracil-rich DNA template using standard procedures as described in sections 2.3.11 to 2.3.17. In all of the reactions the template DNA was prepared from M13mp18 containing the gene for WT BIMP. Mutagenesis reactions were carried out after which 1μl and 4μl of the reaction mixture were transfected into competent JM103 cells. Double-stranded DNA was (1μl) and template DNA (1μl) were used as negative and positive controls. After overnight incubation at 37°C, six plaques were picked for each reaction and grown for 6 hours and used to prepare single-stranded DNA. Potential mutants were identified by dideoxynucleotide chain termination sequencing, the gels for which are shown in Figure 3.7 (a)-(i). The efficiency of mutagenesis for the mutants sequenced, (Table 3.1) agreed closely with that previously predicted (50-70%), by Kunkel, (1985).

Figure 3.6 Oligonucleotide primers used in the production of mutants of recombinant bovine inositol monophosphatase.

WT	5' ACT AAC TTT GTA CAT GGA TTT CCT TTT 3'
H100Q	5' ACT AAC TTT GTA **CAG** GGA TTT CCT TTT 3'
WT	5' TGC CTT CCC ATC CAT GGG ATC CGG GGT 3'
H188Q	5' TGC CTT CCC ATC **CAG** GGG ATC CGG GGT 3'
WT	5' TCT GTG GCA GCT GGG GAA AAA AGT ATC 3'
G76S	5' TCT GTG GCA GCT **TCT** GAA AAA AGT ATC 3'
WT	5' CAC AGT TTC ATT GGT GAG CAA TCT GTG 3'
G69S	5' CAC AGT TTC ATT **TCT** GAG CAA TCT GTG 3'
WT	5' GCG CTC AAG AAT GAA ATG AAT ATT ATG 3'
E30P	5' GCG CTC AAG AAT **CCG** ATG AAT ATT ATG 3'
WT	5' ATC CAT GGG ATC CGG GGT GTT GGA ACA 3'
R191A	5' ATC CAT GGG ATC **GCT** GGT GTT GGA ACA 3'
WT	5' GAA ATT CAG ATA ATA CCT CTT CAA AGA 3'
I269SC	5' GAA ATT CAG ATA **TAA** CCT CTT CAA AGA 3'
WT	5' ATG GGG ATC CAC TGC TGG GAT GTT GCA 3'
C218D	5' ATG GGG ATC CAC **GAC** TGG GAT GTT GCA 3'
WT	5' CAC AGT TTC ATT GGT GAG CAA TCT GTG 3'
G69D	5' CAC AGT TTC ATT **GAC** GAG CAA TCT GTG 3'

Figure 3.7 DNA sequencing gels for (a) G76S, (b) G69S, (c) H188Q, (d) E30P, (e) C218D, (f) I269SC, (g) G69D, (h) R191A and (i) H100Q.

(a) G76S

A C G T

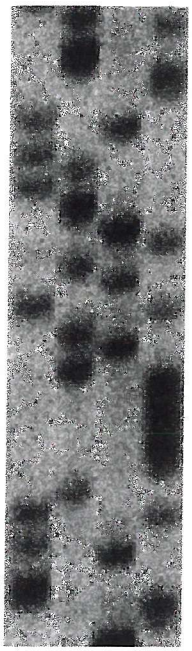

(b) G69S

A C G T

(c) H188Q

A C G T

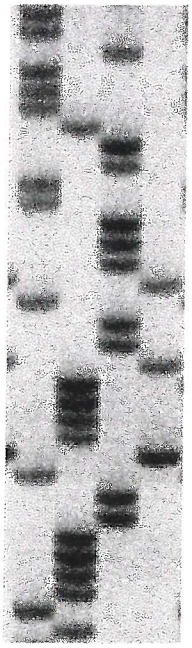

(d) E30P

A C G T

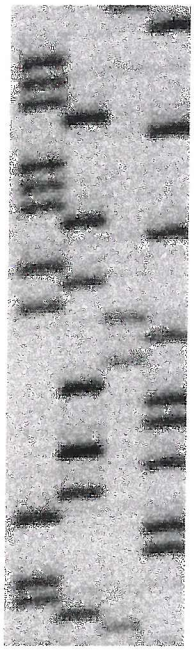

(e) C218D

A C G T

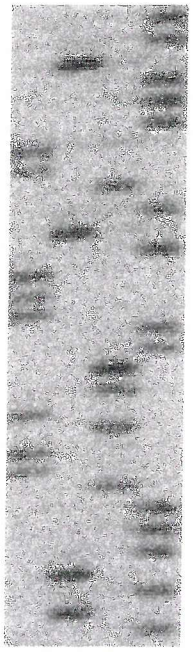

(f) I269SC

A C G T

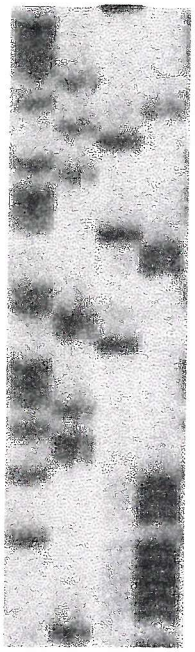

(g) G69D

A C G T

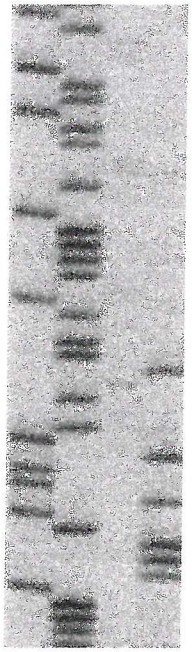

(h) R191A

A C G T

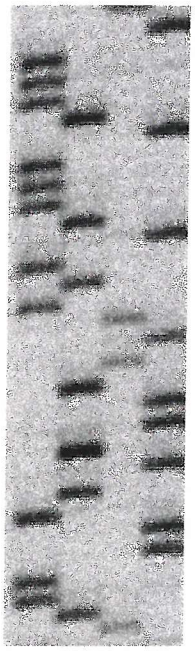

(i) H100Q

A C G T

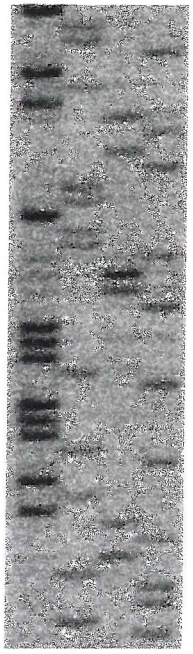

The H188Q mutant DNA was transfected into competent JM103 cells and used for the production of double-stranded DNA (Figure 3.8(a)) and subsequently the gene was excised with restriction enzymes *Nde I* and *Hind III* (Figure 3.8(b)) and isolated from a 0.8% gel using a QIAquick gel extraction kit Qiagen). The gene was then subcloned into *Nde I*/*Hind III* digested and dephosphorylated pRSET5a expression vector. Ligation reaction mixtures were transformed into competent DH5α cells and double-stranded DNA prepared from the resultant colonies. Plasmid DNA was digested with *Nde I* and *Hind III* to screen for recombinants (Figure 3.8(c)). The expression vector was then transformed into *E.coli* BL21(DE3) cells and the recombinant mutant enzymes expressed.

3.5 Expression and purification of mutant enzymes

All mutant recombinant enzymes were expressed and purified as described in section 2.4 for WT BIMP. Since this requires the treatment of the cell extract at 65°C for one hour, it may be expected that if the mutation had resulted in any gross structural changes, a change in this step may be required. The mutant enzymes were eluted from the Q-sepharose column in an analogous way to the WT enzyme and the purity of the protein was tested on SDS PAGE. The standard purification procedure typically yielded 80-160mgs from 4 litres of bacterial culture depending upon the particular mutant protein (Table 3.1). Figure 3.9(a) and 3.9(b) shows examples of SDS-PAGE gels obtained during the purification protocol of the H188Q substituted mutant. Mutants H100Q, R191A and I269 to a stop codon (SC) failed to express any protein. It is unclear as to why R191A and in particular H100Q failed to express. With the I269SC mutant, it is reasonable to presume that the last 8 residues may be crucial for the full expression or folding of the protein or for resistance to proteolysis by cellular proteases. In future work, it would be interesting to synthesise a truncated version of the protein with fewer residues missing. In order to study the kinetic and structural characteristics of the mutant forms of inositol monophosphatase, they have to be purified and compared with WT inositol monophosphatase. Table 3.1 shows the efficiency of mutagenesis and

Figure 3.8 (a-d) Agarose gels showing the subcloning of the H188Q mutant.

(a) Double stranded M13 containing H188Q gene.

Lane 1) Lambda DNA/EcoRI + Hind III Markers.
Lanes 2-8) Double stranded M13 containing H188Q gene.

(b) Restriction digest of double stranded M13 containing H188Q gene.

Lane 1) Lambda DNA/EcoRI + Hind III Markers.
Lane 2) Uncut double stranded M13 containing H188Q gene.
Lanes 3-4) *Nde I* + *Hind III* digest.

(c) *Nde I* + *Hind III* digested fragment.

Lane 1) 831 bp H188Q BIMP gene.
Lane 2) Lambda DNA/ EcoR I + Hind III Marker.

(d) H188Q BIMP gene in pRSET5a vector.

Lane 1) Lambda DNA/ Eco RI + Hind III Markers.
Lane 2) pRSET5a vector containing the WT BIMP gene.
Lanes 3-5) H188Q BIMP gene in pRSET5a vector.

(a)

(b)

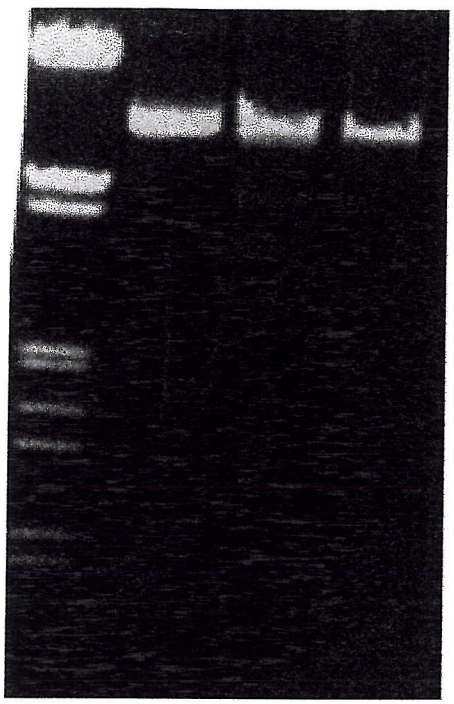

(c)

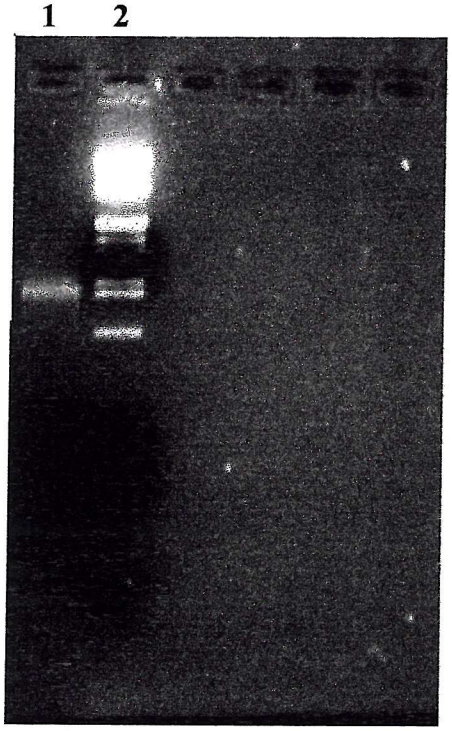

(d)

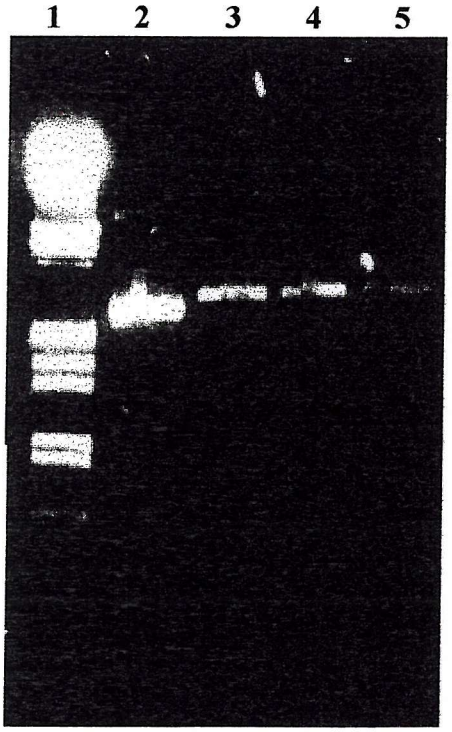

Figure 3.9a) SDS PAGE showing samples obtained during the purification procedure for the H188Q mutant.

Lane 1) WT protein control.
Lane 2) Supernatant 1 (after sonication and spin 1).
Lane 3) Supernatant 2 (after heat treatment at 65°C).
Lanes 4-10) Fractions obtained from a Q-sepharose column during the purification procedure.

b) SDS PAGE showing H188Q BIMP fractions obtained from a Q-sepharose column.

Lanes 1-10) Fractions obtained from a Q-sepharose column during the purification protocol. Fractions corresponding to lanes 1 to 8 were pooled and subsequently stored at 4°C as an 80% ammonium sulfate cut.

(a)

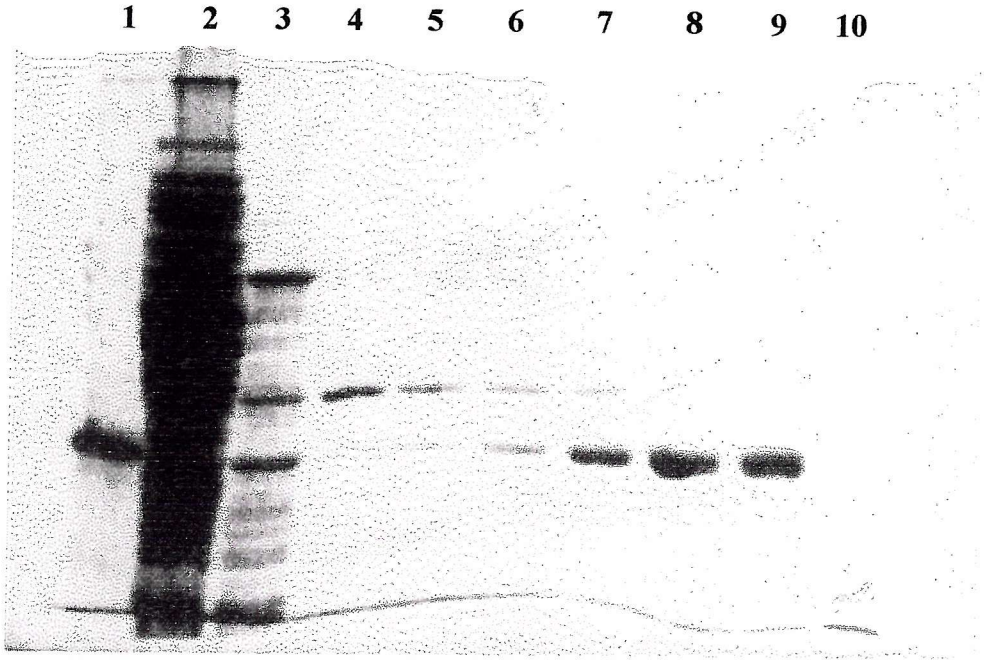

(b)

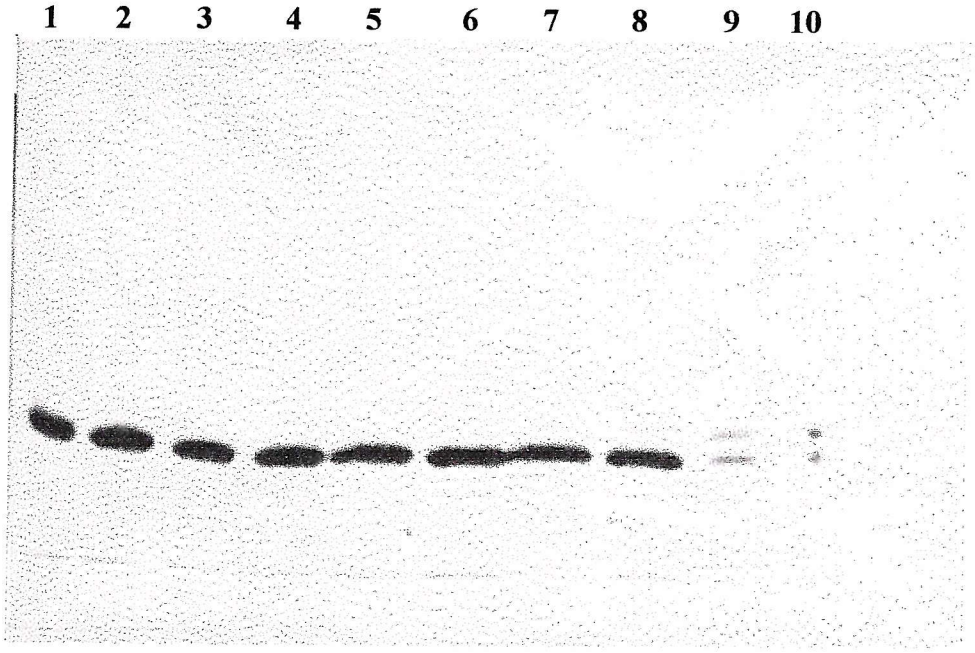

the yield of protein obtained from a typical 4l of bacterial culture for WT and mutant enzymes. Figure 3.10 shows a typical elution profile for H188Q BIMP from a Q-sepharose column at pH 8.0.

Table 3.1 Data for the yield of enzyme obtained from WT and mutant preparations

Enzyme species	% Efficiency	Total protein (mg protein from 4l culture)
WT		154
G76S	50	98
G69S	40	130
H188Q	50	107
E30P	60	93
C218D	50	90
G69D	50	-
H100Q	60	-
R191A	50	-
I269SC	40	-

3.6 CIRCULAR DICHROISM

3.6.1 Introduction

Circular dichroism (CD) is a useful spectroscopic technique which can be used to gain information about the structure and conformation of a protein in solution. CD spectroscopy can provide information on the structural content of the macromolecule, in terms of the secondary and tertiary components together with any motility of flexible regions within the structure. The technique is invaluable for monitoring structural transitions, for example the unfolding from the native to the denatured state can be monitored. In addition, any conformational and local changes arising from ligand binding of molecules such as substrates, cofactors or effectors can also be followed.

Figure 3.10 A typical elution profile for inositol monophosphatase from a Q-sepharose column at pH 8.0. The plot shows the elution of H188Q enzyme as a single peak.

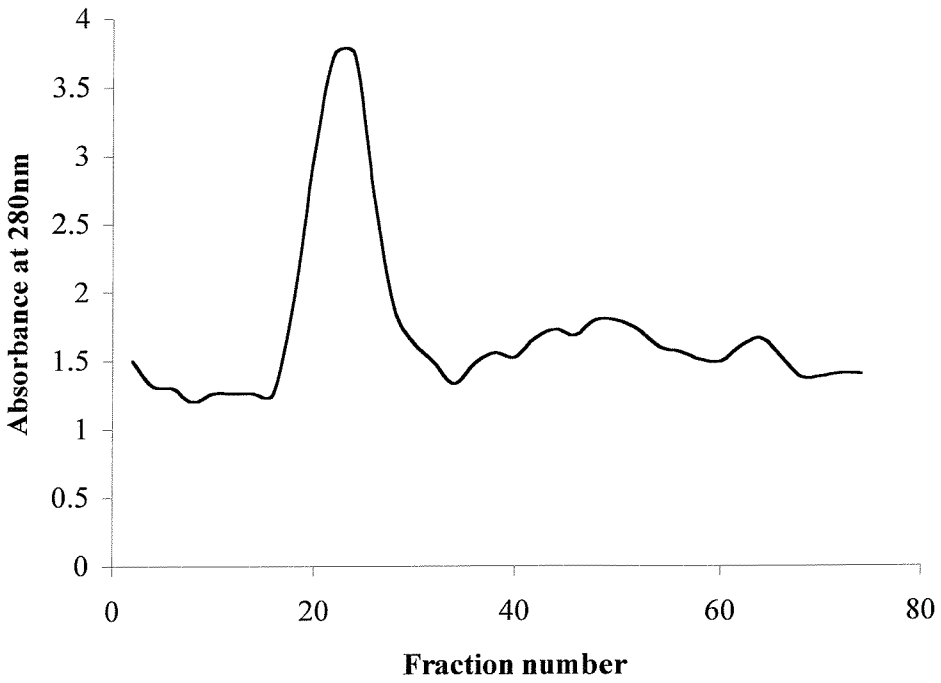
Absorbance at 280nm
4
3.5
3
2.5
2
1.5
1
0.5
0
0
20
40
60
80
Fraction number

3.6.2 Principles of circular dichroism

Circular dichroism (CD) is a form of spectroscopy, which measures the difference in extinction coefficients for left and right circularly polarised radiation (ε_L and ε_R respectively) by a sample containing asymmetric chromophores. CD bands can either be positive or negative, depending on which circular component is absorbed more strongly: in practice, the difference in optical density for the two circularly polarized components (A_L and A_R respectively) is measured directly and converted to a difference in extinction coefficients using the Beer-Lambert law:

$$\Delta\varepsilon = (\varepsilon_L - \varepsilon_R) = (A_L - A_R)/cl = \Delta A/cl$$

Where c is the molar concentration of the sample and l is the path length in cm. CD causes plane polarised light (which may be considered the superimposition of left and right coherent circularly polarised components of equal amplitude) to become elliptically polarised. The ellipticity is defined as the angle whose tangent is the ratio of the minor to the major axis, and may be related to the CD by the expression (Velluz *et al.*, 1965):

$$[\theta_m] = 3300\ \Delta\varepsilon$$

Where the molar ellipticity $[\theta_m]$ has the units deg.cm^2/decimole.
The angle θ is measured in mdeg, and converted to molar ellipticity:

$$[\theta_m] = \theta MRW/10cl$$

where MRW is the mean residue weight (115) for all amino acids, c is the concentration (g/ml), and l is the path length (cm).

3.6.3 CD of proteins

CD is particularly suitable for the study of proteins since it studies molecules in solution and because all amino acids (with the exception of glycine) are asymmetric. In addition, the technique requires only a small quantity of protein and is extremely sensitive to its conformation making it ideal for monitoring conformational changes arising from changes in temperature, pH, salt concentration, solvent composition, ligand binding and quaternary structure. For protein work the molar ellipticity is expressed per decimole of amino acid residues (mean residue weighting):

$$[\theta]MRW = [\theta]/N$$

Where N is the number of amino acid residues in the protein.

Although it is not currently possible to directly relate the measured spectrum to the asymmetric charge distributions that give rise to it, it is nevertheless distinctive for a given protein and may be used empirically to probe its structure. The CD of proteins is conventionally divided into two regions; the far UV (170-250nm) and the near UV (250-320nm).

In the far UV region, the CD is primarily that of peptide bond transitions; although this bond is symmetric, there is usually an asymmetric α-carbon on either side which gives rise to a CD signal which is very sensitive to secondary structure (since α-helical, β-sheet and random coil structures each have characteristic ϕ and ψ backbone dihedral angles). Comparison of the far UV CD spectrum of the sample protein with that of reference spectra determined using proteins comprising entirely of α-helices or β-sheet or random coil can be used to estimate the relative contribution from each type of secondary structure to the measured spectrum (Figure 3.11).

The far UV CD spectrum of an α-helix comprises of three bands, all due to spectral transitions associated with peptide bonds arranged in a right-handed helical array. The longest wavelength negative band at 222nm has a small

3.11 The CD spectra shows the different secondary structure elements (adapted from "Proteins structure"- Creighton, T. E. (1990).

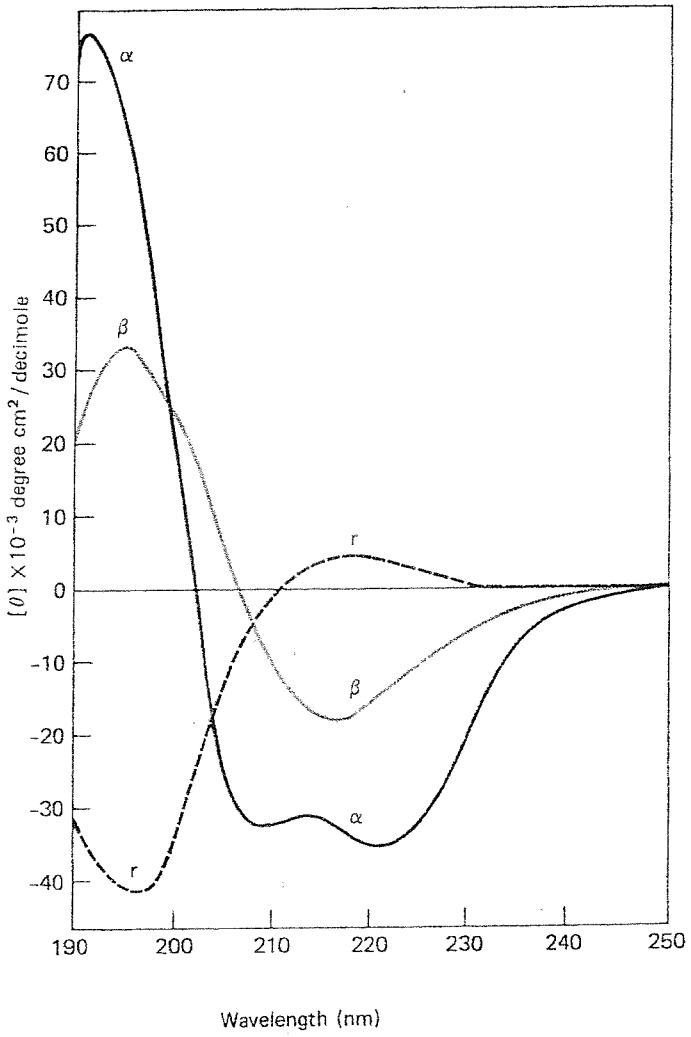
α
β
r
70
60
50
40
30
20
10
0
-10
-20
-30
-40
[θ] ×10⁻³ degree cm² / decimole
190
200
210
220
230
240
250
Wavelength (nm)

extinction coefficient and is often not distinctly perceived. The two shorter wavelength bands, one negative with a shoulder at 207nm and the other positive with a maximum at 190nm are more intense (Woody, 1968). Both parallel and anti-parallel β-sheet structures show a negative CD band at 220 nm and an intense positive band at 200nm (Woody, 1969). β-turns which involve three successive amide groups give a low intensity band at 228nm and two intense CD bands of roughly equal magnitude, but opposite sign at 208 and 190nm respectively (Woody, 1974). Often amides in a protein cannot be classified into one of the above categories of secondary structure. The CD spectrum for such an amide may be approximated by the CD spectrum for a disordered polypeptide (random coil) which has a positive band of low intensity at 217 nm, a negative band of moderate intensity at about 190nm, and a negative band of low intensity at about 175nm. The strongest and most characterstic spectrum arises from α-helices, with β-sheets and random coils being identified less easily. The far UV CD spectrum of a particular protein can be used to estimate the secondary structure composition by applying various mathematical procedures (Provencher and Glockner, 1981; Yang *et al.*, 1986), which essentially assumes that the overall spectrum is a simple accretion of the contribution from the various elements of secondary structure. The method of Provencher and Glockner estimates structure by fitting the sample protein spectrum to spectra from proteins of known secondary structure, while that developed by Yang *et al.*, (1986) uses pure secondary structure elements as standard spectral references.

The near-UV CD spectra of proteins arises from transitions of the aromatic side chains (primarily from Trp, Phe, and Tyr residues) and disulfide bonds and by providing information about the environment of the aromatic amino acid residues, the near UV CD is a sensitive probe of any changes in the tertiary structure of a protein. The positions and intensities of the CD signal of the aromatic residues depends on their local environment within the protein. Tryptophan residues generate ellipticity bands in the 240-320nm spectral interval and tyrosine residues exhibit prominent ellipticity bands at 275nm (Beychok, 1966). Phenylalanine residues generate very weak bands at

wavelengths longer than 240nm and these are often visible as fine structure on the smoother envelopes of the other two aromatics (Moscowitz *et al.*, 1965). Any optical activity in the near UV in the absence of aromatic residues is attributed to disulphide bonds and the spectrum generated is usually broader than that due to aromatic residues (Bayley, 1973; Strickland, 1974). Therefore this region can be used to gain information on the changes in protein conformation brought about by ligand binding.

3.6.4 Previous circular dichroism studies on inositol monophosphatase.

Studies by Ganzhorn *et al.*, (1993) using far UV CD in combination with fluorescence, Raman spectroscopy and empirical prediction methods (based on amino acid sequence analysis) have been used to predict the α-helical and β-sheet content of bovine recombinant inositol monophosphatase. Their studies showed that the enzyme belongs to the α/β class of proteins with 33% α-helix and 29% β-sheet. The Raman spectrum also demonstrated that the three tryptophan residues in inositol monophosphatase are not exposed to solvent and residue W5 was predicted to lie on the hydrophobic face of an amphiphilic helix, W87 was predicted to be part of a short hydrophobic stretch of β-sheet and W219 was located on a hydrophobic part close to the C-terminal (Ganzhorn *et al.*, (1993). In addition, the heat stability of the enzyme was monitored by following the CD signal at 222nm, the mid-point of the transition was determined to be 87°C.

The structural studies carried out by Bone *et al.*, (1992) using the human enzyme further confirmed the prediction of Ganzhorn *et al.*, (1993) mentioned above in that the enzyme is composed of an alternating αβαβα pentalayered structure. According to Manavalan and Johnson, (1983), most proteins containing alternating αβ type structures, contain the following characteristics in the far UV CD spectrum, a maximum at 190nm, a minimum at 222nm and a broad shoulder of ellipticity at 208nm.

The sensitivity of the CD spectrum of inositol monophosphatase to the presence of Mg^{2+} ions has allowed metal ion interactions in both the far UV and near UV CD regions to be investigated. In particular, the binding of Mg^{2+} ions to metal depleted enzyme causes a decrease in molar ellipticity (~15%) at 220nm, yielding a K_m value of 2mM (Pineda *et al.*, (1996)). The authors demonstrated that Mg^{2+} ions function to stabilise the secondary structure relative to the metal-depleted apoenzyme.

The binding of Mg^{2+} ions to IMPase results in an increase in positive ellipticity of approximately 25% at 275nm in the near UV region (Rees-Milton *et al.*, 1997). Titration of Mg^{2+} ions into WT enzyme yielded a K_d value of 275μM and the K_d values for the H217Q and W219F mutant proteins were found to be 292μM and 302μM respectively. From these studies it was concluded that spectral changes at this wavelength (275nm) display metal binding at site 1 i.e. the high affinity site (Rees-Milton *et al.*, 1997).

The binding of Mg^{2+} ions to IMPase results in a 12% decrease in negative ellipticity at 225nm in the far UV region. Titration of Mg^{2+} ions into WT and H217Q and W219F mutant enzymes provided K_d values of 3.9mM, 6.8mM and 29.1mM respectively. The marked difference in the K_d values determined in the near and far UV regions suggests that the far UV spectral change reports primarily on metal ion binding at the low affinity site (site 2) as determined by kinetic studies (see chapter 5). Li^+ ion binding to the enzyme was also observed to result in a 10% increase in ellipticity at 220nm in the far UV and a K_d value of 0.8mM was determined.

3.7 Results and discussion

3.7.1 Far UV CD spectra of WT and mutants of inositol monophosphatase

Far UV CD spectroscopy was used as a means to compare the secondary structure of the mutants (produced by mutagenesis and described in this

chapter; sections 3.1-3.5) to that of the WT enzyme in order to ensure that they are correctly folded i.e. to confirm that the amino acid substitution has not altered the correct folding of the protein. Far UV CD spectra of WT and mutant enzymes (G76S, G69S, E30P, H188Q and C218D) were measured using a 0.1cm cuvette at 25°C at a protein concentration of 6.6μM in 10mM Tris.HCl pH 8.0. Figure 3.12 depicts the far UV CD spectra of WT enzyme. The far UV CD spectra for WT, G76S, G69S, H188Q, E30P and C218D mutants are identical. The CD spectra of WT and mutant enzymes display a number of characteristic features including a broad negative shoulder of ellipticity between 205nm and 210nm, a feature which is typical of the α-helical content of proteins. The molar ellipticity values at 209nm and 222nm determined from the spectra of the individual proteins are presented in Table 3.2. Previous studies have found that typical values for the molar residue ellipticity minimum at 222nm range from 16,600-17,500 deg.cm^2.dmol^{-1} at 222nm for the WT enzyme (Ganzhorn *et al.*, 1993; Rees-Milton *et al.*, 1997). Although the mutants displayed spectra very similar to WT enzyme, the value for the WT enzyme obtained in this study is slightly higher than some published values. This may have arisen due to different methods of preparing the enzyme since earlier studies did not have access to recombinant protein production (Ganzhorn *et al.*, 1993).

3.8 Conformational stability of WT and mutants of inositol monophosphatase

3.8.1 Introduction

Protein stability is an important concept to consider in the understanding of proteins and their respective mutant forms. The correctly folded conformation of a protein, known as the native state is crucial to the function of the protein. The native protein state is maintained by numerous factors which contribute to stability, including forces such as hydrophobic interactions, hydrogen bonds, disulphide bonds, electrostatic and Van der Waals interactions with each contributing similarly quantitatively to the stability. In addition binding of

Figure 3.12 The far UV CD spectra of WT and mutant proteins. All spectra show 0.2mg/ml enzyme in 10mM Tris.HCl pH 8.0 at 25°C.

Table 3.2 The values of $[\Theta_m]$ at 209nm and 222nm in the far-UV CD region for WT, G76S, G69S, H188Q, E30P and C218D enzymes.

Protein	$[\Theta_m]$ 209nm	$[\Theta_m]$ 222nm
WT	15769	21216
G76S	16888	21671
G69S	16784	21515
H188Q	15822	21291
E30P	16683	21291
C218D	15704	21424

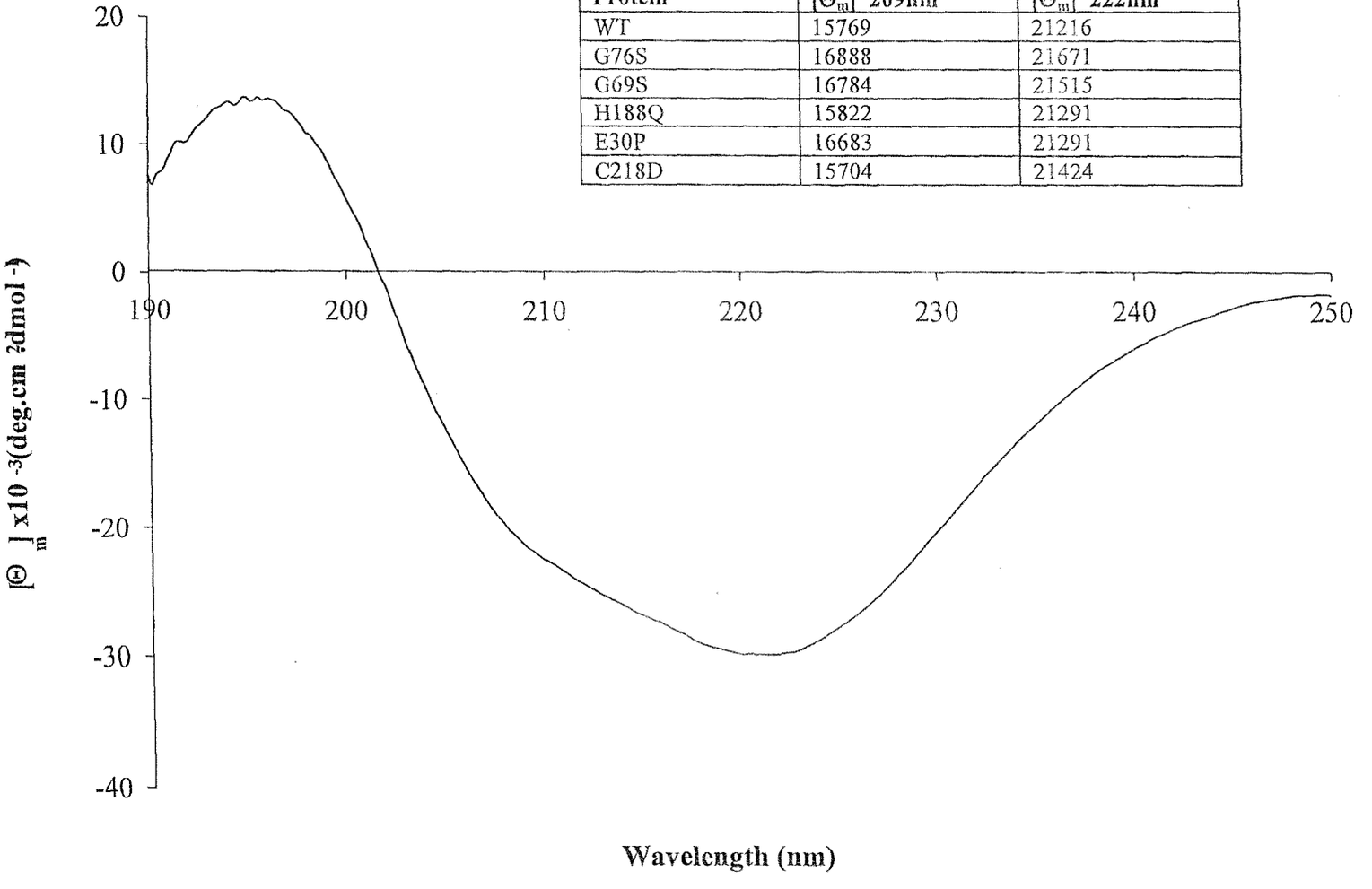

metal ions, and cofactors or substrate act to further increase the stability of some proteins. However, protein stability is easily perturbed by changes such as increases in temperature, pH variation or the addition of a denaturant (urea/guanidinium hydrochloride). This denaturation of the protein structure can result in the disruption of covalent bonds (irreversible chemical denaturation), or reversibly where the covalent bonds remain intact.

Careful study of the conformational stability of a protein can give valuable information about the effects of amino acid substitutions on its secondary, tertiary or quaternary structure (Krauss, 1996). Therefore, controlled unfolding experiments using urea as a denaturant were carried out to investigate whether the mutations made to inositol monophosphatase in these studies result in conformational stability changes.

The unfolding of a protein in the presence of a denaturant may be monitored by a number of techniques including absorption spectroscopy, fluorescence spectroscopy and circular dichroism owing to changes in the spectral properties that occur as it unfolds (Creighton, 1990). Measurement of the extent of unfolding using a range of different techniques should all generate the same curve, which suggests that unfolding is a two-state occurrence, with the fully folded (F) and unfolded (U) states present (Creighton, 1990).

$$F \rightleftharpoons U$$

$$K_{eq} = U/F$$

K_{eq} is used to calculate the free energy change of unfolding, using the equation:

$$\Delta G = -RT\ln K_{eq}$$

$$\Delta G = \Delta G_{H_2O} - m\,[\text{denaturant}]$$

where R is the gas constant (8.315 $Jmol^{-1}$), T is the temperature Kelvin and ΔG_{H_2O} is the difference in free energy between the folded and unfolded states in water and represents the conformational stability of the protein. m is a measure of the dependence of ΔG on denaturant concentration. A plot of ΔG against denaturant concentration provides the value for ΔG_{H_2O} after extrapolation of the line to the y-axis intercept, and the slope of the line determines the value of m.

Typical unfolding curves displays three distinct regions. With initial increases in denaturant concentration, the change in the structure of the protein is minimal (pre-transition region) and any spectral change indicates the effect of the denaturant on the reporter group in the folded protein. This is followed by the transition region that display the unfolding of the protein even with small increments of denaturant concentration. The final post-transition region of the curve shows the variation of the spectral properties of the reporter group with denaturant concentration in the unfolded protein.

Analysis of protein unfolding using these curves is based on the two-state model Pace, (1986) where there is no accumulation of intermediates and only the folded and unfolded species are present. The transition region can then be used to determine the equilibrium constant, K_{eq} of the unfolding followed by ΔG_{H_2O} from the plot of ΔG versus denaturant concentration.

3.8.2 The use of fluorescence spectroscopy as a probe of protein stability

In this chapter fluorescence spectroscopy was employed to measure the conformational stability of WT and mutant forms of inositol monophosphatase in order to determine if the mutation had an overall affect on the stability of the protein.

By monitoring protein fluorescence changes it is possible to follow the unfolding of proteins. Intrinsic protein fluorescence primarily arises due to contribution from three amino acid residues, tryptophan, tyrosine and

phenylalanine. Of the three residues tryptophan, with its higher extinction coefficient gives the greatest fluorescence contribution to the emission from a protein (Szabo, 2000; also see chapter 4). Due to the hydrophobic nature of the indole side-chain of tryptophan, it is usually partially or deeply buried within the tertiary structure of a protein, with an emission maximum around 320-340nm. This decrease in emission maximum is as a result of a decrease in the polarity of the immediate environment when the tryptophan residue is buried and removed from the aqueous solvent. The quantum yield of the tryptophan residue in proteins is also influenced by its microenvironment, for instance by its proximity to quenching groups, namely amino acid side chains, peptide bonds and solvent. Therefore this parameter varies for different proteins as their different tertiary structures place tryptophan residues in unique environments. Therefore the unfolding process can be followed by monitoring the red shift in the wavelength of maximum emission that occurs as a result of increased exposure of the tryptophan to solvent shift and or by the change in fluorescence emission intensity.

3. 8.3 Previous stability studies on inositol monophosphatase

Studies carried out by Gee *et al.*, (1988) demonstrated that incubation of bovine inositol monophosphatase with urea concentrations exceeding 4M resulted in a progressive loss of activity. However, overnight dialysis (or dilution) resulted in complete restoration of the enzyme activity, thus, suggesting the reaction to be reversible. Similarly, inositol monophosphatase isolated from pig brain was also found to display reversible unfolding in guanidine hydrochloride as determined by the complete restoration of catalytic activity after dilution of the guanidine hydrochloride treated samples Kwon *et al.*, (1993). These authors proposed a model in which the dimeric protein unfolds in a single cooperative manner from folded dimer to two unfolded monomers.

The unfolding and refolding processes monitored by stopped-flow fluorescence spectroscopy Moreno *et al.*, (1996) showed that the enzyme unfolded in a single exponential process with rate constants of 80-65s^{-1}

corresponding to guanidine hydrochloride concentrations of 5M to 3.6M respectively at 25°C. The protein was found to refold with a rate between 120 to $65s^{-1}$ in solutions of 1M to 3.6M guanidine hydrochloride at the same temperature. No intermediate forms of inositol monophosphatase were detected during the course of the refolding of inositol monophosphatase from unfolded enzyme Moreno *et al.*, (1996). It was also found that enzyme denatured in 5M Gdn.HCl still displayed terbium (Tb^{3+}) binding, suggesting that some residual structure remains in metal binding site 1 in the denatured enzyme.

More recently, Lau *et al.*, (1998) investigated the stability of porcine inositol monophosphatase in the presence of increasing urea concentrations. The urea-treated enzyme displayed Co^{2+} ion binding with a K_d of 3.3μM. Therefore, the proposal of Kwon *et al.*, (1993) that the dimer dissociates into two unfolded monomers was modified to a model in which the monomeric species retains some folding (perhaps an expanded globular form of inositol monophosphatase) in the presence of 8M urea. Once again it was shown that the affinity of the 8M urea treated enzyme for Tb^{3+} ions was unaffected suggesting that the metal-coordination site 1 of the porcine enzyme is also retained upon exposure to high concentrations of denaturant. In identical assay systems Mg^{2+} ions failed to activate inositol monophosphatase in 8M urea and this was mainly attributed to the lower affinity constants of these metal ions for the enzyme, Lau *et al.*, (1998).

3.9 Results and discussion

In this chapter intrinsic protein fluorescence has been used to observe protein unfolding over increasing concentrations of urea. Fluorescence emission intensity was monitored at both 320nm and 360nm (excitation at 280nm). Measurement of the fluorescence at these wavelengths allows the change in microenvironment of the tryptophan residues of bovine inositol monophosphatase to be monitored. In the folded enzyme the fluorescence at 320nm is indicative of tryptophan residues buried within a protein. The

fluorescence of solvent exposed tryptophan residues tends to show an emission maximum around 360nm. On unfolding, the fluorescence emission intensity at 320nm decreases and the fluorescence emission intensity at 360nm increases with increasing concentrations of urea. This shows that the tryptophan fluorescence is quenched in the folded protein by neighbouring groups. For example, Trp219 is close to Asp217 and to other metal binding ligands such as Asp220. Thus on unfolding the quenching diminishes as the Trp residue moves away from these groups and its quantum yield increases. The ratio of the intensities at the two wavelengths was calculated and plotted against the concentration of denaturant used. This method of data handling has the added advantage that it automatically corrects for slight differences in protein concentrations.

3.9.1 The stability of WT and mutants forms of inositol monophosphatase in the absence and presence of Mg^{2+} ions

Figure 3.13(a) shows a typical unfolding curve, in this case obtained for the WT enzyme in the absence of 10mM Mg^{2+} ions together with the secondary plot (Figure 3.13(c) used to determine the ΔG_{H2O} value. These parameters for the WT and mutated enzymes are listed together with the values of m in Table3.3.

3.9.2 G76S mutant

The conformational stability of G76S (11.0 ± 0.5kJmol^{-1}) is slightly lower than the value determined for WT enzyme (13.3 ± 0.7kJmol^{-1}). However, the increase in stability in the presence of 10mM Mg^{2+} ions for both G76S and WT is in the same order (c.f. 15.5 ± 0.8kJmol^{-1} and 17.7 ± 1.1kJmol^{-1} for G76S and WT respectively), being ~ 4.1kJmol^{-1}. This stabilising effect of the Mg^{2+} ions on the tertiary structure of the enzyme (detected by Trp fluorescence changes) is in agreement with previous controlled unfolding studies (using CD and GdnHCl as the denaturant) that showed that Mg^{2+} ions

Figure 3.13(a) The unfolding of WT BIMP in urea in 50mM Tris.HCl buffer pH 8.0 at 32°C (without Mg^{2+}), (b) The percentage of WT BIMP unfolded and (c) the ΔG of unfolding of WT BIMP.

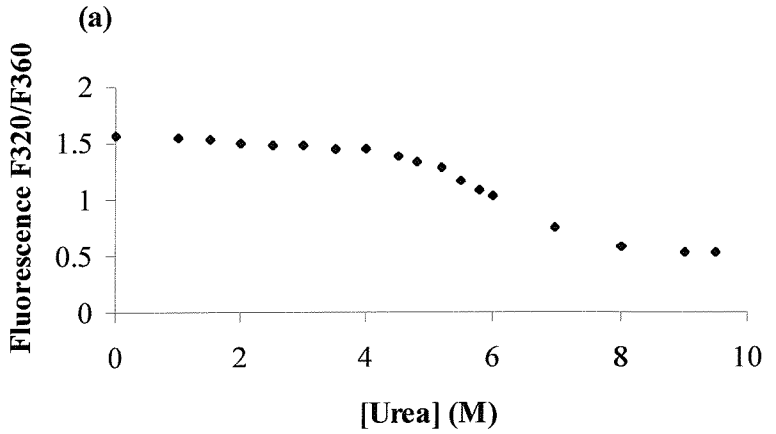
(a)
Fluorescence F320/F360
2
1.5
1
0.5
0
0
2
4
6
8
10
[Urea] (M)

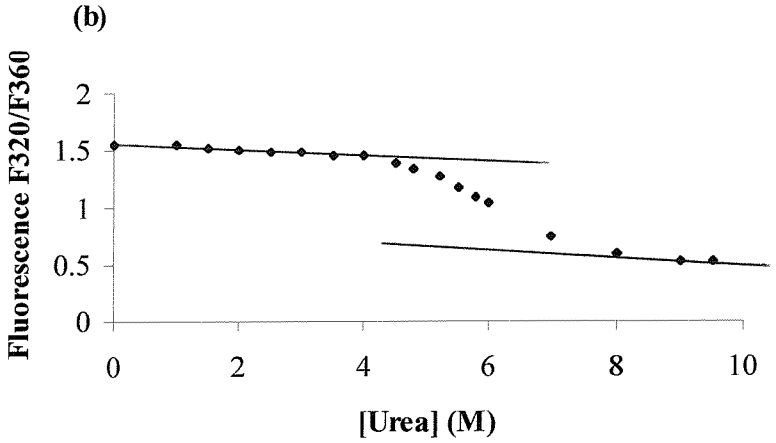
(b)
Fluorescence F320/F360
2
1.5
1
0.5
0
0
2
4
6
8
10
[Urea] (M)

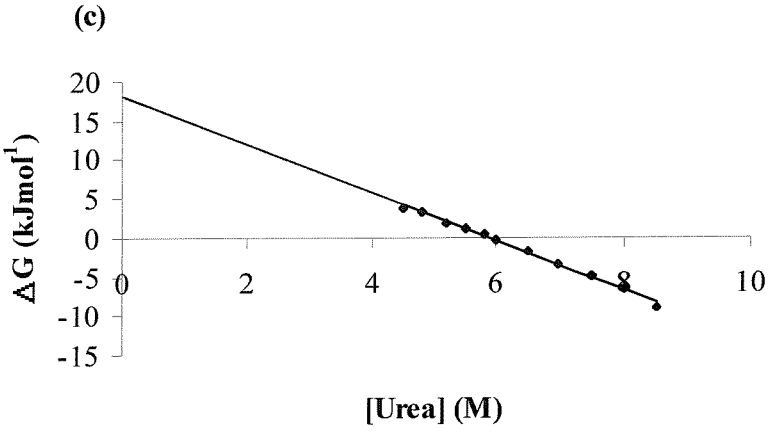
(c)
ΔG (kJmol-1)
20
15
10
5
0
-5
-10
-15
0
2
4
6
8
10
[Urea] (M)

have a stabilising effect on the secondary structure of the enzyme (Pineda *et al.*, 1996).

3.9.3 G69S mutant

The G69S mutant displays the most marked reduction in conformational stability compared to that of WT enzyme (8.9 ± 0.8kJmol^{-1} compared to 13.3 ± 0.7kJmol^{-1} respectively. In chapters 4 and 5, it was demonstrated that the affinity of G69S for Mg^{2+} ions (in particular at site 1, but also at 2) was decreased significantly and it is possible that this loss of stability results in a reduced affinity for Mg^{2+} ions. Since this residue is not catalytically important, the same cause could underlie the decreased value of the maximum specific activity shown in chapter 5. The stability of this mutant in the presence of Mg^{2+}, is increased by only 3.3kJ mol^{-1} compared to the higher values observed for the other mutants (see Table 3.3).

3.9.4 E30P mutant

The conformational stability of E30P mutant (11.4 ± 0.7kJmol^{-1}) is slightly less than that of WT (13.3 ± 0.7kJmol^{-1}), in fact it is very close to that of G76S and displays a similar increase in stability (~4kJmol^{-1}) in the presence of 10mM Mg^{2+} (see Table 3.3).

3.9.5 H188Q mutant

The stability of H188Q (12. ± 0.1kJmol^{-1}) shows a slight decrease with respect to WT (13.3 ± 0.7kJmol^{-1}). However, the effect of the additional presence of Mg^{2+} is somewhat less than that observed for the other mutants i.e. the value for ΔG is increased by only 1.5kJmol^{-1} compared to values ranging from 4 to 4.5kJmol^{-1} for WT and most of the other mutant enzymes. The decreased conformational stability value in the presence of Mg^{2+} could be due to the reduced affinity of Mg^{2+} at site 2.

3.9.6 C218D mutant

The C218D mutant shows a slight increase in the conformational stability in the absence of Mg^{2+} ions ($14.5 \pm 0.4 kJmol^{-1}$) compared to that of WT enzyme ($13.3 \pm 0.7 kJmol^{-1}$), however, the value in the presence of 10mM Mg^{2+} ions shows only a $3kJmol^{-1}$ increase to $17.6 \pm 0.9 kJmol^{-1}$.

3.9.7 Conclusions

Thus the amino acid substitutions carried out have generated proteins with different conformational stabilities ranging from $13.3 \pm 0.7 kJmol^{-1}$ for the WT enzyme to $8.9 \pm 0.8 kJmol^{-1}$ for the G69S mutant. These experiments have shown that stability measurements are more sensitive probes of structural differences than CD experiments that suggested that the global folding of these proteins is similar (Table 3.2). However, comparison with similar experiments carried out with other proteins (Krauss, 1996; Drewett, 1997) suggest that these changes (with the possible exception to that of the G69S mutant) are not very large. Almost certainly the best measurement of the effect of mutations on the structure of an enzyme is the kinetic parameters K_m and V_{max}. These are the subject of studies described in chapter 5.

Table 3.3 A summary of the unfolding parameters for WT and mutant forms of inositol monophosphatase

Protein	ΔG ($kJmol^{-1}$) without Mg^{2+} m (kJ)	ΔG ($kJmol^{-1}$) with Mg^{2+} m (kJ)
WT	13.3 ± 0.7 (m = 2.3)	17.7 ± 1.1 (m = 2.4)
G76S	11.0 ± 0.5 (m = 1.6)	15.7 ± 0.8 (m =3.14)
G69S	8.9 ± 0.8 (m = 2.9)	12.3 ± 0.4 (m = 2.2)
E30P	11.4 ± 0.7 (m = 2.1)	15.4 ± 0.4 (m = 2.3)
H188Q	12.0 ± 0.1 (m = 2.5)	13.5 ± 0.7 (m =3.5)
C218D	14.5 ± 0.4 (m = 2.4)	17.6 ± 0.9 (m = 2.8)

CHAPTER 4

THE USE OF FLUORESCENCE SPECTROSCOPY TO STUDY EQUILIBRIUM AND PRE-EQUILIBRIUM BINDING

CHAPTER 4

The use of fluorescence spectroscopy to study equilibrium and pre-equilibrium binding

4.1.1 Introduction

The absorption of a quantum of light by an electron in a molecule can result in its transition from the ground state to an excited state of higher energy level. Following this event, the electron drops to the lowest vibrational level of the excited state. During this process internal conversion takes place and energy is lost as heat. The return of the electron to the ground state results in the energy being either re-emitted as radiation (i.e. the process of fluorescence) or in non-radiative processes such as heat, resonance energy transfer or by quenching. Since some energy is lost in the internal conversion process as heat, the emitted light is at a lower frequency and therefore a longer wavelength (i.e. lower energy) than the wavelength of incident light (see scheme1). This phenomenon is referred to as the Stoke's Shift (Stoke, 1852). The non-radiative processes provide an alternative mechanism for molecule to return to the ground state, and thus results in a lower quantum yield of fluorescence. Consequently the fluorescence intensity and λ_{max} are very sensitive to the environment.

Scheme 1:

The energy (E) of a quantum of energy is represented by the expression

$$E = hv$$

where h is Planck's constant (6.02×10^{-27} Js^{-1}), v is the frequency of light. Consequently a decrease in E results in a concomitant decrease in v and this results in an increase in λ (termed the Stoke's shift).

The lifetime of fluorescence (τ, the period of time in which the molecule spends in the excited state) is of the order of 10^{-9} to 10^{-8} seconds and is influenced by the environment of the fluorophore. Therefore this feature allows fluorescence spectroscopy to be used in the investigation of structural and conformational changes taking place in macromolecules.

Quantum yield (ϕ) is an important factor in determining the likelihood of fluorescence. It represents the percentage of absorbed energy, which can be re-emitted as fluorescence and is represented by the following ratio:

$$\phi = \frac{\text{number of quanta emitted}}{\text{number of quanta absorbed}}$$

The process of fluorescence makes use of two types of fluorophores, either intrinsic (contained within the protein) or extrinsic (require addition to the protein). Proteins contain 3 intrinsic fluorophores - phenylalanine, tyrosine and tryptophan. These can be used to investigate conformational changes of proteins or folding and unfolding transitions. In proteins the fluorescence is dominated by the contribution from tryptophan because although its quantum yield (0.13) is similar to that of tyrosine (0.14, Eftink and Maity, (2000)) its molar extinction coefficient is much higher (5,600M^{-1} cm^{-1}, 1400M^{-1} cm^{-1}, respectively). Consequently more photons of light are absorbed and thus from the definition of quantum yield, more photons are emitted.

Other naturally occurring fluorophores include flavins, chlorophyll, Vitamin A, and NADH. In addition to the naturally occurring fluorophores used in the study of macromolecules, many fluorescent probes can be introduced to the macromolecule by either binding or chemical coupling (Gore, 2000).
For instance a number of lanthanide ions have observable fluorescence properties and therefore can be used as probes for non-fluorescent ions, notably Ca^{2+} and, sometimes Mg^{2+}. For a particular compound to be considered a good extrinsic fluorophore, it has to satisfy a number of criteria: it has to bind tightly to an appropriate site with subsequent fluorescence upon

binding, its fluorescence signal should be sensitive to environmental changes and the fluorophore must not alter the stability or properties of the protein.

4.1.2 Resonance energy transfer

As discussed previously, extrinsic reporter groups are molecules that can bind macromolecules and as a result emit signals that report on changes in their microenvironment. Pyrene maleimide is one such fluorescent reagent that has been used extensively in this study. Pyrene maleimide is a cysteine-specific chemical modification reagent that forms fluorescent adducts with proteins or macromolecules containing sulfhydryl groups (Weltman *et al.*, 1973; Gupte *et al.*, 1983). Pyrene maleimide is usually non-fluorescent, and reaction with an available thiol group generates its fluorescent properties. The label (Figure 4.1(a)) attaches covalently to an available thiol to form a fluorescent adduct with an emission spectrum as shown in Figure 4.1(b). In view of the fact that tryptophan fluoresces at 340nm when excited at 280nm, there is a good spectral overlap for resonance energy transfer (RET) to occur from the donor (tryptophan residue) to the acceptor (pyrene label). This non-radiative form of energy transfer is also accompanied by a quenching of protein fluorescence in the 340nm region upon excitation at 280nm as shown in Figure 4.1(b). The fluorescence emission spectra, for unlabelled protein (λ^{ex} = 280nm) is also included in Figure 4.1(b). There are a number of criteria that need to be met in order for efficient RET to occur: there must be an appreciable overlap between the emission spectrum of the donor fluorophore and the absorption spectrum of the acceptor fluorophore, the two fluorophores involved must be suitably orientated with respect to each other with a typical distance between them being no greater than 25-35nm (Förster, 1949).

4.1.3 Studies on the use of pyrene maleimide as a probe of Mg^{2+} binding to inositol monophosphatase and mutant enzymes

Bovine inositol monophosphatase contains 6 cysteines (8, 125, 141, 184, 201 and 218) while the human enzyme contains an additional residue at position

Figure 4.1 (a) Shows the fluorescent pyrene maleimide label covalently attached to an enzyme thiol group, (b) Fluorescence emission spectra of the modified and unmodified (native) enzyme.

(a)

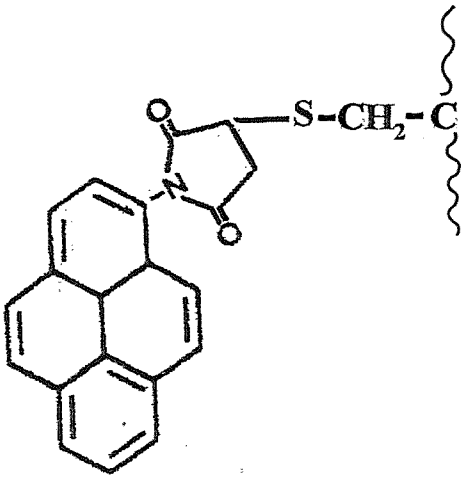

Pyrene-maleimide attached to a cysteinyl side chain

(b)

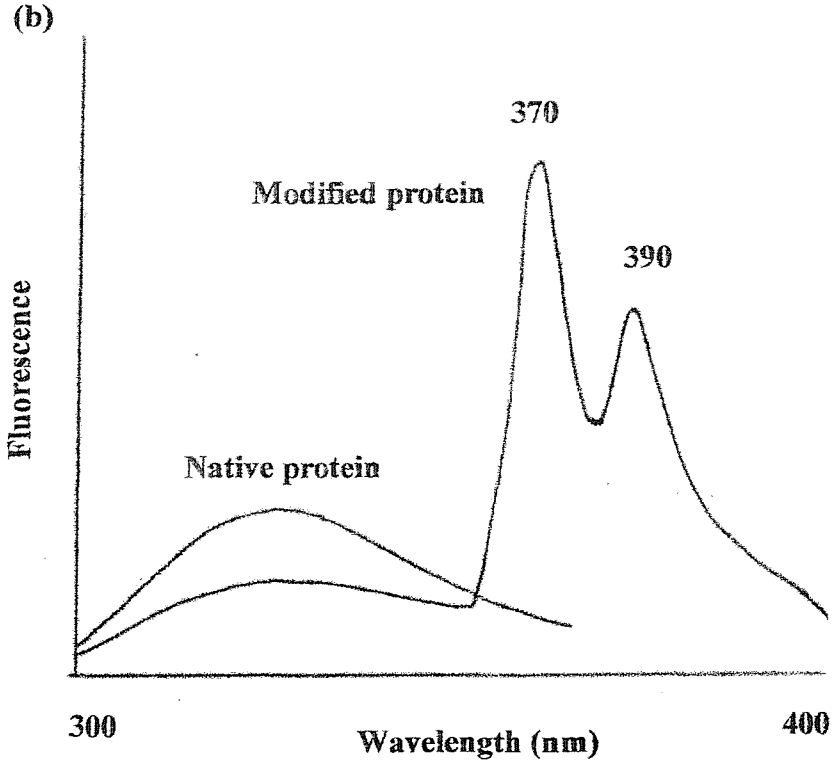

24 (this is an arginine in the bovine sequence). Cysteine 141 and 184 are susceptible to modification by cysteine-specific reagents such as DTNB, iodoacetic acid, and N-ethylmaleimide in a mutually exclusive manner (Knowles *et al.*, 1992; Greasley *et al.*, 1994).

Initial studies on the use of pyrene maleimide as an important reagent for labelling cysteine residues were carried out by Greasley *et al.*, (1994).
There are two residues that have been identified as those modified by this reagent (C141 and C218). The stoichiometric addition of pyrene maleimide to inositol monophosphatase leads to almost exclusive modification of C218 (98%: 2% C218:C141 respectively) with no resultant loss in enzyme activity.
Previous studies in which N-ethylmaleimide was used to covalently label sulfhydryl groups in inositol monophosphatase led to the proposition that C218 lies at or near the active site (Knowles *et al.*, 1992). However, mutagenesis studies changing C218 to alanine led to the conclusion that this residue is not essential for catalytic activity, but that the modification by NEM inhibits the enzyme by steric means (Knowles *et al.*, 1992). The high resolution X-ray crystallographic structure of the human form of the enzyme has confirmed the close proximity of this residue to the active site, in particular to residue D220, which has been shown to be an important metal binding ligand at site 2. Greasley *et al.*, (1994) have shown that the fluorescence properties of the pyrene maleimide label when bound to the protein can be used as a tool to monitor metal ion interactions to the high affinity site 1.

Further to this, residues surrounding the C218 residue have also been mutated in an attempt to assign any functional or structural roles. Residues H217 and W219 were mutated to Gln (Q) or Phe (F) respectively and C218 then labelled using pyrene maleimide for ligand binding studies. Both H217Q and W219F were shown to bind Mg^{2+} ions and the amplitude of the accompanying signal change observed at 380nm upon excitation at 340nm, was found to be typically the same as that for WT enzyme (18-23%). In addition, metal ion titrations conclusively showed that metal binding at site 1 was unaffected in these mutant enzymes (K_d values for H217Q and W219F being 280 ± 35μM

and 271 ± 22μM respectively (Thorne *et al.*, 1996) compared to 300μM for WT enzyme (Greasley *et al.*, 1994)).

In studies reported here C218 has been labelled by the fluorophore in order to to investigate the effects of mutations on the binding of Mg^{2+} to the enzyme. In doing so, the results are compared to WT inositol monophosphatase so as to detect any differences in binding phenomena.

4.2 Results and Discussion

4.2.1 Fluorescence emission spectra of wild type and mutant forms of inositol monophosphatase

Before any fluorescence experiments were attempted it was necessary to examine the spectral properties of the mutated enzymes in case they had been altered by the mutation. Figure 4.2 illustrates the fluorescence emission spectra of WT, G76S, G69S, H188Q, E30P and C218D enzymes. All proteins (3μM) were prepared in 50mM Tris.HCl buffer at pH 8.0 and at 25°C. Using an excitation wavelength of 280nm each of the mutants and WT were scanned and the fluorescence emission spectra obtained. In WT enzyme the emission maximum occurs at 335nm as tryptophan emission dominates the spectrum (Figure 4.2). This is the highest fluorescence intensity shown out of all the proteins studied. The emission from the G76S mutant is approximately 13.5% lower than that of the WT enzyme. All spectra have a wavelength of maximum emission around 335nm, which is characteristic of tryptophan residues buried within the protein. The H188Q mutant, in addition to showing a 17.5% decrease in protein fluorescence intensity, also shows a small blue shift in the emission maximum from 335nm to 330nm. This indicates that a slight change in the polarity of the environment has taken place due to the mutation of the histidine to a glutamine residue. The E30P mutant shows an almost identical spectra, to that of WT with maximal emission intensity at 335nm, but a 15.1% decrease in the quantum yield of emission. This could be due to a structural change, which causes increased exposure of the tryptophan

Figure 4.2 Fluorescence emission spectra for WT (—), G76S (—), G69S (—), H188Q (—), E30P (—) and C218D (—). Fluorescence emission spectra were obtained at 335nm for 3μM enzyme in 50mM Tris.HCl, pH 8.0 at 25°C using an excitation wavelength of 280nm.

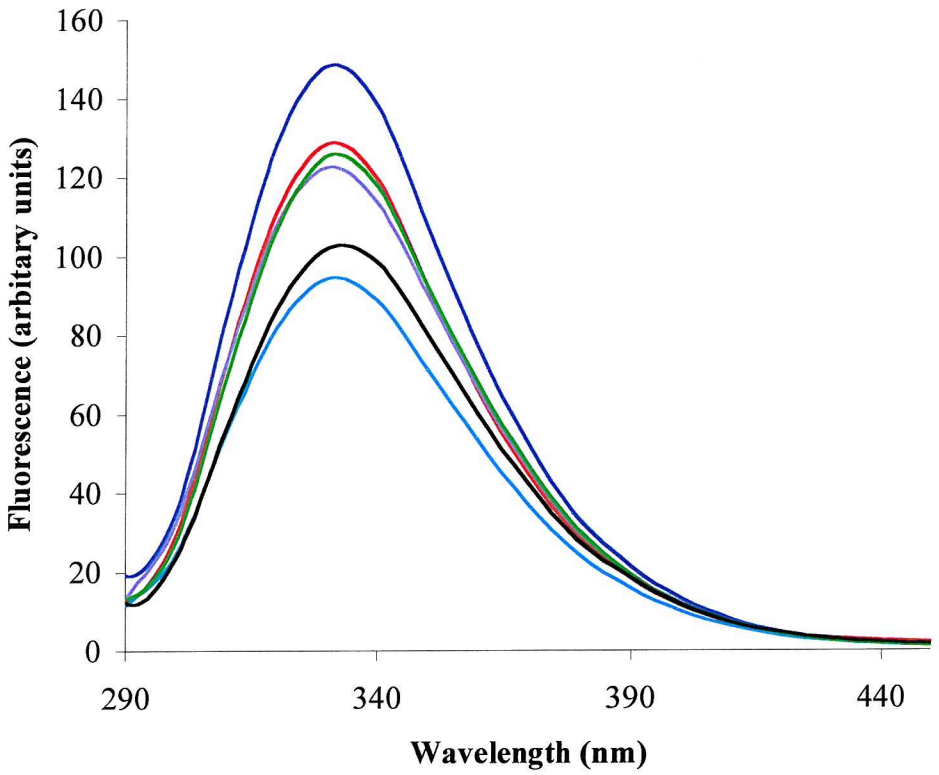
160
140
120
100
80
60
40
20
0
Fluorescence (arbitary units)
290
340
390
440
Wavelength (nm)

residues to the solvent and resulting in increased collisional or static quenching. The spectrum obtained for the C218D mutant protein shows a 30% decrease in the fluorescence emission maximum. This is probably as a result of the addition of a charged aspartate residue, which may cause static quenching of the neighbouring tryptophan residue (W219). The G69S mutant shows a 36.3% decrease in quantum yield of the tryptophan relative to WT enzyme. This could be due to a structural change, resulting in one or more of the more exposed tryptophan residues being quenched by increased collisional or static quenching.

None of the fluorescence emission spectra were altered by the presence of Mg^{2+} ions (data not shown).

4.2.2 Measurement of the stoichiometry and the rate of modification of WT and mutant forms of inositol monophosphatase by pyrene maleimide

Pyrene maleimide was used to modify WT inositol monophosphatase and mutants G69S, G76S, H188Q and E30P. Stoichiometric addition of the reagent to WT enzyme has been shown to result in the sole modification of C218 (Greasley *et al.*, 1994). Figure 4.3 depicts the data from experiments in which 1:1 mol:mol reaction (lower curve) and 1:5.6 mol:mol reaction of WT and mutant enzymes by pyrene maleimide was carried out. The graph shows the increase in fluorescence at 380nm accompanying the covalent attachment of the pyrene label to the wild type or mutant enzymes. The stoichiometry of label incorporation was determined after modification and overnight dialysis (or by passing the sample down a Sephadex G-10 column), the protein concentration was determined using the BCA method and the absorbance at 340nm ($\varepsilon_{340} = 36000\mu M^{-1}\ cm^{-1}$), was used to measure the pyrene label. The ratio describes the number of C218 residues labelled (Table 4.1). From the table it can be seen that the number of residues labelled for wild type, G76S, H188Q and E30P enzymes are similar to previously published values made for wild type bovine inositol monophosphatase labelled under the same conditions (cf. bovine enzyme 1.89 mol ± 0.13 mol of pyrene label per mol enzyme

Figure 4.3 Pyrene maleimide labelling of (a) WT, (b) G76S, (c) G69S, (d) H188Q and (e) E30P. 33μM pyrene maleimide and 33μM protein in 50mM Tris.HCl buffer pH 8.0 at 25°C were reacted and the change in fluorescence intensity at 380nm (λ^{ex} = 280nm) recorded with time (for a 1:1 addition (—)). A 5.6 molar excess of the pyrene maleimide was also reacted with each of the enzymes (—) to label both the C218 and C141 residues.

(a)

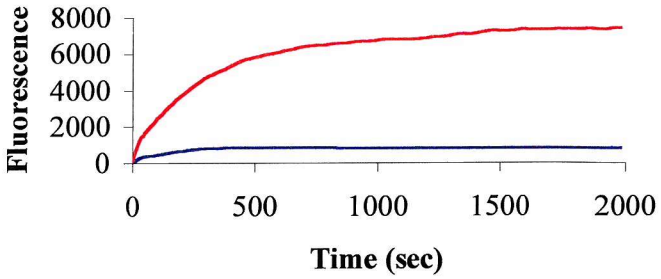
Fluorescence
8000
6000
4000
2000
0
0
500
1000
1500
2000
Time (sec)

(b)

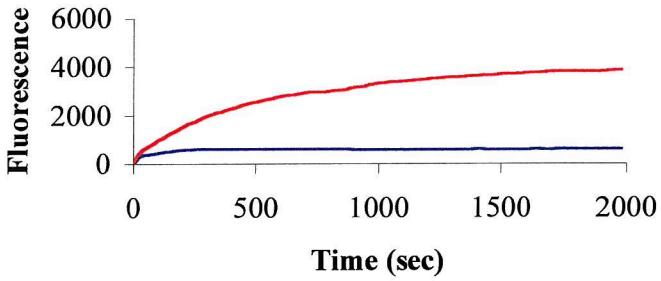
Fluorescence
6000
4000
2000
0
0
500
1000
1500
2000
Time (sec)

(c)

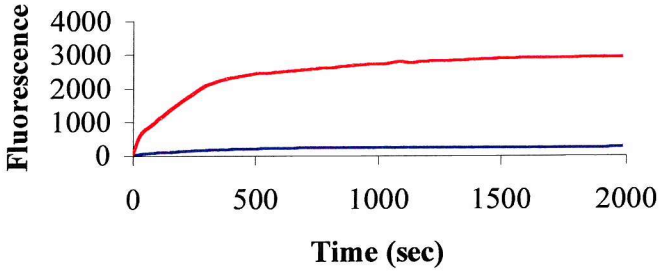
Fluorescence
4000
3000
2000
1000
0
0
500
1000
1500
2000
Time (sec)

(d)

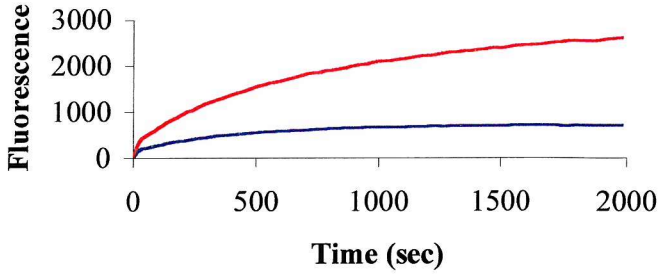
Fluorescence
3000
2000
1000
0
0
500
1000
1500
2000
Time (sec)

(e)

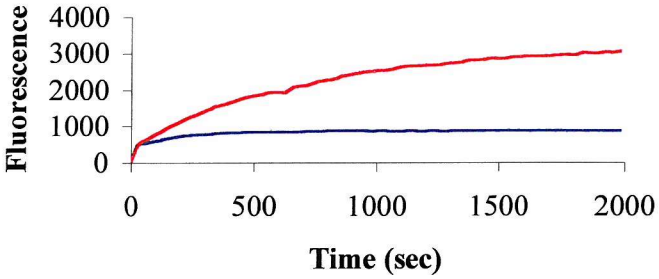
Fluorescence
4000
3000
2000
1000
0
0
500
1000
1500
2000
Time (sec)

Table 4.1 The rates of modification of WT inositol monophosphatase and G76S, G69S, H188Q and E30P substituted mutants by pyrene maleimide. Also shown is the number of residues labelled by a 5.6 molar excess of the fluorescent probe pyrene maleimide. For conditions see text (section 4.2.2).

Protein	Rate of modification (min^{-1})	Number of residues labelled
WT	$k_1 = 5.3 \pm 0.3$ $k_2 = 0.12 \pm 0.01$	1.9
G76S	$k_1 = 5.0 \pm 0.2$ $k_2 = 0.15 \pm 0.003$	1.8
G69S	$k_1 = 4.8 \pm 0.5$ $k_2 = 0.15 \pm 0.004$	1.2
H188Q	$k_1 = 5.0 \pm 0.3$ $k_2 = 0.13 \pm 0.01$	0.9
E30P	$k_1 = 4.9 \pm 0.5$ $k_2 = 0.15 \pm 0.004$	1.8

subunit, Greasley *et al.*, 1994). For H188Q, only 0.9 mol of pyrene label was seen to react per mol of enzyme.

Greasley *et al.*, (1994) have previously shown that excess pyrene labelling occurs in two phases, a fast phase with a rate of 5.45 ± 0.31 min^{-1}, (corresponding to the labelling of C218) and a slow phase with a rate of 0.077 ± 0.31 min^{-1} (corresponding to the labelling of C141). Figure 4.3 illustrates the pyrene maleimide labelling of WT together with mutants of inositol monophosphatse. As mentioned previously, the lower curve depicts a 1:1 mixture of enzyme to pyrene maleimide label (49.5µl of 1mM pyrene label added to 33µM enzyme) and the other the curve generated when the WT and mutant enzymes were reacted with a 5.6 molar excess of this reagent (10µl of 1mM pyrene maleimide to 1.5ml of 1µM enzyme).

Table 4.1 also lists the rate of modification of C218 and C214 residues for the WT and mutant enzymes. The fast rate corresponding to the modification of C218 for mutants G76S, G69S, H188Q and E30P was seen to be the same rate as for WT enzyme (4.8 - 5.0 ± 0.2-0.5 min^{-1} for mutants cf. WT (5.3 ± 0.3 min^{-1}) suggesting that the replacement of G76 and G69 by a serine residue and the replacement of H188 and E30 by glutamate and proline respectively does not affect the accessibility of these residues to the label. Previously published values for this fast reacting residue are in close agreement with those obtained here (WT = 5.45 ± 0.3 min^{-1}, Greasley *et al.*, 1994 and Thorne *et al.*, 1996). The rates of labelling of the slow reacting C141 residue show similar values for the WT, G76S, G69S, H188Q and E30P mutants, reporting unchanged accessibility of the C141 residue for the pyrene maleimide label.

4.2.3 Signal change elicited upon Mg^{2+} binding to pyrene labelled WT and mutant inositol monophosphatase

Figure 4.4 shows spectra obtained upon the addition of 20mM Mg^{2+} to each of the mutants and WT. With the exception of G69S, all mutant enzymes display

Figure 4.4 Fluorescence emission spectra of pyrene-maleimide labelled (a) WT, (b) G76S, (c) G69S, (d) H188Q, (e) E30P and (f) C218D enzymes (—) and the signal change on addition of 20mM Mg^{2+} ions (—).

(a)

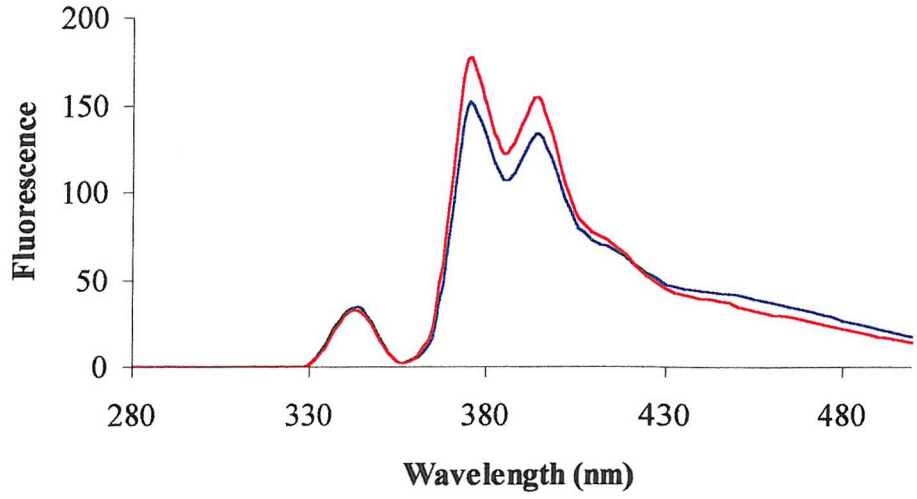
Fluorescence
200
150
100
50
0
280
330
380
430
480
Wavelength (nm)

(b)

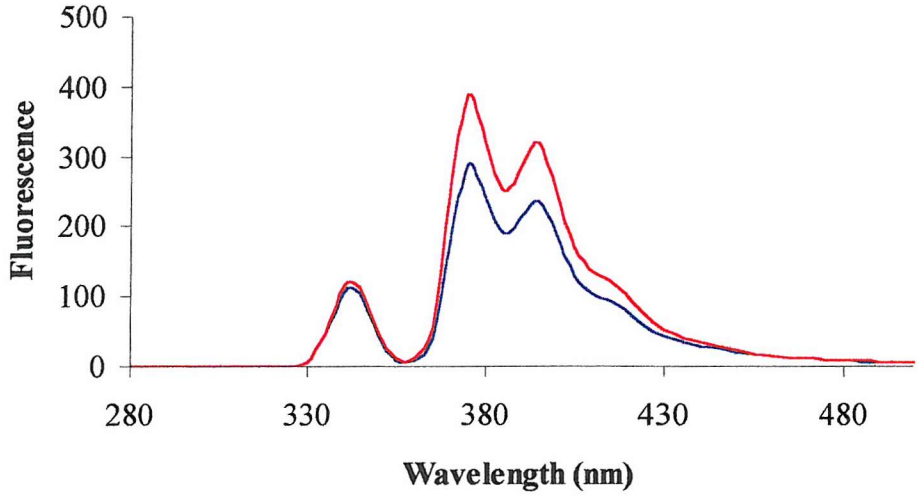
Fluorescence
500
400
300
200
100
0
280
330
380
430
480
Wavelength (nm)

(c)

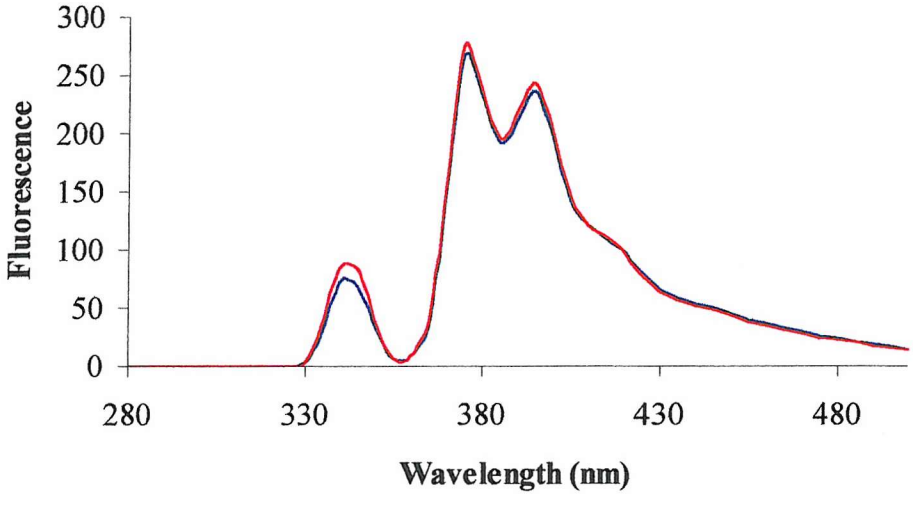
Fluorescence
300
250
200
150
100
50
0
280
330
380
430
480
Wavelength (nm)

(d)

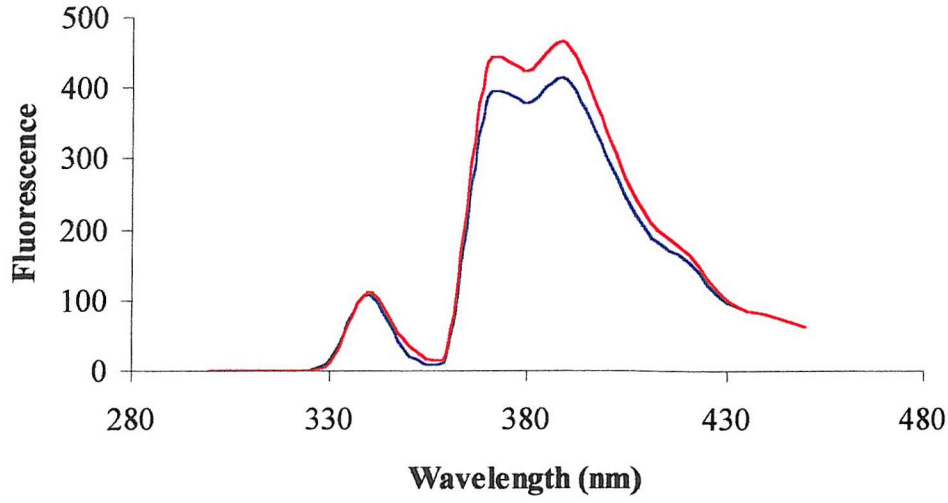
Fluorescence
500
400
300
200
100
0
280
330
380
430
480
Wavelength (nm)

(e)

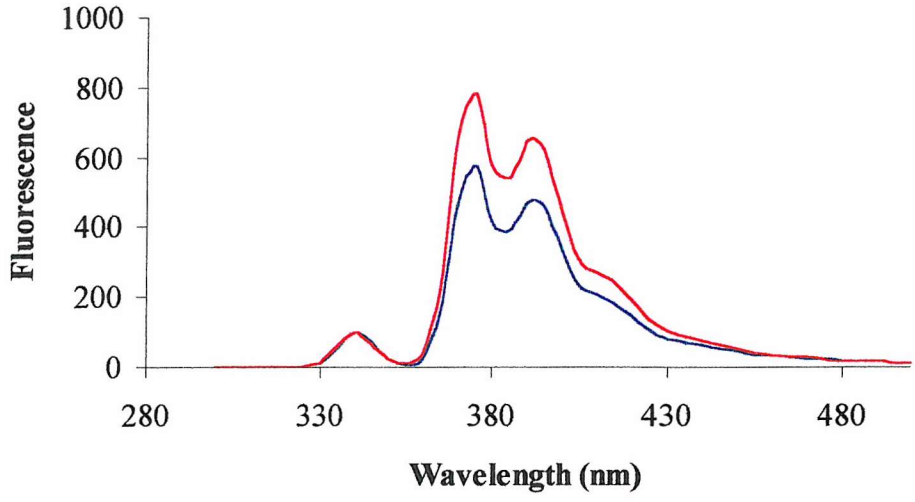
Fluorescence
1000
800
600
400
200
0
280
330
380
430
480
Wavelength (nm)

(f)

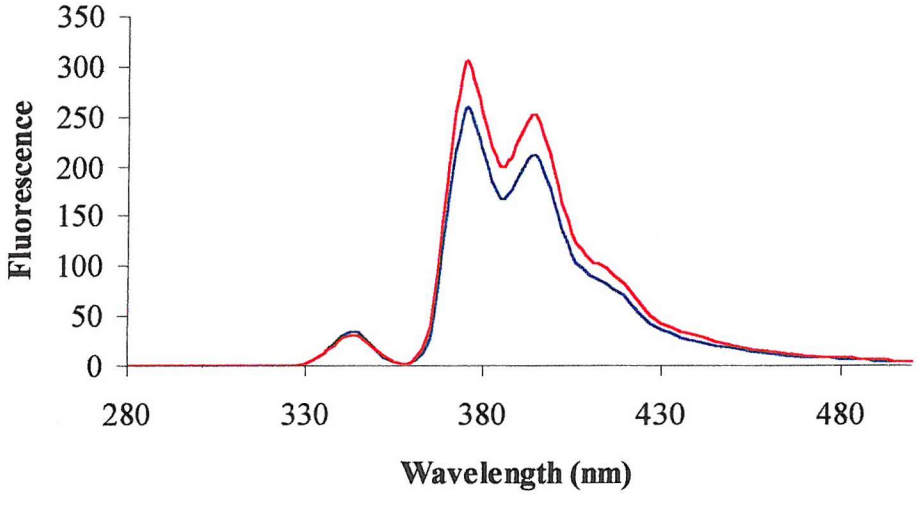
Fluorescence
350
300
250
200
150
100
50
0
280
330
380
430
480
Wavelength (nm)

12-40% increase in signal change upon Mg^{2+} binding. G69S mutant showed no significant signal change upon addition of 20mM Mg^{2+} (< 1%). Since residue G69 is located in a conserved loop region of the enzyme sequence (motif C, residues 69-72), the introduction of a slightly bigger residue may lead to a structural change which might affect Mg^{2+} ion binding to the metal depleted enzyme. The failure of G69S pyrene-labelled enzyme to report Mg^{2+} binding at site 1 could either be due to the mutation removing metal binding at site 1 or to it decreasing the affinity of this site for Mg^{2+} ions. This could be due to its close proximity to a residue known to interact with site 1, namely E70. E70 is an important site 1 metal binding residue, which is believed to ligate $Mg^{2+}1$ and is responsible for activating a nucleophilic water molecule through its interaction with this site 1 Mg^{2+}. It is also significant that this mutant has only about 38% of the specific activity of the wild type enzyme (see chapter 5, section 5.2.4). Mutant enzymes G76S, H188Q, C218D, E30P and WT reported increases of 32.6%, 12.2%, 17.1%, 40% and 20% in signal change upon addition of 20mM Mg^{2+} ions. This increase in the fluorescence emission of the pyrene maleimide modified protein upon addition of 20mM Mg^{2+} ions could be due to two reasons: the binding of Mg^{2+} ions may result in charge neutralisation on closely situated groups which in turn result in decreased fluorescence quenching; or there may be a conformational change upon Mg^{2+} ion binding resulting in increased pyrene florescence.

4.2.4 Titration of Mg^{2+} ions into pyrene maleimide labelled WT and mutant enzymes

Titration experiments were carried out in order to determine if the mutations had altered the affinity for metal ions at site 1. Mg^{2+} ions were titrated into pyrene-labelled WT enzyme and mutant enzymes and monitored at 380nm after excitation at 340nm. Figure 4.5 depicts the binding curves obtained by the titration of Mg^{2+} ions and Table 4.2 shows the values of K_d determined for Mg^{2+} ions by fitting the data to a Michaelis-Menten analysis. K_d and the maximum change in fluorescence values were initially obtained by analysing the data using the Michaelis-Menten and Lineweaver-Burk analysis (Figure

Figure 4.5 Titration of Mg^{2+} ions into (a) WT, (b) G76S, (c) G69S, (d) H188Q, (e) E30P and (f) C218D enzymes in 50mM Tris.HCl containing 250mM KCl pH 8.0 at 25°C.

(a)

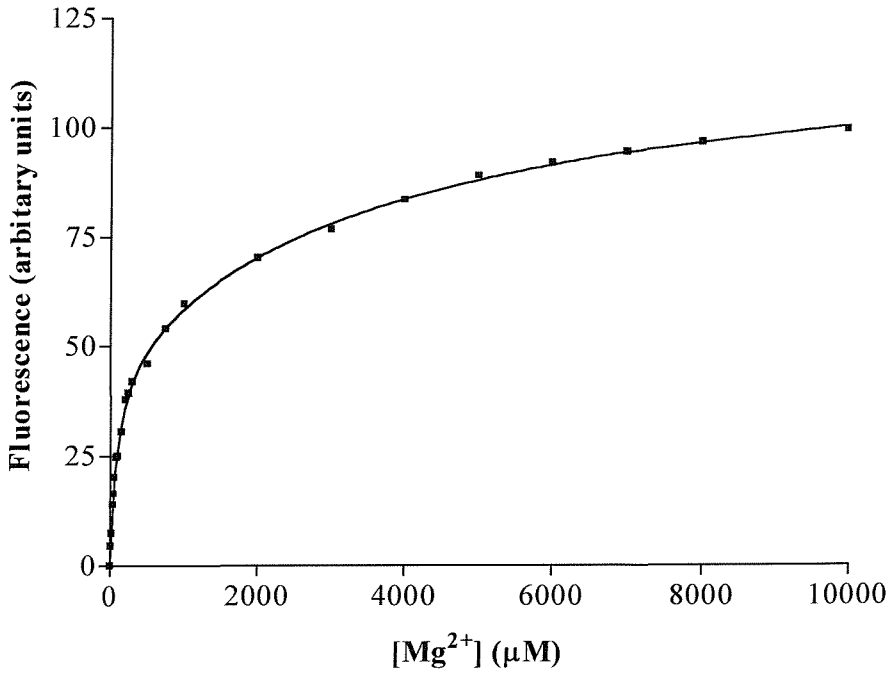
125
100
75
50
25
0
Fluorescence (arbitary units)
0
2000
4000
6000
8000
10000
[Mg2+] (μM)

(b)

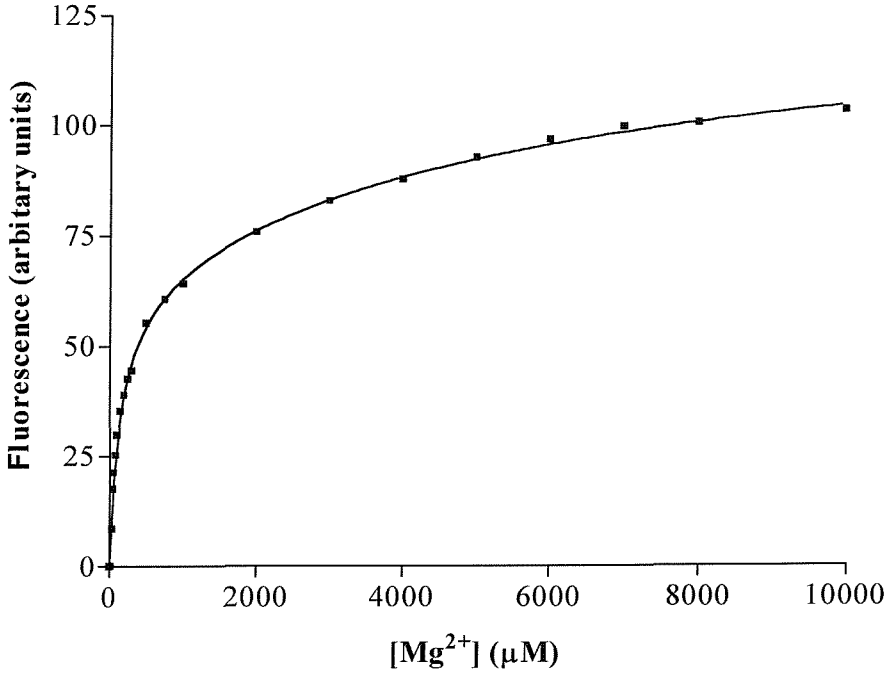
125
100
75
50
25
0
Fluorescence (arbitary units)
0
2000
4000
6000
8000
10000
[Mg2+] (μM)

(c)

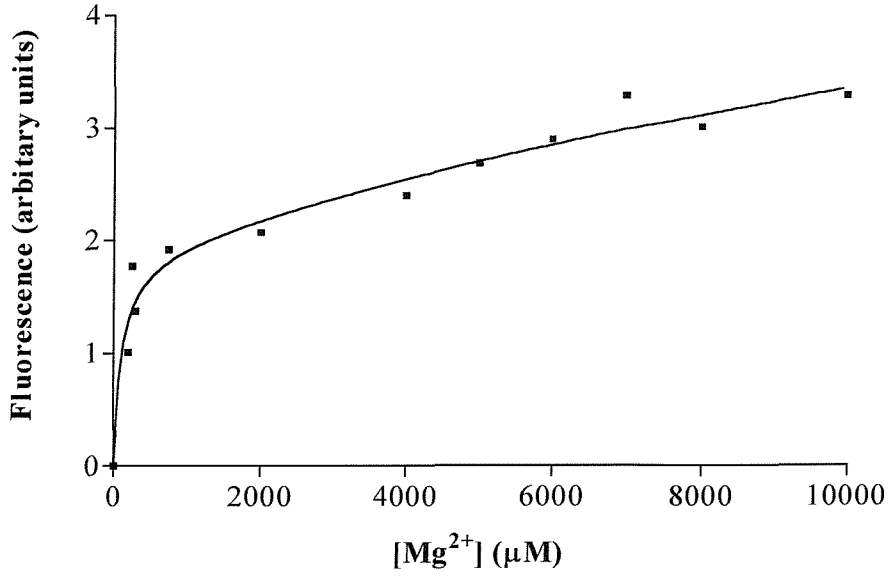
Fluorescence (arbitary units)
0
1
2
3
4
0
2000
4000
6000
8000
10000
[Mg2+] (μM)

(d)

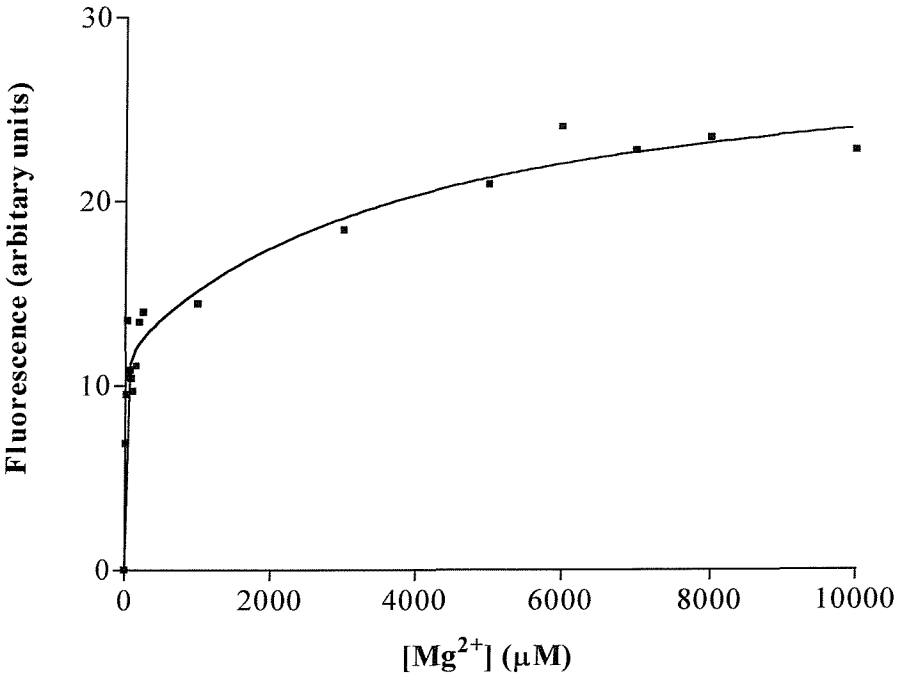
Fluorescence (arbitary units)
0
10
20
30
0
2000
4000
6000
8000
10000
[Mg2+] (μM)

(e)

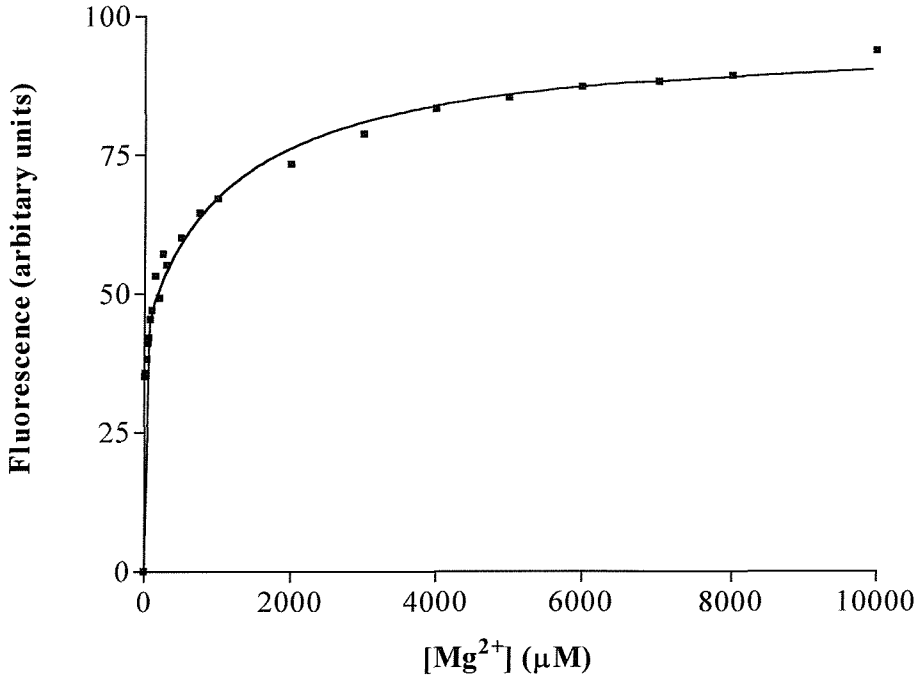
Fluorescence (arbitary units)
100
75
50
25
0
0
2000
4000
6000
8000
10000
[Mg2+] (μM)

(f)

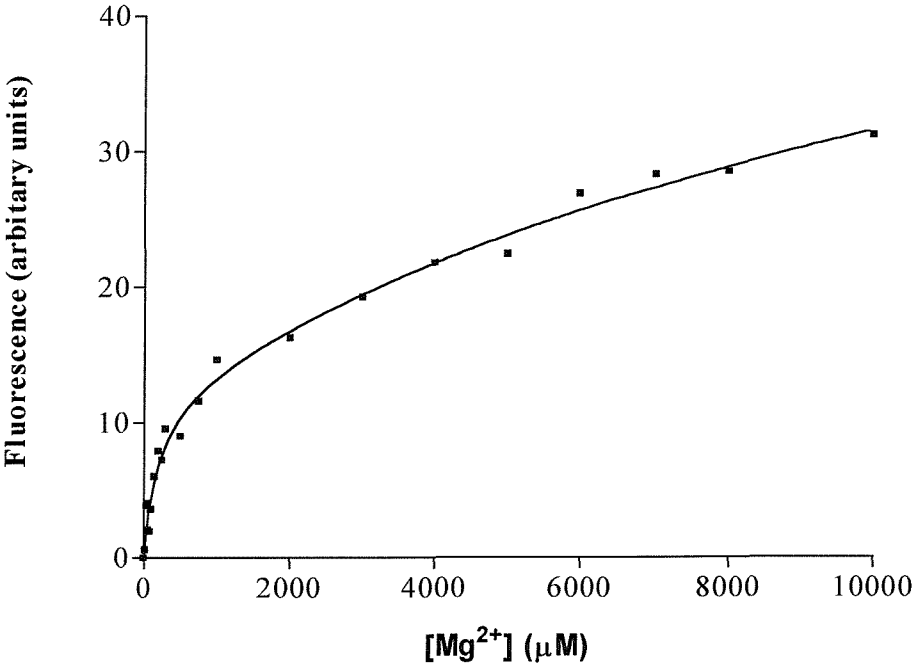
Fluorescence (arbitary units)
40
30
20
10
0
0
2000
4000
6000
8000
10000
[Mg2+] (μM)

4.5 (a)-(f)). These values are comparable to previously published values also derived using the same method of analysis.

Analysis of the titration curve for WT inositol monophosphatase provides a K_d of 430 ± 37.3μM, which is somewhat higher than the previously determined value of 300μM for WT pyrene labelled enzyme (Greasley *et al.*, 1994 and Thorne *et al.*, 1996). However, further analysis of the titration data using the Prism graph analysis package shows that the data are not best fitted to a Michaelis-Menten hyperbolic plot. In particular, the higher data points corresponding to Mg^{2+} ion concentrations exceeding 600-1500μM do not conform to the hyperbolic curve. Upon further analysis, the shape of the saturation curve for the metal ion titrations was clearly seen to show biphasic binding of ligand to the enzyme. Subsequently, the data were fitted to a two site binding (hyperbola) analysis, the values for which are also shown on Table 4.2. This type of analysis considers the titration curve in two distinct parts; the first part analysing all points preceding 1.5mM (site 1) and the second part considers all data points following this lower limit (i.e. 1.5mM to 10mM corresponding to site 2), thus giving rise to two K_d values (Table 4.2). The results for WT enzyme gave rise to a site 1 K_d value of 91 ± 14.5μM and a site 2 K_d value of 3201 ± 65μM. Consequently it was initially thought that the titration of Mg^{2+} ions into pyrene labelled enzyme could be reporting binding of Mg^{2+} at both the high affinity site (site 1) and that of the low affinity site 2 as determined by kinetic studies. Certainly the magnitude of the site 2 K_d value being in the millimolar region supports this hypothesis. The X-ray structure of Bone *et al.*, (1994(b)), revealed a third metal binding site in the Mn^{2+} enzyme structure which was absent in the $Mn^{2+}$and phosphate structure. Recent structural and kinetic data suggest that three metal ions may be involved in the mechanism of human inositol monophosphatase (Ganzhorn *et al.*, 1999). The X-ray crystallographic structure resolved to 2.5Å, in the presence of Ca^{2+} ions and substrate (D-Ins(1)P) has shown that the phosphate of the D-Ins(1)P moiety interacts with all three Ca^{2+} ions (Ganzhorn *et al*, 1997). Furthermore, our studies of the structure of the bovine enzyme complexed with Mg^{2+} ions (solved to 1.6Å resolution, chapter 6) also provides

support for the existence of this third metal ion (site 3/ Mg^{2+} 3). It may therefore be possible that the second metal binding site measured in the pyrene titration experiments could be monitoring this third site, which has not yet been characterised. If so, then this would suggest that binding of metal ions at site 2 cannot be monitored by fluorescence spectroscopy.

4.2.5 G76S mutant

Residue G76 is located in a loop region (loop 2) of the enzyme structure. The solution of the HIMP X-ray structure reveals that residues 70-75 adjacent to this residue, form a two turn α-helical type structure, which in addition to containing a crucial metal binding ligand (E70), moves away from the metal binding site by 2-3Å in the absence of Mg^{2+} ions (Bone *et al.*, 1994b). The K_d value obtained from the titration of Mg^{2+} ions into pyrene labelled enzyme was determined to be 306.1 ± 32.2μM which agrees closely with the value for WT enzyme (430 ± 37.3μM). Similarly, the value for site 1 obtained using a two phase binding model is in close agreement with that determined for WT enzyme (127.7 ± 24.1μM c.f. 91.1 ± 14.5μM).

Although the G76S mutation does not alter metal binding at site 1 with respect to wild type enzyme, reported previously (Greasley *et al.*, 1994), a greater enhancement in pyrene fluorescence at 380nm (λ^{ex} = 280nm), upon addition of 20mM Mg^{2+} ions into labelled G76S enzyme was observed (32.6%). This could mean that the introduction of the serine residue has somehow reduced quenching effects from active site carboxylic residues upon Mg^{2+} binding, as this region of the enzyme structure moves towards the active site on metal binding.

4.2.6 G69S mutant

Residue G69 is another loop region residue located adjacent (from amino acid sequence analysis) to the 70-75 α-helical segment mentioned above for G76. In addition, this residue is contained within a conserved region of the enzyme

sequence (motif C). Titration of Mg^{2+} ions into pyrene labelled G69S enzyme failed to elicit any signal change (<1%). Nevertheless, attempts were made to titrate metal ions into G69S, shown in Figure 5.5(c) after correction for dilution effects. The fluorescence intensity decreased with addition of Mg^{2+}ions or buffer solution indicating protein degradation was occurring.
The failure of the G69S mutant to report significant Mg^{2+} binding to site 1 could be due to the mutation either removing metal binding at this site or it could be that it has decreased the affinity of this site for Mg^{2+}. Certainly, residue E70 next to this residue in the sequence is an important metal site 1 ligand, which functions by activating a water molecule for nucleophilic attack in the reaction mechanism.

Studies in which residue E70 was replaced by a glutamine only displayed 0.01% of the specific activity of wild type (Pollack *et al.*, 1994). However, in these studies the G69S mutant had 38% of the specific activity of the WT enzyme which suggests that the mutation may merely decrease the reporting of the metal ion binding by fluorescence methods.

4.2.7 H188Q mutant

The K_d value of 413.4 ± 71.2 μM shows that the affinity of metal ions at site 1 is not affected significantly by the H188 to glutamine substitution, although the signal change on addition of 20mM Mg^{2+}ions is only 12.2%, approximately half of that observed for WT enzyme. The latter observation, together with kinetic studies (chapter 5) support the hypothesis that the substitution of H188 for a Q residue has only altered the ability of the enzyme to bind metal ions at the low affinity site (site 2). The unchanged binding constant for Mg^{2+} at site 1 is not surprising since H188 is not at or near the metal binding site. Crystallographic studies have shown H188 stabilises the dimeric form of the enzyme by sharing a hydrogen bond with H100 in the partner subunit. However, no evidence of increased dissociation due to this mutation has been found. Studies in which another histidine residue H217,

also mutated to a glutamine, also showed metal binding at site 1 to be unaffected (Gore *et al.*, 1993).

4.2.8 E30P

Residue E30P is located in a loop region of the enzyme that spans between secondary structural elements and it has been proposed from crystallographic studies carried out here (see chapter 6) and previously (Bone *et al.*, 1994(b)) that this region undergoes a conformational change upon metal ion binding. The mutant E30P, as has been mentioned before displays the greatest enhancement of pyrene fluorescence at 380nm of all of the mutants studied; the addition of 20mM Mg^{2+} ions caused a 40% signal increase. The titration data show that this mutation has increased the affinity for Mg^{2+}ions at site 1, yielding a low K_d value of 47.1 ± 9.3μM. The results therefore suggest that although this residue is not important for catalytic activity, it lies in a peptide region that influences how the metal ion binds at site 1.

4.2.9 C218D

It is interesting that this mutant reacted with pyrene maleimide at all. Since previous studies have shown that C218 is the prime target for this reagent. However, other reagents such as ICH_2COOH have been shown to react at Cys141 and Cys184 with half of each residue being modified per subunit (Knowles *et al.*, 1992). This mutant only showed a 17.1% signal change on addition of 20mM Mg^{2+} ions to pyrene labelled enzyme. This is almost the same as that determined for WT enzyme although this signal is not as a result of pyrene maleimide labelling residue C218. The K_d value, however, was found to be 1246 ± 130.8μM, significantly different from that determined for the WT enzyme (430 ± 37.3μM). The replacement of C218 with an aspartate residue has decreased the affinity of Mg^{2+} for site 1.

Table 4.2 Values of K_d for Mg^{2+} binding site 1 for WT and mutants of inositol monophosphatase.

Protein	K_d μM (single binding site analysis) μM (n = 3)	K_d (two binding site analysis-site1) μM (n = 3)	K_d (two binding site analysis-site2) μM (n = 3)
WT	430 ± 37.3	91.1 ± 14.5	3201 ± 65
G76S	306.1 ± 32.2	127.7 ± 24.1	4405 ± 109
G69S	-	-	-
H188Q	413.4 ± 71.2	143.1 ± 23.8	
E30P	47.1 ± 9.3	5.7 ± 1.5	1069 ± 90
C218D	1246 ± 130.8	138.1 ± 25.1	9339 ± 74.1

4.3 Changes in the far UV CD region on titration of Mg^{2+} ions into WT enzyme

Titration of Mg^{2+} ions whilst observing CD spectral changes in the far UV region has been used previously to monitor metal-protein interactions (Rees-Milton, 1997; Thorne, 1996). This is a method of measuring the K_d for metal ion binding at site 2 only and is useful when the mutants show little catalytic activity e.g. E70Q (Silva, 1999). Those studies have shown that the K_d determined by this method is the same or very close to that obtained by steady state kinetics. A typical CD spectrum of WT enzyme in the absence and presence of 30mM Mg^{2+} ions is shown in Figure 4.6. Titration of Mg^{2+} ions into WT enzyme produced an 8% signal change at 220nm in this region, giving rise to a K_d value of 7.7mM. This agrees closely with the value determined for site 2, using steady state kinetics (c.f. 7.5 ± 1.1mM), however, this value is approximately twice that determined by Rees-Milton *et al.*,

Figure 4.6 The far UV CD spectra of WT enzyme in the absence (—) and presence (…) of 30mM Mg^{2+} and (b) the titration of Mg^{2+} ion into WT enzyme monitored by spectral changes at 222nm.

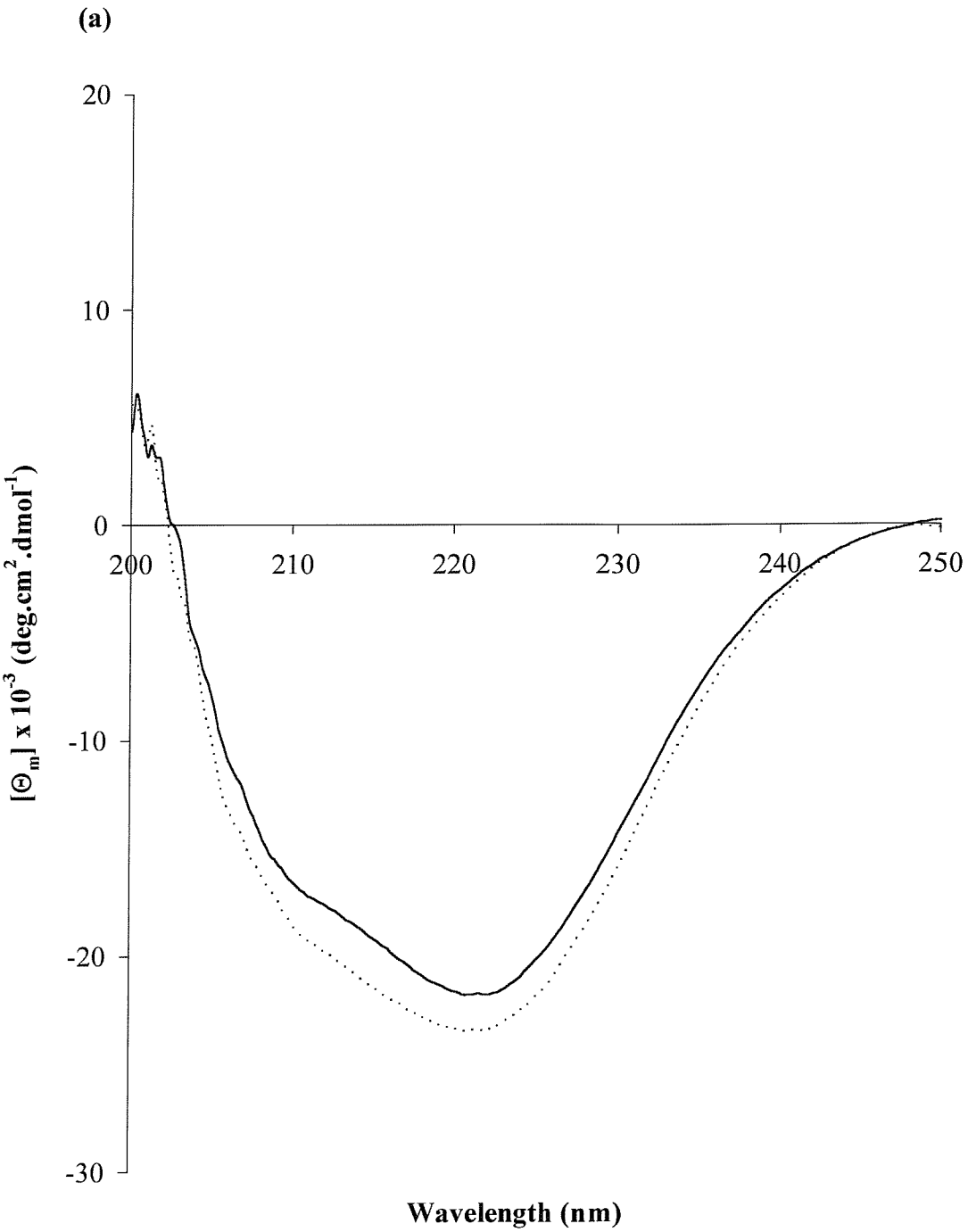
(a)
20
10
0
-10
-20
-30
200
210
220
230
240
250
$[\Theta_m] \times 10^{-3}$ (deg.cm^2.dmol^{-1})
Wavelength (nm)

(1997) (K_d = 3.9mM). The magnitude of the spectral shift reported by Rees-Milton *et al.*, (1997) was also noted to be slightly higher (12%).

X-ray crystallographic studies carried out by Bone *et al.*, (1994a) report on movement of various regions of the enzyme structure in the absence of metal ions and it has been suggested that movement of such regions reports these structural changes upon addition of Mg^{2+} ions, monitored using the far UV CD region.

However, in these studies, all mutants showed specific activity values of the same order of magnitude as WT and therefore steady state kinetics were used to monitor metal ligand interactions at site 2 (see chapter 5).

4.4 Titration of Mg^{2+} ions into WT and mutant enzymes in the near UV region.

The near UV region of a CD spectrum reports on the environment of the aromatic residues present within proteins. In previous studies, the spectral changes in this region have been used to report on ligand binding to inositol monophosphatase. For instance, Rees-Milton *et al.*, (1997) reported a signal change of 25% upon titration of 2mM Mg^{2+} ions into WT enzyme. Furthermore, mutant enzymes H217Q and W219F provided similar signal changes upon addition of the same concentration of Mg^{2+} at 275nm in the near UV region, thus suggesting that the signal change cannot be due to W219. However, it could be that these signal changes in this region of the CD spectrum are reporting on the environment of W5 or W87 or both.

Figure 4.7(a) shows the near UV CD spectral change observed for WT enzyme upon the addition of 10mM Mg^{2+} ions and Figure 4.7(b) the titration curve generated for the WT enzyme. The spectral change at 275nm was determined to be 31% upon the addition of Mg^{2+}, yielding a K_d value of 445.8 ± 40.8μM, which is slightly higher than the previously determined K_d value for Mg^{2+} ions identified by Rees-Milton, (1994) for WT enzyme (275μM), but

Figure 4.7(a) The near UV CD spectra of WT BIMP in the absence (—) and presence (—) of 10mM Mg^{2+} ions and (b) the titration of Mg^{2+} into WT BIMP monitored by a signal change at 275nm.

(a)

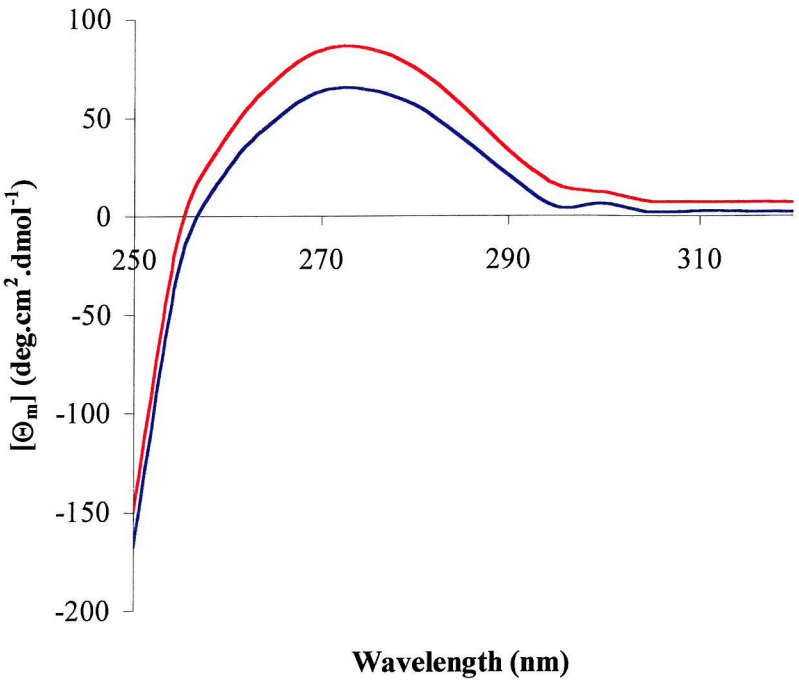
100
50
0
-50
-100
-150
-200
250
270
290
310
[Θm] (deg.cm2.dmol-1)
Wavelength (nm)

(b)

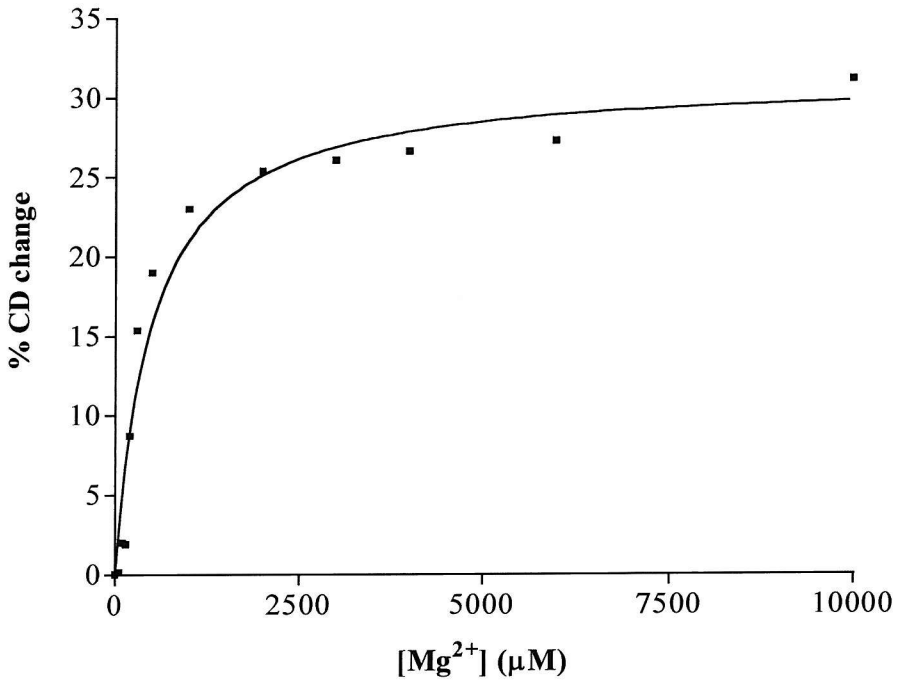
35
30
25
20
15
10
5
0
0
2500
5000
7500
10000
% CD change
[Mg2+] (μM)

it agrees closely with the value demonstrated using fluorescence spectroscopy (430 ± 37.3μM, in chapter 4). The similarity of the magnitude of the K_d value determined here to that measured using pyrene fluorescence suggests that this region of the CD region monitors metal binding at site 1.

The change in positive ellipticity at 275nm was determined to be 36% upon addition of 10mM Mg^{2+} ions to the G76S enzyme (Figure 4.8 (a)). Titration of Mg^{2+} into G76S produced a saturation curve with a (Figure 4.8 (b)) a K_d value of 321.2 ± 20.7μM and this value agrees closely with the previously determined K_d value of 306.1 ± 32.2μM using pyrene labelled enzyme (presented earlier in this chapter).

The G69S mutant enzyme failed to show an increase in positive ellipticity at 275nm upon addition of 10mM Mg^{2+} ions (Figure 4.9 (a)). This is in agreement with fluorescence experiments made using pyrene labelled enzyme, which also failed to report Mg^{2+} binding to site 1, thus suggesting the Mg^{2+} ions are either not binding to site 1 or that the affinity of site 1 for these ions is much reduced.

The H188Q mutant shows a 17% increase in ellipticity at 275nm upon addition of 10mM Mg^{2+} ions (Figure 4.10(a)) which is just over half of that displayed by WT BIMP in these studies. The saturation curve generated upon titration of 10mM Mg^{2+} into H188Q enzyme (Figure 4.10 (b)) gave rise to a K_d value of 268.4 ± 33.6μM. This value is significantly higher than the value determined from fluorescence spectroscopy using pyrene labelled enzyme (413.4 ± 71.2μM, section 4.2.7).

The mutant E30P reported a very interesting observation, it showed an approximately 1.4-fold higher increase in ellipticity at 275nm (42%) compared to that seen for WT enzyme (31%). This magnitude of this signal change (Figure 4.11(a)) is analogous to the fluorescence signal change reported by Mg^{2+} binding to pyrene labelled E30P enzyme (see section 4.2.8). From the titration curve (Figure 4.11 (b)) a K_d value of 67.29 ± 9.51μM was determined

Figure 4.8(a) The near UV spectral changes on the addition of 10mM Mg^{2+} ions (—) to G76S (—) and (b) the titration upon Mg^{2+} binding to G76S enzyme.

(a)

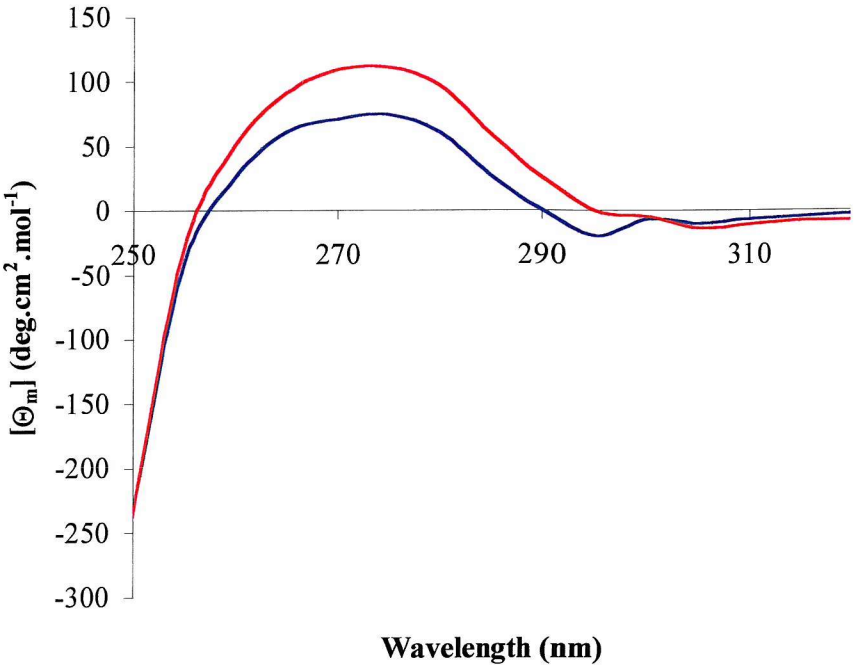
150
100
50
0
-50
-100
-150
-200
-250
-300
250
270
290
310
[Θm] (deg.cm2.mol-1)
Wavelength (nm)

(b)

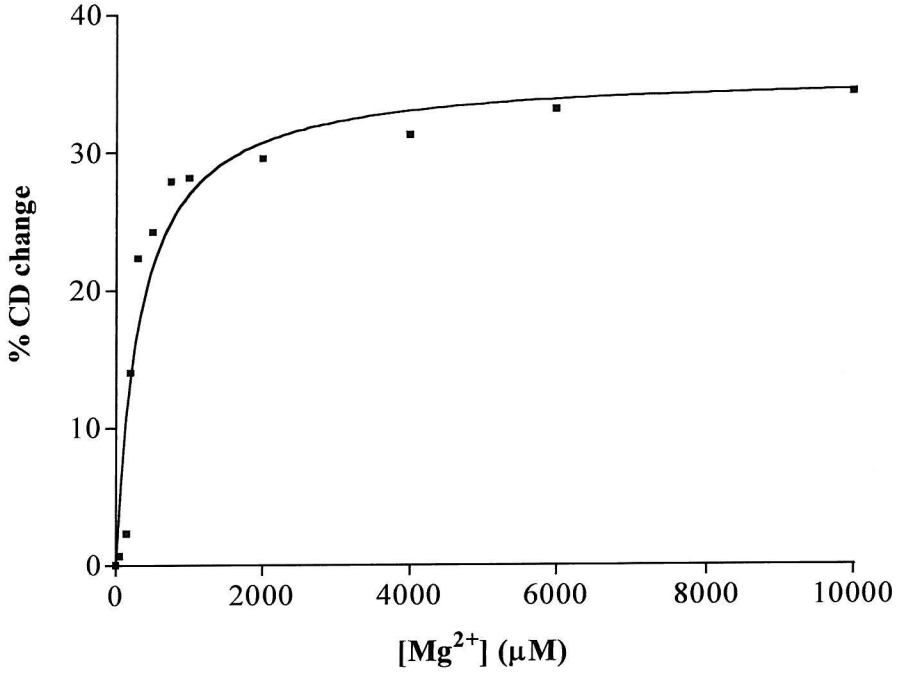
40
30
20
10
0
0
2000
4000
6000
8000
10000
% CD change
[Mg2+] (μM)

Figure 4.9(a) The near UV CD spectra of G69S in the absence (—) and presence (—) of 10mM Mg^{2+} ions.

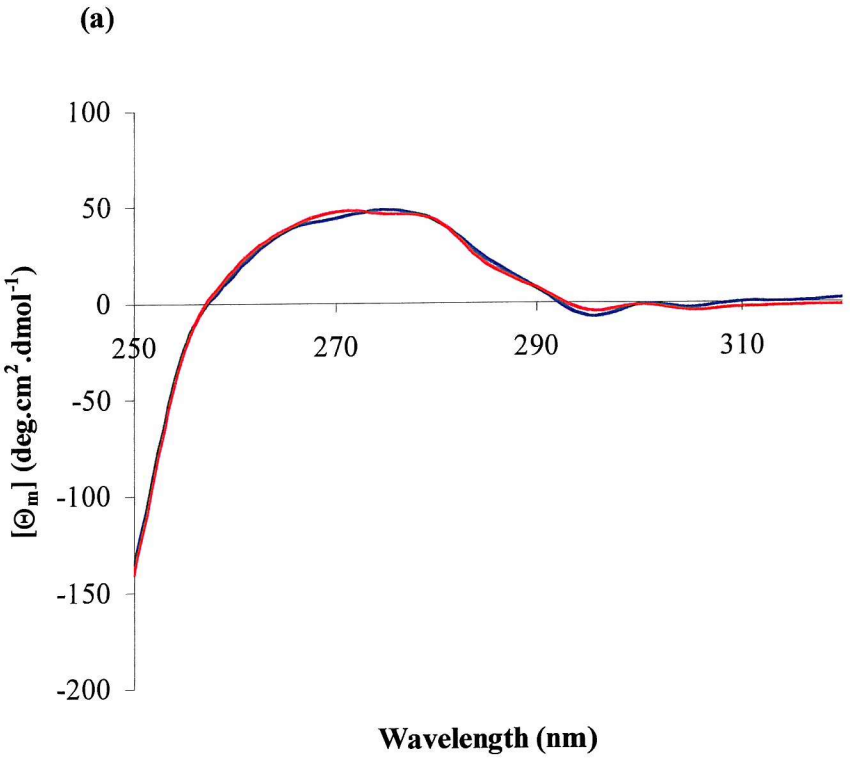
(a)
100
50
0
-50
-100
-150
-200
250
270
290
310
[Θm] (deg.cm2.dmol-1)
Wavelength (nm)

Figure 4.10(a) The near UV spectral changes on the addition of 10mM Mg^{2+} ions (—) to H188Q (—) and (b) the titration curve upon Mg^{2+} binding to H188Q enzyme.

(a)

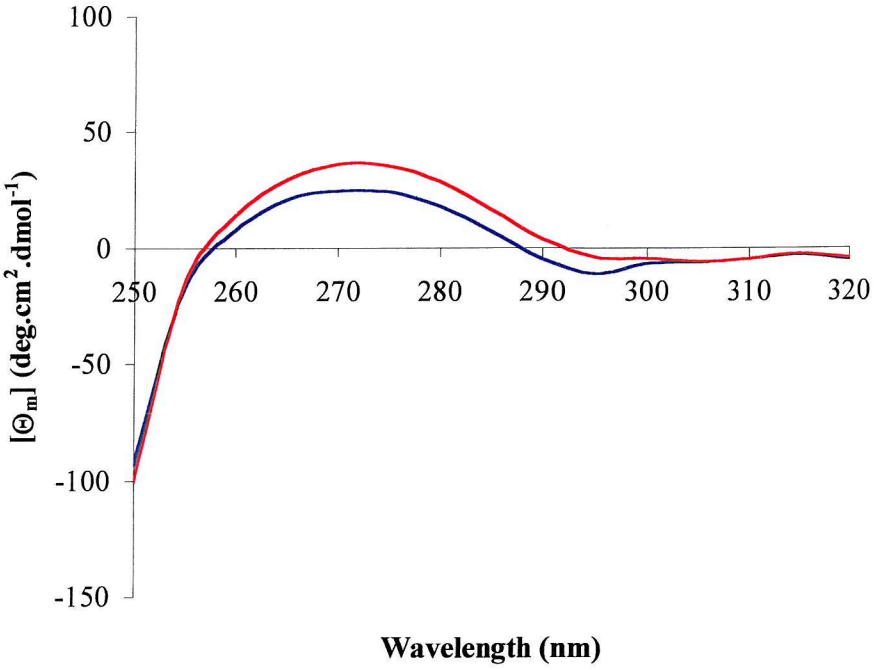
100
50
0
-50
-100
-150
250
260
270
280
290
300
310
320
[Θm] (deg.cm2.dmol-1)
Wavelength (nm)

(b)

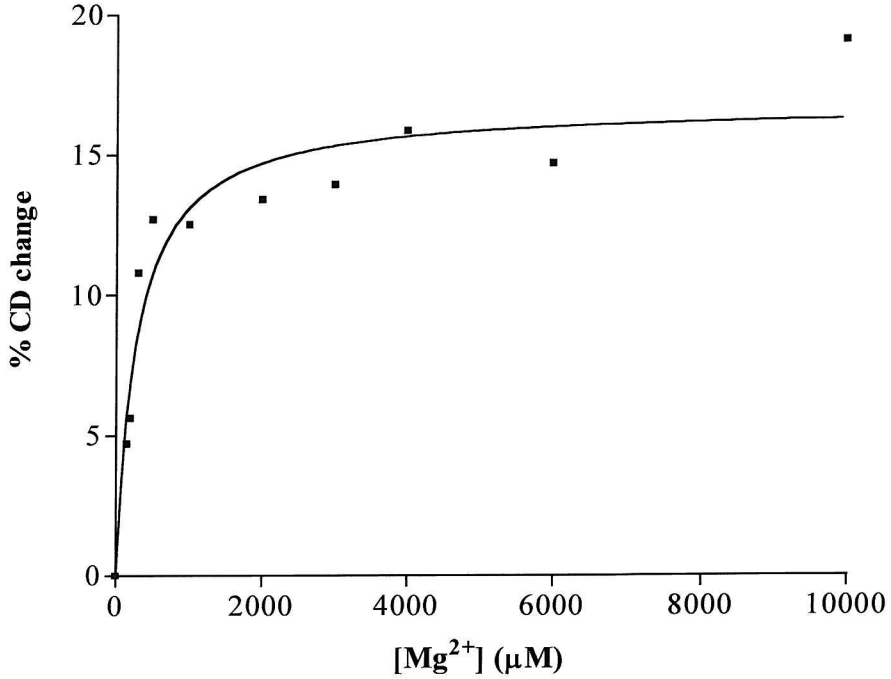
20
15
10
5
0
0
2000
4000
6000
8000
10000
% CD change
[Mg2+] (μM)

Figure 4.11(a) The near UV CD spectra of E30P in the absence (—) and presence (—) of 10mM Mg^{2+} ions and (b) the titration of Mg^{2+} into E30P monitored by a signal change at 275nm.

(a)

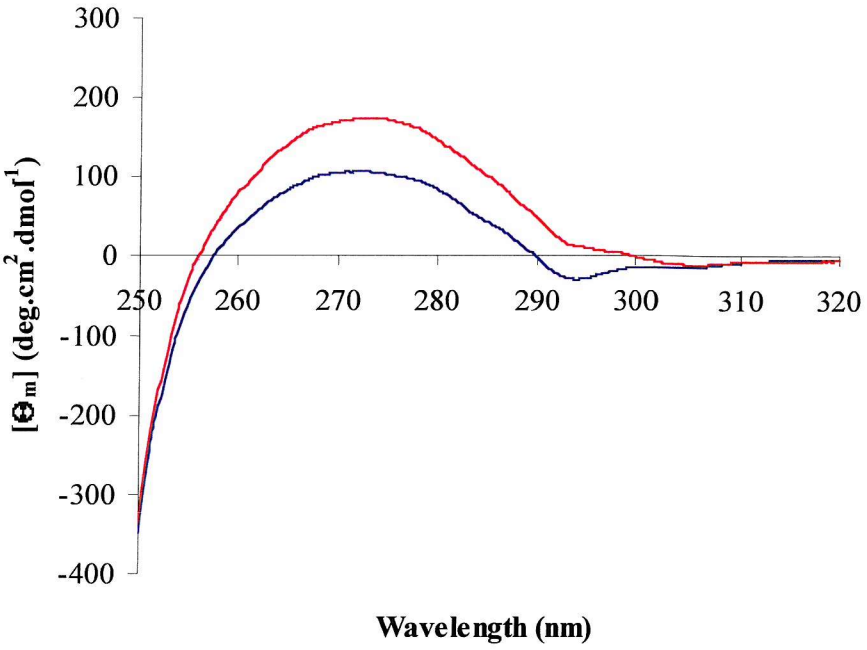
300
200
100
0
-100
-200
-300
-400
250
260
270
280
290
300
310
320
[Θm] (deg.cm2.dmol-1)
Wavelength (nm)

(b)

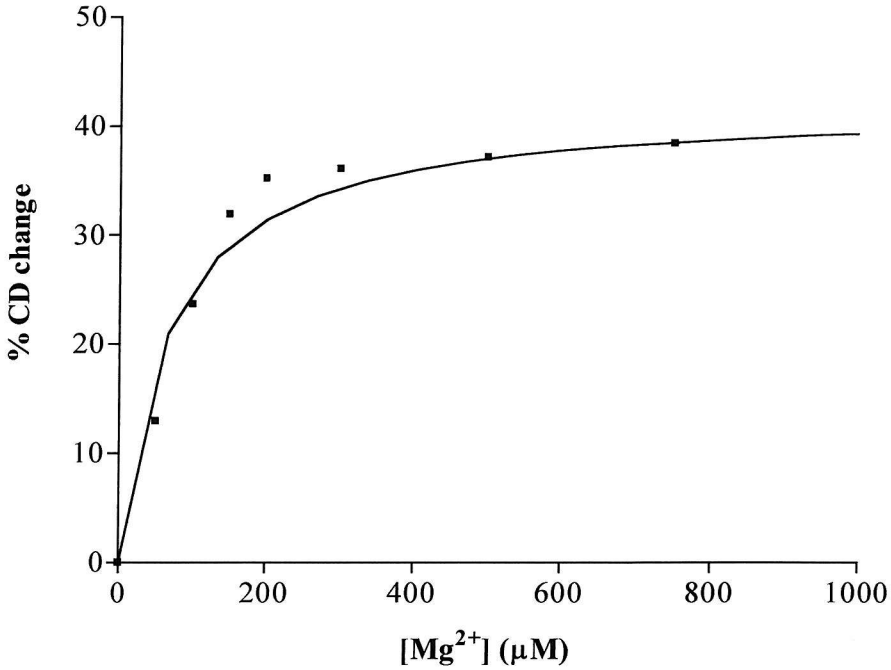
50
40
30
20
10
0
0
200
400
600
800
1000
% CD change
[Mg2+] (μM)

which corroborates previous findings in section 4.2.8 where a K_d value of 47.1 ± 9.3μM was demonstrated for this enzyme indicating that the mutation results in a high affinity for metal ions at site 1.

The C218D mutant enzyme demonstrated a 25% signal change upon addition of 10mM Mg^{2+} to metal depleted enzyme at 275nm (Figure 4.12 (a)). The corresponding saturation curve (Figure 4.12 (b)) gave rise to a K_d value of 1048 ± 150.7μM. This agrees very closely with the K_d determined for Mg^{2+} binding monitored using pyrene labelled enzyme (1246 ± 130.8μM, see section 4.2.9).

Table 4.3 The near UV K_d values for WT and G76S, G69S, E30P, H188Q, and C218D mutants.

Protein	**Near-UV CD K_d value for Mg^{2+} (n = 3) (μM)**
WT	445.8 ± 40.8
G76S	321.2 ± 20.7
G69S	-
H188Q	268.4 ± 33.6
E30P	67.3 ± 9.5
C218D	1048 ± 150.7

Figure 4.12(a) The near UV CD spectra of C218D in the absence (—) and presence (—) of 10mM Mg^{2+} ions and (b) the titration of Mg^{2+} into C218D monitored by a signal change at 275nm.

(a)

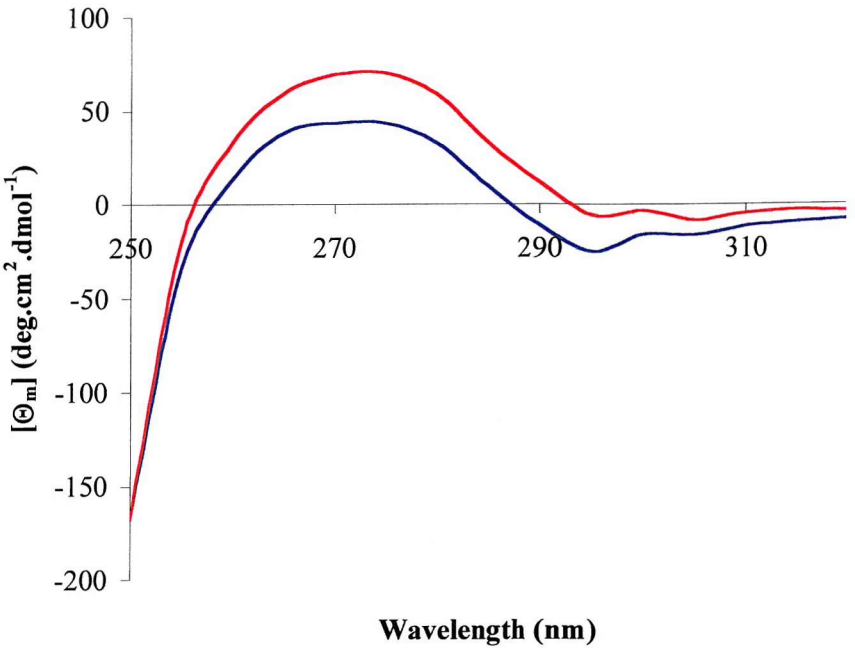
100
50
0
-50
-100
-150
-200
250
270
290
310
[Θm] (deg.cm2.dmol-1)
Wavelength (nm)

(b)

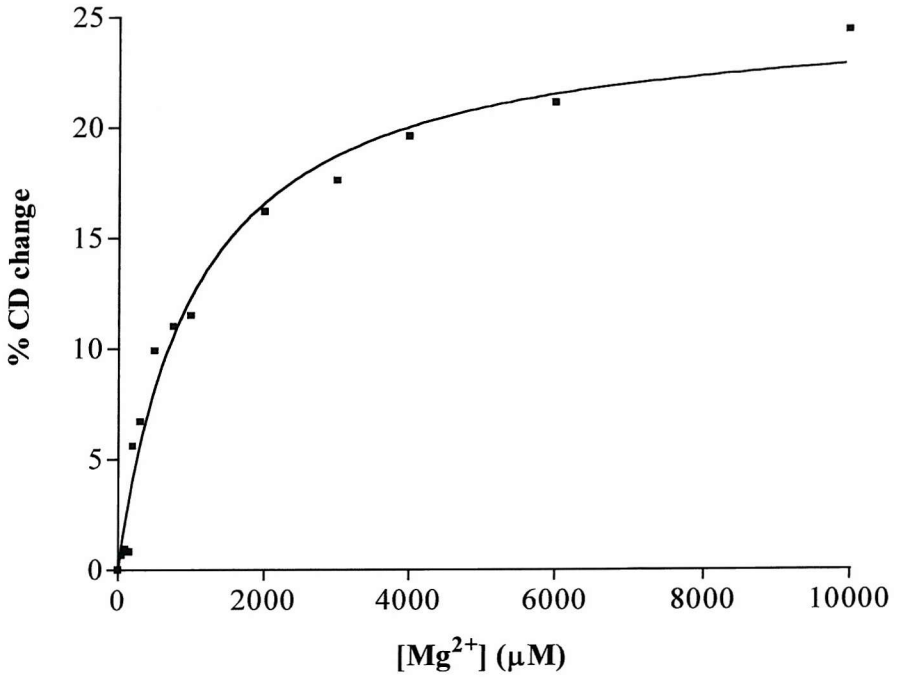
25
20
15
10
5
0
0
2000
4000
6000
8000
10000
% CD change
[Mg2+] (μM)

4.5 Observation of Mg^{2+} - inositol monophosphatase interactions by pre-equilibrium fluorescence spectroscopy

4.5.1 Introduction

Simple binding reactions between two molecules such as the formation of a complex between an enzyme and its substrate or cofactors normally takes between 10 and 200ms to complete. Specialised instrumentation is required for their study and stopped-flow spectroscopy is usually the technique chosen. This is a simple system that has been developed from continuous flow instrumentation. Reactants are placed into syringes with pistons that can be rapidly driven by compressed air so that a small sample of each is mixed and delivered to an optical detector within 1 - 2ms. The flow continues until the reactants push the piston of a third syringe up against a physical barrier that stops the flow. The reaction therefore "ages" from the time the flow stops and the resultant change in signal can be recorded on a computer via an appropriate analogue - digital converter. In the studies described here the method of detecting the reaction progress was fluorimetry based upon the fluorescence changes that occur when metal ions bind to pyrene-maleimide labelled BIMP.

The excitation light is provided by a 150W Xenon lamp and the wavelength is selected by a monochromator. The fluorescence emission from the reaction cell is subsequently selected by a cut-off filter that permits light above a selected wavelength (360nm for pyrene emission) to pass through, but absorbs light at lower wavelengths.

4.5.2 Data analysis

The reaction between BIMP and Mg^{2+} ions, shown in the equation below, is second order, the rate of which will depend upon the concentration of both reactants.

$$E + Mg^{2+} \underset{k_{-1}}{\overset{k_1}{\rightleftharpoons}} E.Mg^{2+} \quad (1)$$

In which k_1 and k_{-1} are the rate constants for the forward and reverse reactions respectively. The velocity of the forward direction $v_f = k_1[E][Mg^{2+}]$ and the velocity of the reverse direction $v_r = k_{-1}[E.Mg^{2+}]$. At equilibrium the two velocities are the same ie. $v_f = v_r$ and thus

$$k_1 [E][Mg^{2+}] = k_{-1} [E.Mg^{2+}] \quad (2)$$

and therefore

$$k_{-1}/k_1 = [E][Mg^{2+}] / [E.Mg^{2+}] = K_d \quad (3)$$

i.e. the ratio of the rate of dissociation to the rate of association of the complex = K_d, the dissociation constant for the equilibrium. For simple systems the value of K_d determined by equilibrium experiments (such as the fluorescence titrations as described in this chapter) is normally the same as that determined by pre-equilibrium techniques.

The second order rate constant k_1 ($M^{-1}s^{-1}$) is can be determined if the experiment is carried out so that one reagent (in these experiments Mg^{2+} ions) is in excess over the other. Then, the rate of loss of the limiting component is a pseudo-first order process that will have the same rate as the formation of product.

The reaction progress curve observed from a 'shot' of the stopped-flow is the accumulated rates $k_1[Mg^{2+}] + k_{-1}$ and is called the apparent rate (k_{app}). If the dependence of the value of k_{app} on Mg^{2+} ion concentration is determined then the second order rate constant k_1 can be calculated. Therefore reactions are carried out in which a fixed concentration of BIMP is reacted with various concentrations of Mg^{2+} ions and the values of k_{app} determined by a first order analysis algorithm. A plot of $k_{app}(s^{-1})$ against Mg^{2+} ion concentration yields a straight line with a slope of k_1 ($M^{-1}s^{-1}$). When the concentration of Mg^{2+} ions = 0, then $k_1[Mg^{2+}]$ also = 0 and therefore the intercept on the ordinate is equal to

k_{-1} (s^{-1}). In practice, only the concentration of Mg^{2+} ions needs be known accurately.

4.5.3 Results

In Figure 4.13 a typical reaction progress curve is shown in which 3μM enzyme is reacted with 400μM Mg^{2+} ions at pH 8.0, 25°C. The rapid increase in fluorescence intensity from the pyrene label (k_{app} approximately = $292s^{-1}$) is followed by a slower (k_{app} = $10.6s^{-1}$) further increase in intensity. Both parts of the reaction progress curve can be analysed either by use of a double exponential algorithm (see section 2.6.5) or by selection of data from each section of the progress curve and its subsequent analysis by a single exponential algorithm.

Other experiments carried out using a range of concentrations of Mg^{2+} ions allowed the data to be plotted (see Figure 4.14) to obtain the value of the second order rate constant k_1 (slope) and k_{-1} (intercept on ordinate). These data are given in Table 4.4. Using these data the value of K_d was estimated to be 663μM under these conditions. This is higher than the value at equilibrium (445.8μM, see Table 4.4) determined in CD studies under the same conditions. This may be due to a structural rearrangement that leads to an increase in affinity.

Table 4.4 The values of k_1, k_{-1}, k_{app} and K_d determined from stopped-flow fluorescence studies. Also shown are the values of K_d determined by CD spectropolarimetry and fluorescence spectroscopy.

Protein	k_1 ($M^{-1}s^{-1}$)	k_{-1} (s^{-1})	K_d Pre-equilibrium μM	K_d (μM) at equilibrium (CD)	K_d (μM) at equilibrium (fluorescence)
WT	2.7×10^5	179 ± 7.8	663	430 ± 37.3	445.8 ± 40.8
G76S	2.8×10^5	194 ± 10.5	692	306.1 ± 32.2	321.2 ± 20.7

Figure 4.13 A typical reaction progress curve observed when 3μM enzyme is reacted with 400μM Mg^{2+} ions at pH 8.0, 25°C. The lower plot describes the residuals to the curve which in this case was fitted by a double exponential algorithm. Rate 1 was $292s^{-1}$ and rate 2 was $10.6s^{-1}$. The concentrations quoted are final concentrations after mixing.

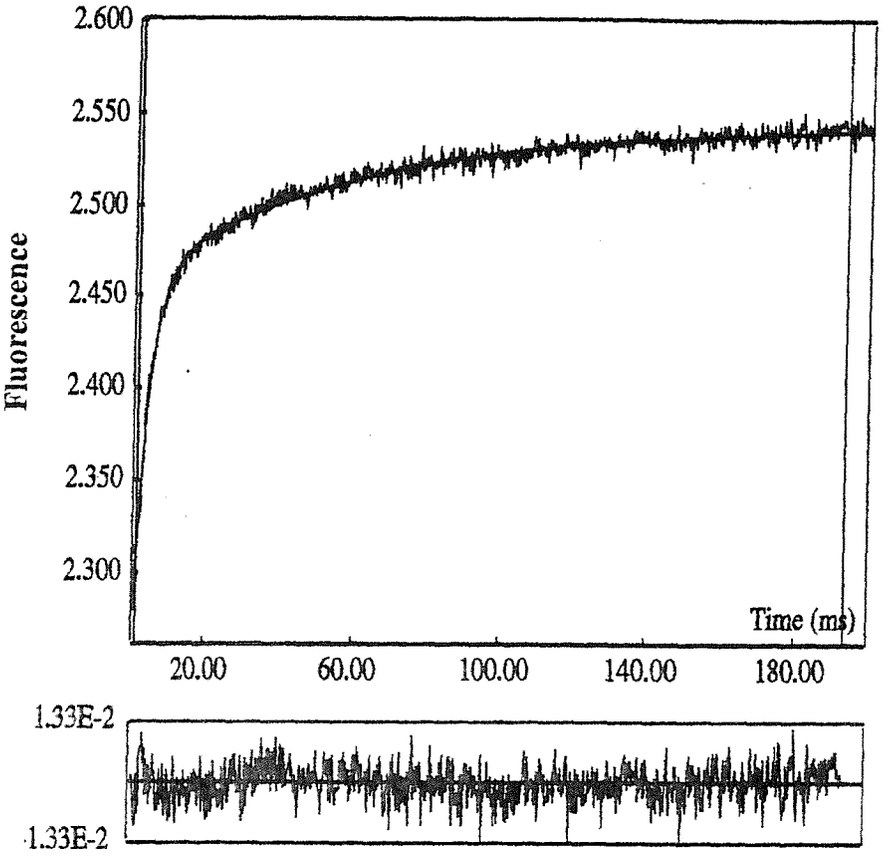
2.600
2.550
2.500
2.450
2.400
2.350
2.300
Fluorescence
Time (ms)
20.00
60.00
100.00
140.00
180.00
1.33E-2
-1.33E-2

Figure 4.14 The relationship between k_{app} and the final concentration of Mg^{2+} ions. The conditions were as for Figure 4.13 and are described in the text.

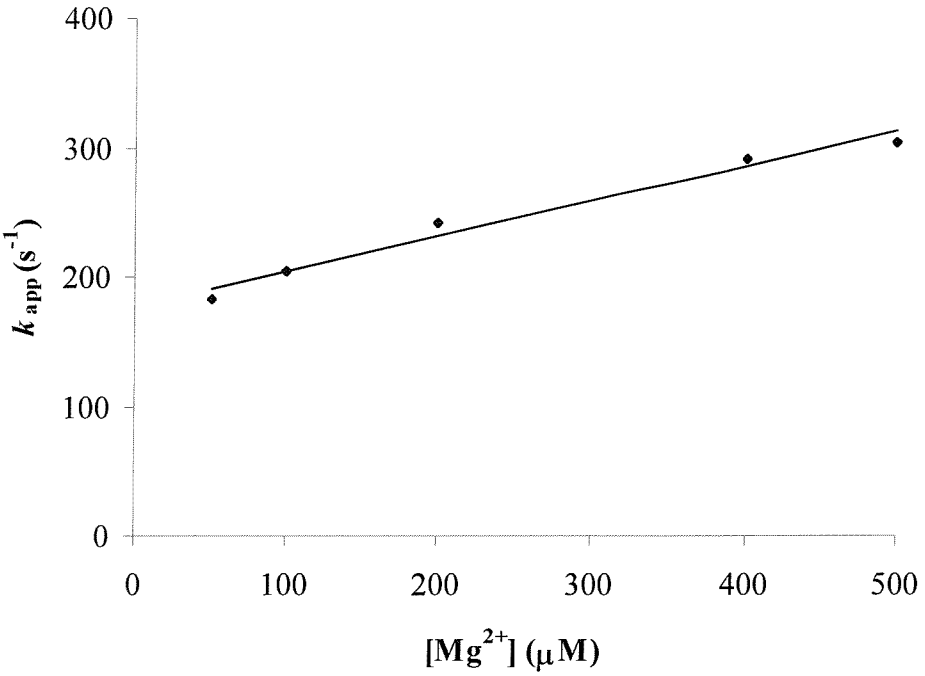
400
300
200
100
0
k_{app} (s^{-1})
0
100
200
300
400
500
[Mg^{2+}] (μM)

The observed rate of the slower increase in fluorescence under these conditions was around 8-10s^{-1}. Figure 4.15 shows that this rate changed little with Mg^{2+} ion concentration which supports the concept of a protein structural change.

Experiments to determine the rate of the reverse process(es) were carried out by diluting a pre-formed complex of E*. Mg^{2+} (6μM enzyme + 400μM Mg^{2+} ions) with an equal volume of 1–50mM EDTA. The chelation of the free metal ions causes the complex to dissociate and give rise to a decrease in fluorescence intensity. Figures 4.16 show a typical reaction progress curve from such an experiment. There is a rapid decrease in fluorescence intensity with a first order rate of 190s^{-1} at pH 8.0, 25°C. The inset to Figure 4.16 shows that the rate of this part of the dissociation reaction is independent of the concentration of EDTA used, thus showing that this factor is not rate limiting. The curve in Figure 4.16, and others in this type of experiment, is best fitted by a double exponential algorithm with a second slow rate of 11.9s^{-1}.
Figure 4.17 shows that the rate of the dissociation reaction reflected by the change in fluorescence is sensitive to pH and the curve confirms that groups with low pKa values are involved with metal ligation. In these experiments it was not possible (due to the instability of the enzyme in low pH solutions) to obtain a full pH profile and estimate the pKa of the participating residues but it is clear that the midpoint must be at a pH below 5.0–5.5 and therefore corresponds to acidic side chains as indicated by the X-ray data (see chapter 6).

Parallel studies with mutant enzymes gave very similar results. Data for the G76S mutant is provided in Table 4.4. These data show that the binding process for this mutant is similar to that of the WT enzyme.

4.5.4 Discussion

These results are in agreement with previous reports (Thorne *et al.*, 1996) who showed that the binding reaction appears to take place in two stages.

Figure 4.15 The dependence of the second phase of the reaction on the final concentration of Mg^{2+} ions.

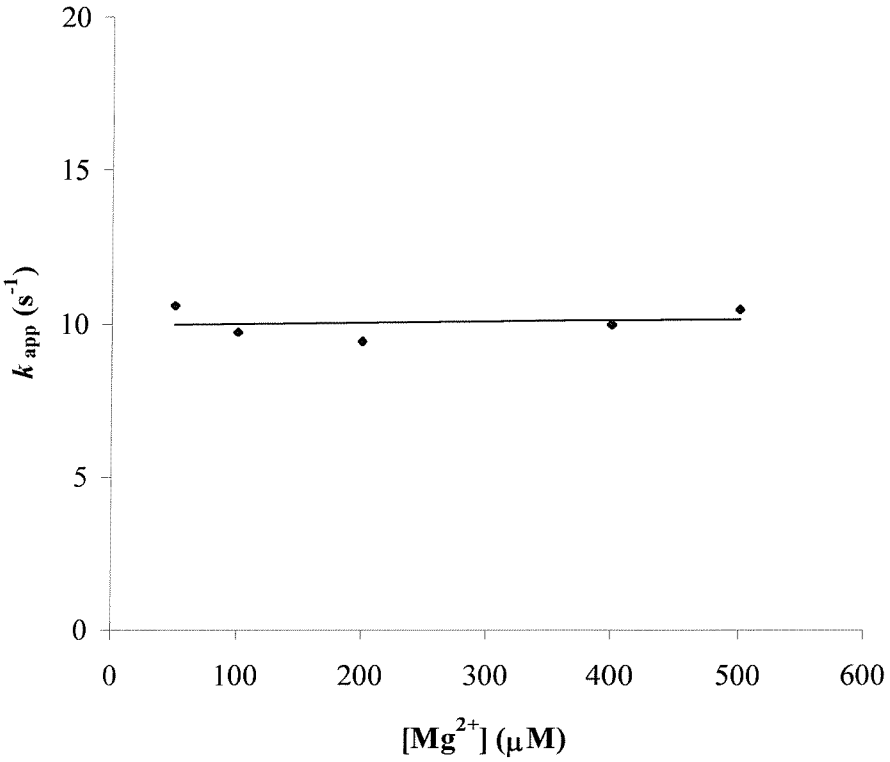
20
15
10
5
0
k_{app} (s^{-1})
0
100
200
300
400
500
600
[Mg^{2+}] (μM)

Figure 4.16 The decrease in fluorescence intensity when a solution of 6μM enzyme containing 400μM Mg^{2+} is rapidly mixed with an equal volume of a solution of EDTA. The buffer used was 10mM Hepes, pH 8.0, 25°C.

Inset:
The dependence of the fast rate of decrease of fluorescence intensity on the concentration of EDTA. The concentration of EDTA is the final concentration after mixing.

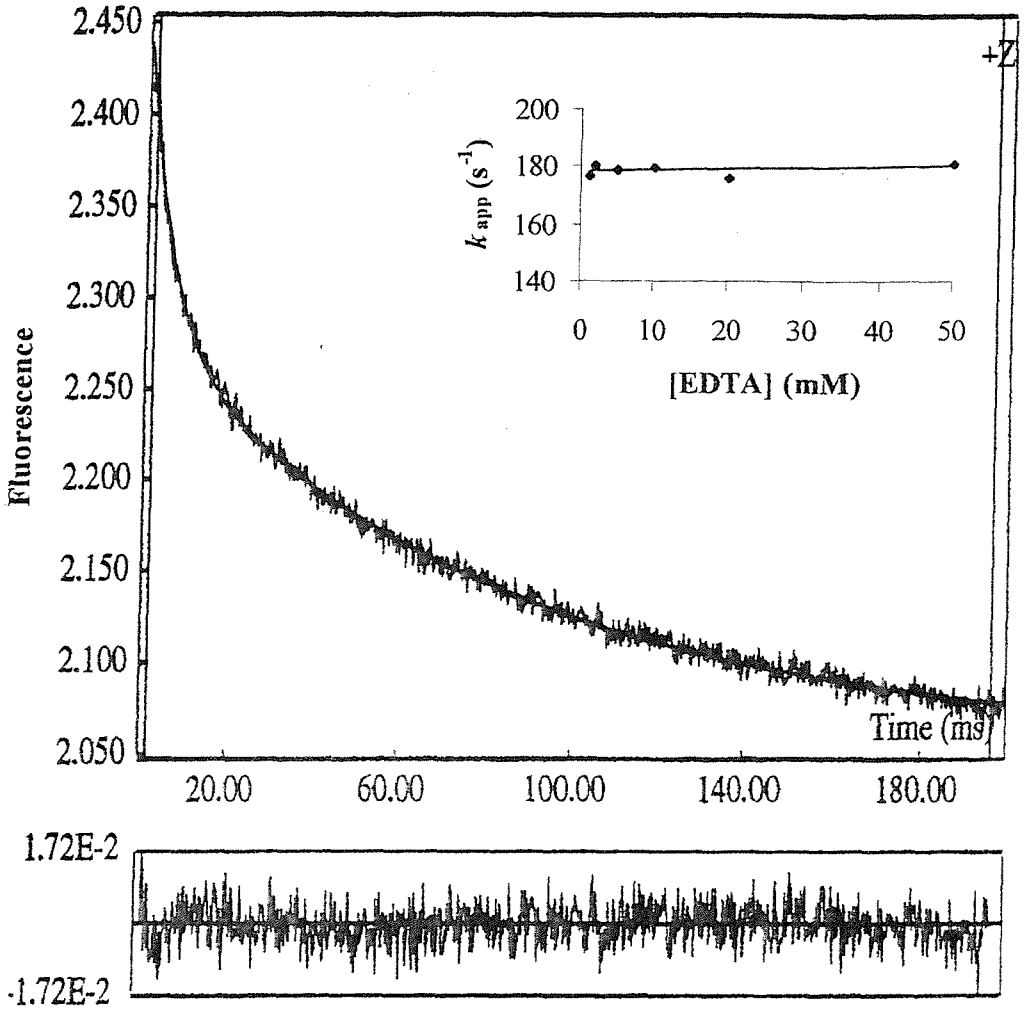
2.450
2.400
2.350
2.300
2.250
2.200
2.150
2.100
2.050
Fluorescence
+Z
Time (ms)
20.00
60.00
100.00
140.00
180.00
200
180
160
140
k_{app} (s^{-1})
0
10
20
30
40
50
[EDTA] (mM)
1.72E-2
-1.72E-2

Figure 4.17 The rapid decrease in fluorescence intensity noted when a solution of 6μM pyrene-labelled enzyme, 400μM EDTA in 10mM Tris-HCl buffer containing 250mM KCl, pH 8.0 is reacted with an equal volume of 10mM EDTA in 10mM Hepes buffer adjusted to the pH required to generate the final pH indicated. The inset shows a plot of the value of k_{app} (s^{-1}) against the pH of the resultant solution.

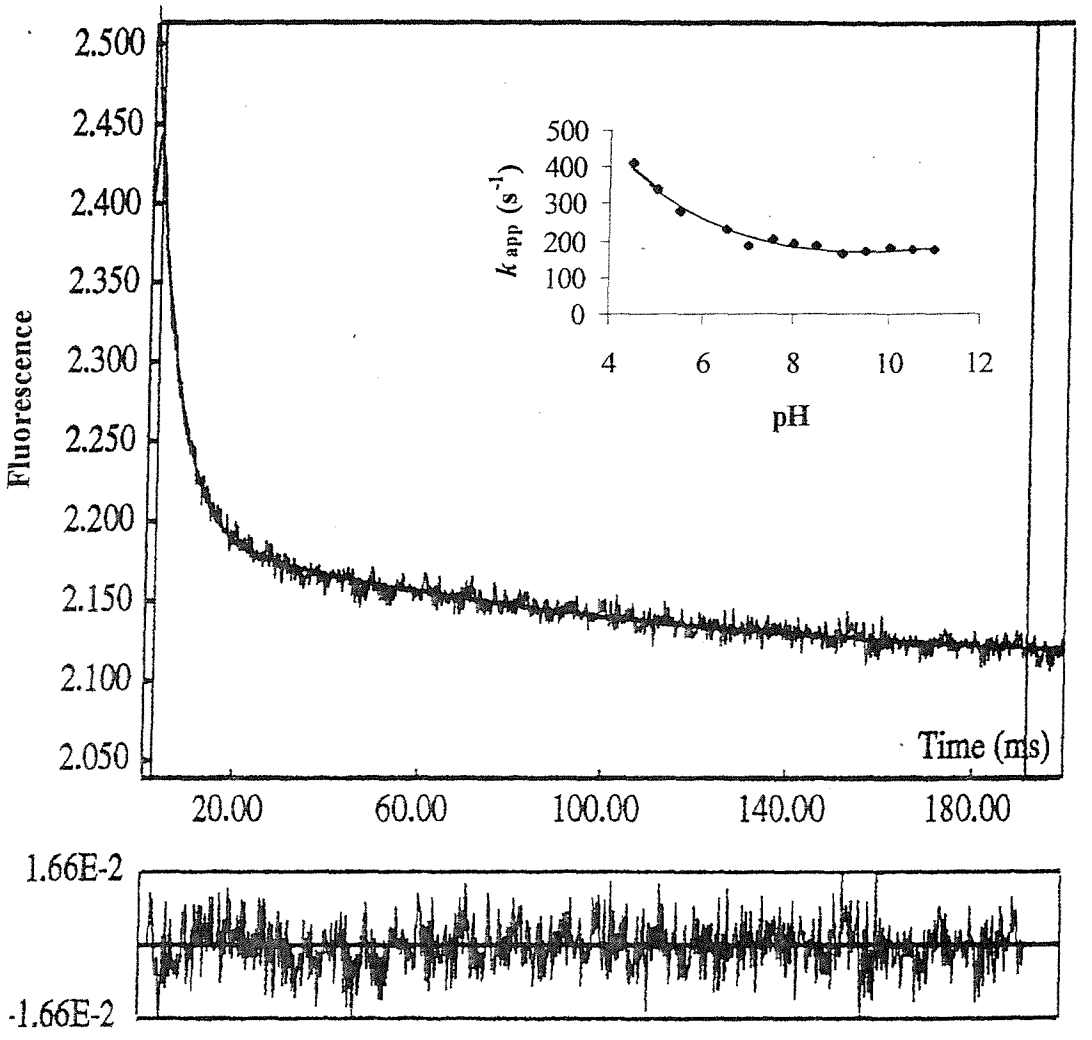
2.500
2.450
2.400
2.350
2.300
2.250
2.200
2.150
2.100
2.050
Fluorescence
Time (ms)
20.00
60.00
100.00
140.00
180.00
500
400
300
200
100
0
k_{app} (s^{-1})
4
6
8
10
12
pH
1.66E-2
-1.66E-2

Two possible models may explain such phenomena;

(a) a binding reaction followed by a conformational change

$$E + Mg^{2+} \underset{k_{-1}}{\overset{k_1}{\rightleftharpoons}} E.Mg^{2+} \underset{k_{-2}}{\overset{k_2}{\rightleftharpoons}} [E.Mg^{2+}]^* \qquad (4)$$

Here a rapid increase in fluorescence occurs on the formation of the 'encounter' binary complex $E.Mg^{2+}$ and the slow change in fluorescence occurs as this complex isomerises to $[E.Mg^{2+}]^*$. This model has been proposed for a number of other protein-ligand systems (Beckingham *et al.*, 1999; Chaiyen *et al.*, 1997; Wallis *et al.*, 1995). Here, k_1 ($M^{-1}s^{-1}$) is the second order rate constant for the formation of the initial binary complex and k_{-1} (s^{-1}) is the first order rate of dissociation of this complex. The rate of the fast change of fluorescence intensity is proportional to Mg^{2+} concentration and represents the rate of formation of E. Mg^{2+}. If the rate of formation of the encounter complex E. $Mg^{2+}$is rapid compared to the conformational change then the two parts of the process can be considered as two separate reactions. Thus, k_1 and k_{-1} may be derived from the slope and intercept, respectively, of a plot of k_{app} against the final concentration of Mg^{2+} and the K_d for the encounter complex is given by k_{-1} / k_1.

The apparent rate for the conformational change (k_{2app}) is given by the equation:

$$k_{2app} = k_{-2} + k_2 \frac{[Mg2+]}{Kd+[Mg2+]} \qquad (5)$$

i.e. k_{-2} plus the value of k_2 corrected for the fraction of the enzyme in the initial binary complex. If the concentration of Mg^{2+} ions used are much higher than the K_d of the pre-equilibrium complex E. Mg^{2+} then it can be ignored and then

$$k_{2app} = k_{-2} + k_2 \qquad (6)$$

and no correction to k_2 is required.

In the case of a conformational change that does not involve further binding reactions, the rate of the process will be independent of the concentration of

metal ions. The further increase in fluorescence intensity would result from either the reaction equilibrium being pulled further to the right by a higher affinity for metal ions as a result of the structural change, or as a result of a increase in quantum yield from the reporter group as the conformational change proceeds.

The second possible model to explain the two-phase kinetics;
(b) an equilibrium between two states of the enzyme, only one of which binds metal ions strongly.

$$E \underset{k_r}{\overset{k_f}{\rightleftharpoons}} E^* + Mg^{2+} \underset{k_{-1}}{\overset{k_1}{\rightleftharpoons}} E^*.Mg^{2+} \qquad (7)$$

In this scheme, k_f is the forward rate of a conformational change between two forms of the enzyme, E (unable to bind metal ions / binds metal ions very weakly) and E* (able to bind metal ions with a high affinity). k_r is the rate of the reverse reaction. k_1 and k_{-1} are the forward and reverse rates of the formation of the binary complex, respectively. In this model, the change in fluorescence may also occur as the pyrene-labelled enzyme binds Mg^{2+} ions. Thus, the rapid phase would occur as the Mg^{2+} ions react with existing E* and the slower phase from the re-equilibration that would occur between E and E* due to the loss of E* from the equilibrium.

The data obtained in these studies supports model (b) above in contrast to the conclusion drawn in previous studies where some data were not available. If we consider the reverse direction of the binding reaction then in model (a) the rate observed should be either k_{-2} or k_{-1}, whichever is the slower. This should be k_{-2} since the observed rate in the forward direction (k_{2app}) is only around $10s^{-1}$ and equation (6) this is equal to $k_2 + k_{-2}$. Thus, k_{-2} must be slower than $10s^{-1}$. However, the data from these experiments show that the observed rate of decrease in fluorescence intensity is approximately 170 - $420s^{-1}$ and approximates k_{-1} (at pH 8.0) given from the data in Figure 4.17. Therefore model (a) is unlikely to be correct. Model (b) is more plausible since the above data does support the observed reverse rate being the dissociation of an enzyme. Mg^{2+} ion complex (e.g. E*. Mg^{2+}). The reverse of the conformational

change (k_r) is probably represented by the second rate, $11.9s^{-1}$, seen in Figure 4.16. As the binary complex dissociates there will be an increase in the concentration of E* and this will re-equilibrate with E. As this occurs, more $E^*.Mg^{2+}$ complex will dissociate with a resultant further decrease in fluorescence intensity with a rate equal to that of the E* - E isomerisation process. If this is correct then it suggests that the E:E* equilibrium is approximately in the ratio 11.9 /10 ie. 1.19 : 1 in the absence of metal ions and in these conditions.

Thus, the structural differences between the apo-enzyme and the Mg^{2+} - enzyme shown in the X-ray data (see chapter 6) may reflect the stabilisation of one form of the enzyme (E*) that is able to bind metal ions with a relatively high affinity in comparison to E.

CHAPTER 5

OBSERVATION OF THE EFFECT OF MUTAGENESIS ON METAL ION AND SUBSTRATE BINDING BY STEADY STATE KINETICS

CHAPTER 5

Observation of the effect of mutagenesis on metal ion and substrate binding by steady state kinetics

5.1 Introduction

5.1.1 Metal binding to inositol monophosphatase

Inositol monophosphatase has an absolute requirement for Mg^{2+} ions for catalytic activity (Hallcher and Sherman, 1980). With the *in vivo* substrate inositol-1-phosphate (Ins-1-P), the activity of the enzyme increases in a sigmoidal manner with increasing concentrations of Mg^{2+} ions (Ganzhorn *et al.*, 1990 and Leech *et al.*, 1993), although at high concentrations (> 10mM Mg^{2+}) it behaves as an uncompetitive inhibitor mutually exclusive with Li^{+} (Ganzhorn *et al.*, 1990). Ganzhorn and Chanal, (1990) have previously demonstrated that the concentration of Mg^{2+} ions resulting in half maximal activity is influenced by the nature of the substrate used. With some substrates e.g. 4-nitrophenyl phosphate or 4-methylumbelliferyl phosphate, the increase in activity with increasing concentrations of Mg^{2+} ion does not follow sigmoidal kinetics. This may arise because the reactions with these substrates have different rate limiting steps. The rate limiting step in the reaction using Ins-1-P as substrate is the breakdown of the $E.Mg^{2+}.Pi$ complex, whereas, with 4-nitrophenyl phosphate as substrate it is believed that ester hydrolysis is the main rate-limiting step. This is because 4-nitrophenyl phosphate lacks the hydroxyl group that was shown to enhance catalysis when Ins(1)P is used as the substrate (Baker *et al.*, 1989), which functions to position the second Mg^{2+} ion. With 4-methylumbelliferyl phosphate, used in these studies, which also lack the hydroxyl groups, stabilisation of the leaving group by the second metal ion may not be so important since the aromatic system functions to stabilise the developing negative charge, (Strasser *et al.*, 1995). The specific activities of the enzyme using these substrates are 12.9μmol/min/mg, 0.54μmol/min/mg and 0.39μmol/min/mg respectively (Gore *et al.*, 1992;

Strasser *et al.*, 1995). Using these substrates no cooperativity is noted with Mg^{2+} ions which greatly simplifies kinetic analyses.

Mg^{2+} and substrate binding to inositol monophosphatase is a complex process, with a structural rearrangement occurring at some point in complex formation. Therefore one of the main reasons behind the design of the mutants studied in this thesis was to investigate the effect of mutating loop-region residues (each shown by sequence alignment and X-ray crystallographic studies to be conserved in this enzyme, the human inositol monophosphatase (Gee *et al.*, 1988; Diehl *et al.*, 1990), rat (Takimoto *et* al., 1985) and human brain (McAllister *et al.*, 1992) and the fructose 1,6 bisphosphatase (Zhang *et al.*, 1993a and 1993b) on the enzymes ability to bind Mg^{2+} ions or substrate and on the ability to undergo a conformational change that has been reported (Gee *et al.*, 1989; Greasley *et al.*, 1994).

Site-directed mutagenesis has been used to engineer the following mutants G76S, G69S, E30P H188Q and C218D and kinetic studies were employed in order to determine if the amino acid substitutions had affected metal ion binding at site 2, the binding site characterised by the K_m for the metal ion. The kinetic studies were carried out using the fluorescent substrate, 4-methylumbelliferyl phosphate in a continuous fluorescence assay as described by Gore *et al.*, (1993).

5.2 Results and Discussion

The kinetic data were fitted to the Michaelis-Menten equation, which is a simple measure of the relationship existing between the initial rate and substrate concentration. There are a few assumptions made in the application of the Michaelis-Menten equation. If we consider the reaction:

$$E + S \underset{k_{-1}}{\overset{k_1}{\rightleftharpoons}} E.S \underset{k_{-2}}{\overset{k_2}{\rightleftharpoons}} E + P$$

in which E is enzyme, S is substrate and P is product then Michaelis and Menten assumed that E , S and ES are in equilibrium i.e. that k_2 is very small and is the rate limiting step of the reaction. This latter assumption is not always valid and the Michaelis Menten model was later modified by Briggs and Haldane, (1925). They assumed that at the start of the reaction, the concentration of P is low and therefore k_{-2} can be ignored and that the concentration of ES remains constant over the initial part of the reaction and that over this time the reaction has a steady state.

The rate of production of product will be = v = k_2[ES]

The concentration of ES depends upon its rate of synthesis. i.e. k_1[E][S] and its rate of breakdown i.e. k_{-1}[ES] + k_2[ES]
Over the first part of the reaction the rates are the same i.e.

$$k_1[E][S] = k_{-1}[ES] + k_2[ES]$$

If [E] is renamed [E_{total} – ES], then

$$k_1[E_{total} - ES]\,[S] = k_{-1}[ES] + k_2[ES]$$

and

$$k_1[E_{total}]\,[S] - k_1[ES]\,[S] = [ES]\,(k_{-1} + k_2)$$

$$k_1[E_{total}]\,[S] = [ES]\,(k_{-1} + k_2 + k_1\,[S])$$

solving for ES

$$[ES] = \frac{k_1[E_{total}]\,[S]}{k_1[S] + k_{-1} + k_2}$$

and

$$\frac{[E_{total}]\,[S]}{[S] + (k_{-1} + k_2)/k_1}$$

The ratio of the rate constants $(k_{-1} + k_2) / k_1$ is termed the Michaelis constant, K_m

Therefore $[ES] = \frac{[E_{total}][S]}{K_m + [S]}$ and since v = k_2[ES]

then

$$v = \frac{k_2 [E_{total}] [S]}{K_m + [S]}$$

when all of the enzyme is saturated by substrate then $V_{max} = k_2[E_{total}]$

and thus we get the Michaelis Menten equation

$$v = \frac{V_{max} [S]}{K_m + [S]}$$

While kinetic constants such as K_m and V_{max} can be calculated using the Michaelis-Menten equation, its use is subject to error owing to the difficulty of measuring initial rates at high substrate concentrations and therefore of extrapolating the hyperbolic curves to give an accurate value of V_{max}. Consequently linear transformations of the Michaelis-Menten equation are often used. The Lineweaver-Burk plot is an example and is obtained by taking the reciprocal of the Michaelis-Menten equation and a plot of 1/v against 1/ [S] results in the direct graphical determination of the K_m and V_{max} (Figure 5.2b).

$$\frac{1}{v} = \frac{K_m}{V_{max}} \cdot \frac{1}{[S]} + \frac{1}{V_{max}}$$

An alternative plot often used to analyse the same data is the Hane's plot represented by the following equation:

$$\frac{[S]}{v} = \frac{K_m}{V_{max}} + \frac{[S]}{V_{max}}$$

5.2.1 K_m and V_{max} values for Mg^{2+} and substrate binding to WT and mutants of inositol monophosphatase

The activity of inositol monophosphatase using the fluorescent compound 4-methylumbelliferyl phosphate (4-MUFP) was measured using the continuous assay described by Gore *et al.*, (1992). This assay makes use of the difference in fluorescence properties of 4-methylumbelliferyl phosphate and

its fluorescent product, 4-methylumbelliferone (4-MUFone). For the calculation of specific activity values, the fluorimeter was initially calibrated by titrating in fixed amounts of 1mM 4-methylumbelliferone (product) into 2ml of 50mM Tris-HCl pH 8.0 at 37°C (Figure 5.1). Subsequently, all assays were carried out using 10 μg of enzyme buffered in 50mM Tris-HCl, pH 8.0 at 37°C. For experiments to determine the V_{max} and K_m values for Mg^{2+} ions, 3mM substrate was used in each of the assays. Although this is only high enough to cause 77% saturation of the enzyme (based upon a K_m of 0.92mM under these conditions (Gore *et al.*, 1992)), higher concentrations were difficult to use in practice. Therefore the data presented have been multiplied by 100/77 to correct for this factor (Table 5.1).

Figure 5.2 (a-l) depicts the Michaelis-Menten curves and corresponding Lineweaver-Burk plots obtained for WT and mutant enzymes. This analysis was repeated for the G76S, G69S, H188Q, E30P and C218D mutant enzymes, with the kinetic parameters V_{max} and K_m summarised in Table 5.1.

5.2.2 WT

The V_{max} and K_m values for WT inositol monophosphatase were found to be 492.6 ± 16.0 nmoles/min/mg and 7.5 ± 1.1mM, both slightly higher than previously published values using the same substrate (390nmole/min/mg and 7.19mM respectively, Gore *et al.*, 1992). As was shown in the above study, no inhibition was observed up to Mg^{2+} concentration of 100mM. The K_m for substrate binding was calculated to be 1.3 ± 0.1mM (Figure 5.3).

5.2.3 G76S

The V_{max} of the G76S mutant obtained corrected for 3mM substrate is 38 % greater than that for the WT enzyme (681.1 ± 14.6nmol/min/mg). By examining the K_m value for Mg^{2+} and substrate binding shown in Table 5.1, it can be seen that the mutant displays a 25% increase in K_m for Mg^{2+} (5.6 ± 0.7mM) and an increase in the K_m for substrate (1.8 ± 0.2mM). No inhibition

Figure 5.1 A calibration curve of the fluorescence of fixed concentrations of product 4-methylumbelliferone (4-MUFone). The fluorescence emission of the product was measured at 450nm upon excitation at 388nm at 37°C.

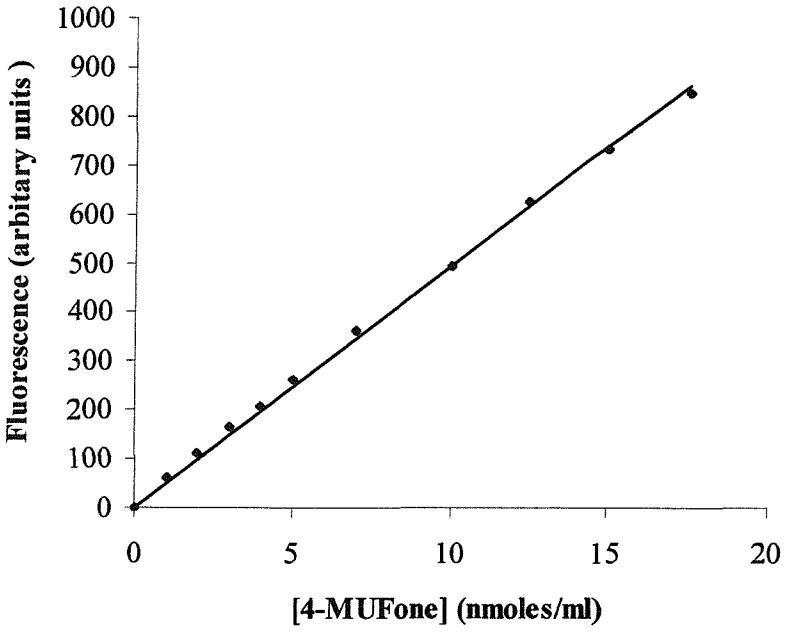
Fluorescence (arbitary units)
1000
900
800
700
600
500
400
300
200
100
0
0
5
10
15
20
[4-MUFone] (nmoles/ml)

Figure 5.2 Michaelis-Menten curves for Mg^{2+} binding at site 2 for (a) WT, (c) G76S, (e) G69S, (g) H188Q, (i) E30P and (k) C218D and the corresponding Lineweaver-Burk plots represented by (b), (d), (f), (h), (j) and (l) respectively for the enzymes listed above.

(a)

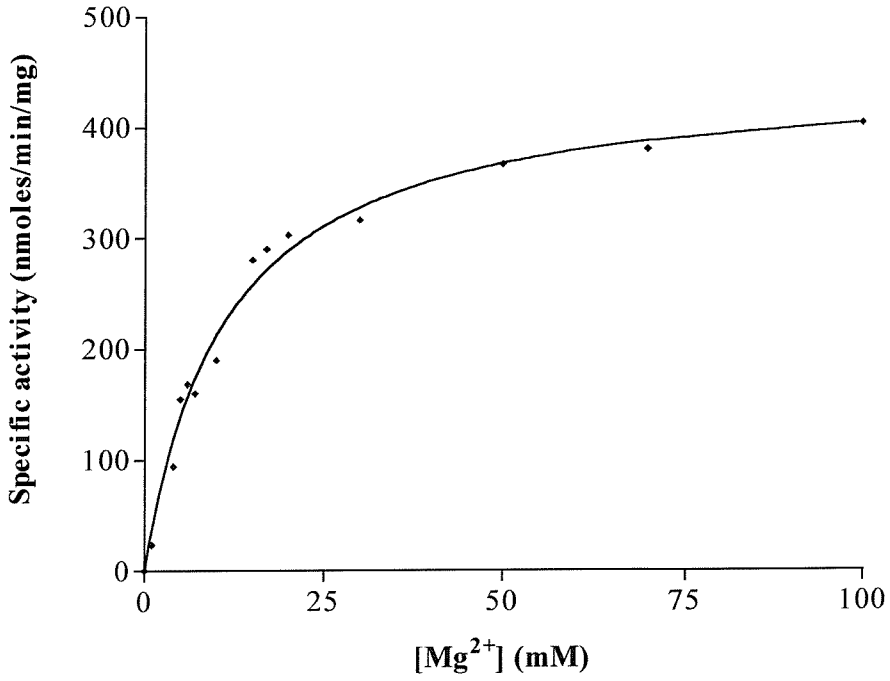
Specific activity (nmoles/min/mg)
500
400
300
200
100
0
0
25
50
75
100
[Mg2+] (mM)

(b)

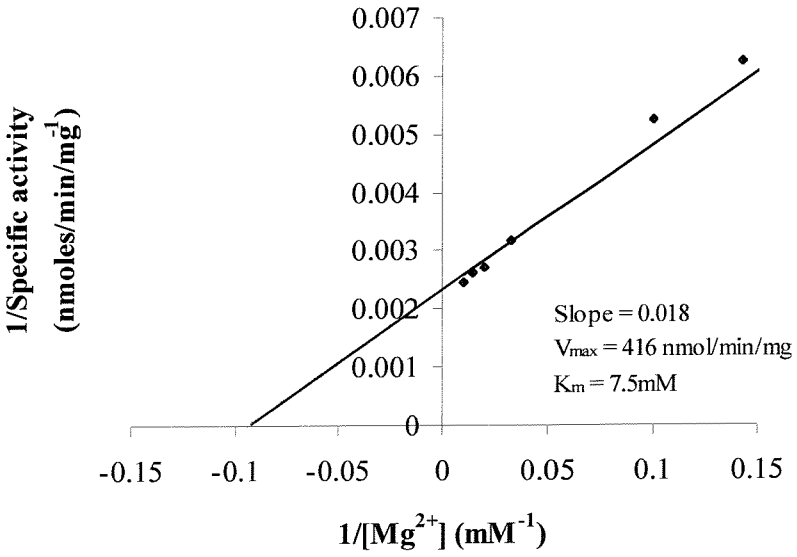
1/Specific activity (nmoles/min/mg-1)
0.007
0.006
0.005
0.004
0.003
0.002
0.001
0
-0.15
-0.1
-0.05
0
0.05
0.1
0.15
1/[Mg2+] (mM-1)
Slope = 0.018
Vmax = 416 nmol/min/mg
Km = 7.5mM

(c)

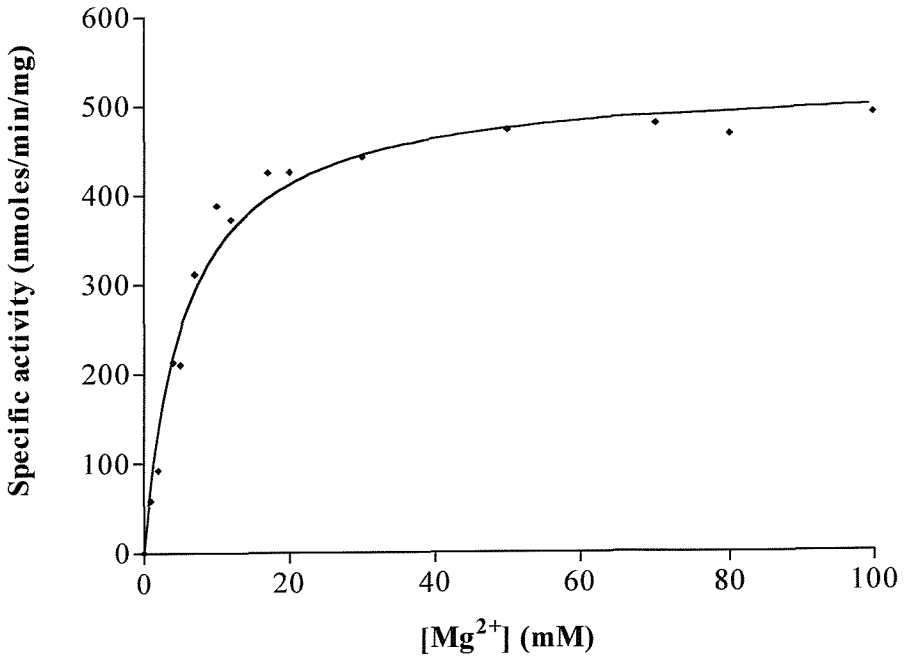
Specific activity (nmoles/min/mg)
600
500
400
300
200
100
0
0
20
40
60
80
100
[Mg2+] (mM)

(d)

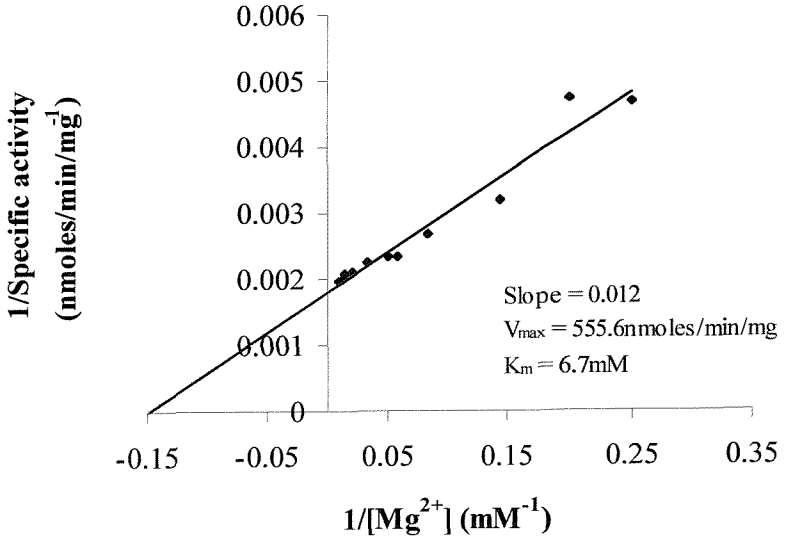
1/Specific activity (nmoles/min/mg-1)
0.006
0.005
0.004
0.003
0.002
0.001
0
-0.15
-0.05
0.05
0.15
0.25
0.35
1/[Mg2+] (mM-1)
Slope = 0.012
Vmax = 555.6nmoles/min/mg
Km = 6.7mM

(e)

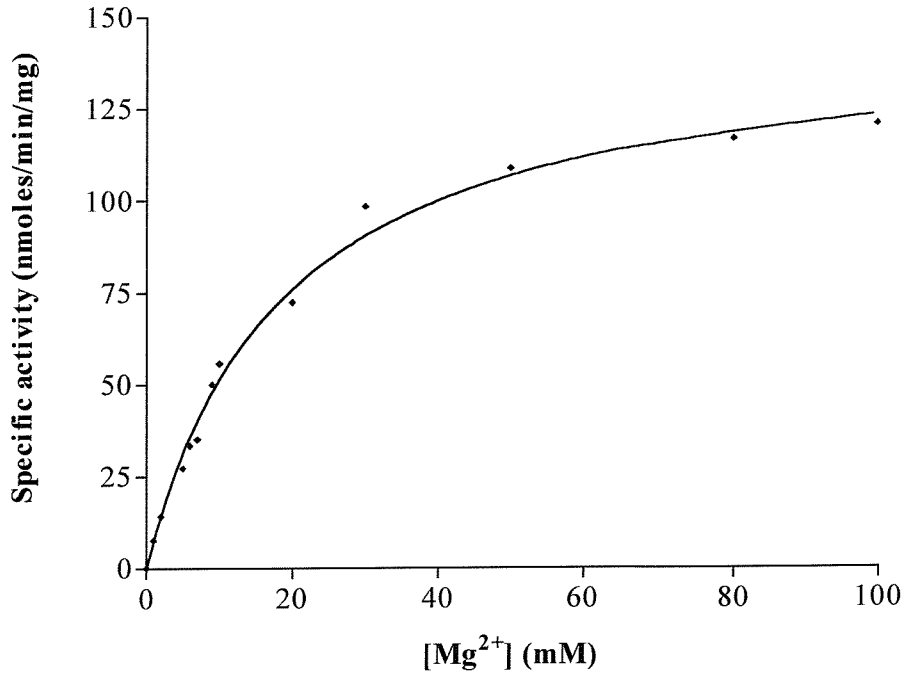
Specific activity (nmoles/min/mg)
150
125
100
75
50
25
0
0
20
40
60
80
100
[Mg2+] (mM)

(f)

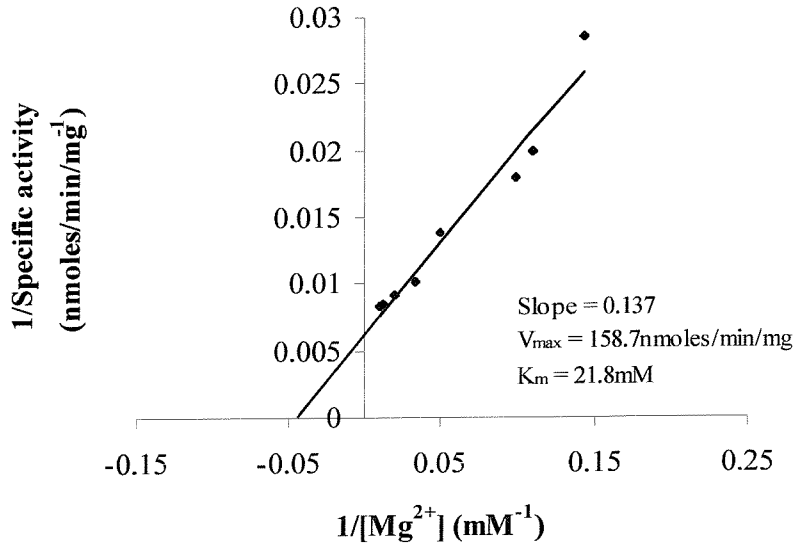
1/Specific activity (nmoles/min/mg-1)
0.03
0.025
0.02
0.015
0.01
0.005
0
Slope = 0.137
Vmax = 158.7nmoles/min/mg
Km = 21.8mM
-0.15
-0.05
0.05
0.15
0.25
1/[Mg2+] (mM-1)

(g)

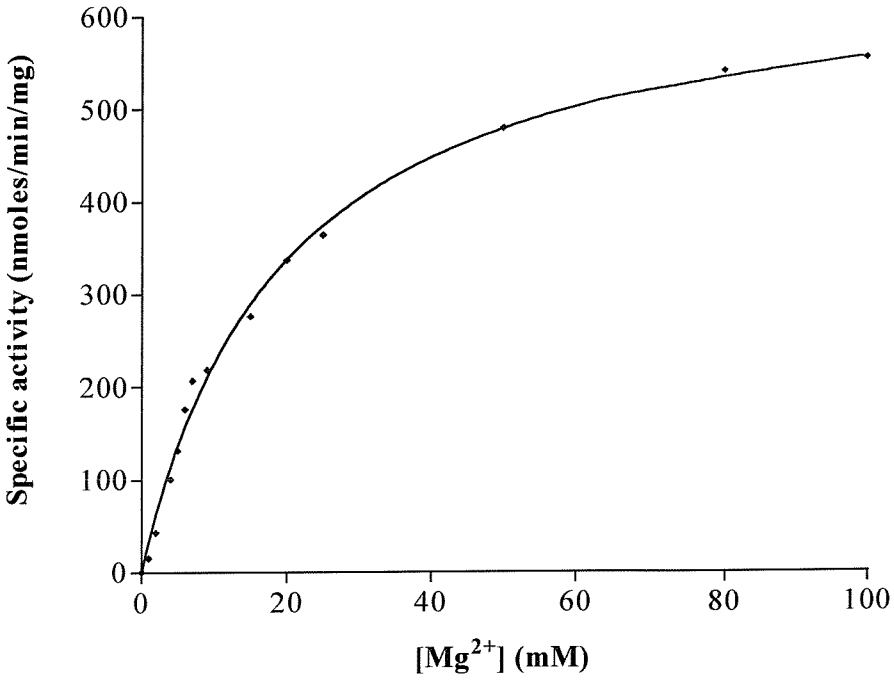
Specific activity (nmoles/min/mg)
600
500
400
300
200
100
0
0
20
40
60
80
100
[Mg2+] (mM)

(h)

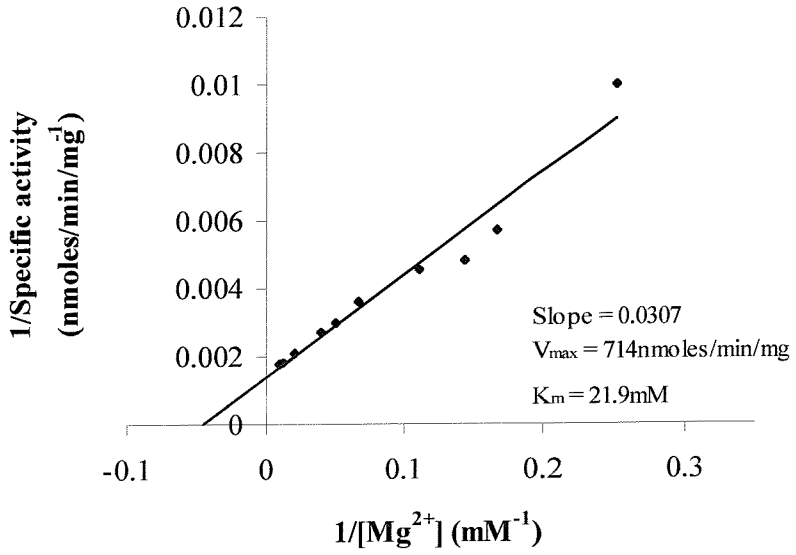
1/Specific activity (nmoles/min/mg-1)
0.012
0.01
0.008
0.006
0.004
0.002
0
-0.1
0
0.1
0.2
0.3
1/[Mg2+] (mM-1)
Slope = 0.0307
Vmax = 714nmoles/min/mg
Km = 21.9mM

(i)

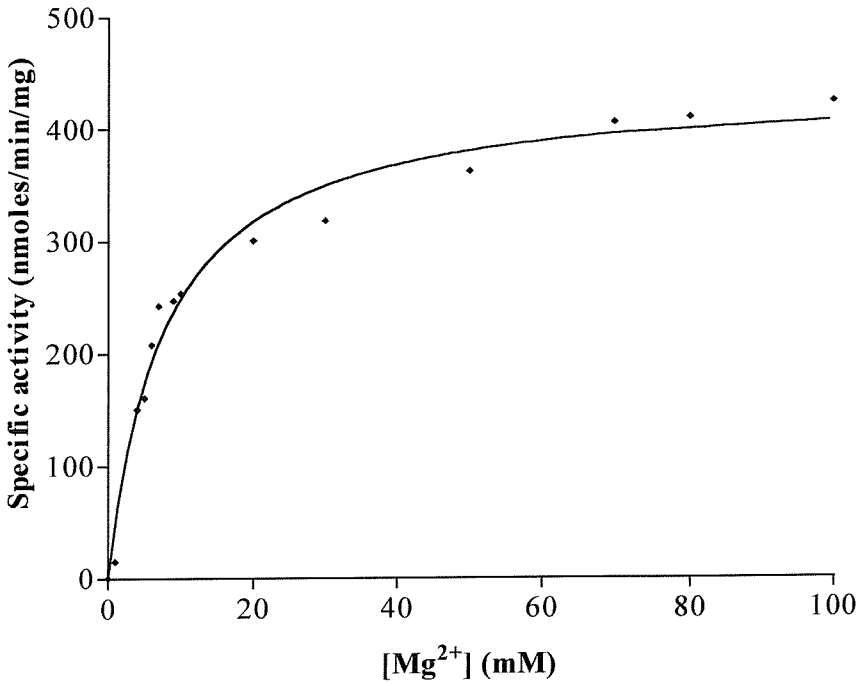
Specific activity (nmoles/min/mg)
500
400
300
200
100
0
0
20
40
60
80
100
[Mg2+] (mM)

(j)

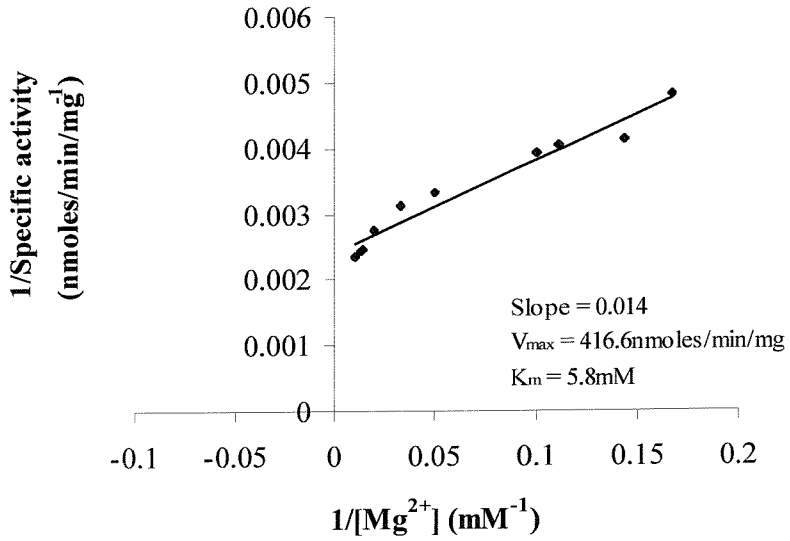
1/Specific activity (nmoles/min/mg-1)
0.006
0.005
0.004
0.003
0.002
0.001
0
Slope = 0.014
Vmax = 416.6nmoles/min/mg
Km = 5.8mM
-0.1
-0.05
0
0.05
0.1
0.15
0.2
1/[Mg2+] (mM-1)

(k)

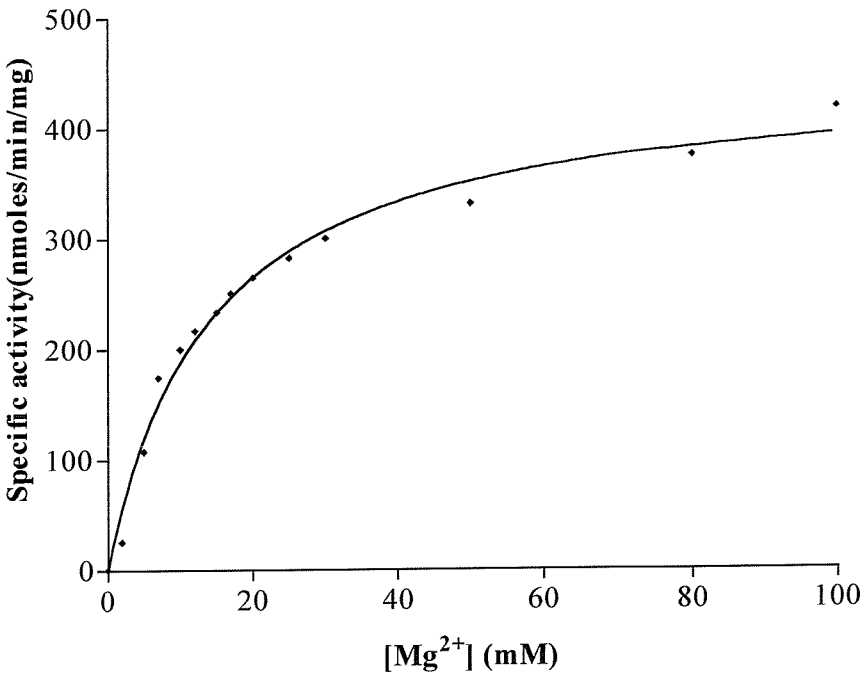
Specific activity(nmoles/min/mg)
500
400
300
200
100
0
0
20
40
60
80
100
[Mg2+] (mM)

(l)

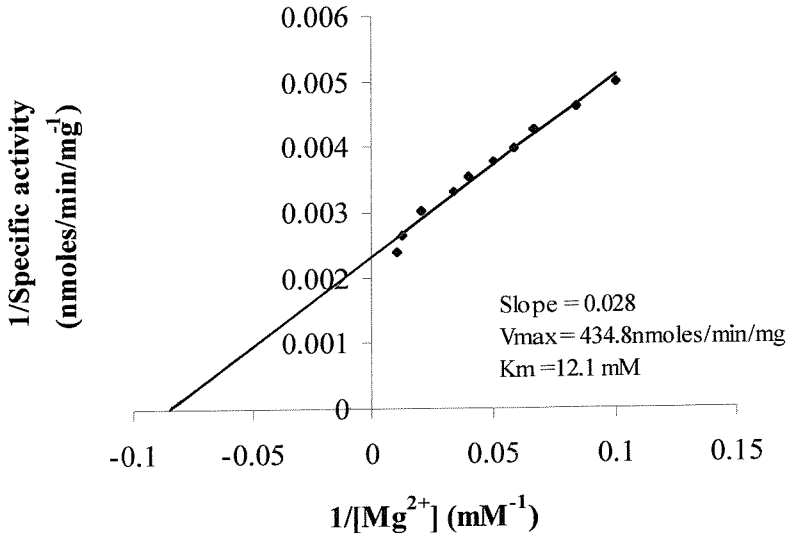
1/Specific activity (nmoles/min/mg-1)
0.006
0.005
0.004
0.003
0.002
0.001
0
-0.1
-0.05
0
0.05
0.1
0.15
1/[Mg2+] (mM-1)
Slope = 0.028
Vmax = 434.8nmoles/min/mg
Km = 12.1 mM

Figure 5.3 Michaelis-Menten plot for 4-MUFP binding to (a) WT enzyme and a Lineweaver-Burk analysis of the same data.

(a)

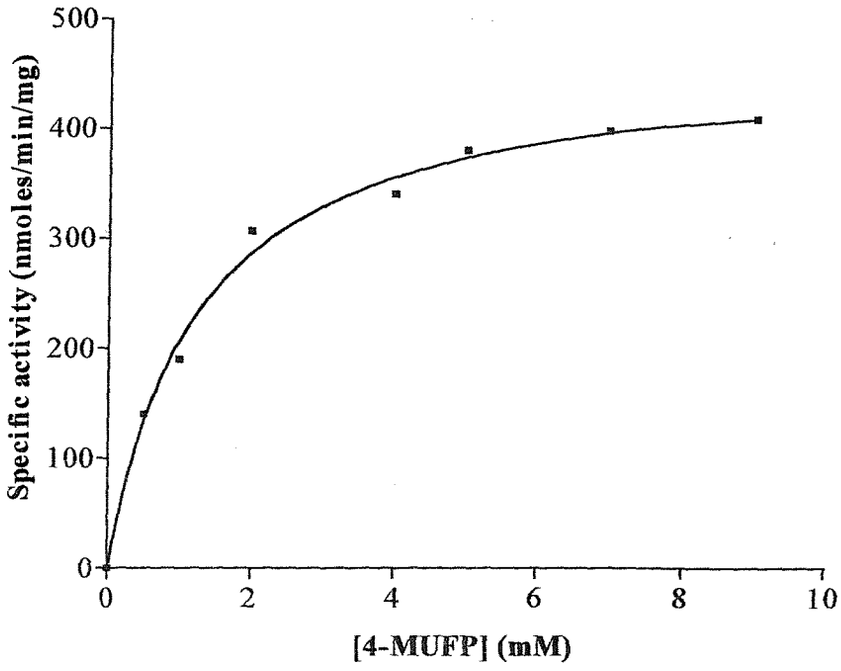
Specific activity (nmoles/min/mg)
500
400
300
200
100
0
0
2
4
6
8
10
[4-MUFP] (mM)

(b)

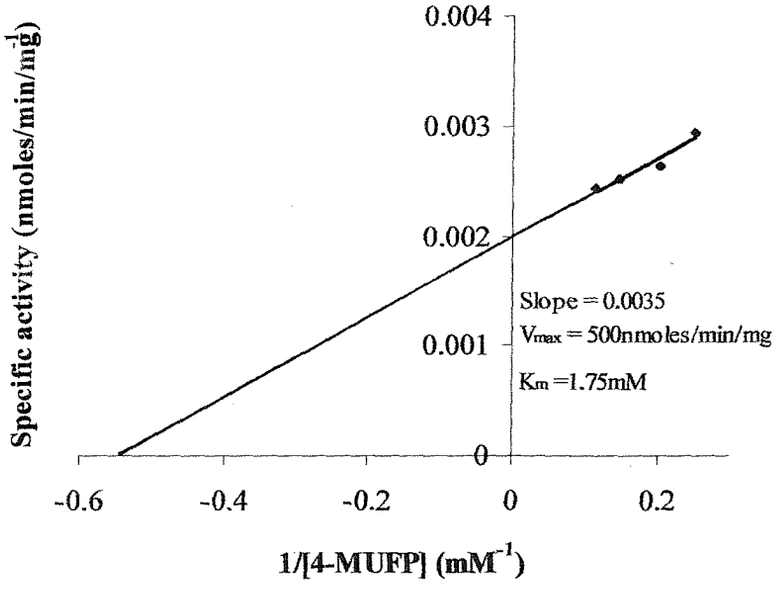
Specific activity (nmoles/min/mg^{-1})
0.004
0.003
0.002
0.001
0
Slope = 0.0035
V_{max} = 500nmoles/min/mg
K_m =1.75mM
-0.6
-0.4
-0.2
0
0.2
1/[4-MUFP] (mM^{-1})

of activity was noted at concentrations of Mg^{2+} ions as high as 100mM. This implies that the G76S mutation has had very little effect on the enzyme and its interaction with the substrate. Furthermore, it demonstrates that the mutation does not make the enzyme more susceptible to inhibition at high metal ion concentrations.

5.2.4 G69S

G69S has a specific activity of 188.7 ± 15.1 nmol/min/mg) which is approximately 38% of that of the WT enzyme. This shows that the location of this residue (G69) is important structurally, although it has no function in the catalytic mechanism. From the data shown in Table 5.1, it can be seen that these changes in maximal activity are accompanied by changes in the affinity of the G69S mutant enzyme for both Mg^{2+} and substrate. The G69S mutant displays a 2.5 fold increase in K_m for Mg^{2+} (18.5 ± 1.4mM) and a 5-fold increase in K_m for substrate (6.6 ± 0.9mM) when compared to the WT enzyme. These data suggest that the geometry of the active site has been perturbed by the mutation. These large reductions in the affinity of the G69S enzyme for both $Mg^{2+}$and the substrate may be due to its position of the substitution in the enzyme structure. The slightly bulkier serine residue may restrict mobility at this position as well as increasing hydrophilicity. It is located next to E70, which is an important residue in binding metal ions at site 1, and in addition it activates a nucleophilic water molecule during the catalytic mechanism (Bone *et al.*, 1992). The G69S mutation adjacent to E70 may also affect the ability of site 2 to bind Mg^{2+} since disturbance of the binding of Mg^{2+} ions at site 1 will probably result in an effect on Mg^{2+} binding at site 2. Since the crystal structure of HIMP (Bone *et al.*, 1992, Bone *et al.*, 1994(b)) has demonstrated that M1 (site 1 Mg^{2+}) ligates to residues E70, D90 and Ile92, and that this ligation is necessary for subsequent substrate phosphate binding. In addition, mutation of the E70 residue to a glutamine dramatically effects both the specific activity (0.26nmoles/min/mg ± 0.008) and the K_m for Mg^{2+} (24.56 ± 3.8mM) (Pollack *et al.*, 1994) and it is therefore probable that a near neighbour mutation may also effect the kinetic parameters

either by distorting the position of the carboxylate group or by changing its pKa.

5.2.5 H188Q

Determination of the V_{max} for H188Q showed it to be 1.5 fold higher than that for WT enzyme (857.6 ± 17.2 nmol/min/mg), however, the K_m for Mg^{2+} and substrate K_m show a 2.7 fold (20.9 ± 1.5mM) and 4.5 fold (4.5 ± 0.6mM) increase suggesting that this mutation has markedly impaired the Mg^{2+} binding ability at site 2 together with substrate binding.

5.2.6 E30P

The E30P mutant has a similar V_{max} to that of WT BIMP (566.4 ± 15.4nmoles/min/mg) and K_m values for Mg^{2+} and substrate binding are almost the same as for the native enzyme (7.6 ± 0.8mM and 1.5 ± 0.2mM respectively) indicating that the more conformationally rigid proline residue at this position in the protein has little effect on metal binding at site 2 or substrate binding. This finding is surprising since it is believed that the amino terminal region of the protein moves during the catalytic cycle and that the presence of the proline residue may impair this movement (Gee *et al.*, 1988).

5.2.7 C218D

The V_{max} for C218D mutant is very similar to that of the WT enzyme (0.2 fold higher, 580.1 ± 17.7mM), while the K_m values for Mg^{2+} and substrate binding were 13.9 ± 1.3mM and 2 ± 0.5mM respectively. This amino acid substitution has increased the K_m for Mg^{2+} binding at site two i.e. it has lowered the affinity of the metal ion for this catalytic site. Previous studies in which C218 was changed to an alanine residue have shown that the mutant enzyme retained full activity with the same K_m for substrate as the native enzyme, but with an increased K_m for Mg^{2+} (Greasley *et al.*, 1993).

All data presented here was also fitted to the Hanes plot analysis in order to confirm the validity of the values obtained. These graphs and the results are shown in Figure 5.4 and it can be seen that the values agree closely with those determined using Michaelis-Menten analysis (Table 5.1).

Table 5.1(a) The K_m and V_{max} values obtained for WT and mutant proteins (n =3).

PROTEIN	WT	G76S	G69S	H188Q	E30P	C218D
K_m Mg^{2+} (mM)	7.5 ± 1.1	5.6 ± 0.7	18.5 ± 1.4	20.9 ± 1.5	7.6 ± 0.8	13.9 ± 1.3
V_{max} Mg^{2+} (nmoles/min/mg)	492.6 ± 16.0	681.1 ±14.6	188.7± 15.1	857.6 ± 17.2	566.4 ± 15.4	580.1 ± 17.7
K_m 4MUFP (mM)	1.3 ± 0.1	1.8 ± 0.2	6.6 ± 0.9	4.5 ± 0.6	4.5 ± 0.6	2.0 ± 0.5

Table 5.1(b) The k_{cat} and the specificity constant (k_{cat}/K_m) values obtained for WT and mutant proteins.

PROTEIN	WT	G76S	G69S	H188Q	E30P	C218D
k_{cat} (min^{-1}) 4-MUFP	1.48	2.04	0.57	2.58	1.7	1.74
k_{cat}/K_m 4-MUFP	1.18	1.12	0.11	0.57	1.11	0.56
k_{cat} (min^{-1}) Mg^{2+}	1.48	2.05	0.57	2.58	1.70	1.74
k_{cat} / K_m	0.19	0.37	0.03	0.12	0.22	0.13

The data shown in Table 5(b) indicate that the mutant G69S has a lower specificity constant than the others both for the substrate and the Mg^{2+} ion suggesting that the active site has been most distorted by this mutation.

Figure 5.4 Hanes plot analysis for Mg^{2+} binding to (a) WT, (b) G76S, (c) G69S, (d) H188Q, (e) E30P and (f) C218D enzymes.

(a)

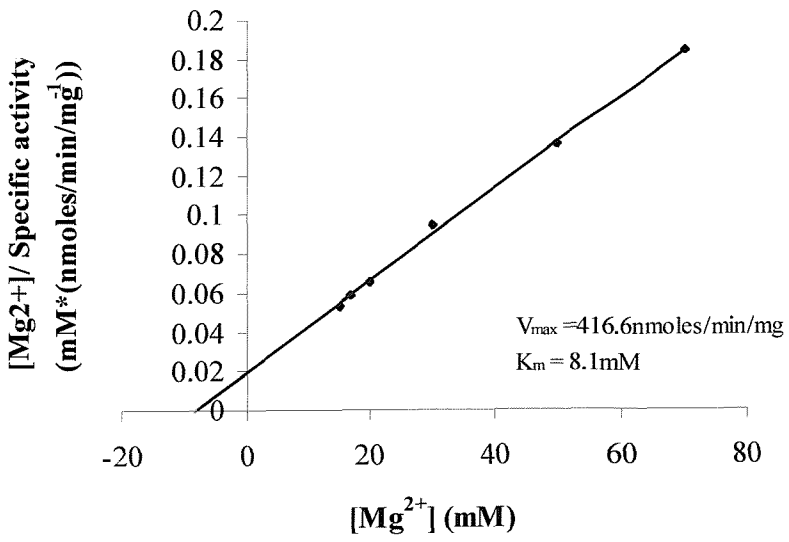
[Mg2+]/ Specific activity (mM*(nmoles/min/mg-1))
0.2
0.18
0.16
0.14
0.12
0.1
0.08
0.06
0.04
0.02
0
-20
0
20
40
60
80
[Mg2+] (mM)
Vmax =416.6nmoles/min/mg
Km = 8.1mM

(b)

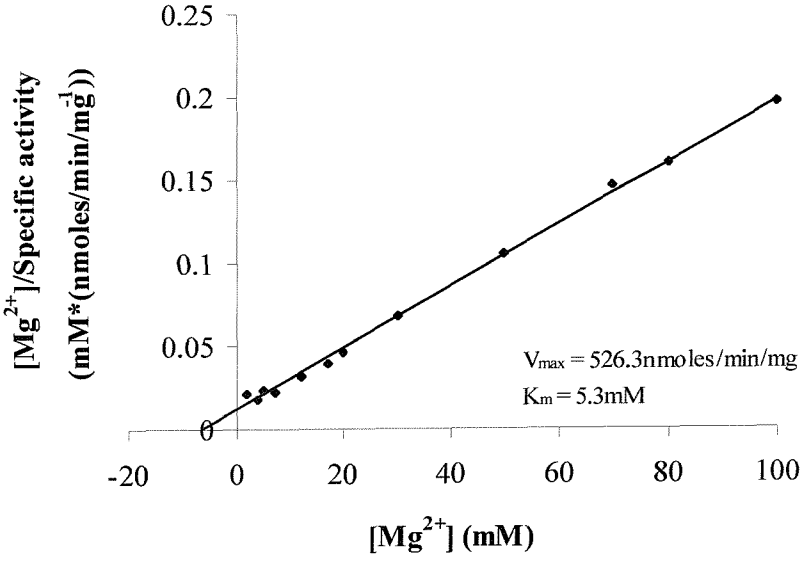
[Mg2+]/Specific activity (mM*(nmoles/min/mg-1))
0.25
0.2
0.15
0.1
0.05
0
-20
0
20
40
60
80
100
[Mg2+] (mM)
Vmax = 526.3nmoles/min/mg
Km = 5.3mM

(c)

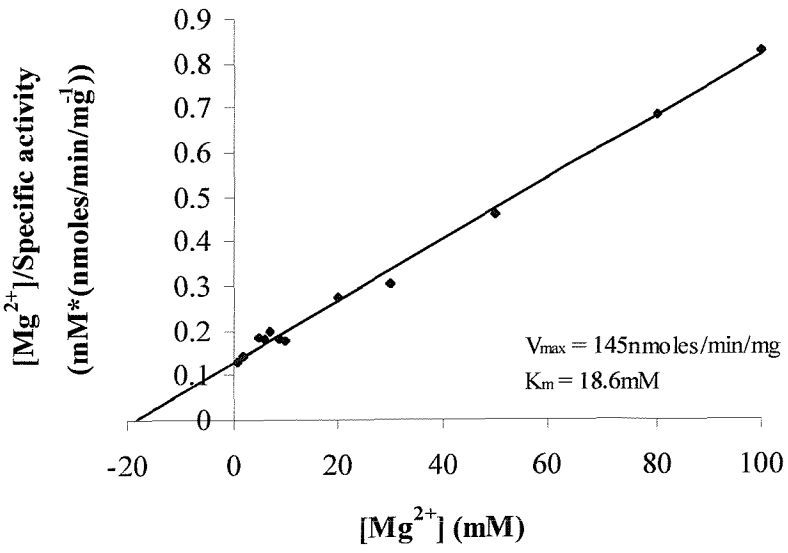
0.9
0.8
0.7
0.6
0.5
0.4
0.3
0.2
0.1
0
-20
0
20
40
60
80
100
[Mg2+]/Specific activity (mM*(nmoles/min/mg-1))
[Mg2+] (mM)
Vmax = 145nmoles/min/mg
Km = 18.6mM

(d)

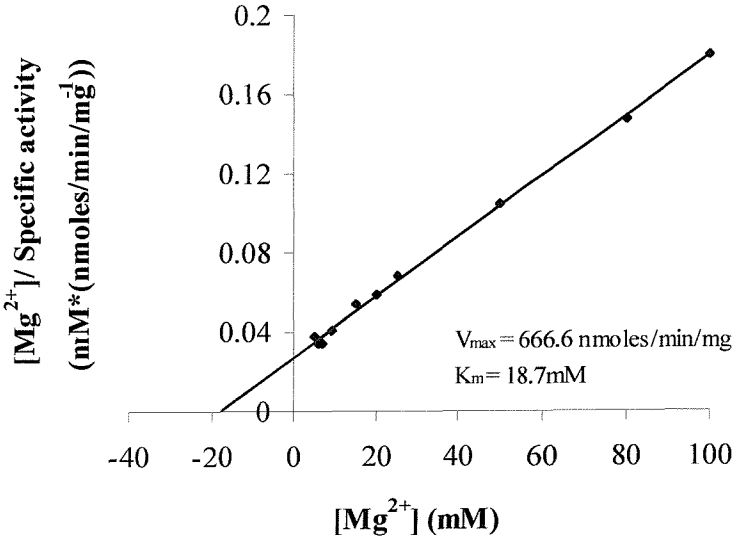
0.2
0.16
0.12
0.08
0.04
0
-40
-20
0
20
40
60
80
100
[Mg2+]/ Specific activity (mM*(nmoles/min/mg-1))
[Mg2+] (mM)
Vmax = 666.6 nmoles/min/mg
Km = 18.7mM

(e)

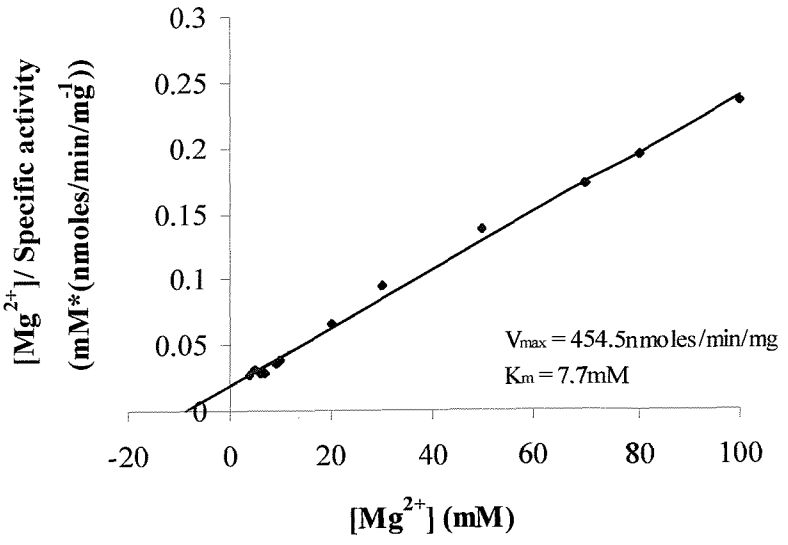
0.3
0.25
0.2
0.15
0.1
0.05
0
-20
0
20
40
60
80
100
[Mg2+]/ Specific activity (mM*(nmoles/min/mg-1))
[Mg2+] (mM)
Vmax = 454.5nmoles/min/mg
Km = 7.7mM

(f)

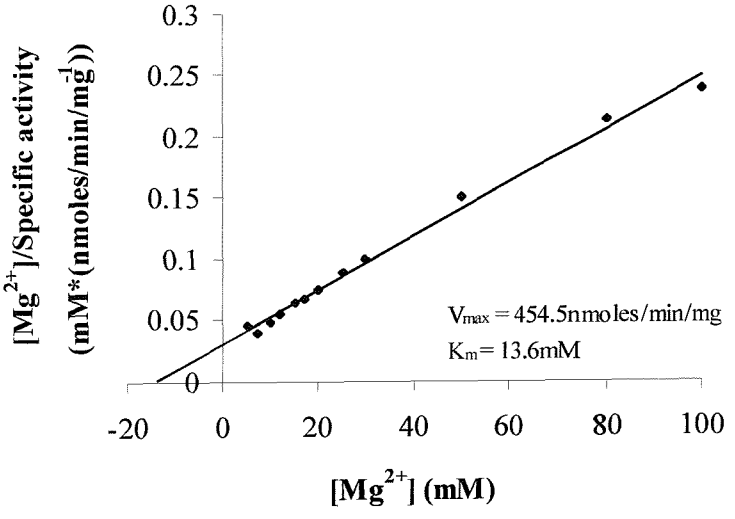
0.3
0.25
0.2
0.15
0.1
0.05
0
-20
0
20
40
60
80
100
[Mg2+]/Specific activity (mM*(nmoles/min/mg-1))
[Mg2+] (mM)
Vmax = 454.5nmoles/min/mg
Km = 13.6mM

5.3 Studies of Li^+ inhibition of inositol monophosphatase

Inositol monophosphatase is uncompetitively inhibited by lithium with respect to the natural substrate inositol-1-phosphate (Ins(1)P). This is of primary interest in the study of inositol monophosphatase since this monovalent ion is used in the treatment of manic-depressive disorders. It was therefore necessary to show that the assay involving 4-MUFP is sensitive to this monovalent cation. Inhibition of bovine inositol monophosphatase by Li^+ occurs when 4-MUFP is the substrate with a K_i value of 16mM (Gore *et al.*, 1992). This is quite different from the value of 0.26mM obtained using the natural substrate (Ins(1)P) (Hallcher and Sherman, 1980). Therefore the values suggest that the inhibition of inositol monophosphatase by Li^+ ions when 4-MUFP is the substrate is much less (60 fold) than when the natural substrate is used. This finding is to be expected since it is probable that the ester hydrolysis is rate limiting using this substrate, and that Li^+ traps an $E.Mg^{2+}.P_i$ intermediate. Consequently there will be less of the $E.Mg^{2+}.P_i$ complex for the Li^+ to bind to when 4-MUFP is the substrate.

Kinetic experiments were carried out using 5, 10,15, 20, 30 and 50mM LiCl in the presence of a fixed concentration of substrate and varying concentrations of Mg^{2+}. The data were analysed using the Lineweaver-Burk equation modified for competitive inhibition. In the presence of a competitive inhibitor the Lineweaver-Burk equation becomes:

$$1/v = (K_m / V_{max}) \,.\, (1/ [S]) \,.\, (1 + [I]/ K_i) + 1/ V_{max}$$

where [I] denotes the concentration of the inhibitor, [S] is the concentration of $[Mg^{2+}]$ and K_i is the dissociation constant of the enzyme-inhibitor complex.

5.3.1 Li^+ inhibition of WT and mutant forms of inositol monophosphatase

Lithium binding was examined using fixed Li^+ concentrations over a range of Mg^{2+} ion concentrations using the standard assay described by Gore *et al.*,

(1992). The assay mixture contained 10μg of inositol monophosphatase, 3mM 4MUFP, Li^+ ions (5, 10, 20, 30 or 50mM), in 50mM Tris.HCl together with Mg^{2+} ions which were varied in an analogous manner, to the standard assay used for the determination of the K_m for Mg^{2+}. Double reciprocal plots of specific activity against the concentration of Mg^{2+} concentrations at fixed Li^+ ion concentrations demonstrate that the V_{max} values for the different Li^+ concentrations are not significantly different form each other (they intersect at a common point on the y-intercept above the horizontal axis), however, the $K_m$app can be seen to increase with increasing concentrations of Li^+, indicating competitive inhibition with respect to Mg^{2+} (Figure 5.4(a)-(e)). With competitive inhibition, the inhibitory effect was seen to be removed, at high Mg^{2+} concentrations.

The K_i value for Li^+ obtained for WT inositol monophosphatase (8 ± 0.2mM) is only half the published value obtained during the characterisation of 4MUFP as a substrate (K_i = 16mM), although the mode of inhibition observed from the Lineweaver-Burk plot was shown to be identical (Gore *et al.*, 1992). The mode of inhibition at high concentrations of Li^+ (~50mM) was shown to be competitive with respect to Mg^{2+}.

The G76S and H188Q mutants exhibited K_i values for Li^+ of 13 ± 0.7mM and 12.8 ± 0.9mM respectively which are in good agreement with the previously published value of 16mM (Gore *et al.*, 1992).

For the G69S mutant the sensitivity to Li^+ inhibition was reduced slightly (K_i value of 20.3 ± 1.5mM). This could in part be accounted for by the low specific activity of this mutant (38% of that of WT enzyme).

The K_i value for Li^+ for E30P was shown to be 24.1 ± 1.6mM which is approximately 3 fold higher than that determined for WT enzyme in this study. It is unclear as to why this may be so, since from Mg^{2+} binding studies, the specific activity value and the K_m for Mg^{2+} binding site 2 (501.2 ± 13.6

Figure 5.5 Lineweaver-Burk plots for Li^+ inhibition of (a) WT, (b) G76S, (c) G69S, (d) H188Q and (e) E30P enzymes.

The concentrations of Li^+ used in the experiments carried out were:

(a) 0mM, 5mM, 25mM and 50mM.

(b) 0mM, 10mM, 20mM, 30mM and 50mM.

(c) 0mM, 5mM, 10mM, 15mM, 20mM and 30mM.

(d) 0mM, 10mM, 15mM, 30mM and 50mM.

(e) 0mM, 15mM, 25mM and 50mM.

(a)

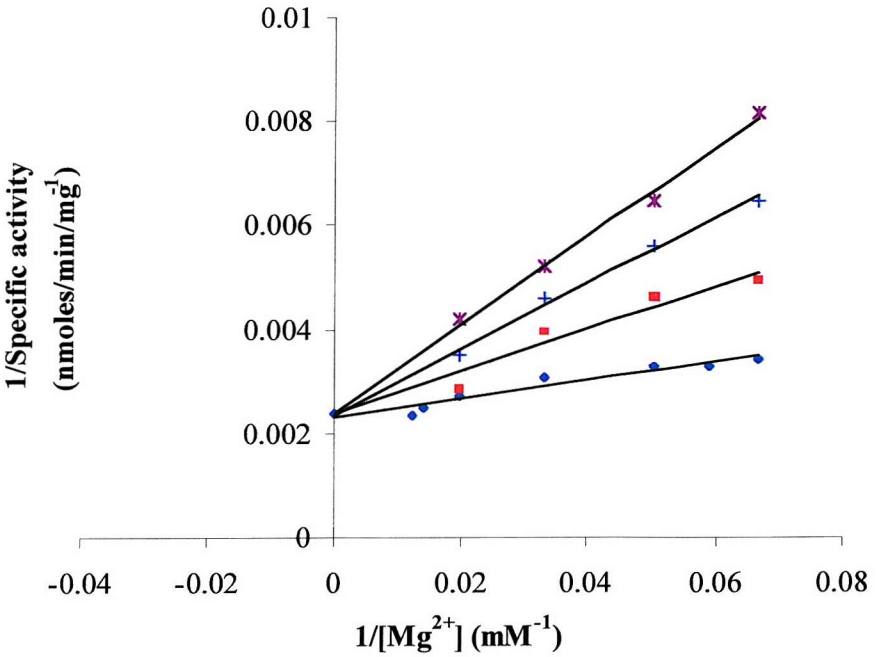
0.01
0.008
0.006
0.004
0.002
0
-0.04
-0.02
0
0.02
0.04
0.06
0.08
1/Specific activity (nmoles/min/mg-1)
1/[Mg2+] (mM-1)

(b)

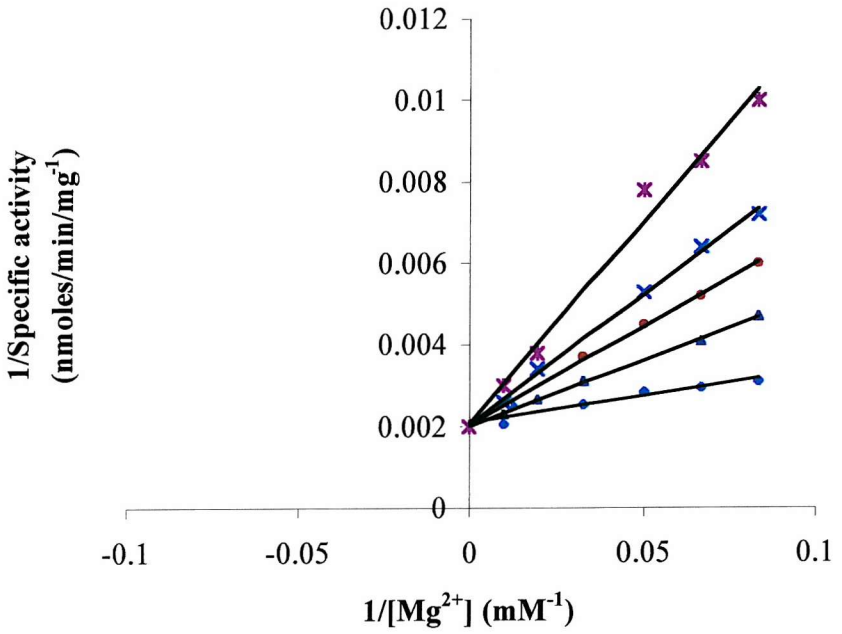
0.012
0.01
0.008
0.006
0.004
0.002
0
-0.1
-0.05
0
0.05
0.1
1/Specific activity (nmoles/min/mg-1)
1/[Mg2+] (mM-1)

(c)

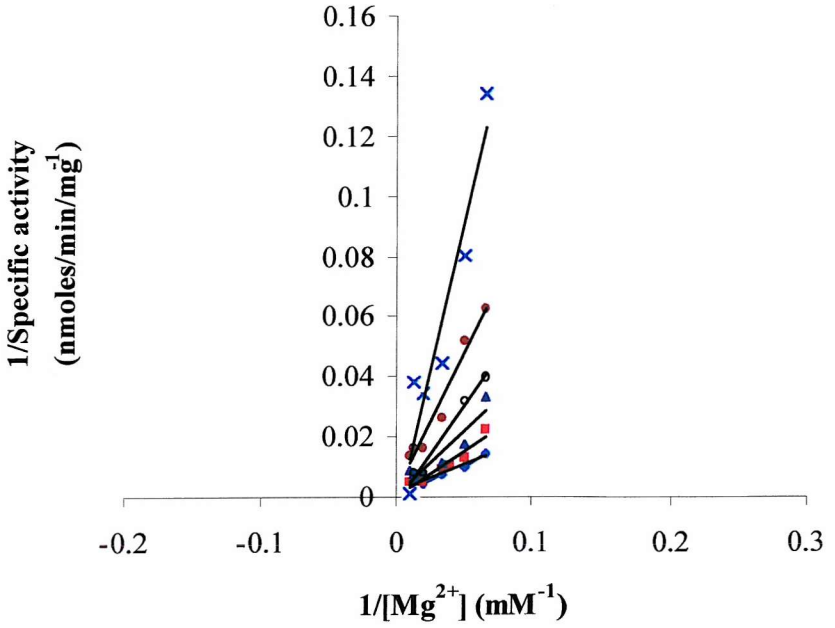
0.16
0.14
0.12
0.1
0.08
0.06
0.04
0.02
0
-0.2
-0.1
0
0.1
0.2
0.3
1/Specific activity (nmoles/min/mg-1)
1/[Mg2+] (mM-1)

(d)

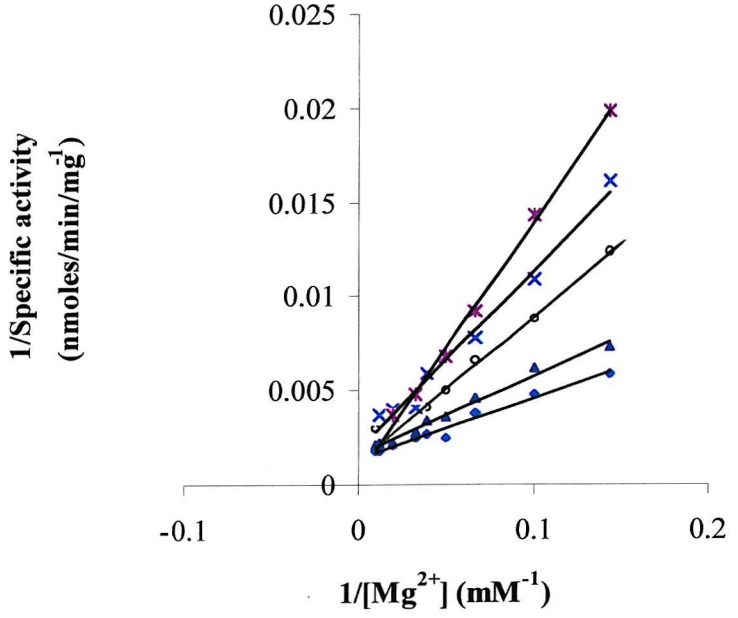
0.025
0.02
0.015
0.01
0.005
0
-0.1
0
0.1
0.2
1/Specific activity (nmoles/min/mg-1)
1/[Mg2+] (mM-1)

(e)

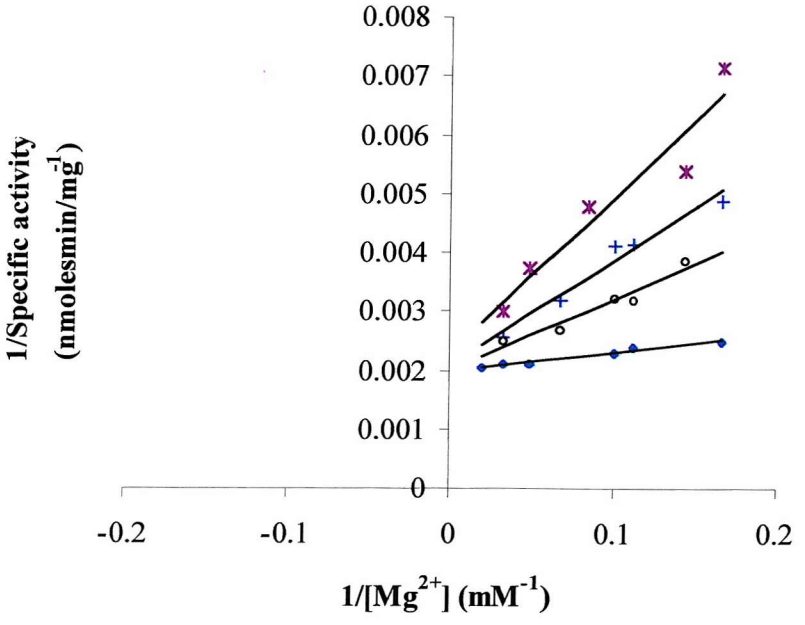
0.008
0.007
0.006
0.005
0.004
0.003
0.002
0.001
0
-0.2
-0.1
0
0.1
0.2
1/Specific activity (nmolesmin/mg-1)
1/[Mg2+] (mM-1)

nmoles/min/mg and 7.6 ± 0.8mM respectively) clearly demonstrates that this E30 residue is not important for Mg^{2+} binding to site 2 or catalytic activity.
X-ray crystallographic studies also show that none of the above residues are important for Mg^{2+} and therefore for Li^{+} ion binding at metal binding site 2 (Bone *et al.*, 1994(a)).

Table 5.3 Shows the K_i values for Li^{+} obtained for WT and mutant inositol monophosphatase (n=2).

PROTEIN	WT	G76S	G69S	H188Q	E30P
K_i for Li^{+} (mM)	8.0 ± 0.2	13 ± 0.7	20.3 ± 1.5	12.8 ± 0.9	24.1 ± 1.6

It has previously been demonstrated by Ganzhorn and Chanal, (1990) that inhibition of the enzyme by Li^{+} is dependent on the nature of the substrate used. This is in agreement with previous studies carried out by Attwood *et al.*, (1998) and Gee *et al.*, (1988). Consequently since 4-MUFP displays only 0.3% of the specific activity of the natural substrate (Ins(1)P, 0.12mM) and yet displays a 2-fold higher K_m for Mg^{2+}ions (K_m for Mg^{2+} with Ins(1)P, 3mM) than when Ins(1)P is used as substrate, it would be expected that Li^{+} ions would inhibit the enzyme less effectively when 4-MUFP is the substrate. Comparison of the K_i values for Li^{+} inhibition using Ins(1)P (0.26mM) and 4MUFP (16mM) show this observation to be correct. Studies in which residues in close proximity or at the active site were mutated (K36I, D90N, T95A, T95S, H217Q and C218A) showed parallel reductions in both the K_m for Mg^{2+} and K_i for Li^{+} ions, consistent with the hypothesis that Mg^{2+} and Li^{+} share a common binding site Pollack *et al.*, (1993).

It has been proposed that Li^{+} binds after the second Mg^{2+} leaves the

$E.Mg^{2+}.P_i$. Mg^{2+}complex to form $E.Mg^{2+}.P_i.L_i$ thereby preventing the dissociation of the P_i product (Leech *et al.*, 1993). However, with 4-MUFP as substrate where ester hydrolysis is the rate-limiting step, $E.Mg^{2+}.P_i$ does not accumulate (i.e. phosphate release is not rate-limiting as with Ins(1)P) which in turn means that inhibition by Mg^{2+} is negligible (as seen from the previous studies in Section 5.2.2). With Li^+, however, in the presence of Mg^{2+} it is believed that the ion binds either the enzyme-Mg^{2+} or the enzyme-substrate complex to form either $E.Mg^{2+}.Li^+$ or $E.Mg^{2+}.S.Li^+$, in competition with the activating Mg^{2+} ion.

CHAPTER 6

CRYSTALLISATION AND STRUCTURAL DETERMINATION OF RECOMBINANT BOVINE INOSITOL MONOPHOSPHATASE

CHAPTER 6

Crystallisation and structural determination of recombinant bovine inositol monophosphatase

6.1 Introduction

The structure of human inositol monophosphatase has been determined at 2.6Å resolution in the presence of Mn^{2+} ions (Bone *et al.*, 1994b). This structure suggests that 3 Mn^{2+} ions bind to each monomer, one of which is displaced upon the binding of the inorganic phosphate ion. The absence of the substrate molecule in this structure led to the question as to whether the third metal ion is necessary for catalysis and most studies to date propose the existence of a 2 metal ion mechanism. Since much of the kinetic work and binding studies presented here and elsewhere (Hallcher and Sherman, 1980; Faraci *et al.*, 1993; Gore *et al.*, 1993; Pollack *et al.*, 1994; Greasley *et al.*, 1994 and Thorne *et al.*, 1996) have been carried out with the bovine enzyme, crystallisation of the enzyme leading to the determination of the structure in the presence of the natural metal ligand Mg^{2+} would be most rewarding. The attainment of a high resolution structure is essential for full interpretation of the data. Previous attempts at obtaining bovine inositol monophosphatase crystals have failed mainly due to impure protein preparations or proteolysis at the highly susceptible proteolytic site (K36-Ser37) (Greasley *et al.*, 1993). It would also be of great interest to crystallize the enzyme in the presence of Li^{+} ions. Since Li^{+} ions, which have only 3 electrons, are difficult to visualize using X-ray analysis (Bone *et al.*, 1992), only a high resolution structure (1-1.3Å) would allow Li^{+} ions to be observed and this in turn would allow the metal binding site to be elucidated together with the appropriate ligands involved.

Currently X-ray crystallography and NMR are the two most commonly used techniques employed to solve the three-dimensional structures of proteins. Both techniques may take a long time for complete determination of the structure. X-ray crystallography requires a number of prerequisites including

the need for large quantities of protein, diffraction quality crystals, maintaining the crystals in their native state and a knowledge of the primary structure. For NMR, the structure of the protein of interest can be determined in solution, however, as for crystallography the protein is required in large quantities and the technique can only be used for proteins <15kDa in size.

6.2 Protein purity

The purity of the protein used for crystal growth is one of the most important factors for growing diffraction quality crystals (McPherson *et al.*, 1995). Crystallisation is affected by microheterogeneity, which may arise as a result of chemical modification, cysteine oxidation or proteolysis. Microheterogeneity is difficult to detect, however, it can be detected by native gel electrophoresis or light scattering techniques.

6.3 Protein and macromolecular crystals

In a typical protein crystal each protein molecule is accurately positioned in a three-dimensional lattice, with the unit cell being the basic building block from which the whole volume of the crystal is built up by infinite repetition. The unit cell is specified by the cell dimensions a, b and c which correspond to the lengths of the axes and α, β and γ which are the interaxial angles.

Protein and small molecule crystals mainly differ in that the unit cell of the former can typically contain up to 30-80% by volume of solvent. This solution environment means that only a small proportion of the protein surface is involved in contacts with other protein molecules. X-ray structures are very similar to solution structures determined by NMR except for a few surface regions where hydrogen bonds, Van der Waals contacts and hydrophobic interactions serve to stabilize the crystal lattice.

In the absence of surrounding liquid, crystals are very fragile and susceptible to solvent loss by evaporation. As a result of their large solvent environment,

proteins in the crystal lattice are often found to be functional and thus it is possible to react the protein within the crystal lattice; heavy atom isomorphous replacement stems from this phenomenon and is sometimes used to solve macromolecular structures in cases where a homologous model to the protein of interest is absent. In a similar manner, ligands, substrate analogues and inhibitors can be introduced into the active site providing much insight into active sites.

6.4 Protein crystallisation

The search for ideal protein crystallisation conditions is complex; it is often achieved through trial and error and in many cases it represents the main obstacle in crystallographic analysis. There are several methods that exist for setting up crystallisation trials, with the basic principle being the same for most proteins. Crystallisation is essentially brought about by altering the solubility of a protein solution. This can be brought about by varying parameters including protein concentration, the concentration of the precipitant, temperature, pH and buffer type. Polyethylene glycols (PEGs) are commonly used in crystallisation protocols primarily because they are powerful precipitants which work in an analogous manner to salts such as ammonium sulphate (i.e. "salting out").

Hanging drop or vapour diffusion is the most commonly used technique to bring about crystallisation. In this case, the protein (3-10μl) is mixed with an equal volume of final precipitant solution and pipetted onto a siliconised 22mm glass cover slip. The cover slip is then inverted over a sealed chamber containing the same precipitant solution and the system is allowed to reach equilibrium via diffusion of water vapour from the drop to the precipitating solution. A very basic knowledge of the crystallisation process can be gained by considering the two-dimensional solubility diagram (Figure 6.1).

Figure 6.1 A typical two-dimensional phase diagram showing the relationship between the protein and precipitant concentration in a crystallisation experiment.

(A) An unsaturated solution region exists when the protein is present in solution.

(B) With increasing protein and precipitant concentrations, the solution moves into the supersaturation phase. In such a state crystallisation can take place if suitable nuclei are present. This normally takes place on the border of the supersaturation and precipitation phase.

(C) Further increases in the concentration results in precipitation of the protein.

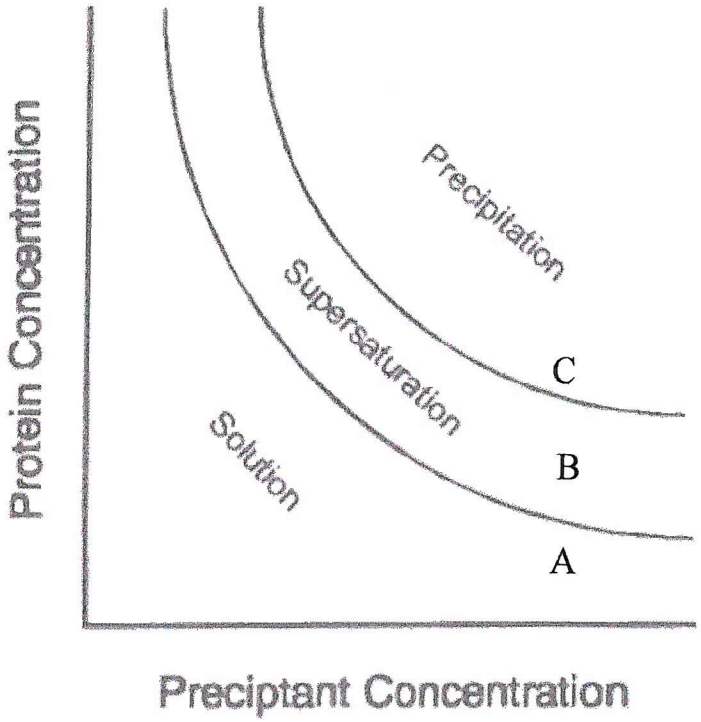
Protein Concentration
Precipitation
Supersaturation
Solution
C
B
A
Preciptant Concentration

6.5 Initial crystallisation screens and results

Recombinant bovine inositol monophosphatase was purified, dialysed and prepared as described in materials and methods (chapter 2, sections 2.4.3, 2.4.7 and 2.9.1). Crystals were grown using the 'hanging drop' or vapour diffusion method (Figure 6.2). An initial screen was set up using the MDL structure screen kit which contains 98 different sterile filtered reagents, with the variables being buffer, pH, salt and precipitant concentrations. These trial crystallisation conditions have been selected on the basis of previously published studies. Multiple hanging drops were used in each well of the crystallisation tray (Linbro plate). 1ml of the crystal screen mixture was placed in the reservoir of a 24 well Linbro plate. 2µl of the reagent was then mixed with an equal volume of 20mg/ml WT inositol monophosphatase and placed on a siliconised cover slip. This was subsequently repeated for enzyme containing 10mM Mg^{2+} and G76S inositol monophosphatase. Once all the screen reagents had been sampled, the cover slides were then inverted over the well which had been pregreased to form an airtight seal, the trays were sealed and allowed to equilibrate for several weeks at 25°C. This screening method generated a number of crystals, as shown in Table 6.1. Crystals were found using reagents 2, 7, 9, 25, 31, 33, 37, 58, 62, 69, and 86 corresponding to Figure 6.3 (a)-(k) respectively. Table 6.1 lists the conditions giving rise to crystal growth. Comparison of these conditions with those used to crystallise the human enzyme reveals that PEG 4K/8K is common to both sets of conditions together with Tris.HCl buffer (pH 7.5) (Table 6.2, 1IMC.pdb).

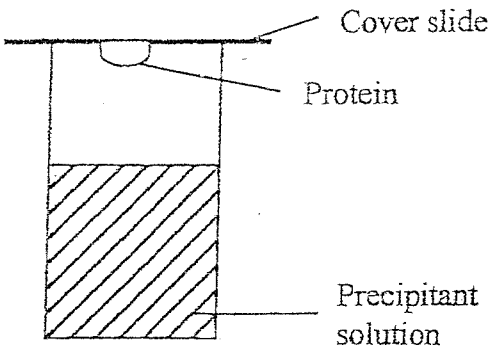

Figure 6.2 Hanging drop method used for the crystallisation of inositol monophosphatase (adapted from Eisenberg and Hill, 1989).

Table 6.1 MDL structure screen reagents used in initial crystallisation trials, which gave rise to crystal growth.

Structure screen reagent number	Buffer	Salt	Precipitant
2	0.1M Na Acetate trihydrate pH 4.6	0.2M Ammonium acetate	30% PEG 4000
7	0.1M tri-sodium citrate dihydrate pH 5.6	0.2M Ammonium acetate	30% w/v PEG 4000
9	0.1M tri-sodium citrate dihydrate pH 5.6	None	20% w/v 2-propanol, 20% w/v PEG 4000
25	0.1M Na Hepes pH 7.5	0.2M tri-sodium citrate dihydrate	20% v/v 2-propanol
31	0.1M Na Hepes pH 7.5	None	10% v/v 2-propanol, 20% w/v PEG 4000
33	0.1M Tris.HCl pH 8.5	0.2M Magnesium chloride hexahydrate	30% w/v PEG 4000
37	0.1M Tris.HCl pH 8.5	0.2M Sodium acetate trihydrate	30% w/v PEG 4000
58	0.1M Tris.HCl pH 9.0	0.2M Ammonium phosphate monobasic	50% v/v MPD
62	0.1M Hepes pH 7.5	None	10% w/v PEG 6000, 5% v/v MPD
69	0.1M Hepes pH 7.5	None	10% v/v PEG 8000, 8% v/v EG
86	0.1M Sodium acetate pH 4.6	0.2M NaCl	30% w/v PEG 4000

Figure 6.3 Initial screen hits using the MDL crystal screen kit. The figure shows low resolution images of crystals formed in some test conditions. Crystals shown in (a)-(k) were grown using the reagents corresponding to 2, 7, 9, 25, 31, 33, 37, 58, 62, 69 and 86 respectively outlined in Table 6.1.

a)

b)

c)

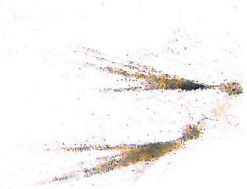

d)

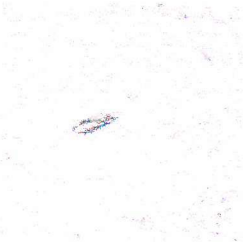

e)

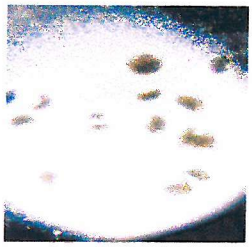

f)

g)

h)

i)

j)

k)

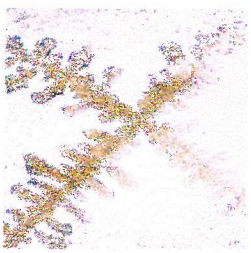

Table 6.2 The crystallisation conditions used to produce human inositol monophosphatase crystals (adapted from Bone *et al.*, 1992; Bone *et al.*, 1994(a) and (b)).

Structure	Crystallisation conditions
1AWB	18% PEG 8000, 100mM sodium cacodylate pH6.5, 200mM calcium acetate, 1mM EDTA, 4mM DTT, 40mM D-inositol-1-phosphate.
1IMA	20mM Tris.HCl pH7.8, 1mM EGTA, 2mM o-phenanthroline, 5mM glutathione, 3mM NaN_3, 2-6mM $Gd_2(SO_4)_3$, 10mg/ml HIMP, 70% Li_2SO_4 (pH 7) and 200mM D-inositol-1-phosphate.
1IMB	20mM Tris.HCl pH7.8, 1mM EGTA, 2mM o-phenanthroline, 5mM glutathione, 3mM NaN_3, 2-6mM $Gd_2(SO_4)_3$, 10mg/ml HIMP, 70% Li_2SO_4 (pH 7) and 100mM L-inositol-1-phosphate.
1IMC	20mM Tris.HCl pH7.5, 10 PEG 8000, 5mM glutathione, 5mM $MnCl_2$, 3mM NaN_3, 50mM 4-morpholinepropanesulfonic acid (pH 7.5), 1mM EGTA, 2mM o-phenanthroline, and 10-15mg/ml HIMP.
1IMD	20mM Tris.HCl pH7.4, 10% PEG 8000, 5mM glutathione, 40mM potassium phosphate, 3mM NaN_3, 50mM 4-morpholinepropanesulfonic acid (pH 7.4), 1mM EGTA, 2mM o-phenanthroline, and 10-15mg/ml HIMP.
1IMF	20mM Tris.HCl pH7.4, 25% PEG 4000, 3mM glutathione, , 3mM NaN_3, and 10-15mg/ml HIMP.
2HHM	20mM Tris.HCl pH7.8, 1mM EGTA, 2mM o-phenanthroline, 64-68% Li_2SO_4 (pH 7), 5mM glutathione, 3mM NaN_3, 2-6mM $Gd_2(SO_4)_3$, and 10mg/ml HIMP

6.6 Optimisation of crystallisation conditions

Crystallisation conditions were optimised via factorial screening by altering the precipitant concentration (0-37.5%), the salt concentration (0.1M-0.3M Na acetate) and the buffer type (0.1M Tris.HCl / 0.1M Na Hepes) or pH (7.5-8.5) (Figure 6.4). A crystal of WT BIMP was obtained one month after the optimised set up in 15% PEG 4K, 0.1M Na Hepes pH 8.5 containing 0.1M Na acetate. Figure 6.5 shows a crystal of wild type recombinant bovine inositol monophosphatase with the appropriate dimensions labelled.

6.7 Cryocrystallography

There are two methods commonly used for preparing crystals for data collection. Diffraction experiments can either be carried out at room temperature, where the crystal is mounted in a glass or quartz capillary, or at low temperature, usually 100 K, where the crystal is soaked in a cryoprotectant and mounted in a fibre loop for freezing prior to data collection. The cryoprotectant acts as an "antifreeze" by preventing the formation of ice in the solvent channels of the protein crystal which would cause cracking and disorder. It achieves this by transforming the liquid surrounding the crystal into glass, a process known as vitrification. The main reason for freezing crystals is to reduce radiation damage caused by free radicals.

A crystal (0.6mm x 0.4mm x 0.1mm; Figure 6.5) for low temperature data collection was prepared by soaking it for a short time in a solution of mother liquor (which already contained 15% PEG 4K). The crystal was then mounted in a mohair loop that supports it by the surface tension of the surrounding liquid. Once mounted, the crystal was flash cooled by plunging it initially into liquid ethane and then quickly into liquid nitrogen after which it was sealed in a cryovial for transportation. Once at the synchrotron the crystal was rapidly placed in the nitrogen stream of a cryostream (Oxford Cryosystems), which maintained its temperature at 100K. Ice formation was prevented by a stream of dry air surrounding the nitrogen stream.

Figure 6.4 Optimisation of crystallisation conditions using the factorial screening technique. Labelled WT* and G76S* denotes conditions under which diffraction quality crystals were obtained.

Precipitant

1) No Na acetate

PEG 4K ⟶

	0%	7.5%	15%	22.5%	30%	37.5%
0.1M Tris.HCl pH 7.5						
0.1M Tris pH 8.5						
0.1M Na Hepes pH 7.5						
0.1M Na Hepes pH 8.5						

2) 0.1M Na acetate

PEG 4K ⟶

	0%	7.5%	15%	22.5%	30%	37.5%
0.1M Tris.HCl pH 7.5						
0.1M Tris.HCl pH 8.5						
0.1M Na Hepes pH 7.5						
0.1M Na Hepes pH 8.5			**WT***			

3) 0.2M Na acetate

PEG 4K ⟶

	0%	7.5%	15%	22.5%	30%	37.5%
0.1M Tris.HCl pH 7.5						
0.1M Tris.HCl pH 8.5						
0.1M Na Hepes pH 7.5						
0.1M Na Hepes pH 8.5						

4) 0.3M Na acetate

PEG 4K ⟶

	0%	7.5%	15%	22.5%	30%	37.5%
0.1M Tris.HCl pH 7.5						
0.1M Tris.HCl pH 8.5				**G76S***		
0.1M Na Hepes pH 7.5						
0.1M Na Hepes pH 8.5						

Figure 6.5 Crystal of WT BIMP obtained using the hanging drop method. The crystal grew over a one-month period in 0.1M Na Hepes pH 8.5, 0.1M Na acetate, 15% v/v PEG 4K and 10mM Mg^{2+} ions at 25°C.

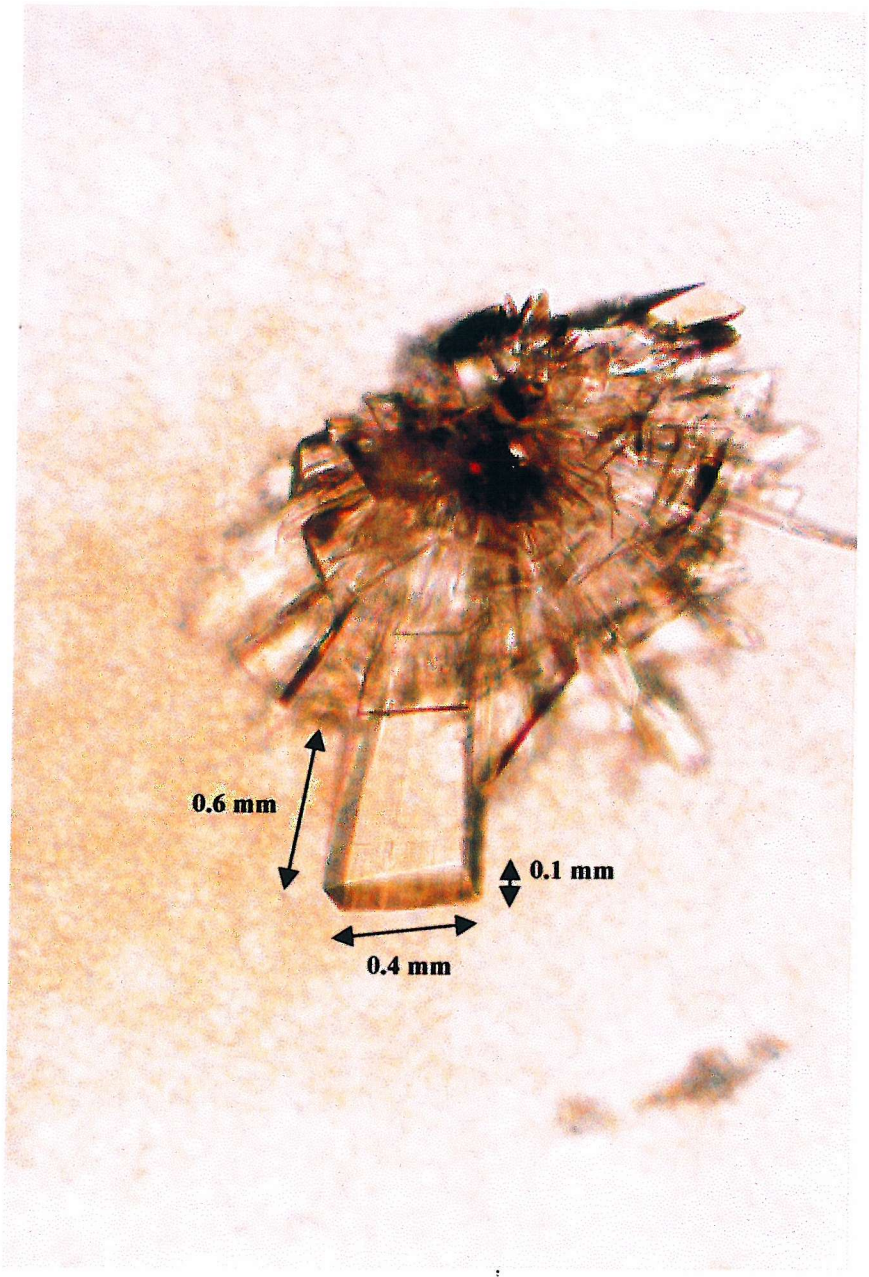
0.6 mm
0.1 mm
0.4 mm

6.8 The oscillation method

In this method reflections are produced in accordance with the Bragg equation ($\lambda = 2d\sin\theta$) by varying ϕ through a small oscillation at a given X-ray wavelength λ. The crystal is mounted with its rotation axis perpendicular to the X-ray beam and rotated through small angles while the detector is kept stationary at a fixed distance. The oscillation angle is chosen so as to collect as many reflections per exposure without overlap (usually between 0.25° and 2°). Multiple oscillations can be performed within each exposure to average out any fluctuations in the beam intensity. The crystal is rotated about ϕ taking as many exposures as required to collect a full data set (This depends on the symmetry within the crystal).

6.9 Data Collection

X-ray data were collected at the ESRF synchrotron (Grenoble, France), at station ID14-EH3 with a 30cm Mar CCD detector by Dr Jon Cooper and P. Ershine. 180 images of 1° oscillation were collected, one of which is shown in Figure 6.6. The diffraction pattern is a two-dimensional image representing a slice of reciprocal space. This image is distorted as a result of the collection geometry and for successful data reduction this distortion must be corrected.

6.10 Data Processing

The raw data was processed with the package MOSFLM (Leslie, 1994) and programs from the Collaborative Computing Project number 4 (CCP4) suite.

Determination of the crystal orientation and cell parameters.

The crystal orientation, unit cell parameters and space group are determined from a single rotation image. The MOSFLM subroutine IMSTILLS reads the image and produces a list of spot coordinates along with their intensities. The MOSFLM auto-indexing subroutine REFIX then determines the crystal

Figure 6.6 A 1° oscillation diffraction image of a WT BIMP crystal.

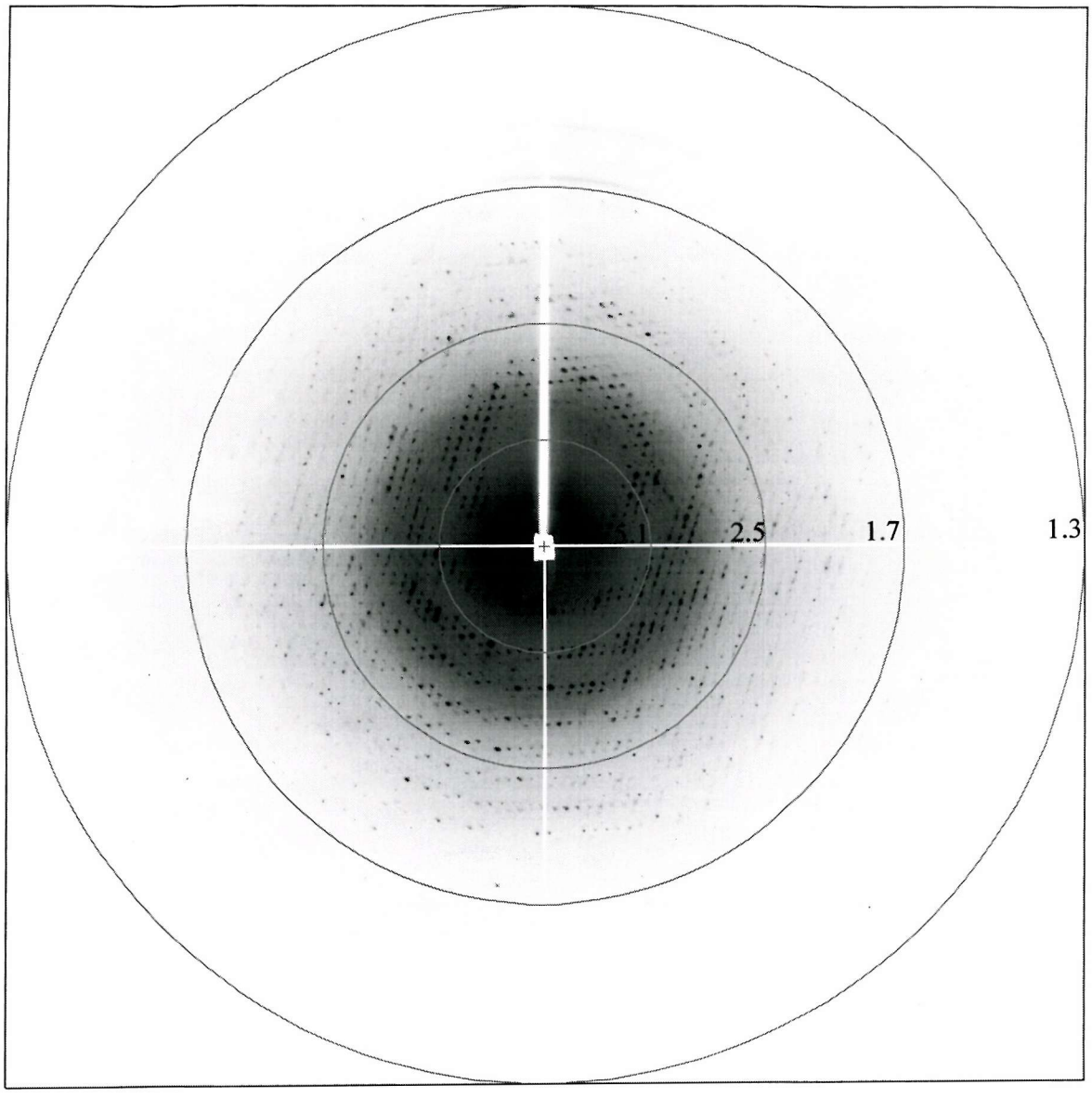
2.5
1.7
1.3

orientation, space group symmetry and unit cell dimensions from the crystal diffraction spots on one or more oscillation images (more accurate cell parameters can be obtained by using data from two or more images that are well separated in ϕ). Post-refinement utilizes the initial estimates of the cell parameters and space group and a number of different "blocks" of data separated in ϕ to refine the crystal orientation, cell parameters and mosaic spread. Post-refinement has the advantage that the unit cell parameters are determined independently of the detector parameters and distortions. The crystal was found to be triclinic (space group P1) with unit cell dimensions:

a = 43.1 Å, b = 54.8 Å, c = 59.3 Å, α = 68.5°, β = 69.2° and γ = 80.7°.

6.11 Crystal solvent content

Knowledge of the unit cell and the space group allows the determination of the number of protein molecules in the asymmetric unit. The method proposed by Matthews, (1968) depends on finding that the ratio of the volume of the unit cell and the molecular weight of the protein (V_M) which lies between 1.7 and 3.5 $Å^3$/ Da, with most values being around 2.15 $Å^3$/Da. Assuming two IMPase subunits (60 kDa) per asymmetric unit, V_M = 2.55 $Å^3$/ Da, corresponding to a solvent content of 52 %.

6.12 Integration of the images and generation of the reflection list.

Once the crystal orientation and unit cell parameters have been refined, the complete data set can be processed by MOSFLM. Profile fitting rather than summation integration of diffraction intensities provides greater accuracy since it makes use of knowledge concerning the expected shape to obtain better estimates of the integrated intensity. Profile fitting also allows deconvolution of overlapping reflections. Standard profiles (obtained by averaging reflections from 5-10 images) are fitted to each image and integrated to give the reflection intensities.

6.13 Data reduction

The CCP4 program SORT lists the set of integrated reflection intensities on hkl. The CCP4 program SCALA adjusts the indexed reflections to a common scale; diffracted intensities vary systematically over the course of data collection owing to variation of the scattering path-length in the crystal. The symmetry equivalent reflections are then averaged (merged). Finally, the CCP4 program TRUNCATE determines the square root of the indexed intensities to generate a list of indexed structure factor amplitudes $|\mathbf{F}|$ and their standard deviation σ. Table 6.3 summarises the data processing statistics.

Table 6.3 The table depicts the data processing statistics for bovine inositol monophosphatase

Resolution	1.6Å
Total number of reflections	102779
Total number of unique reflections	53496
Completeness overall	94.2%
I/σ	5.1
Multiplicity	1.9
R-merge	8.9%

6.14 Molecular Replacement

Reconstruction of the three-dimensional structure of a protein from its X-ray diffraction pattern requires knowledge of not only the indexed structure factor amplitudes $|\mathbf{F}|$ but also of their phases ϕ. This gives rise to the so called "phase problem" of crystallography. Luckily, methods exist to solve the phase problem, one of which (molecular replacement) requires the availability of a known model structure, e.g. of a homologous protein which has a similar tertiary structure (Rossman and Blow, 1962).

In this method, the molecule of known structure (the search model) is the initial model from which one can calculate a first estimate of the phase angles for a given crystal of that structure (in this case in the unit cell of the crystal structure that we wish to determine). The atoms of the search model are then sufficiently close to the real positions of interest to yield phases of sufficient accuracy. Positioning of the search model is achieved by the application of six variables; three rotational and three translational. This transformation can be represented by:

$$X' = [M]\, X + t$$

Where X is the group of vectorial atomic positions of the search model, [M] is the rotation matrix that rotates the coordinates X to a new orientation and t is a vectorial translation. The problem is therefore of finding [M] and t, although this is really the problem of superimposing the two protein structures, only one of which is known; the other is the one we wish to determine. The solution to the problem is to use two mathematical functions (the rotation and translation functions), which do not require knowledge of the unknown structure. Instead the model structure is replaced by a map of inter-atomic vectors instead of atomic positions (a Patterson map) and is calculated directly from the diffraction intensities without any knowledge of the phase angles. The search Patterson map is used initially to orient the search model, via the rotation function and then to superimpose it on the unknown Patterson map, via the translation function. Nowadays, the rotation and translation functions can be calculated with computer programs.

The structure of bovine IMPase was solved by molecular replacement by F. Mohammed and Dr R. Gill (in Professor S. Wood's group) using the program package AMoRe (Navaza, 1994). The search model consisted of the human IMPase dimer with the water molecules and sulphate ion removed. The human structure (2HHM.pdb) is trigonal and this was first placed in the triclinic (P1) cell of the unknown bovine structure. Data in the 10.0 to 3.5Å resolution range were used in the rotation function calculations, with a sphere of integration of

30 Å. The rotation function gave a strong rotation peak at 10.1σ ($\alpha = 205.82°$, $\beta = 13.00°$, $\gamma = 54.95°$), the next peak having a height of 5.3σ above the noise. Several other choices of integration radii gave the same highest peak. Crystal packing of this solution was viewed using MOLPACK (CCP4, 1994) and showed sensible crystal contacts.

Figure 6.7 illustrates a molecule of human inositol monophosphatase (dimer) within the BIMP crystal unit cell. The human form of the enzyme falls into the space group $P3_221$, with a lattice that constrains a, b and c to be identical and the angles between the axes ($\alpha = \beta = \gamma$) to be <120°.

6.15 Refinement and model building

Model refinement is the process of adjusting the atomic coordinates of the model in order to minimize the difference between the experimentally measured structure factor amplitudes (F_{obs}) and those calculated for a hypothetical crystal containing the model (F_{calc}). Refinement is based on the principle of least squares, which states that the best-fit parameters are those that minimise the sum of the squares of the errors. The parameters that need to be refined include atom positions (x, y, z), temperature factors (B) and occupancy.

Another way to reduce the number of parameters in the refinement is to apply non-crystallographic symmetry (NCS) which implies redundancy within the asymmetric unit, for example it may contain two or more copies of the same protein subunit which are structurally identical. In this case (two molecules per asymmetric unit) refinement is performed on one molecule and the symmetry parameters which relate the two subunits. Towards the end of the refinement the NCS is liberated in order to examine any small conformational differences between the chemically identical subunits.

Further refinement of protein structures can be difficult because of the large number of atoms in the structure. To overcome this problem, refinement

Figure 6.7 An illustration of a molecule of human inositol monophosphatase placed within the unit cell of the bovine enzyme.

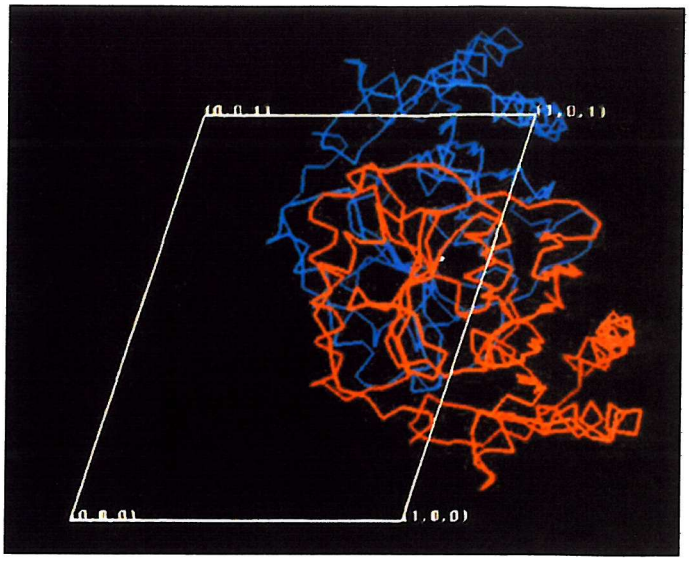
(1,0,1)
(1,0,0)

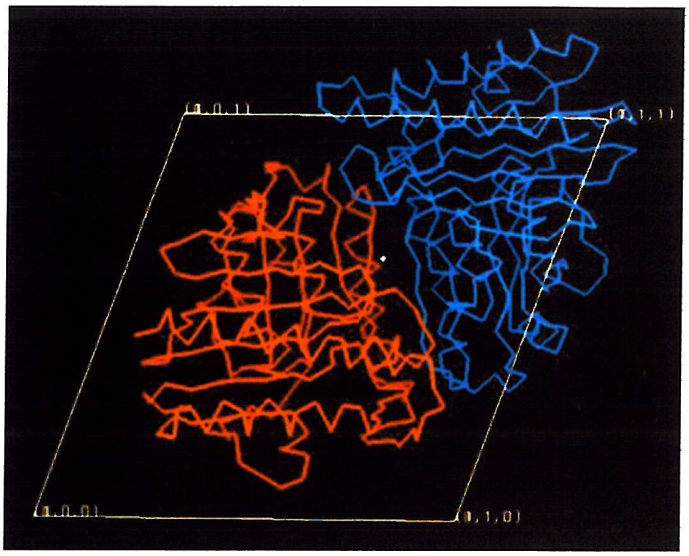
(0,1,1)
(0,1,0)

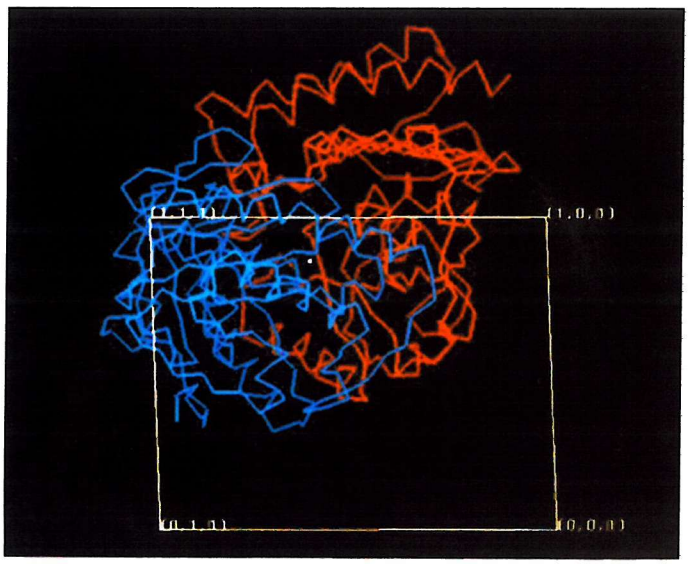
(1,0,0)
(0,0,0)

programs include constraints or restraints, thus further reducing the number of parameters to be refined. The overall function to be minimised by least squares refinement therefore involves two terms, one relating to the crystallographic information and one relating to empirically determined information concerning protein structure.

The initial model is used to calculate the first electron density map (there is little ambiguity in main chain tracing in the case of molecular replacement), which contains features belonging to both the model and the actual structures. After mutation of the search model into the real structure, the necessary side-chain substitutions, insertions and deletions, can be made by inspection of the electron density map and the new structure refined further.

In constrained refinement a whole group of atoms is treated as a rigid-body. All the atoms of the rigid-body move in concert, always occupying the same relative positions. At the beginning of the refinement, the whole molecule can be treated as a rigid-body; this is usually the case for structures solved by molecular replacement, since the search model is only approximately correctly positioned within the unit cell. The concept can then be applied to smaller groups of atoms, for example individual amino acid side chains for which standard bond lengths and angles have been determined from small molecule structures (i.e. fixed bond lengths and angles); in this case only dihedral angles are allowed to vary and therefore the number of parameters for refinement are decreased.

In restrained refinement stereochemical information (for example bond lengths, bond angles, torsion angles and non-bonded interactions) is included in the function to be minimised. This not only increases the number of observations included in the refinement but also helps to ensure good stereochemistry for the molecule.

A number of packages are available for refining protein structures, however, the CNS package was used for this project mainly because it includes numerous refinement protocols including rigid body refinement, positional

refinement, simulated annealing and temperature factor refinement. Refinement is carried out until the diffraction pattern calculated from the model matches the experimentally determined one as well as possible. During refinement, the improvement in the quality of the model can be followed by monitoring the changes in the crystallographic R-factor which is defined as:

$$R = \frac{\Sigma_{hkl} \| F_{obs} | - k | F_{calc} \| }{\Sigma_{hkl} | F_{obs} |} \times 100$$

As refinement converges to the correct structure, the agreement between the observed (F_{obs}) and calculated (F_{calc}) structure factor amplitudes also improves. Typical values for the R-factor range from 0-0.6. An R-factor of 0.6 is obtained when a set of F_{obs} is compared with a random set of amplitudes (i.e. for a random model). For instance, an early model with an R-factor near 0.4 is likely to show improvement with subsequent refinement protocol applications. For a typical protein model refined with data to 2.5Å, the refinement proceeds until the R-factor is around 0.2, which is considered a good value for a protein structure refinement.

6.16 Overall structure of recombinant bovine inositol monophosphatase

As expected, the refined structure of recombinant bovine inositol monophosphatase is similar to the human structure described by Bone *et al.*, 1992 and Bone *et al.*, 1994 (a) and (b). The quality of the model obtained can be judged by the Ramachandran plot shown in Figure 6.8. The plot illustrates that 92.1% of the residues lie in the most favoured regions with the allowed dihedral backbone (ϕ-ψ) angles. The enzyme is organised in a $\alpha\beta\alpha\beta\alpha$ penta-layered fashion for each subunit with an approximate two-fold symmetry existing within the dimer (Figure 6.9). Each active site is located at the base of the two central helices as in the human enzyme (Bone *et al.*, 1992). During the refinement process, four of the N-terminal and 6 of the C-terminal amino acid residues were disordered and consequently these were omitted from the final

Figure 6.8 Ramachandran plot of bovine inositol monophosphatase refined to 1.6Å. 92.1% of residues lie in the allowed most favoured regions and the remaining 7.9% lie in additionally allowed regions. Glycines residues are shown as triangles. There are no residues in disallowed regions.

Ramachandran Plot

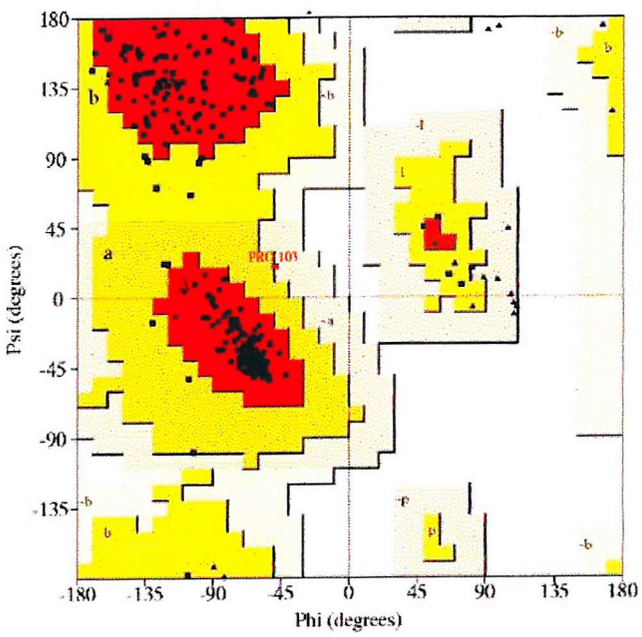

Plot statistics

Residues in most favoured regions [A,B,L]	222	91.3%
Residues in additional allowed regions [a,b,l,p]	16	6.6%
Residues in generously allowed regions [~a,~b,~l,~p]	0	0.0%
Residues in disallowed regions	0	0.0%
Number of non-glycine and non-proline residues	238	100.0%
Number of end residues (excl. Gly and Pro)	2	
Number of glycine residues (shown as triangles)	24	
Number of proline residues	10	
Total number of residues	274	

Figure 6.9 The structure of bovine inositol monophosphatase (dimer), showing three Mg^{2+} ions (shown in green) in the active site of subunit B and three differently located Mg^{2+} ions in subunit A.

refinement and model building studies. The final model of recombinant bovine inositol monophosphatase was refined to an R-factor of 18.9% (R_{free} = 20.7%).

6.17 Active site of the enzyme containing Mg^{2+} ions and interatomic Mg^{2+} distances

The bovine inositol monophosphatase crystal structure with Mg^{2+} clearly reveals the presence of three Mg^{2+} binding sites for subunit B of the dimer, however, site 3 in subunit A appears less well defined. This site 3 in subunit A, is differently located from that in subunit B (Figure 6.10(a)), and could be a low occupancy site since there is no interaction between E70 and this site as there is in subunit B (Figure 6.10(b)).

The metal ions in bovine inositol monophosphatase interact with essentially the same active site residues as in the human structure (Bone *et al.*, 1992 and Bone *et* al., 1994(b)). The active site identified by the location of residues Glu70, Asp90, Ile92, Asp 93, Asp 220, three Mg^{2+} ions and several water molecules is depicted in Figure 6.10(a). This Figure also shows the electron density map in this region together with other amino acid side chains in the immediate vicinity. Figure 6.11 depicts the active site of the human enzyme and the associated metal ions (denoted $Mn^{2+}1$, $Mn^{2+}2$ and $Mn^{2+}3$) together with their ligands. The coordinate files for the generation of these figures were obtained from the Protein Data Bank (1IMC.pdb; Bone *et al.*, 1994b) and the 3 Ca^{2+} ion and D-Ins(1)P structure discussed in section 6.19, (1AWB.pdb; Ganzhorn *et al.*, 1997).

The two main metal ions $Mg^{2+}1$ and $Mg^{2+}2$ are located close together in BIMP with the distance between them being 3.62Å. The distance between metal binding sites 1 ($Mg^{2+}1$) and 3 ($Mg^{2+}3$) was found to be 3.75Å for subunit B (Table 6.4). In addition the distance between sites 2 and 3 was determined to be 5.20Å. The active site of the enzyme is shown in Figure 6.12: with the metal binding sites labelled $Mg^{2+}1$, $Mg^{2+}2$ and $Mg^{2+}3$.

Figure 6.10(a) The active site for subunit A of bovine inositol monophosphatase. The Mg^{2+} ions are shown in green, active site water molecules (blue) and the proposed nucleophile in orange. The electron density around the active site is also shown (blue net).

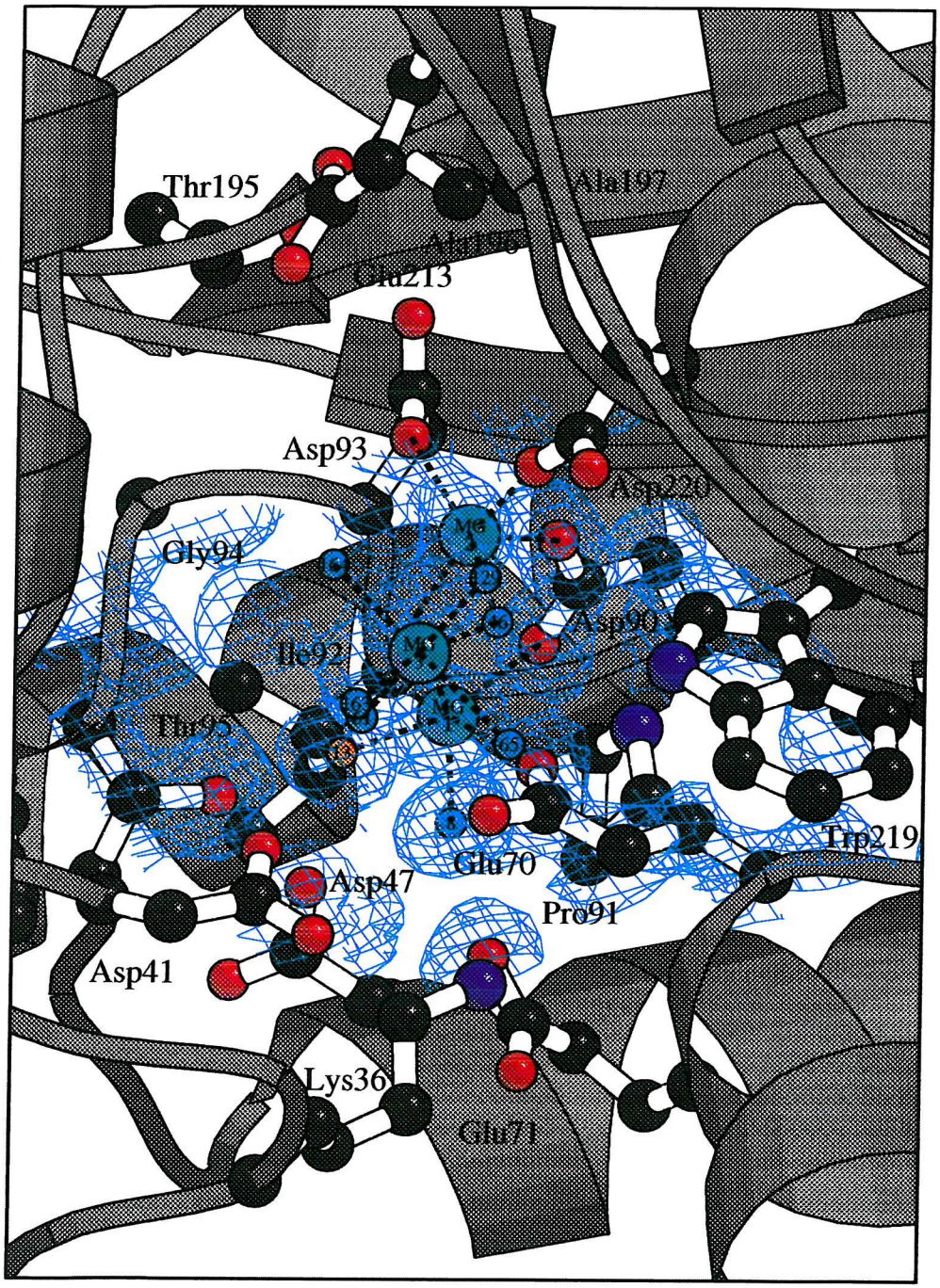
Thr195
Ala197
Glu213
Asp93
Asp220
Gly94
Asp90
Ile92
Thr95
Trp219
Glu70
Asp47
Pro91
Asp41
Lys36
Glu71

Figure 6.10(b) The active site for subunit B of bovine inositol monophosphatase showing the three Mg^{2+} ions at the active site (shown in green), the active site waters (blue) and the proposed nucleophile (orange). The electron density around the active site is also shown (blue net).

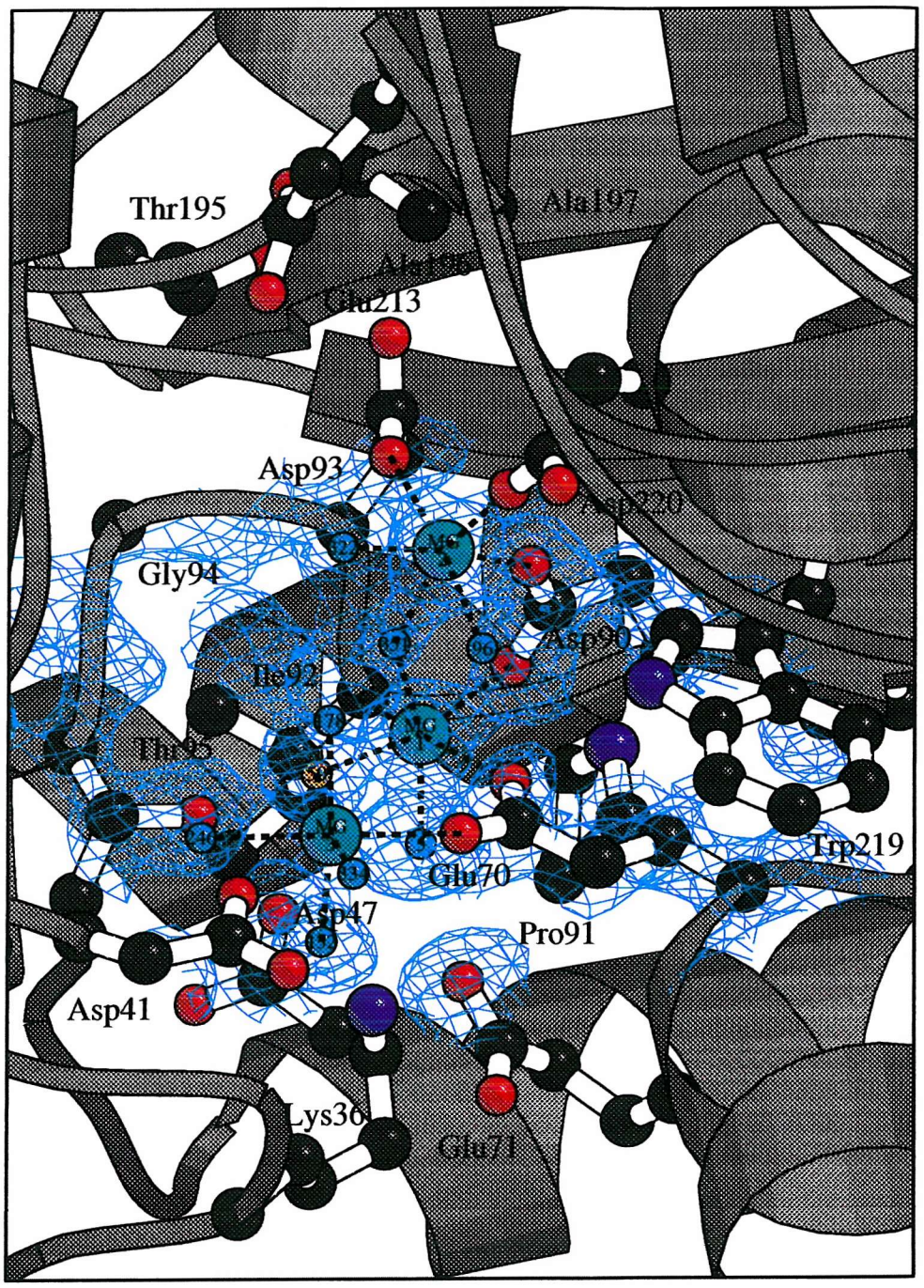
Thr195
Ala197
Glu213
Asp93
Asp220
Gly94
Asp90
Ile92
Thr95
Trp219
Glu70
Asp47
Pro91
Asp41
Lys36
Glu71

Figure 6.11 The active site structure of human inositol monophosphatase, complexed to Mn^{2+} and Cl^- ions. Metal ions are labelled 1-3, shown in light blue and coordinate bonds to Mn^{2+} and Cl^- ions are shown as dashed lines. Water molecules are shown in blue and labelled 1-3.

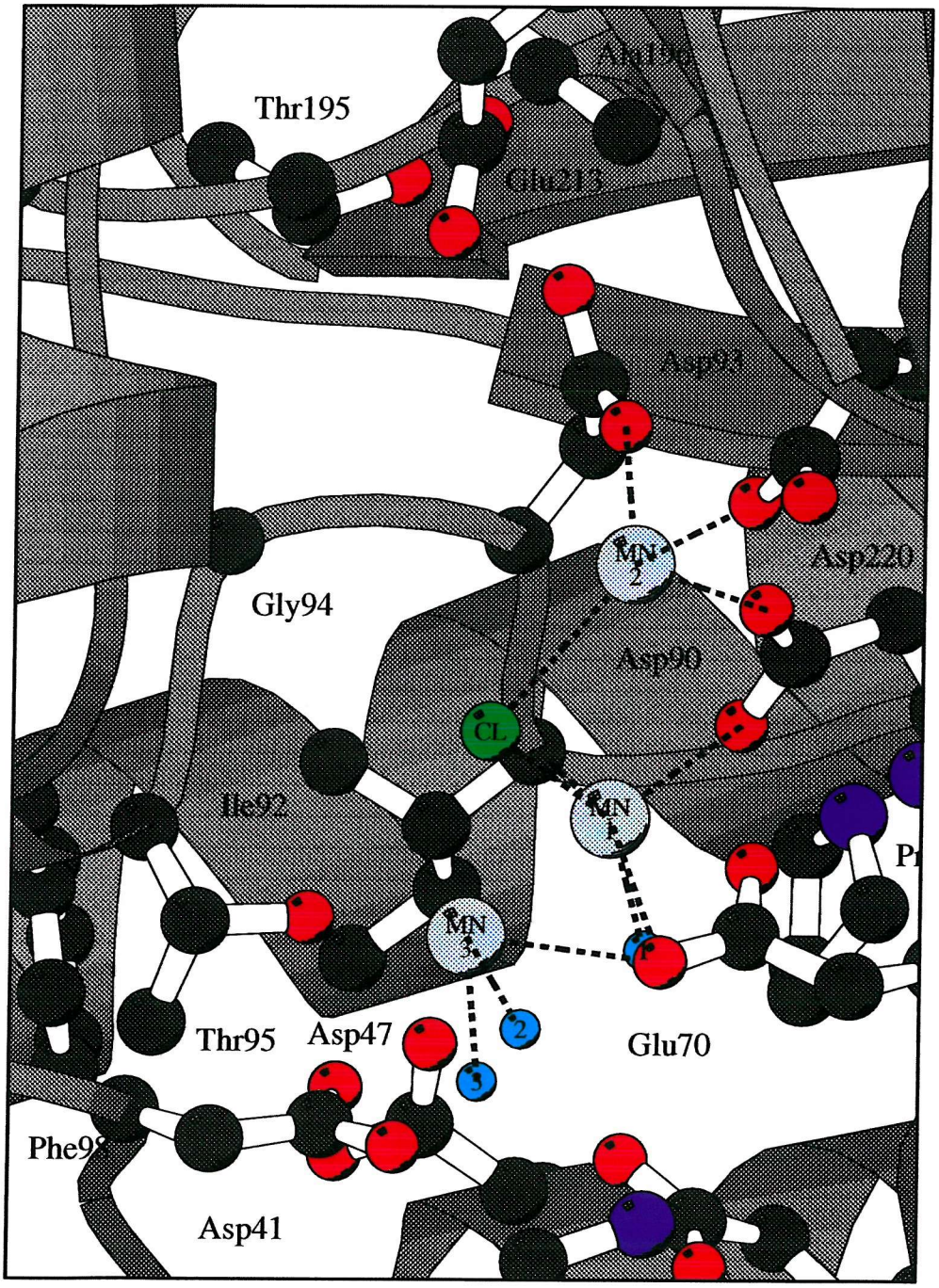
Thr195
Glu213
Asp93
Asp220
MN 2
Gly94
Asp90
CL
Ile92
MN 1
MN 3
Thr95
Asp47
Glu70
Asp41

(i) Mg^{2+} coordination in binding site1

Mg^{2+} binding site1 is coordinated to six ligands: Glu70, Asp90, Ile92, and three water ligands (W5, W50 and W351) with octahedral coordination geometry as shown in Figure 6.12.

Mg^{2+} site 1 is located 2.04Å from the carboxylate oxygen (OE1) of Glu70, 2.08Å from the carboxylate oxygen (OD1) of Asp90 and 2.14Å from the carbonyl oxygen (O) of Ile 92. In addition there are 3 water molecules which act as ligands: W5, W50 and W351 which form hydrogen bonds with Mg^{2+} at site 1 with lengths of 2.05Å, 2.15Å and 1.99Å respectively.

(ii) Mg^{2+} coordination in binding site 2

Mg^{2+} 2 is hexa-coordinated by Asp90, Asp93 and Asp220 and three water molecules W96, W322 and W351 also arranged in an octahedral conformity, where Mg^{2+} site 2 is located 2.03Å from the carboxylate oxygen (OD2) of Asp90, 1.99 Å from the carboxylate oxygen (OD1) of Asp93 and 2.00 Å from the carboxylate oxygen (OD1) of Asp220 and ligated to 3 water molecules, namely W96 (O), W322 (O) and W351 (O) at distances of 2.52Å, 2.42Å and 1.87Å respectively. W351 bridges across both metal binding sites (sites 1 and 2).

(iii) Mg^{2+} coordination in binding site 3

A third Mg^{2+} site (Figure 6.12) was noted at a distance of 2.14Å from residue Glu70, in agreement with the observations made by Bone *et al*, (1994(b)) and Ganzhorn *et al.*, (1997). In addition, there are 5 water molecules coordinated to this third Mg^{2+} ion, W50, W132, W178, W246 and W334, at distances of 2.14Å, 2.02Å, 2.04Å, 2.25Å and 2.08Å respectively. In this case, W50 bridges across metal sites 1 and 3, resulting in octahedral coordination geometry.

From the structure of BIMP, Thr95 was seen to be too far away from the metal ions to act as a metal binding ligand, however, its OG1 atom is 2.59Å from a

Figure 6.12 The active site of bovine inositol monophosphatase showing the positions of the three Mg^{2+} ions (shown in green) and their corresponding ligands. Coordinate bonds are shown as dashed lines.

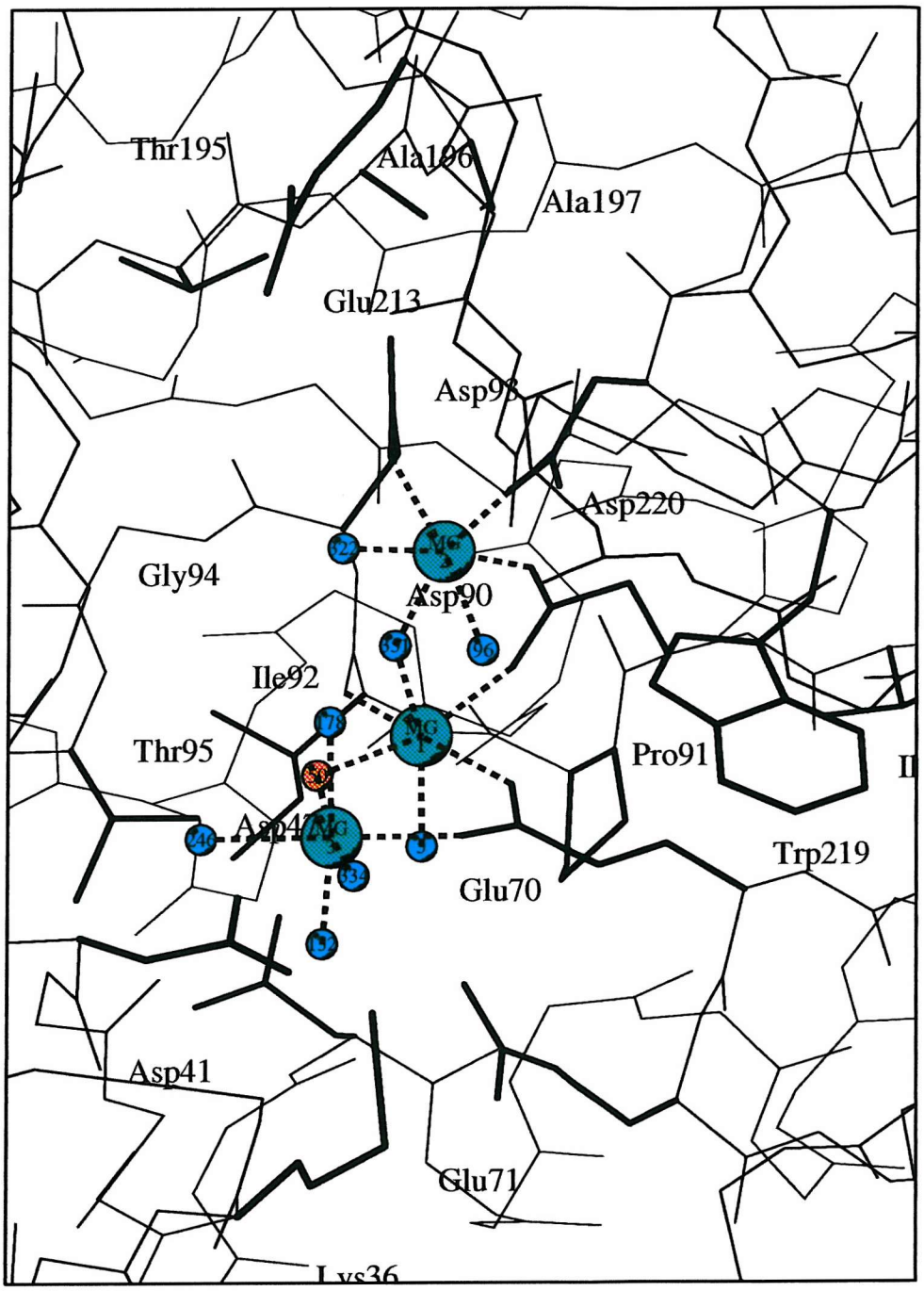
Thr195
Ala196
Ala197
Glu213
Asp93
Asp220
Gly94
Asp90
Ile92
Thr95
Pro91
Asp41
Trp219
Glu70
Asp41
Glu71
Lys36

water molecule (W50) which does coordinate to both Mg^{2+} ions 1 and 3. Previous structural studies suggest that this water is activated by interaction with residues E70 and Thr95 (Bone *et al.*, 1994 (a) and (b)). Consequently, based upon these previous findings together with the observations made in this study, it is highly probable that W50, located approximately 2.15Å from residue E70, is the nucleophile that participates in the catalytic mechanism in BIMP.

6.18 Comparison of subunits A and B

Comparison of subunits A and B demonstrates that site 3 in subunit B is in fact identical to that proposed for the $3Mn^{2+}$ structure (Bone *et al.*, 1994(b)). Table 6.5 shows that the protein-metal ion interatomic distances for sites 1 and 2 are almost identical for the two subunits. For subunit A the distances are E70 (OE1), D90 (OD1) and I92 (O) are 2.07Å, 2.11Å and 2.11Å respectively and these values agree closely with those for subunit B: E70 (OE1), D90 (OD1) and I92 (O) being 2.04Å, 2.08Å and 2.41Å respectively. Similarly for site 2 the Interatomic distances for D90, D93 and D220 are 2.16Å, 2.09Å and 2.13Å (subunit A) and 2.03Å, 1.99Å and 2.00Å (subunit B). However, site 3 for subunit A differs in only having 6 water ligands compared with 1 protein ligand (E70 (OE2)) and 5 water ligands in subunit B. Site 3 is also located in a different position relative to the other two sites (c.f. Figures 6.13(a) and (b)). An interesting finding from analysis of these 2 subunits is that although the coordinating water molecules are numbered differently for subunits A and B, all of the water molecules in subunit A occupy equivalent positions in subunit B (Figures 6.13(a) and (b)). These are listed in equivalent rows in adjoining columns in Table 6.5. This is also true for the proposed water nucleophiles for the two subunits (i.e. W*13 and W*50 in subunits A and B correspondingly) (Table 6.5). These findings together with findings elsewhere (Ganzhorn *et al.*, 1997) provide support for the existence of this third site.

Figure 6.13(a) Subunit A. This illustrates the active site structure of bovine inositol monophosphatase complexed to Mg^{2+} ions (shown in green). Metal ions are labelled 1, 2 and 3 together with water molecules (blue) and the proposed nucleophile (orange).

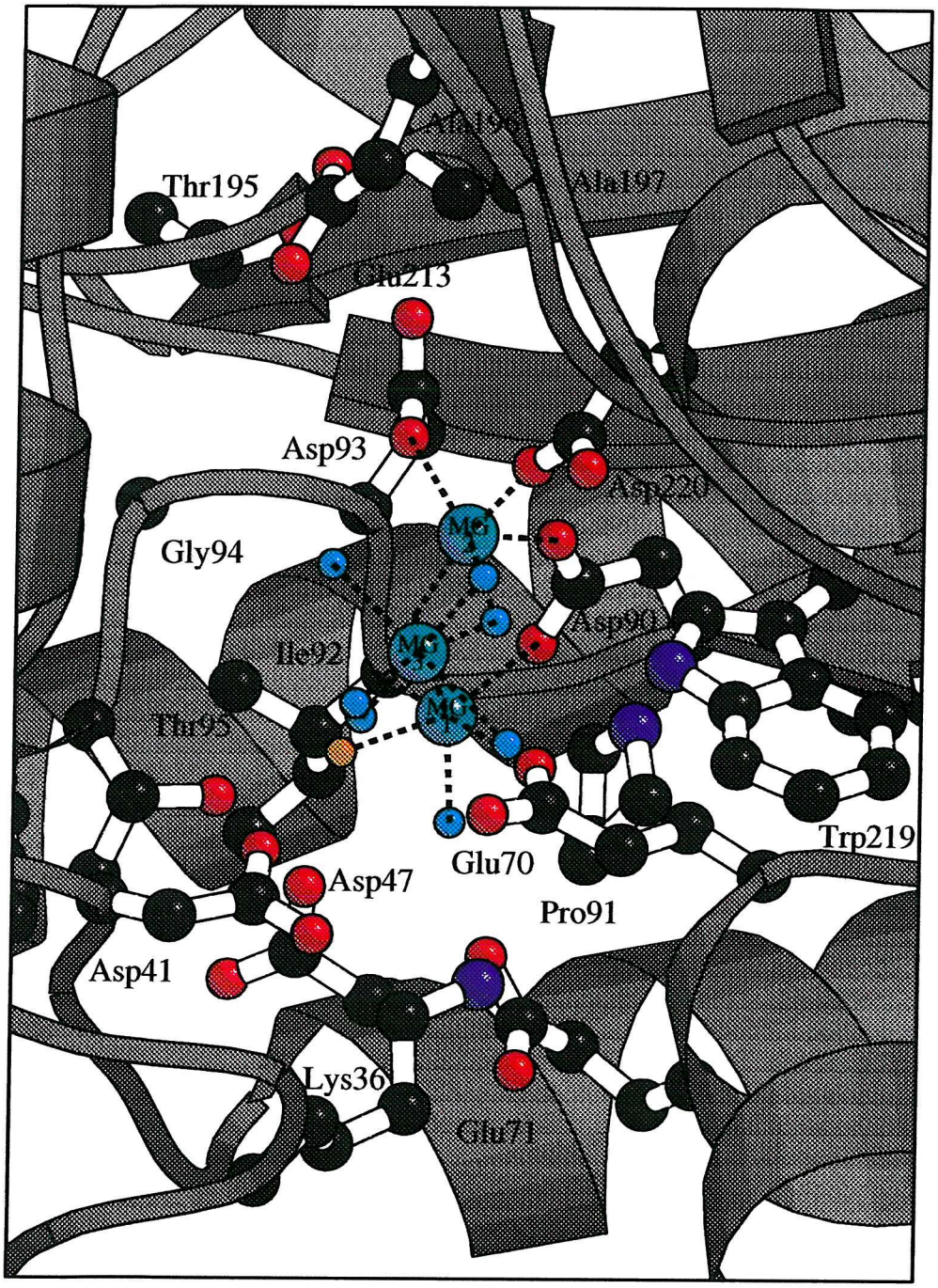
Thr195
Ala197
Glu213
Asp93
Asp220
Gly94
Mg
Asp90
Ile92
Thr95
Trp219
Glu70
Asp47
Pro91
Asp41
Lys36
Glu71

Figure 6.13(b) Subunit B. This illustrates the active site structure of bovine inositol monophosphatase complexed to Mg^{2+} ions (shown in green). Metal ions are labelled 1, 2 and 3 together with water molecules (blue) and the proposed nucleophile (orange).

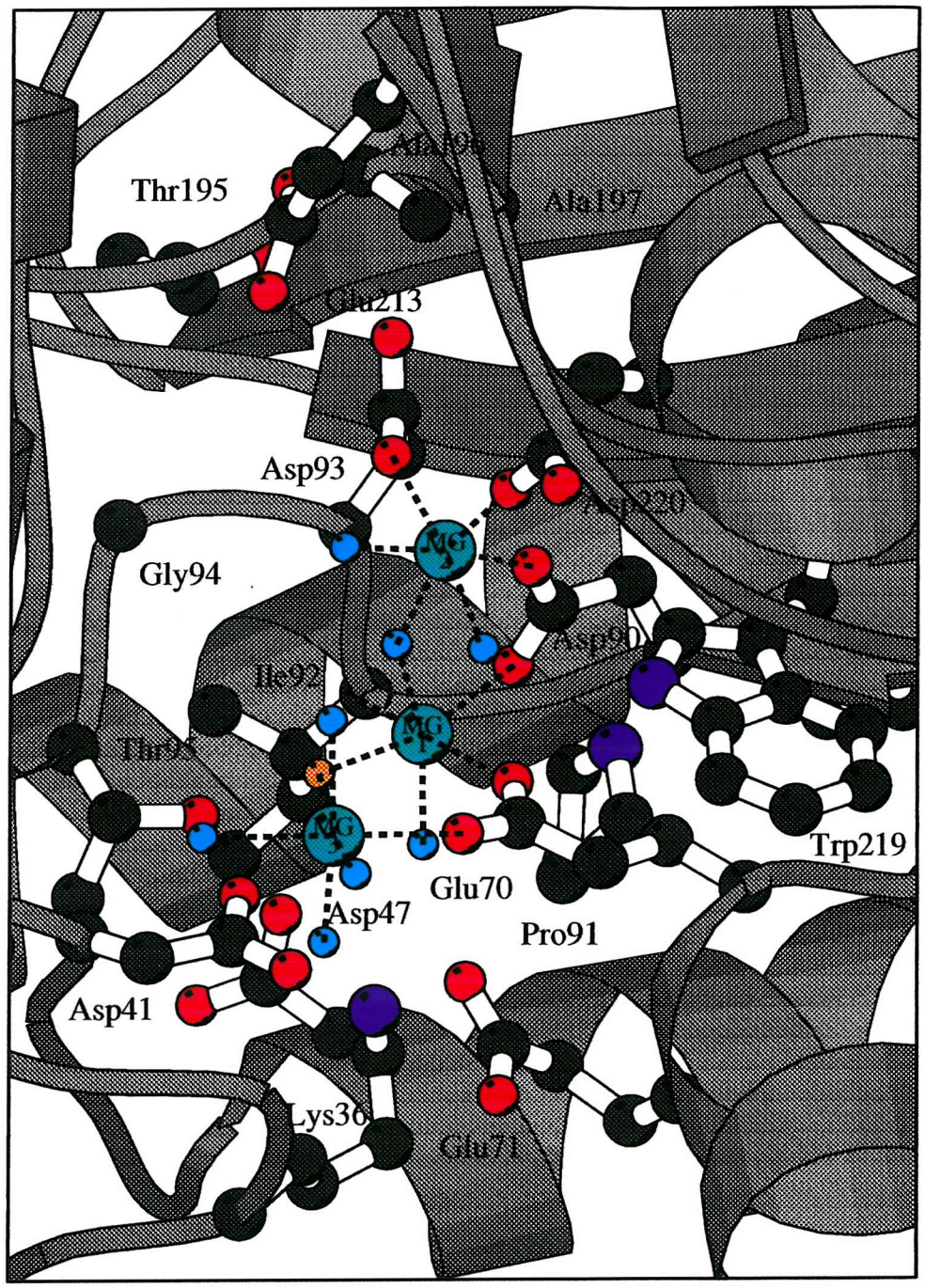
Thr195
Ala197
Glu213
Asp93
Gly94
Ile92
Thr95
Asp41
Asp47
Glu70
Pro91
Trp219
Lys36
Glu71
MG
MG
MG

6.19 Comparison of subunit B of WT BIMP and the $3Ca^{2+}$ and D-Ins(1)P structure

The structure of human inositol monophosphatase at 2.5Å resolution complexed with Ca^{2+} and D-Ins(1)P also implies the existence of a third metal binding site Ganzhorn *et al.*, (1997). Since Ca^{2+} ions are inhibitory with respect to the essential activating Mg^{2+} ions, it was possible to observe the resulting complex with the natural substrate (D-Ins(1)P). In addition to coordinating to the same residues (E70, D90 and I92) as in the BIMP structure, the site 1 Ca^{2+}, interacts with the O7 of the phosphate moiety of the substrate and two water molecules in an octahedral ligand field (Table 6.5). Figure 6.14 shows that the $3Ca^{2+}$ and substrate containing complex sequesters the three metal ions in positions analogous to those in the BIMP structure. The metal ligand distances for the Ca^{2+} containing structure are slightly longer (2.12Å (E70; OE1), 2.26Å (D90; OD1) and 2.14Å (I92; O)) than those for the bovine enzyme (cf., 2.03Å (E70; OE1), 2.08Å (D90; OD1) and 2.17Å (I92; O)), since the Ca^{2+} ion has a slightly larger ionic radius than Mg^{2+} ions. In addition, Ca^{2+} can have up to a maximum of 7 ligands while Mg^{2+} the value is only 6. The distances between the metal ions are also comparable to those determine for the bovine structure. In particular, the distance between $Ca^{2+}1$ and Ca^{2+} 2 is 3.64Å (Table 6.6) which agrees closely with that determined for the bovine enzyme (3.62Å). However, the distances between $Ca^{2+}1$ and $Ca^{2+}3$ together with those between $Ca^{2+}2$ and $Ca^{2+}3$ differ significantly, being 4.40Å and 5.35Å (Table 6.6) respectively (c.f. in the bovine structure, the distance between $Mg^{2+}1$ and $Mg^{2+}3$ is 3.75Å and the distance between $Mg^{2+}2$ and $Mg^{2+}3$ is 5.20Å).

6.20 Substrate binding determinants of BIMP

Superposition of the substrate binding region of BIMP (monomer B) on that of the HIMP structure complexed either with Gd^{3+} and D-inositol(1)P (1IMB.pdb) or with Ca^{2+} and D-inositol(1)P (1AWB.pdb), (Fig 6.15(a)) demonstrates that not only are the substrate binding side chains (Gln 213, Asp 93, Asp 220) conserved between both structures, but the protein backbones are

Figure 6.14 The human inositol monophosphatase structure complexed with $3Ca^{2+}$ (shown in orange) and D-Ins(1)P (Ganzhorn *et al.*, 1997, 1AWB.pdb).

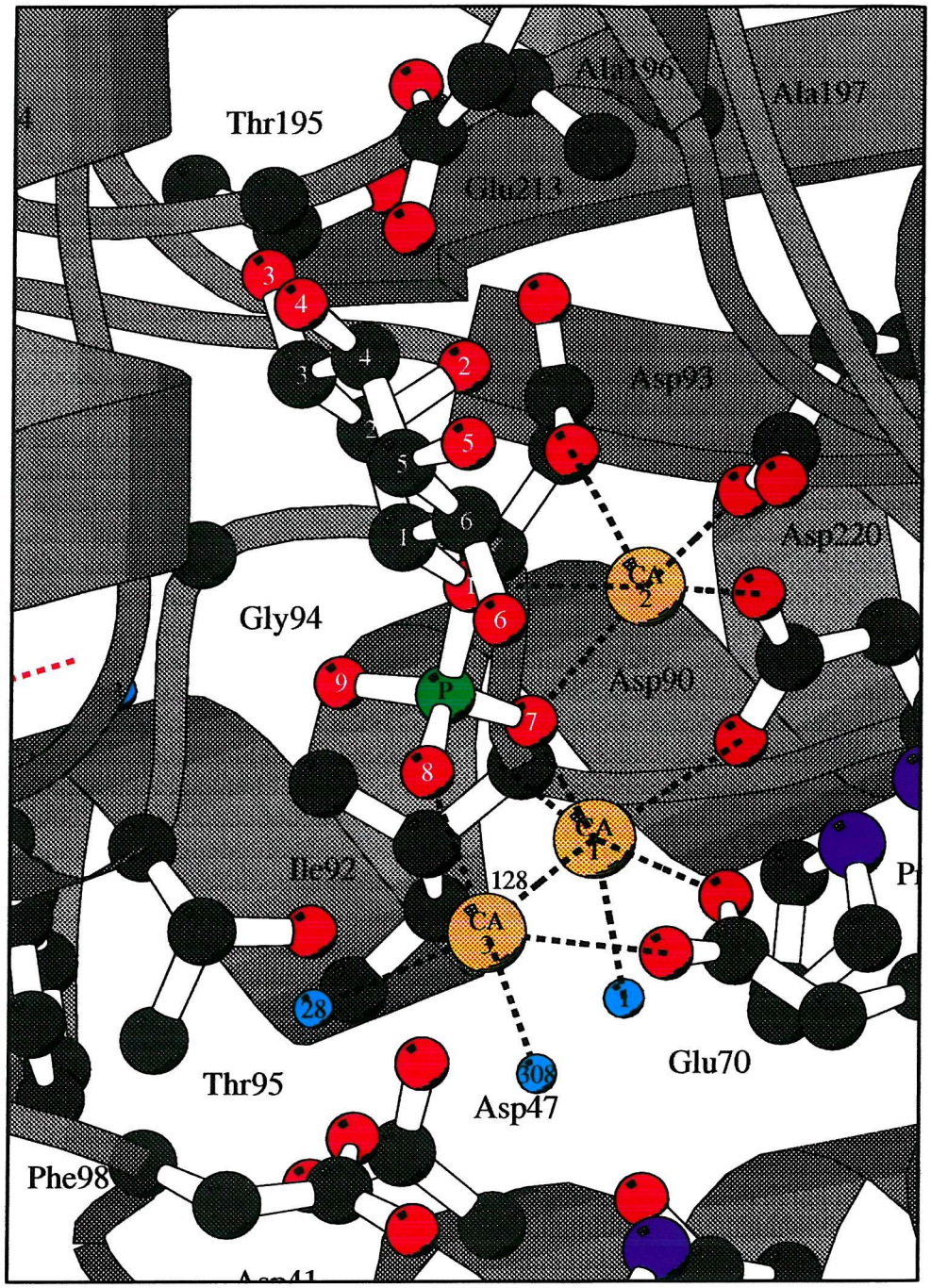
Ala196
Ala197
Thr195
Glu213
Asp93
Asp220
Gly94
Asp90
Ile92
128
Glu70
Thr95
Asp47
Phe98

also well superposed. Consequently, substrate binding to BIMP must be identical to substrate binding to HIMP and the slightly lower affinity of L-Inositol(1)P for BIMP must arise from neighbouring sequence differences in the region affecting flexibilty.

Similarly, superposition of the substrate binding region of BIMP (monomer B) on that of the HIMP structure complexed with Gd^{3+} and L-inositol(1)P (1IMA.pdb) (Fig 6.15(b)) demonstrates that the analysis above applies equally to both isomers of Inositol(1)P.

6.21 Discussion

The structure of human inositol monophosphatase complexed with (a) Mn^{2+}or (b) Mn^{2+} and PO_4 have been determined at 2.6Å resolution (Bone *et al.*, 1994(b)). The Mn^{2+} only complex shows that the metal binding site 1 (Mn^{2+}) has octahedral geometry while the geometry of site 2 is tetrahedral (Bone *et al.*, 1994(b)). This coordination pattern differs from that seen for the BIMP structure crystallized in the presence of Mg^{2+}ions. As mentioned above the bovine structure site 1 Mg^{2+} has octahedral geometry with 3 enzyme ligands (Glu70, Asp90 and Ile92), and three water molecules (W5, W50 and W351) completing the octahedron. Comparison with previously determined structures complexed with Gd^{3+} and substrate (Bone *et al.*, 1992) and enzyme structures complexed with Mn^{2+} and phosphate (Bone *et al.*, 1994(b)) demonstrate conclusively that Mg^{2+} binding site 1 is in the same location and retains the same protein ligands.

The coordination geometry for the site 2 Mg^{2+} differs from that published for the human enzyme in that it has 6 direct ligands; the carboxyl oxygen of residues Asp90, Asp 93 and Asp 220 and three water molecules (W96, W322 and W351) with one of these (W351) bridging across the two metal binding sites (sites 1 and 2). This substantiates the findings reported by Bone *et al.*, 1994b concerning the protein structure complexed with Mn^{2+} although additional water ligands in the bovine structure may serve mainly to fill the

Figure 6.15(a) Superposition of the substrate binding region of BIMP (monomer B; shown in red) on that of the HIMP structure complexed either with Gd^{3+} and D-Inositol(1)P (1IMB.pdb; shown in blue) or with the Ca^{2+} and D-Inositol(1)P (1AWB.pdb; shown in purple).

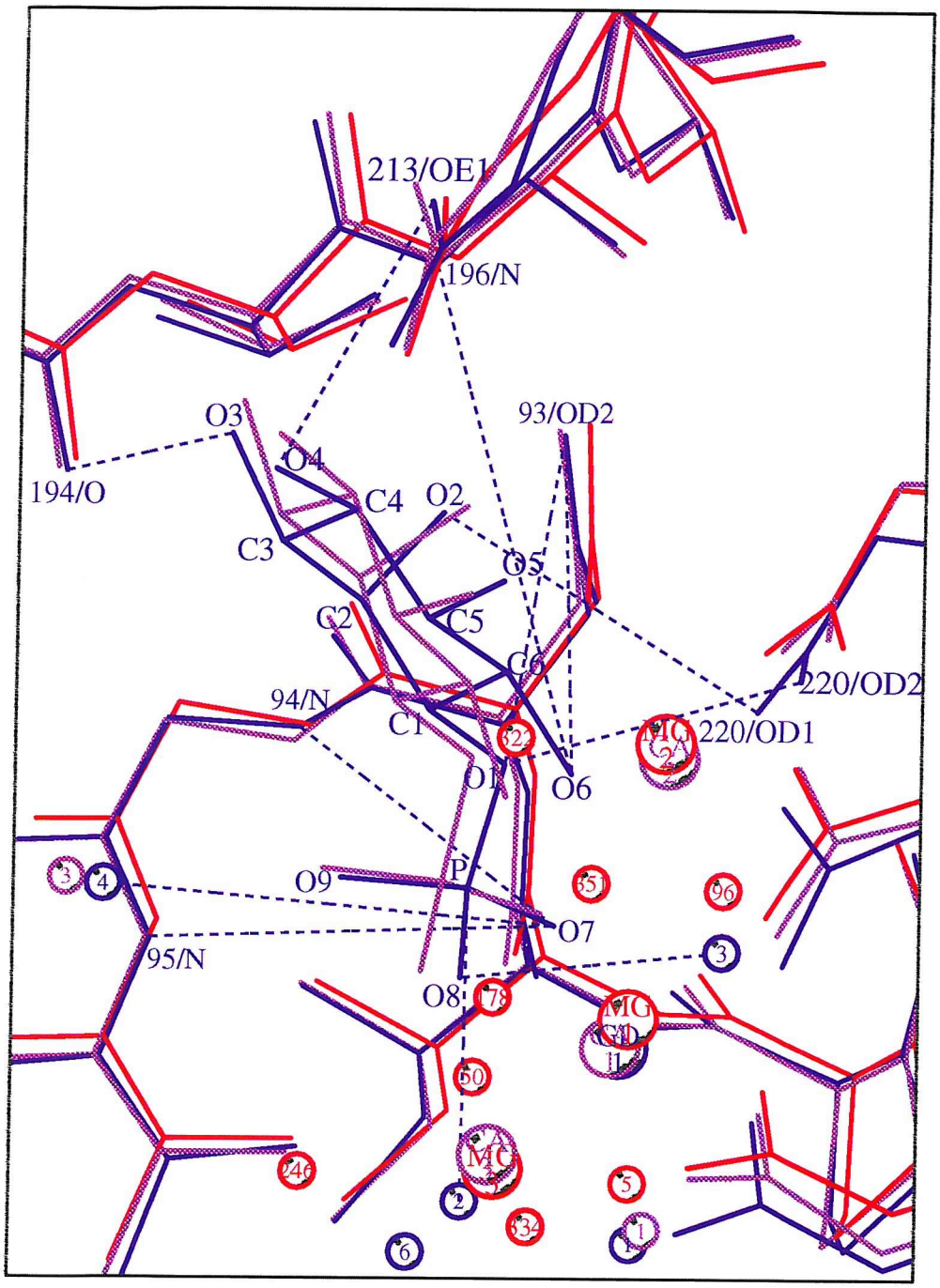
213/OE1
196/N
O3
O4
194/O
C4
O2
C3
O5
93/OD2
C2
C5
C6
220/OD2
94/N
C1
220/OD1
O1
O6
P
O9
O7
95/N
O8
MG

Figure 6.15(b) Superposition of the substrate binding region of BIMP (monomer B; shown in red) on that of the HIMP structure complexed with Gd^{3+} and L-Inositol(1)P (1IMA.pdb) (shown in blue).

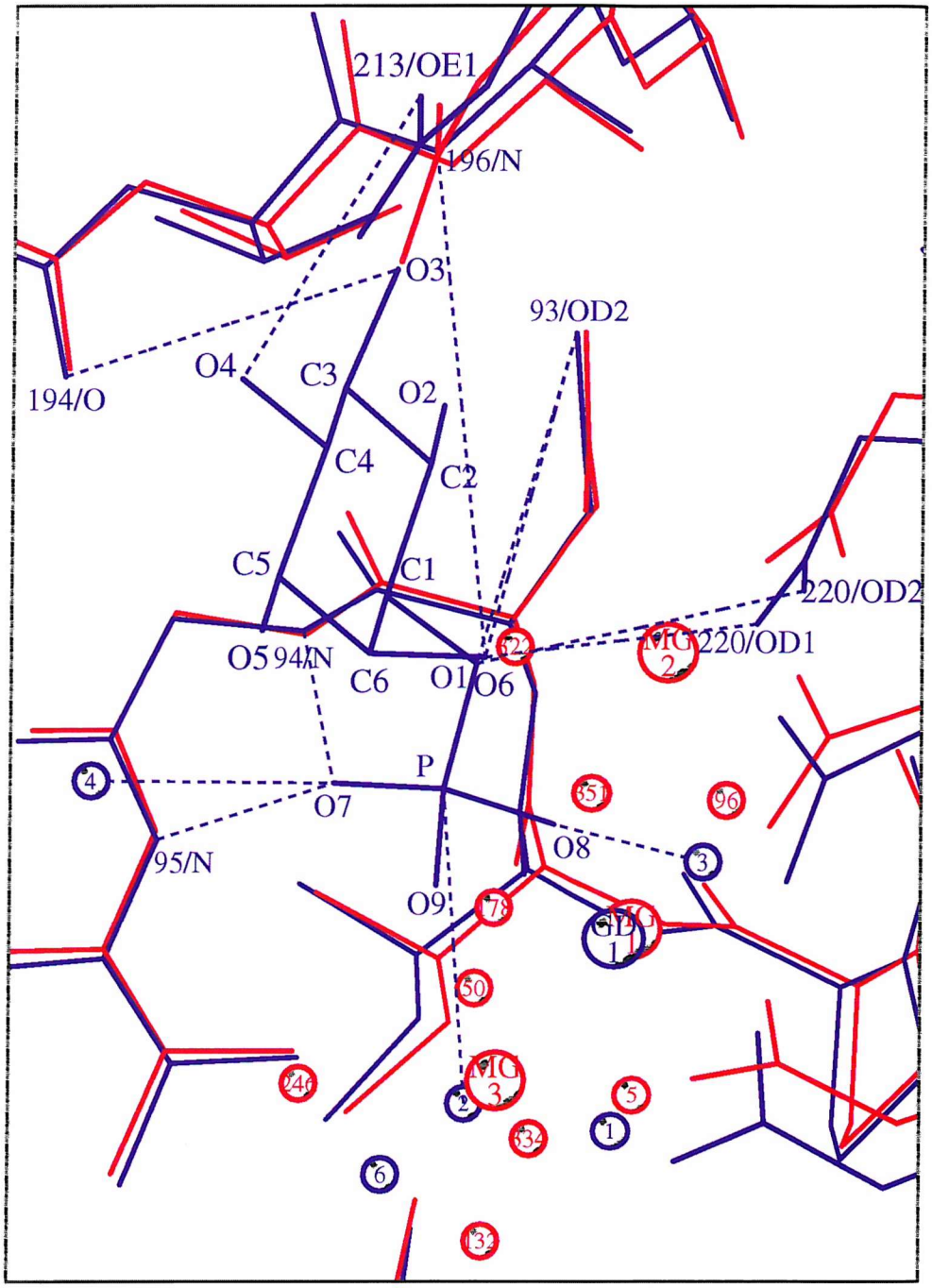
213/OE1
196/N
O3
93/OD2
O4
C3
194/O
O2
C4
C2
C5
C1
220/OD2
O5
94/N
C6
O1
O6
MG
2
220/OD1
P
O7
O8
95/N
O9
MG
3

coordination spheres of the two Mg^{2+} metal ions in the absence of the substrate.

A third Mg^{2+} binding site, also with octahedral coordination geometry, has been observed in the BIMP crystal structure, coordinated by only one enzyme ligand (E70) and an additional 5 water molecules (W50, W132, W178, W246 and W334). Studies carried out by Bone *et al.*, (1994(b)) using Mn^{2+} crystals have also demonstrated the presence of this third metal binding site, however, this third Mn^{2+} was expelled from the active site when crystals were soaked in phosphate. It is still unclear as to whether this third site is involved in catalysis or whether it is an inhibitory site. The coordination geometry of this third site in the bovine enzyme differs from that shown by Bone *et al*, (1994(b)), in being octahedral as opposed to tetrahedral. The Mg^{2+}-E70 distance for the bovine enzyme (2.04Å) is less than the Mn^{2+}-E70 distance for the human enzyme, (2.57Å).

Comparison of the structure of human inositol monophosphatase with Fructose-1,6-bisphosphatase (F-1,6-BP) and inositol polyphosphate 1-phosphatase (IPP) showed that although they share minimum amino acid identity, they share a common $\alpha/\beta/\alpha/\beta$ structural fold (Zhang *et al.*, 1993, York *et al.*, 1994 and Liang *et al.*, 1993). The metal binding sites of the three proteins are all conserved even though their quaternary structures vary (IPP is a monomer, F-1,6-BP a homotetramer, while both HIMP and BIMP are homodimers). In particular, the three enzymes share a conserved metal binding site sequence motif, D-P-I/L-D-G/S-T/S (York *et al.*, 1995).

The metal binding sites of F-1, 6-BP, which utilizes 2 Mg^{2+} ions in its catalytic mechanism, are very similar to those of HIMP and to those of IPP (Zhang *et al.*, 1993 and York *et al.*, 1994). In IPP the two Mg^{2+}ions are located 3.88Å apart while the two equivalent residues in F-1, 6-BP are located approximately 3.7Å apart. This compares well with the values obtained for the BIMP enzyme. The two main metal ions Mg^{2+} 1 and Mg^{2+} 2 are close in space with the distance between them being 3.67Å while the distance between Mg^{2+} 1 and Mg^{2+} 3 was found to be 3.75Å for subunit B.

Based upon these findings and kinetic studies by Pollack *et al.*, (1994) a two metal ion mechanism has been proposed in which metal ion 1 ($Mg^{2+}1$) activates a water molecule for nucleophilic attack, and metal ion 2 ($Mg^{2+}2$) functions by stabilizing the leaving inositol oxyanion group. Since the third metal ion has only one protein ligand, this implies that it is not involved in catalysis. Most studies to date (Pollack *et al.*, (1994), Greasley *et al.*, (1994)) support this two metal ion model, however recently the structure of human inositol monophosphatase complexed with Ca^{2+} (inhibitory metal ion) and D-Ins(1)P has been determined to 2.5Å resolution and this suggests an alternative mechanism (Ganzhorn *et al.*, 1997). A combination of structural and kinetic studies suggest that a mechanism with more than two metal ions may be present in which metal ions $Ca^{2+}1$, $Ca^{2+}2$ and $Ca^{2+}3$ bind to the phosphate oxygens of the substrate, thereby stabilising the negative charge in the transition state, with M1 and M2 still playing the same roles as in the proposed two metal ion mechanism (Ganzhorn *et al.*, 1997). Comparable three metal ion clusters referred to as co-catalytic sites, have been observed for Zn^{2+} in alkaline phosphatase, phospholipase C and P1 nuclease (Vallee *et al.*, 1993). Now, three Mg^{2+} binding sites have also been observed in the active site of bovine inositol monophosphatase, however, it is presently unclear as to whether the third site is involved in catalysis.

6.22 Crystallisation trials with Li^{+} ions, Zn^{2+}ions and inhibitors

The factorial screening technique giving rise to WT BIMP crystals in the presence of Mg^{2+} ions has also been successful for G76S BIMP (Figure 6.16). Diffraction quality crystals have been isolated and work is currently under way to solve the structure at 1.3Å. In addition, trials were set up using; (a) Mg^{2+} and inhibitor I, (b) Mg^{2+} and inhibitor II, (c) Li^{+} and inhibitor I, (d) Mg^{2+} and Li^{+}, (e) Zn^{2+}, (f) Zn^{2+} and inhibitor I, (g) Zn^{2+} and inhibitor II, (h) Zn^{2+}, Li^{+} and inhibitor I (i) Li^{+}, Mg^{2+} and inhibitor I, (j) Li^{+}, Mg^{2+} and inhibitor II and (k) Li^{+}, and inhibitor I. These screens utilise the same buffer, and precipitant concentrations as for WT enzyme and look extremely promising (see Figure 6.17).

Figure 6.16 Crystal of G76S BIMP obtained using the hanging drop method. The crystal grew in 0.1M Tris.HCl pH 8.5, 0.3M Na acetate, 22.5% v/v PEG 4K and 10mM Mg^{2+} ions at 25°C.

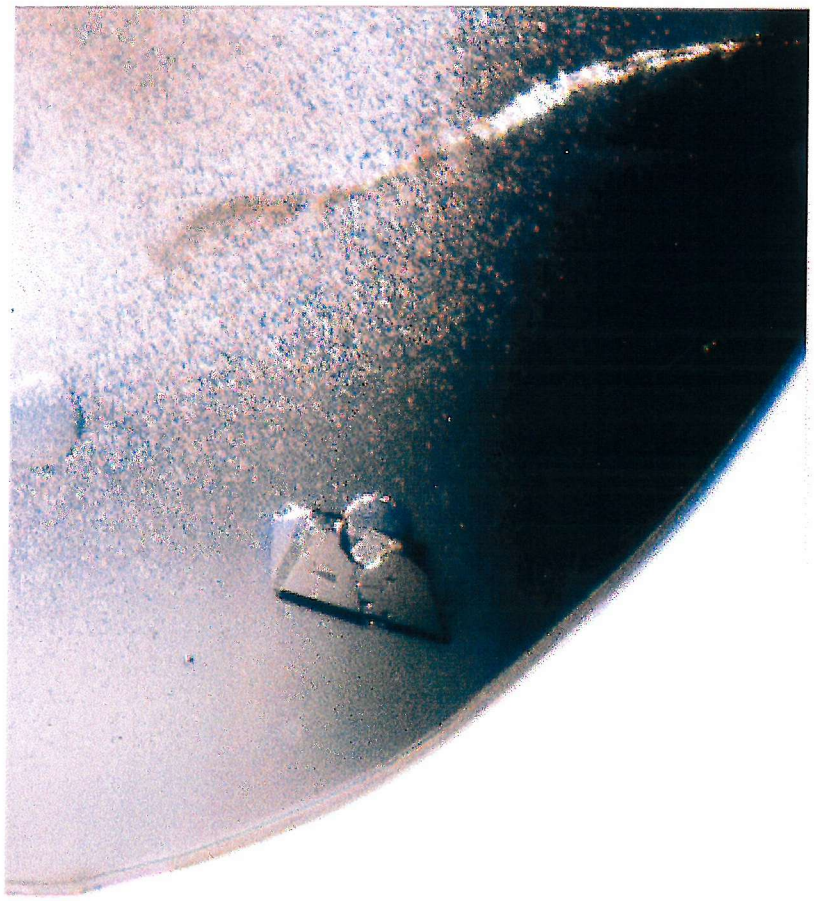

Figure 6.17 Shows low resolution images of crystals formed in the presence of (a) Mg^{2+} and inhibitor I, (b) Mg^{2+} and inhibitor II, (c) Li^{+} and inhibitor I, (d) Mg^{2+} and Li^{+}, (e) Zn^{2+}, (f) Zn^{2+} and inhibitor I, (g) Zn^{2+} and inhibitor II, (h) Zn^{2+}, Li^{+} and inhibitor I (i) Li^{+}, Mg^{2+} and inhibitor I, (j) Li^{+}, Mg^{2+} and inhibitor II and (k) Li^{+}, and inhibitor I.

(a)

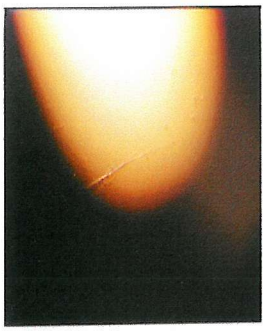

(b)

(c)

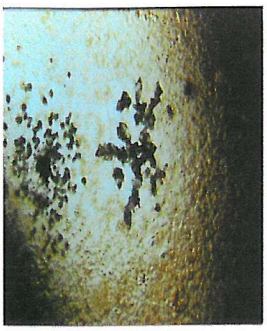

(d)

(e)

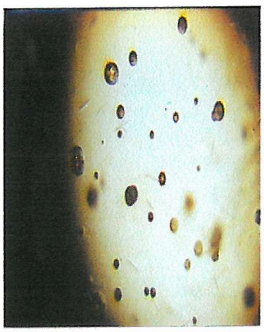

(f)

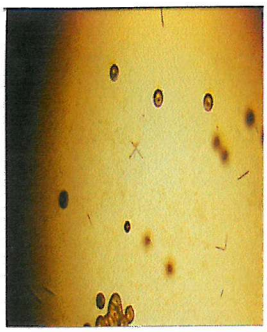

(g)

(h)

(i)

(j)

(k)

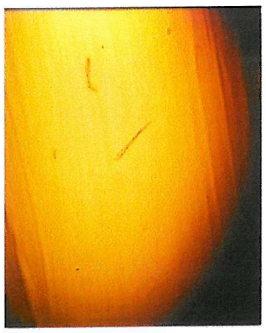

6.23 Summary

A high resolution structures have for the first time been successfully achieved for bovine inositol monophosphatase in the presence of the catalytic Mg^{2+} ions. Improvement in resolution achieved by crystals produced as described above is now close to yielding data that will locate the binding site for inhibitory Li^{+} ions. Other studies presented here (Gore *et al.*, 1993) and elsewhere have shown that Li^{+} ions will bind to the enzyme in the absence of Mg^{2+} ions with a K_d of around 0.1mM. This binding is at site 2, but this site will almost certainly not be the same as the site that leads to uncompetitive inhibition of the enzyme when in the form $E.Mg^{2+}.P_i.Li^{+}$. Crystallisation trials are now under way using appropriate conditions in an attempt to obtain crystals of both of these complexes.

Table 6.4 The distances between Mg^{2+} ions in the BIMP structure.

Mg^{2+} binding sites in BIMP structure	**Distances between metal ions subunit A (Å)**	**Distances between metal ions in subunit B (Å)**
Site 1-Site 2	3.64	3.62
Site 1-Site 3	5.52	3.75
Site 2- Site3	3.97	5.20

Table 6.5 Metal ligand distances in the human and bovine inositol monophosphatase structures. Interatomic distances for the (i) Mn^{2+} and (ii) Ca^{2+} and D-Ins(1)P structures were obtained from Bone *et al.*, (1IMC.pdb; 1994(b)) and from Ganzhorn *et al.*, (1AWB.pdb; 1997) respectively. An asterix denotes the putative nucleophilic water molecules.

		Interatomic distances between metal ions and ligands (Å)			
		Human structure		**Bovine structure**	
Metal binding site	**Ligand**	**Mn^{2+} structure (1IMC.pdb)**	**Ca^{2+} and D-Ins(1)P structure (1AWB.pdb)**	**Subunit A**	**Subunit B**
Site 1	E70 (OE1)	2.12	2.15	2.07	2.04
	D90 (OD1)	2.26	2.40	2.11	2.08
	I92 (O)	2.14	2.35	2.11	2.14
		2.08 (W1; O)	2.31 (W88; O)	2.09 (W-8)	2.05 (W-5)
		2.71 (Cl^-)	2.20 (W128; O)	2.09 (W*-13)	2.15 (W*-50)
			2.20 (Ins(1)P;O7)	2.1 4 (W-90)	1.99 (W-351)
Site 2	D90 (OD2)	2.35	2.18	2.16	2.03
	D93 (OD1)	2.27	2.19	2.09	1.99
	D220 (OD1)	2.13	2.09	2.13	2.00
		2.58 (Cl^-)	2.48 (Ins(1)P;O1)	2.29 (W-46)	2.53 (W-96)
			2.26 (Ins(1)P;O7)	1.79 (W-90)	1.87 (W-351)
					2.42 (W-322)
Site 3	E70 (OE2)	2.57	2.41	2.29 (W-46)	2.15
		2.11 (W3; O)	2.43 (W28; O)	2.12 (W-61)	2.04 (W-178)
		2.09 (W4; O)	2.63 (W128; O)	2.15 (W-65)	2.03 (W-132)
		2.11 (W5; O)	2.20 (W208; O)	2.02 (W-129)	2.15 (W*-50)
			2.24 (Ins(1)P;O8)	2.00 (W-163)	2.25 (W-246)
				2.06 (W-164)	2.08 (W-2.08)

Table 6.6 The distances between Ca^{2+} ions in the HIMP structure.

Ca^{2+} binding sites in HIMP structure	**Distances between metal ions subunit A (Å)**	**Distances between metal ions in subunit B (Å)**
Site 1-Site 2	3.73	3.64
Site 1-Site 3	4.33	4.40
Site 2- Site3	5.26	5.35

CHAPTER 7

GENERAL DISCUSSION

CHAPTER 7

General discussion

Inositol monophosphatase is a dimeric enzyme of identical 30kDa subunits, that is responsible for the hydrolysis of the phosphate moiety from all inositol monophosphates with the exception of Ins(2)P and it has an absolute requirement for Mg^{2+} ions for catalytic activity. There were two main aims for the work carried out in this thesis; firstly work was carried out in order to identify residues that may play a role in the structure of the enzyme. A second aim was to purify the enzyme in sufficient quantities for X-ray crystallographic studies.

Chemical modification, spectroscopic studies, together with kinetic studies, structural considerations have previously proposed the presence of two metal binding sites in the enzyme (site 1 with a K_d of 300μM and site 2 with a K_m of 3mM). Based upon the previous structure of HIMP, residues for mutation were selected some of which were contained in conserved regions of the protein structure. Site directed mutagenesis was used to create mutants G76S, G69S, E30P, H188Q and C218D. These mutations were characterised by a range of different techniques in an attempt to ascribe specific roles to individual residues.

Titration experiments using CD and fluorescence spectroscopy were carried out to determine K_d values for site 1 (using native or pyrene-labelled enzyme, respectively). Unlabelled enzyme was used to determine the K_m values for the second lower affinity site using steady state kinetics. These studies revealed that Mg^{2+} ion binding was not altered significantly by the G76S and E30P mutations but that a dramatic increase in Km was observed for mutations G69S, H188Q and a smaller increase noted for the C218D enzyme. G69S was an interesting mutant in that the affinity for both Mg^{2+} and substrate were decreased (by 2.5 fold increase (18.5 ± 1.4mM) and 5-fold respectively (6.6 ±

0.9mM)). This manifested as a 62% decrease in the specific activity of this mutant. Surprisingly, fluorescence titration studies failed to provide a K_d value suggesting that metal binding at site 1 has been eliminated, although it is possible that metal binding occurs without eliciting a fluorescence change.

For H188Q, Mg^{2+} affinity to site 1 was unaffected, however, both the affinity for Mg^{2+} at site 2 and for substrate was markedly lowered showing 2.7-fold and 4.5 fold decreases respectively. Since H188 residue is not near or at the active site, but located at the dimer interface, it must subtly alter the structure at the dimer interface and propagate a conformational change which affects substrate binding at the active site.

Interestingly the C218D mutation reacted with stoichiometric quantities of pyrene maleimide and titration of Mg^{2+} yielded a K_d value approximately 3-fold higher than that determined for WT enzyme. Although this change in fluorescence is not as a result of pyrene binding to C218, it is probably due to reaction of the other cysteine residues (C141 and C184). This together with the decreased affinity (~2-fold) for both Mg^{2+} ions and substrate (0.5-fold) suggests that this substitution has altered the environment of the active site, perhaps owing to its close proximity to D220, an important site 2 ligand. Near UV CD titrations using Mg^{2+}, gave similar K_d values to those determined using pyrene labelled enzyme and fluorescence spectroscopy.

Stopped flow studies, examining the binding interactions between the enzyme and Mg^{2+} ions, showed that there are two steps involved with metal binding but only one observable step in metal dissociation. A model has been proposed in which two different forms of the enzyme are in equilibrium with each other and only one of these forms is able to bind metal ions at site 1 with high affinity. Thus, the movement of the loop region of the enzyme, shown by crystallographic data in chapter 6, may occur in the absence of the metal ion but becomes stabilised by the formation of the $E.Mg^{2+}$ complex.

All mutants show similar conformational stabilities to that of the WT enzyme in the absence of Mg^{2+}. However, the increase in stability for H188Q in the

presence of Mg^{2+} is only ~0.3-fold of that observed for WT and the other mutants.

WT BIMP was successfully crystallized and its structure resolved to 1.6Å for the first time. The X-ray structure displays differences in the two subunits of the dimer; subunit B contains 3 metal binding sites, identical to those revealed by Mn^{2+} and Ca^{2+} bound HIMP, whereas subunit A has a partially occupied site 3 at a different location (see Figures 6.13(a) and (b)). The metal ligands involved are identical to those determined previously by Bone *et* al., (1994(b)) and have similar interatomic distances to those determined for the human WT enzyme.

The data presented in this thesis confirm that the third metal binding site as shown by Ganzhorn *et al.*, (1997), demonstrated to exist in HIMP for Mn^{2+} and Ca^{2+} ions is also present in BIMP. Although, studies using pyrene labelled enzyme provides saturation curves that appear to be monitoring Mg^{2+} binding at two sites. It could be that this third site is being monitored in these studies. The significance, if any of the third Mg^{2+} site in the mechanism of the IMPase remains to be elucidated.

Future work

Work is currently under way to solve the structure of the G76S mutant crystal which has diffracted data to 1.3Å at ESRF Grenoble. Attempts are being made to crystallise the enzyme in the presence of Li^{+} ions which are only visible at 1.0-1.3Å. This would allow determination of the proposed E. Mg^{2+}.S*.Li^{+} complex and elucidate the mechanism of action of the Li^{+} ion as well as the existence of the third metal binding site.

REFERENCES

REFERENCES

Allison, J. H, Blisner, M. E, Holland, W. H, Hipps, P. P, Sherman, W. R (1976) Biochem.Biophys.Res.Commun. 2, **71,** 664-669.

Atack, J. R., Broughton, H. B. and Pollack, S.J. (1995) FEBS Lett. **361**, 1-7.

Atack, J. R., Cook, S.M, Watt, A.P, Fletcher, S.R. and Ragan, C.I. (1993) J. Neurochem. **60**, 652-658.

Attwood, P. V., Ducep, J. B. and Chanal, M. C (1988) Biochem. J. **253,** 387-394.

Baker, R. Kulagowski, J. J. Billington, D.C. Leeson, P. D. Lennon, I. C. and Liverton, N (1989) J.Chem. Soc. Chem. Commun. 1383-1385.

Baker, R., Leeson, P. D., Lennon, I.C. and Liverton, N. (1990) J. Chem. Soc. Chem. Commun. 462-464.

Baker, R. Carrick, C. Leeson, P. D. Lennon, I. C and Liverton, N. J. (1991) J. Chem. Soc. Chem. Commun. 298-300.

Baker, G. R. and Gani, D. (1991) Bioorganic and Med Chem Lett. **1**, (4) 193-196.

Bayley, P. (1973) Prog. Biophys. Molec. Biol. **27**, 3.

Berridge, M.J.and Irvine, R.F. (1984) Nature **312**, 315-320.

Berridge , M.J. and Irvine, R.F. (1989) Nature **341**, 197-205.

Berridge, M. J. Downes, C. P. and Hanley, M. R. (1989) Cell **59,** 411-419.
Beychok, S. R. (1966) Science **154**, 1288.

Bone, R., Springer, J.P and Atack, J. R. (1992) Proc. Natl. Acad. Sci. U. S. A. **89**, 10031-10035.

Bone, R. Frank, L. Springer, J. P. Pollack, S. J. Osborne, S. Atack, J. R. Knowles, M. R. McAllister, G. Ragan, C. I, Broughton, H. B. Baker, R. and Fletcher, S. R. (1994a) Biochemistry **33**, 9460-9467.

Bone, R. Frank, L. Springer, J. P and Atack, J.R. (1994b) Biochemistry **33**, 9468-9476.

Bottomley, M. J., Salim, K. and Panayotou, G. (1998) Biochim. Biophys. Acta. **1436**, 165-183.

Briggs, G.E. and Haldane, J.B.S. (1925) Biochem. J. **19**, 338 – 339.

Brown, S. B. "An Introduction to Spectroscopy for Biochemists" (1980) Academic Press, London.

Chen, I. W. and Charalampous, F. C. (1996) Arch. Biochem .and Biophys. **177**, 154-157.

Chen, L. and Roberts, M. F. (1998b) App. Environ. Microbiol. **64** (7) 2609-2615.

Churchich, J. E. and Kwok, F. (1991) Analytical Biochemistry **198**, 375-378.

Chou, P. Y. and Fasman, G. D. (1974) Biochemistry **13**, 222-224.

Chou, P. Y. and Fasman. G. D. (1978) Adv. Enzymol. **47**, 45-148.

Cole, G. A. and Gani, D. (1994) J. Chem. Soc. Chem. Commun. 1139-1141.

Cornish-Bowden, A. (1986) FEBS. Lett. **203**, 3-6.

Cornish-Bowden, A. (1995) "Fundamentals of Enzyme Kinetics", Portland Press, U.K.

Creighton, T. E. (1990) "Protein Structure: a practical approach", IRL Press.
Creighton, T. E, (1990) Biochem. J. **270**, 1-16.

Diehl, R.E., Whiting, P., Potter, J., Gee, N., Ragan, C.I., Linemeyer, D., Downes, C.P. and MacPhee, C.H. (1989) Eur. J. Biochem.**193**, 1-8.

Diehl, R. E., Whiting, P., Potter, J., Gee, N., Ragan, C. I., Linemeyer, D., Schoepfer, R., Bennett, C. and Dixon, R. A. F. (1990) J. Biol. Chem. **265**, 5946-5949.

Drewett, V.L. (1998) Ph.D Thesis, University of Southampton.

Eftink and Maity (2000) "Spectrophotometry and Spectrofluorimetry: a practical approach", (Gore, M.G.) Oxford University Press.

Eisenberg, F. Jr. (1967) J. Biol.Chem. **242**, 1375-1382.

Faraci, W. S., Zorn, S. H., Baker, A. V., Jackson, E. and Pratt, K. (1993) Biochem. J. **291**, 369-374.

Fauroux, C. M. J., Lee, M., Cullis, P. M., Douglas, K. T., Freeman, S. and Gore, M. G. (1999) J. Amer. Chem. Soc. **121**, 8385-8386.

Fletcher, S. R. (1994a) Biochemistry **33**, 9460-9467.

Förster, Z. (1949) Naturforsch. A: Astrophys. Phys. Chem. **4**, 321-324.

Friefelder, D., (1976) "Physical Biochemistry Applications to Biochemistry and Molecular Biology", Freeman, London.

Gani, D., Downes, P. C., Batty, I., and Bramham,, J (1993) Biochem. et Biophys. Acta. **1177**, 253-269

Ganzhorn, A. J. and Chanal, M. C. (1990) Biochemistry. **29,** 6065-6071.

Ganzhorn, A. J., Vincendon, P. and Pelton, (1993) Biochem. Biophys. Acta. **1161**, 303-310.

Ganzhorn, A. J., Lepage, P., Pelton, P. D., Strasser, F. Vincendon, P. and Rondeau, J. M. (1996) Biochemistry 35, 10957-10966.

Ganzhorn, A. J. and Rondeau, J. M (1997) Protein Engineering **10**, 61.

Garnier, J. (1978) J. Mol. Biol. **120**, 97-120.

Gee, N. S., Howell, S., Ryan, G. and Ragan, C. I. (1989) Biochem. J. **264,** 793-798.

Gee, N. S, Knowles, M. R., McAllister, G. and Ragan, C. I. (1991) FEBS.Lett. **284**, 95-97.

Gee, N. S., Ragan, C. I., Watling, K.J., Aspley, S., Jackson, R.G., Reid, G. R., Gani, D. Gani, D. and Shute, J. K. (1988) Biochem. J. **249**, 883-889.

Gibson, T. J., Hyvönen, M., Musacchio, A., Saraste, M. and Birney, E. (1994) Trends Biochem. Sci. **19**, 349-353.

Gore, M.G. "Spectrophotometry and Spectrofluorimetry: a practical approach", Oxford University Press.

Gore, M.G., Greasley, P.J. and Ragan, C. I. (1992) J. Biochem.Biophys. Methods. **25**, 55-60.

Gore, M.G., Greasley, P.J. McAllister, G. and Ragan, C. I. (1993) Biochem. J. (1993) **296**, 811-815.

Greasley, P. J., Gore, M. G., Rees-Milton, K. J. and Ragan, C. I. (1993) FEBS. Lett. **319**, 49-53.

Greasley, P. J. and Gore, M. G. (1993) FEBS. Lett. **331**, 114-118.

Greasley, P. J., Hunt, L. G. and Gore, M. G. (1994) Eur. J. Biochem. **222**, 453-460.

Gupte, S. S. Lane, L. K. (1983) J. Biol. Chem. **258**, 5005-5012.

Hallcher, L.H. and Sherman, W.R (1980) J. Biol. Chem. **255**, 10896-10901.

Hartridge, H. and Roughton, F. J. W (1923) Proc. R. Soc. London A. **104**, 376-394.

Jackson, R. J., Gee, N. S. and Ragan, C. I. (1989) Biochem. J. **264**, 419-422.

Ke, H., Thorpe, C. M., Seaton, B. A., Marcus, F. and Lipscomb, W. N. (1989) Proc. Natl. Acad. Sci. U.S.A. **86**, 1475-1479.

Knowles, M. R. (1980) Ann. Rev. Biochem. **49**, 877-919.

Knowles, M. R., Gee, N., McAllister, G., Ragan, C.I., Greasley, P. J. and Gore, M. G. (1992) Biochem. J. **285**, 461-468.

Krauss, O. (1996) Ph.D Thesis, University of Southampton.

Kulagowski, J. J., Baker, R. and Fletcher, S. R. (1991) J. Chem. Soc. Chem. Commun. 1649-1650.

Kunkel, T.A, (1985) Proc. Natl. Acad. Sci. **82**, 488-492.
Kunkel, T.A., Roberts, J.D and Zakour, R.A. (1987) Methods. Enzymol. **154**, 367-382.

Kwok, F., Lo, S-C. and Churchich, J. E. (1994a) Biochem. Mol. Biol. Int. **32**, (2), 325-330.

Kwon, H. Y., Lim, B. H., Park, H. S., Lee, Y. L., Lee, E. H., Choi, S.Y. and Park, H. J. (1998) J. Biochem. Mol. Biol. **31**, (3) 274-280.

Kwon, O., Lo, S. C. L., Kwok, F. and Churchich, J. E. (1993) J. Biol. Chem **268** (11) 7912-7916.

Laemmli, U. K. (1970) Nature **277**, 680-684.

Lau., C. K, Lo, S.C., Churchich, D. R., Kwok, F. and Churchich, J. E. (1998) Journal of Protein Chemistry, **17** (8) 789-796.

Leech, A. P., Baker, G. R., Shute, J. K. Cohen, M. A. and Gani, D. (1993) Eur. J. Biochem. **212**, 693-704.

Lemmon, M. A., Falasca, M., Ferguson, K. M. and Schlessinger, J. (1997) Trends in Cell Biol. **7**, 237-242.

Lowenthal, R., Sancho, J and Fersht, A. R (1992) J. Mol. Biol. **224**, 759-770.

Manavalan, P. and Johnson, W. C. Jr. (1983) Nature **305**, 831-832.
1983.

Maniatis, T., Fritsch, E.F., and Sambrook, J. (1982) "Molecular cloning: A Laboratory Manual", C.S.H.N.Y.

Matthews, B. W., (1968) J. Mol. Biol. **33**, 491-497.

McPherson, A., Malkin, A. J. and Kuznetsov, Y. G., (1995) "The Science of Macromolecular Crystallisation Structure", **3**, 759-768.

McAllister, G., Whiting, P., Hammond, E.A., Knowles, M. R., Atack, J.R., Bailey, F.J., Maigetter, R. and Ragan, C.I. (1992) Biochem. J. **284**, 749-754.

Moffat, B. A. and Studier, F. W. (1986) J. Mol. Biol. **189**, 113-118.

Moreno, C. S., Garcia Blanco, F., Gore, M. G., Rees-Milton, K., and Churchich, J. E. (1996) Eur. J. Biochem. **240**, 435-442.

Moscowitz, A., Rosenberg, A. and Hansen, A. E. (1965) J. Amer. Chem. Soc. **87**, 1813.

Needham, J. V., Chen, T. Y. and Falke, J. J. (1993) Biochemistry **32**, 3363-3367.

Nahorski, S.R., Ragan, C.I and Challis, R.A.J.(1991) Trends. Pharmacol. Sci. **12,** 297-303.

Navaza, J., (1994) Acta. Crystallogr. **50**, 157-163.

Neuwald, A. F., York, J. D. and Majerus, P. W. (1991) FEBS Lett. **294**, 16-18.

Nishuzuka, Y. (1992) Science **258,** 597-614.

Norris, F. A., Wilson, M. P., Wallis, T. S., Galyov, E. E. and Majerus, P. W. (1998) PNAS. **95** (24), 14057-14059.

Pace, C.N. (1986) Methods in Enzymology **131**, 266-279

Parthasarathy, R. and Eisenberg, F, (1986) Biochem. J. **235**, 313-322.

Parthasarathy, R. Vadnal, R. E., Ramesh, T. G., Syamaladevi, C. S. Parthasarathy, R., (1993) Arch of Biochem and Biophys. **304** (1) 94-101.

Parthasarathy, R., and Parthasarathy, L, and Vadnal, R. (1997) Brain Res. **778** 99-106.

Parthasarathy, R., and Parthasarathy, L, and Vadnal, R. (1997b) Gene **191,** 81-87.

Pineda, T., Thorne, M. R., Gore, M. G. and Churchich, J. (1996) Biochem. et Biophys. Acta. **1292**, 259-264.

Pollack, S. J., Knowles, M. R., Atack, J. R., Broughton, H. B., Ragan, C. I., Osborne, S. and McAllister, G. (1993) Eur. J. Biochem. **217**, 281-287.

Pollack, S. J., Atack, J. R., Knowles, M. R., McAllister, G., Ragan, C.I., Baker, R., Fletcher, S. R., Iversen, L. L. and Broughton, H. B. (1994) Proc. Natl. Acad. Sci. U.S.A. **91**, 5766-5770.

Provencher, S. W. and Glockner, J. (1981) Biochemistry. **20**, 33-40.

Rees-Milton, K. J., Greasley, P. J. Ragan, C. I. and Gore, M. G. (1993) FEBS Lett. **321**, 37-40.

Rees-Milton, K. J. (1994) Ph.D Thesis.

Rees-Milton, K. J., Thorne, M., Greasley, P, Churchich, J. and Gore, M.G. (1997) Eur. J. Biochem. **246**, 211-217.

Rossmann, M. G., Blow, D. M. (1962) Acta. Crystallogr. **15**, 24-31.

Sanger, F. Nicklen, S. and Coulson, A. R., (1977) Proc. Natl. Acad. Sci. USA. **74** (12) 5463-5467.

Saudek, V. (1996) E. J. Biochem. **240**, 288-291.

Schoepfer, R., Bennett, C. and Dixon, R.A.F. (1990) J. Biol. Chem. **265**, 5946-5949.

Schoepfer, R (1993) Gene **124**, 83-85.

Shears, S.B, (1989) Biochem. J. **260**, 313-324.

Schulz, J., Wilkie, J., Lightfoot, P., Rutherford, T., and Gani, D., (1995) J. Chem. Soc. Chem. Commun. 2353-2355.

Shute, J. K., Baker, R., Billington, D. C. and Gani. D. (1988) J. Chem. Soc. Chem. Commun. 626-628.

Silva, N.M. (1999) Ph.D Thesis, University of Southampton.

Spector, R. and Lorenzo, A. V. (1975) Am. J.Physiol. **228**, 1510-1518.

Stokes, G. G. (1852) Phil. Trans. R. Soc. London **142**, 463-562.

Strasser, F., Pelton, P. D. and Ganzhorn, A.J. (1995) Biochem. J. **307**, 585-593.

Szabo, A. G. (Gore, M.G. Editor, (2000)) "Spectrophotometry and Spectrofluorimetry: a practical approach".

Strickland, E. H. (1974) Crit. Rev. Biochem. **2**, 113.

Takimoto, K., Okada, M., Matsuda, Y. and Nakagawa, H. J. (1985) Biochem. **98**, 363-370.

Taylor, J. W., Ott, J. and Eckstein, F. (1985b) Nuc. Acids. Res. **13**, 8764-8774.

Taylor, J. W., Schmit, W., Cosstick, R., Okruszek, A. and Eckstein, F. (1985a) Nuc. Acids. Res. **13**, 8779-8784.

Thorne, M. R. Greasley, P. J. and Gore, M. G (1996) Biochem. J. **315**, 989-994.

Vadnal, R.E., Parthasarathy, R., Parthasarathy, L., Ramesh, T. G., and Shyamaladevi, C. S (1992) Biochem. Int. **26** (5) 935-941.

Vadnal, R. E., Heng, H. H. Q., Parthasarathy, L. and Parthasarathy, R., (1998) Neuroreport. **9** (4) 683-685.

Vallee, B. L. and Auld, D. S. (1990) Biochemistry. **29** (24) 5647-5659.

Vallee, B. L. and Auld, D. S. (1993) Biochemistry. **32**, 6493-6500.

Velluz, L., Legrand, M, and Grosjean, M. (1965) "Optical circular dichroism", Academic Press, New York.

Waldman, A.D.B., Hart, K.W., Clarke, A.R., Wigley, D. B., Barstow, D.A.., Atkinson, T., Chia, W.N. and Holbrook, J.J. (1988). Biochem. Biophys. Res. Commun. **150**, 752-759.

Weltman, J. K., Searo, R. P., Frackelton Jnr., A.R., Dowben, R. M., Bunting, J. R. and Cathow, R. E (1973) J. Biol. Chem. **248**, 3173-3177.

Whiting, P., Gee, N. S., Potter, J., Howell, S. and Ragan, C. I. (1990) Biochem. J. **272**, 465-468.

Woody, R. W. (1968) J. Chem. Phys. **49**, 4797.

Woody, R. W. (1969) Biopolymers. **8**, 669.

Woody, R. W. (1974) "Peptides, Polypeptides and Proteins" (Blout, E. R., Bovey, F. A., Goodman, M. and Lotan, N. Eds.), John Wiley and Sons inc., New York, 338.

Yang, J. T., Wu, C. S. C. and Martinez, H. M. (1986) Methods in Enzymol. **130**, 208.

Yenush, L., Bellés, J. M. López-Coronado, J. M, Gil-Mascarell, R, Serrano, R. and Rodríguez, P. L. (2000) FEBS Lett. **467**, 321-325.

York, J. D., Chen, Z. W., Ponde, J. W., Chauhan, A. K., Matthews, F. S. and Majerus, P. W. (1994a) J.Mol. Biol. **236**, 584-589.

York, J. D., Ponder, J. W., Chen, Z. W., Matthews, F. S. and Majerus, P. W. (1994b) Biochemistry **33**, 1364-1371.

Zhang, Y., Liang, J. Y. and Lipscomb, W. N. (1993) Biochem.Biophys, Res. Commun. **190**,1080-1083.

Zhang, Y., Liang, J. Y., Huang, S., Ke, H. and Lipscomb, W.N. (1993) Biochemistry **32**, 1844-1857.